



**THE IMPACT OF PHYSICOCHEMICAL
PROPERTIES AND PHYSIOLOGICAL
CLEARANCE MECHANISMS ON OCULAR
DRUG DISTRIBUTION**

**By
Jenifer Mains**

A Thesis submitted to the University of Strathclyde in fulfilment of the
requirement for degree of Doctor of Philosophy

September 2011

DECLARATION OF AUTHENTICITY AND AUTHOR'S RIGHTS

'This thesis is the result of the author's original research. It has been composed by the author and has not been previously submitted for examination which has led to the award of a degree.'

'The copyright of this thesis belongs to the author under the terms of the United Kingdom Copyright Acts as qualified by University of Strathclyde Regulation 3.50. Due acknowledgement must always be made of the use of any material contained in, or derived from, this thesis.'

Signed:

Date:

This thesis is dedicated to Jean Reid and Megan Scott.

ACKNOWLEDGMENTS

Let me first start by thanking my supervisors, Professor Clive Wilson and Doctor Andrew Urquhart. I would like to thank Clive for his guidance and advice throughout the project and for giving me the opportunity to work across a depth of subjects, in a variety of interesting places. Thanks to Andrew for being an excellent supervisor, considering I was his first PhD student, and for his guidance and support throughout. A special thank you for being young enough to remember the highs and lows of being a PhD student.

A number of other people have helped me out during the project and ensured that my research could progress in the right direction. Special thanks to Professor John Girkin of Durham University, Doctor Valeriu Damian-Iordache of GSK, Philadelphia, Doctor Eileen McBride of AstraZeneca, Macclesfield and Anthony Atkinson of AstraZeneca, Charnwood. I would like to thank AstraZeneca for funding this project and my industrial supervisors, Paul Gellert and Ash Bahl for getting it off the ground.

From the University of Strathclyde I would like to thank, Doctor Blair Johnson for his help with SIMCA, Doctor Lay Ean Tan for assistance with the perfusion set up and Doctor Dave Watson and Doctor Zong Tang for their analytical expertise. I would also like to thank the technical staff, workshop staff and the secretarial staff for helping this work to run as smoothly as possible.

For being there throughout this work I would like to thank all my fellow PhD students who I have met over the years, especially my friends Gemma, Shonagh, Lisa, Gracie, Joe and Ruairidh, with a special mention to Scott and Gordon for being there from the enthusiastic start to the bitter end.

To my excellent friends Susan, Oni, Emma and Joanna, for being there whenever I have needed them. To Donna, Laura, Lauren and Nicola for being loving, supportive but at the same time hilarious. To Jenny, Bev, Hazel, Rachelle and Cat for being great friends and reminding me on a regular basis why I am doing this and not doing community pharmacy. To everyone at the Griphouse, Glasgow for providing a very welcome distraction and to the others who have come and gone over the years, you know who you are.

Last but not least, I would like to thank my family. To my parents for getting me to this point and for supporting me through every decision I have made and every direction I have taken. Your love and belief in me has meant a lot, I couldn't have done it without you. To my wonderful Papa who has championed me throughout my life. To my brother Steven, in times of trouble you are my first port of call and not only a brother but a great friend, in addition I would like to thank you for being super competitive and making me want to be better at everything than you are, hence the PhD. Finally, a special thank you to Daniel for your patience, support and understanding throughout. Your ability to pick me up and make me laugh at the drop of a hat will always be appreciated.

Contents

CHAPTER 1. Introduction.....	2
1.1. Structure of the eye.....	2
1.1.1. Outer coat of the eye.....	3
1.1.2. Middle coat of eye: Uveal tract.....	6
1.1.3. The inner layer of the eye.....	10
1.1.4. Periocular structures.....	12
1.1.5. Blood supply.....	15
1.2. Posterior eye disease and treatment.....	16
1.2.1. Glaucoma.....	17
1.2.2. Retinitis pigmentosa.....	17
1.2.3. Cytomegalovirus retinitis.....	18
1.2.4. Age-related macular degeneration.....	19
1.2.5. Diabetic retinopathy.....	21
1.3. Pharmacokinetics.....	22
1.3.1. Basic principles.....	22
1.3.2. Pharmacokinetic modelling systems.....	24
1.3.3. Drug disposition in eye.....	33
1.3.4. Flow within the vitreous.....	33
1.3.5. Clearance from the vitreous.....	37
1.4. The role of transporters in drug disposition.....	41
1.4.1. The role of the blood-retinal barrier.....	41
1.4.2. Role of transporters in drug administration.....	42
1.5. Aims and objectives of the thesis.....	49
CHAPTER 2. Development and validation of a liquid chromatography mass spectrometry method for the simultaneous quantification of a drug series in ocular tissues.....	50
2.1. Introduction.....	50
2.1.1. Cassette dosing.....	50
2.1.2. Ultra performance liquid chromatography.....	53
2.2. Materials and methods.....	54
2.2.1. Chemicals.....	54

2.2.2. Instrumentation.....	54
2.2.3. Chromatographic conditions	55
2.2.4. Mass spectrometry conditions	55
2.2.5. Sample preparation.....	55
2.2.6. Tissue extraction study	57
2.3. Results and discussion	61
2.3.1. UPLC-MS compound separation	61
2.3.2. Validation of UPLC-MS/MS method.....	67
2.4. Conclusions.....	84
CHAPTER 3. Pharmacokinetic study of a drug series in the isolated perfused ovine eye.....	85
3.1. Introduction.....	85
3.2. Methods.....	88
3.2.1. Chemicals and reagents	88
3.2.2. Perfusion materials	88
3.2.3. Perfusion system design	89
3.2.4. Perfusion fluid	91
3.2.5. Ovine eye cannulation procedure	94
3.2.6. Perfusion procedure.....	95
3.2.7. Viability parameters	97
3.2.8. Intravitreal injection	101
3.2.9. Study design and tissue processing	102
3.3. Results and discussion	103
3.3.1. Number of successfully perfused eyes	103
3.3.2. Tissue weights	104
3.3.3. Viability parameters	107
3.3.4. Effect of physicochemical properties on drug distribution	109
3.4. Conclusion	121
CHAPTER 4. ToF-SIMS analysis of ocular tissues to reveal biochemical differentiation and drug distribution	122
4.1. Introduction.....	122
4.2. Materials and methods	127
4.2.1. Ocular tissue preparation.....	127

4.2.2. ToF-SIMS analysis.....	128
4.2.3. Multivariate statistics.....	128
4.3. Results and discussion	128
4.3.1. Principle Component 1 versus Principle Component 2.....	130
4.3.2. Principle Component 2 versus Principle Component 3.....	139
4.4. Conclusions.....	142
CHAPTER 5. ToF-SIMS analysis of dexamethasone distribution - in the isolated perfused eye.....	143
5.1. Introduction.....	143
5.2. Materials and methods	146
5.2.1. Chemicals	146
5.2.2. Isolated ovine eye preparation.....	146
5.2.3. Intravitreal administration of dexamethasone phosphate disodium	147
5.2.4. Tissue preparation	147
5.2.5. Drug sample preparation	148
5.2.6. ToF-SIMS analysis.....	148
5.3. Results and discussion	149
5.3.1. ToF-SIMS spectra analysis.....	149
5.3.2. Dexamethasone phosphate disodium distribution in the non-perfused eye.....	153
5.3.3. Dexamethasone phosphate disodium distribution in the perfused eye.....	159
5.4. Conclusions.....	164
CHAPTER 6. A finite element model of brimonidine distribution in the rabbit eye.....	166
6.1. Introduction.....	166
6.2. Materials and methods	169
6.2.1. Geometry	169
6.2.2. Conditions	169
6.2.3. Brimonidine pharmacokinetics.....	171
6.3. Results and discussion	171
6.4. Conclusion	185
CHAPTER 7. Summary and future work	187
7.1. Summary.....	187

7.2. Future work..... 189

Abbreviations

ABC	ATP Binding Cassette
AIDS	Acquired Immunodeficiency Syndrome
AH	Aqueous Humor
AMD	Age-related Macular Degeneration
APP	Arterial Perfusion Pressure
AUC	Area Under Curve
ATP	Adenosine Triphosphate
BAPSG	Benzylamine phenyl
BRB	Blood Retinal Barrier
CB	Ciliary Body
C _{Max}	Maximum Concentration
CMV	Cytomegalovirus
DR	Diabetic Retinopathy
FEM	Finite Element Model
FG	FluoresceinGlucuronide
FS	Fluorescein Sodium
HAART	Highly Active Antiretroviral Therapy
HCl	Hydrochloric Acid
HPLC	High Performance Liquid Chromatography
IOP	Intraocular Pressure
IS	Internal Standard
LAT	Large neutral amino acid transporter
LC-MS	Liquid Chromatography Mass Spectrometry
LDH	Lactate Dehydrogenase
LLE	Liquid-Liquid Extraction
L-Phe	L-Phenylalanine
MALDI	Matrix Assisted Laser Desorption Ionisation
MDP	Multi-drug Resistant Protein
MDR	Multi-drug Resistant

MRI	Magnetic Resonance Imaging
MS	Mass Spectrometry
MVA	Multivariate Analysis
NPDR	Non Proliferative Diabetic Retinopathy
NMR	Nuclear Magnetic Resonance Imaging
Oat	Organic Anion Transporter
Oct	Organic Cation Transporter
PC	Principal Component
PCA	Principal Component Analysis
PCR	Polymerase Chain Reaction
PDR	Proliferative Diabetic Retinopathy
PLS	Partial Least Square
P-gp	P-glycoprotein
PK	Pharmacokinetics
PP	Protein Precipitation
RP	Retinitis Pigmentosa
RPE	Retinal Pigmented Epithelium
RSD	Relative Standard Deviation
SIM	Selective Ion Monitoring
SPE	Solid Phase Extraction
SRM	Selective Reaction Monitoring
T _{Max}	Time of maximum concentration
Tof-SIMS	Time of flight secondary ion mass spectrometry
UHV	Ultra High Vacuum
UPLC	Ultra Performance Liquid Chromatography
UV	Ultraviolet
VEGF	Vascular Endothelial Growth Factor
VH	Vitreous Humor

Abstract

This thesis presents an investigation into the distribution of drug compounds administered to the eye, focussing on the impact the drug's physicochemical properties and the physiological clearance mechanisms operating within the eye will have on the extent of drug distribution.

At the outset, a fast and effective UPLC-MS/MS method was developed to enable the simultaneous quantification of a drug series in ocular tissues. Using the developed method, a study utilising the methods of cassette dosing and the perfused ovine eye model demonstrated that for a series of beta adrenoreceptor antagonists, lipophilicity is a key physicochemical property that governs drug distribution. Following intravitreal injection, lipophilic beta adrenoreceptor antagonists penetrate to the posterior eye where they bind to the choroid and reside in the retina at greater concentrations than more hydrophilic beta adrenoreceptor antagonists, which preferentially penetrate to the anterior eye.

In order to improve our understanding of drug distribution further, time-of-flight secondary ion mass spectrometry (ToF-SIMS) was used to spatially map model drug distribution through a tissue cross section. Initial difficulties arose in identifying drug fragments and principle component analysis was employed to demonstrate the presence of model drug predominantly across the vitreous. ToF-SIMS was then successfully utilised to characterise and demonstrate the spatial distribution of dexamethasone within ocular tissues, showing that in the living eye, the drug was shown to distribute within the vitreous and penetrate to the back of the retina and also into the lens.

Finally, using finite element modelling, our understanding of spatial ocular drug distribution was enhanced further by modelling the distribution of brimonidine into the posterior eye following topical administration. Brimonidine was shown to penetrate into the posterior eye tissues via the cornea route, the conjunctival route and finally through entering into the systemic circulation.

CHAPTER 1. INTRODUCTION

In 2002 it was estimated that visual impairment affected 161 million of the world's population with 90% of the visually impaired residing in the developing world. On a global scale, 37 million people are considered blind and although this is a reduction from the 1990s, the incidence of blindness attributed to conditions associated with longer life spans has increased (WHO 2004). The magnitude and scale of the problem of visual impairment has lead to increased understanding of the structure of the eye and the conditions it is affected by, with a desire to improve the treatment options available.

1.1. STRUCTURE OF THE EYE

The eye enables arguably one of the most important of the five senses: sight. The ability to visualise our surroundings is a very complex process, requiring detection and conversion of light into neural pulses, before transmission to the brain. As such, the eye is a very intricate organ built from various different structure with varying roles to play in the visual process (Smith, Kincaid et al. 1999). The eye itself can be divided into four sections: the outer coat, the middle coat, the inner coat and the periocular structure (Figure 1-1). The structure of each section of the eye varies in relation to the differing functions of each of the sections.

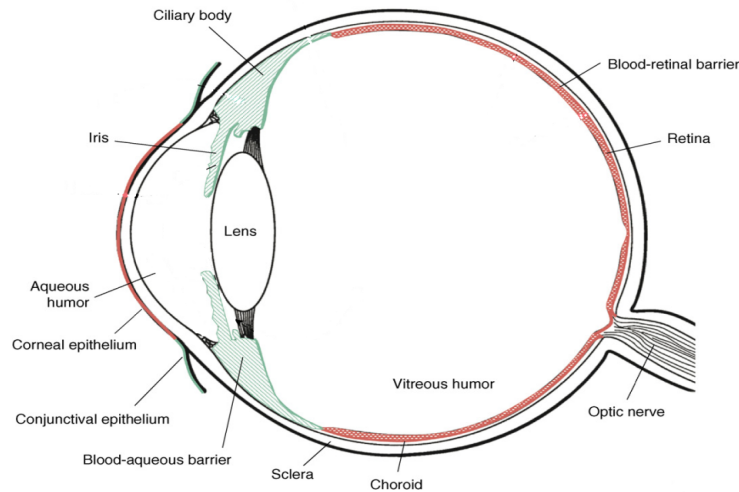


Figure 1-1 Diagram of the structure of the human eye in cross section. Adapted from Amo and Urtti 2008.

1.1.1. OUTER COAT OF THE EYE

The outer section of the eye is in contact with external structure surrounding the eye and as a result, the main role of the outer section of the eye is in the protection of the internal structure. The outer section of the eye is lined by the conjunctiva and can be further divided into the anterior section and the posterior section. The limbus connects the anterior and posterior sections together with the anterior section consisting of the cornea and the posterior section made up from the sclera.

1.1.1.1. SCLERA

The sclera, often referred to as the ‘white of the eye’, is a dense structure and due to its ability to withstand force, it plays a key role in protecting the internal structure of the eye. The sclera is a fibrous structure containing fibroblasts dispersed within the main bulk of collagenous lamella (Figure 1-2), with collagen forming 90% of the sclera (Zorn, Hernandez et al. 1992). Type I collagen predominates and is packed closely at the front of the eye - accounting for the white appearance - however, towards the posterior eye the collagen becomes much thinner. The collagen structure of the sclera provides it with viscoelastic properties, enabling a small degree of distension and contraction when minor variations in intraocular occur

(Forester, Dick et al. 2002). Alongside the collagen structure of the sclera, the thickness of the sclera also varies depending on positioning in the eye. In the human eye the sclera is approximately 0.53 mm thick at the limbus and becomes slightly thinner at the equator (approximately 0.39 mm) before thickening again at the optic nerve to about 1 mm. The surface area occupied by the sclera is about 16.3 cm², which is large in comparison to other ocular structures (Olsen, Aaberg et al. 1998).

The sclera receives its blood supply through the small branches of the ciliary artery, which penetrate through the sclera. Ciliary nerves also penetrate the sclera along with the four vortex veins which drain the four quadrants of the eye (Saude 1993). Finally, the sclera covers 5/6 of the eyeball and due to its large surface area and high permeability, even to larger molecules, it is an alternative route to the cornea for drug entry to the eye (Ranta and Urtili 2006).

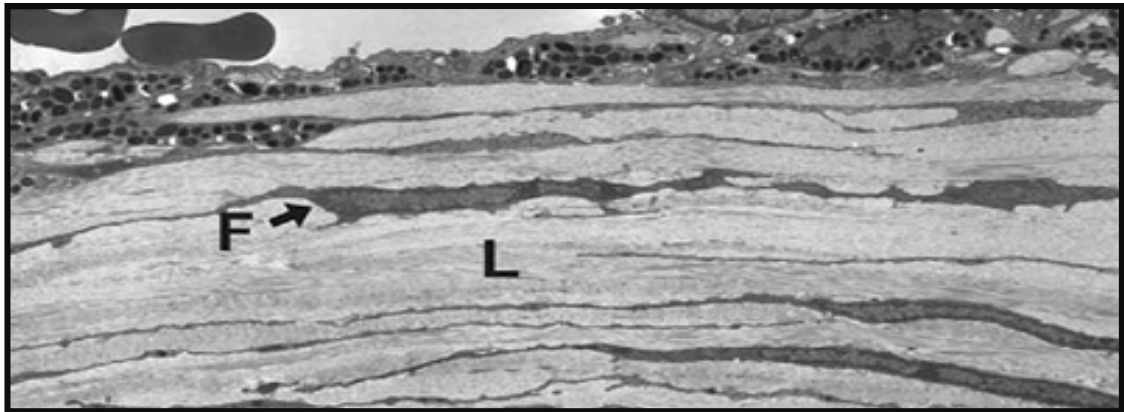


Figure 1-2 Cross section of mouse sclera detailing fibroblast structure (F) dispersed within the collagenous lamella (L) (Summers Rada, Shelton et al. 2006).

1.1.1.2. CORNEA

The cornea is the transparent tissue of the anterior eye that sits at the front of the iris and ciliary body. It is a multilayered structure made up of the corneal epithelium, Bowman's membrane, stroma, Descemet's membrane and the corneal endothelium (Figure 1-3). The thickness of the cornea varies from the limbus to the central position, with thickness at the pupillary centre averaging around 520 µm (Ashwin, Shah et al. 2009). The outer layer of the cornea consists of the corneal

epithelium, which is approximately five to six cells thick and is of a low permeability. The low permeability of the epithelium prevents the free passage of molecules into the eye and specifically compounds that are ionised at physiological pH or are of a hydrophilic nature will have difficulty penetrating. The Bowman's layer sits immediately beneath the corneal epithelium and it is composed of randomly arranged collagen fibres, which connect the corneal epithelium to the stroma. The stroma forms the main bulk of the cornea, occupying approximately 90% of the structure and it is composed of water with parallel running collagen fibres bound together by extracellular mucopolysaccharides (Saude 1993). The stroma is the opposite of the cornea, in that it enables passage of hydrophilic compounds, but will inhibit the passage of lipophilic compounds. This can be problematic in drug treatment of the eye, as the candidate drug will require both hydrophilic groups and lipophilic groups to penetrate through the entirety of the cornea. The inner most layer of the cornea is the endothelium. The endothelium is responsible for maintaining corneal transparency by ensuring fluid is kept out of the stroma. Differing from the epithelium, the endothelium poses a weak barrier to compound penetration, enabling compounds to pass through this structure more freely (Smith, Kincaid et al. 1999).

In order to enable light to pass through, the cornea is a transparent structure. The transparency of the cornea is controlled by glycosaminoglycan and proteoglycan bridges between the collagen fibres present in the cornea (Forester, Dick et al. 2002). This enables light to pass freely though the cornea to the back of the eye without the problem of light scattering (Smith, Kincaid et al. 1999). As expected from its transparency, the cornea is an avascular structure but derives some nutrients from the ciliary artery (Saude 1993).

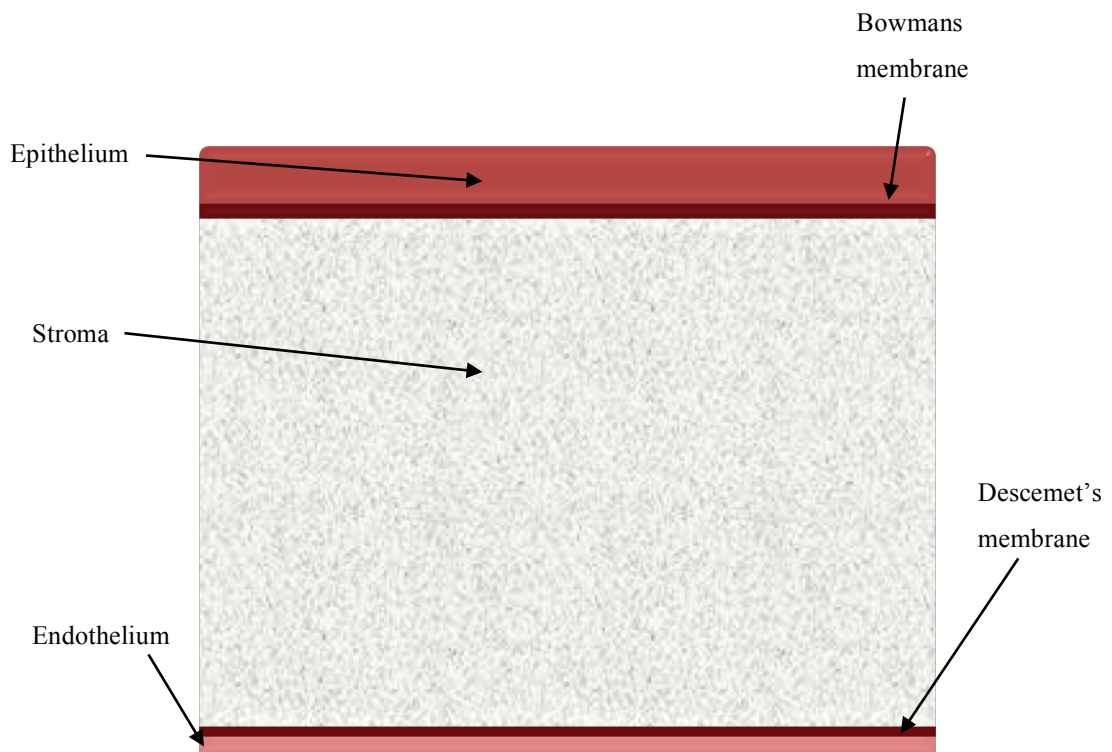


Figure 1-3 Diagram representing the corneal structure.

1.1.2. MIDDLE COAT OF EYE: UVEAL TRACT

The outer section of the eye surrounds the middle coating layer, known as the uveal tract. The uveal tract is a continuous, highly pigmented structure containing two openings: one at the pupil and one at the optic nerve. The continuous uveal tract encompasses the choroid, the iris and the ciliary body and ensures that light enters the eye through the pupil only.

1.1.2.1. CHOROID

The choroid is a vascular structure, positioned between the outer sclera and the inner retina. The main role of the choroid is in elimination of toxins, the elimination of products of metabolism, it provides nutrition to the eye and it is responsible for providing nourishment to the outer part of the retina. The thickness of the choroid can be attributed to its high vascularity and varies depending on

position, with the thickness ranging from 0.15 mm anteriorly to 0.22 mm posteriorly with a thicker section of 0.35 mm present at the macula. The thickness of the choroid will decrease with age due to the collapse of network of veins that are contained within (Tripathi and Tripathi 1984).

The choroid is multilayered, containing the suprachoroidea, the stroma, the choriocapillaris and the Bruch's membrane. The suprachoroidea contains long and short ciliary arteries dispersed throughout this layer. It is composed of collagenous lamellae and this acts as an anchor, attaching on to the sclera. The stroma is composed mainly of collagen, fibroblasts and melanocytes and it contains the larger blood vessels which penetrate through the choroid. The choriocapillaris layer plays an important role in choroidal function, as it is responsible for the nourishment of the retinal pigmented epithelium. In keeping with its important nourishment function, the choriocapillaris layer is composed of a capillary network, which contains highly permeable vessels. The final layer of the choroid is the Bruch's membrane. The Bruch's membrane has been described as a transparent glassy membrane and its role is to separate the capillary network from the retina (Davson 1980; Tripathi and Tripathi 1984). From the composition of the individual layers of the choroid, it is clear that the choroid is of a highly vascular nature. For this reason substances and drug substances can move through the choroid to the inner section of the eye from the systemic circulation with relative ease (Washington, Washington et al. 2001; Amo and Urtti 2008).

1.1.2.2. CILIARY BODY

Following on from the posterior choroid and moving towards the front of the eye, the ciliary body forms part of the pigmented uveal tract positioned within the anterior section. The ciliary body has an important physiological role within the eye and it is responsible for aqueous humor production (including humor flow between the anterior and posterior chambers) and the maintenance of intraocular pressure. The external section of the ciliary body is separated from the choroid and the sclera by the suprachorioidal space, whereas the internal section is in direct contact with the vitreous humor.

The ciliary body forms a circular shape (Figure 1-4) and the thickness varies from 5.2 mm at the upper section, closest to the forehead, to 6.3 mm at the lower section. The internal part of the structure is made up of the smooth posterior section, known as the pars plana, and the ridge-like anterior section, known as the pars plicata. The ridges of the pars plicata are known as the ciliary processes which are composed of both pigmented and non-pigmented epithelium. Along with epithelial cells, the ciliary processes also have an internal vascular connective tissue core and are surrounded by an external vascular layer continuous with the choroid. Blood is supplied to the ciliary body via the anterior ciliary arteries and drainage occurs via the vortex vein. The ciliary processes are a key feature of the ciliary body as they are responsible for the continual production of aqueous humor (Tripathi and Tripathi 1984).

Another key notable feature of the ciliary body is the ciliary muscles. The ciliary muscles have an important role in the visual process as they work together with the lens in focusing light on the retina. The ciliary muscle contracts and relaxes the zonules attached to the lens and adjusts the lens position to focus the light path penetrating through the cornea. Three types of muscle fibres exist: the meridional fibres, the radial fibres and the circular fibres. The radial muscle fibres are the most important in adjusting lens position and are likely to also have a role in widening the uveal trabecular space. The two other types of muscle fibres work with the radial muscles fibres to control lens position, the meridional fibres, in addition to the radial fibres, open up the trabecular space and widen the lumen in Schlem's canal, whereas the circular fibres are thought to relax the zonules around the lens (Donaldson 1973).

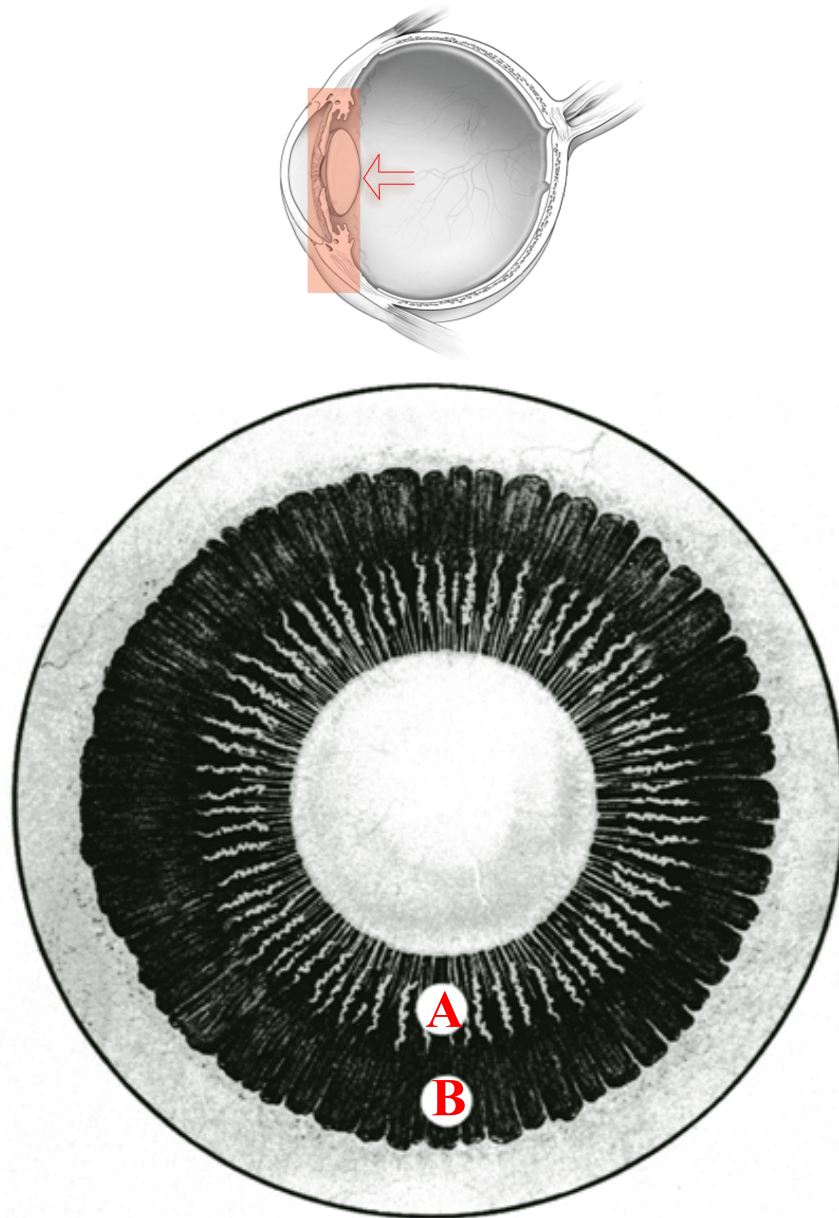


Figure 1-4 Internal view of the ciliary body surrounding the lens as viewed from the posterior pole with lens removed (see inset left). Pars plicata represented by structure A and pars plana represented by B. Figure adapted from (Tripathi and Tripathi 1984).

1.1.2.3. IRIS

The iris is connected to the ciliary body and is the coloured ring surrounding the pupil at the front of the eye. The iris has an approximate diameter of 12 mm and is divided into two zones, the pupillary zone and the ciliary zone, which meet at the collarette. The iris is composed of four layers: the anterior layer, the stroma, the dilator papillary muscle and the posterior pigmented epithelium. All four layers are composed mainly of loose connective tissue, fibroblasts, melanocytes and collagen. The dilator muscle of the iris is under sympathetic control and is responsible for pupil contraction and dilation in response to changing light conditions (Tripathi and Tripathi 1984).

Blood is supplied to the iris via the ciliary body and drains from the iris back into the ciliary body. Blood supply to the iris is rich however due to the structure of the iris, substances cannot move freely into the iris from the systemic circulation. This is due to the numerous tight junctions contained within the iris capillary endothelium and as a result of these tight junctions, the iris plays a key role in the blood ocular barrier. Due to the existence of these tight junctions, the iris is less permeable than other ocular structure to many solutes and prevents movement of substances from the systemic circulation into the internal ocular structure (Forester, Dick et al. 2002).

1.1.3. THE INNER LAYER OF THE EYE

1.1.3.1. THE RETINA

The inner coat of the eye encompasses the retina. The retina is made up of several layers and is responsible for the detection and transmission of light into chemical signals. The sensory retina is made up from photoreceptor cells, consisting of the rods and cones. The rod cells predominate, with approximately 130 million present in the human eye, and are responsible for peripheral vision especially in duller light conditions. The cones exist in three subgroups; long, medium and short. They detect finer vision and colour vision, with the sub grouping of the cones depending on the wavelength of light they detect. A key component of the photoreceptor cells involved in the generation of sight is the membrane bound protein rhodopsin. When a photon of light hits the rhodopsin protein an

isomerisation reaction occurs, converting retinaldehyde from the cis formation to the trans formation. This in turn triggers a series of reactions which ultimately generates a nerve impulse. The nerve impulse is transmitted to the brain and translated into the perception of vision. Another area of the retina concerned with generating visual impulses is the specialised macula. The macula contains a central compartment known as the fovea. The fovea contains only cone cells and its role is in the detection of central and colour vision (Smith, Kincaid et al. 1999; Wilson, Semenera et al. 2007).

The outer layer of the retina consists of the melanin rich, retinal pigmented epithelium (RPE). The RPE is in direct contact with the Bruch's membrane, separating it from the choriocapillaris. It has various functions in substance transport into and out of the retina, including the regulation of ion and fluid balance. The active transport systems of the RPE enable the transfer of materials from the vascular supply into the retina. In addition to this, several ion transport systems are known to be involved in the transfer of ions from the retina into the choroid. As well as enabling material transport, the RPE can also hinder substance movement by creating a tight and effective barrier between the systemic circulation and the retina. This barrier is created via tight junctions which exist between cells thereby preventing the free movement of molecules from the systemic circulation (Leblanc, Jezequel et al. 1998). Alongside substance transport, the RPE also has a role in controlling the visual system, exerting its role through the lysosomes which break down the outer segments of the photoreceptors once they are no longer required (Smith, Kincaid et al. 1999; Mannermaa, Vellonen et al. 2006; Wilson, Semenera et al. 2007).

In order to maintain its key functions, the retina requires a strong blood supply. Blood supply to the retina is provided by the retinal vessels and they supply a rich source of blood into the inner retina, in addition to this, the choroidal circulation provides the outer retina with its vascular source (Smith, Kincaid et al. 1999; Kaufman and Alm 2002).

1.1.4. PERIOcular STRUCTURE

Past the retina and into the central eye are the periorcular structures, consisting of the aqueous humor (towards the front) and the vitreous humor (towards the back), with the lens positioned in-between the two fluids. The two humor based tissues have differing compositions and structure, with the aqueous humor forming a clear, liquid structure, whilst the vitreous forms a gel-like material.

1.1.4.1. LENS

The ocular lens is an oval shaped, transparent structure positioned immediately behind the anterior section of the eye (Figure 1-5). It has an important role in the generation of vision, as it is responsible for focussing light onto the retina, before it is detected and transmitted. The shape of the lens is interesting, in that it has been shown in vitro to increase in size over the course of life. At adulthood the diameter of the lens is about 9 mm and only increases slightly however the volume of the lens is more variable and averages at around 250 μ l (Rosen, Denham et al. 2006). The lens volume is surrounded by an elastic capsule, which is connected to muscles in the ciliary body. The muscles control the lens shape and can adjust the lens positioning to ensure accurate focus.

The lens is composed of cuboidal epithelial cells and elongated fibres cells and both types of cells have different functions. The cuboidal cells play a role in the metabolic function of the lens, whereas the elongated cells enable light to pass through without diffraction and focus onto the retina. Protein content in the lens is very high and the lens is capable of synthesizing its own unique proteins, known as the crystallins (Rafferty 1985). A number of different types of proteins compose the crystallins, with the α crystalline form predominating at approximately 40 – 50% of the total protein content of the lens (Augusteyn and Stevens 1998). Along with the elongated fibres cells, the crystallins are also involved in focusing light onto the retina and ensure light refraction.

An important point to note about the lens is that, unlike the retina, it is a completely avascular structure and therefore it does not obtain nutrients directly from the ciliary artery blood supply going into the eye. Although there is no direct blood supply, it is thought that there is movement of compounds in and out of the lens via

the fluid circulation operating systems that are contained within the lens and this is perhaps controlled by variations in ion concentrations (Beebe 2003).

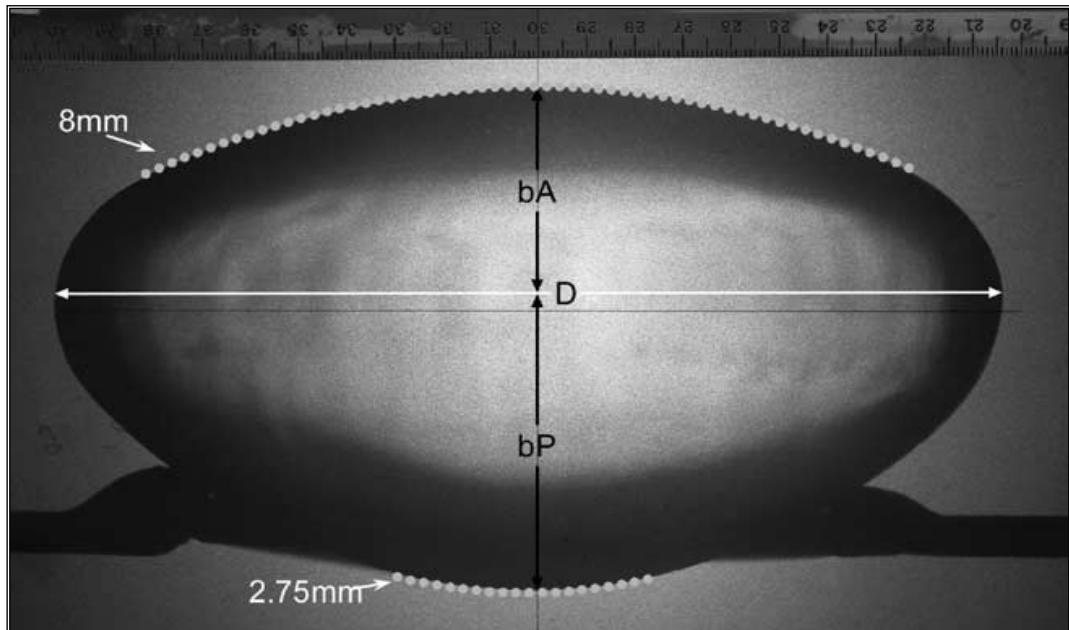


Figure 1-5 Curved structure of the lens, diameter represented by D (Rosen, Denham et al. 2006).

1.1.4.2. VITREOUS

The lens is cushioned by the vitreous and, apart from the section in contact with the lens, is spherical in shape. It is the largest structure in the eye occupying approximately 80% of the eye's total volume and has a volume of approximately 4 ml in the human eye (Wilson, Semenera et al. 2007). The vitreous humor is composed of approximately 99% water but owes its viscoelastic properties to other components contained in the vitreous; including collagen, hyaluronic acid and proteoglycans (Balazs and Denlinger 1984). Various types of collagen are present, with type II collagen dominating. The collagen fibres within the vitreous are arranged in a linear fashion with hyaluronic acid molecules dispersed in spaces between the fibres, trapping the water molecules (Sebag and Balazs 1989). The structure of the vitreous varies between species and in humans it consists of a gel fraction and a liquid

fraction. The gel fraction is in direct contact with structure surrounding the vitreous (including the retina) and the density of the collagen component of the vitreous controls the rigidity of the gel. The liquid fraction is contained within the central part of the vitreous and is less viscous than the gel fraction, with viscosity (originally thought to be controlled by collagen concentration) controlled by hyaluronic concentration (Balazs and Denlinger 1984; Chirlia, Hong et al. 1998). The fluidity of the vitreous increases with age and this is due to a process known as liquefaction, where the structure of the vitreous begins to dissolve and collapse (Lund-Andersen and Sander 2003).

The vitreous humor is responsible for the support and protection of the retina and the lens. It also acts as a diffusional barrier of molecules between the anterior and the posterior eye and ensures light can pass through the posterior eye unrestricted. It has also been described as a 'sink' for some proteins and solutes which are unable to cross over the blood-retinal-barrier (Bito 1977). Flow within the vitreous is mainly by diffusion and this pathway predominates in the movement of low molecular weight molecules, especially ions such as sodium (Maurice 1957; Moseley, Foulds et al. 1984). High molecular weight molecules, on the other hand, tend to move from the anterior vitreous to posterior vitreous eye by bulk flow. Bulk flow in the vitreous however is limited and is thought to account for approximately 30% of movement within the human eye (Lund-Andersen and Sander 2003; Wilson, Semenera et al. 2007).

1.1.4.3. AQUEOUS HUMOR

The aqueous humor is responsible for the maintenance of intro-ocular pressure and provides nutrition to other structures contained within the eye. It is produced via the process of ultrafiltration, controlled by the ciliary processes. Ultrafiltration involves the selective bulk flow of components out of the blood plasma into the ciliary epithelium. This process is aided by a gradient which exists in fluid pressure and the cells then secrete the filtrate as the aqueous humor (Bill 1977). Unsurprisingly the aqueous humor has a similar composition to plasma; however, the concentrations of the individual components contained within differ. Typically differences that exist are; the aqueous humor has much lower protein

content and the aqueous contains approximately 2/3 of the glucose content of plasma. However, the aqueous humor has higher levels of lactate and ascorbate when compared to plasma (Smith, Kincaid et al. 1999).

The aqueous humor has a total volume of approximately 210 μ l and it is produced by the ciliary body at a rate of approximately 2.5 μ l/minute (Jones and Maurice 1966; Wilson, Semenera et al. 2007). It forms a reservoir in the ciliary stroma and is secreted by active secretion across the cell membrane into the posterior chamber, where it moves between the iris and lens via the pupil into the anterior chamber (Kaufman and Alm 2002). The rate of aqueous humor production is heavily influenced by the IOP, with significant increases in IOP inhibiting its production (Green 1984). The aqueous humor exits the anterior chamber via the trabecular meshwork and this involves two mechanisms: the corneoscleral meshwork and the uvealsclera meshwork. The majority of the humor is drained by the corneoscleral meshwork to the canal of schlemm, where it then returns to vascular circulation. However, approximately 35% is removed by the uveolscleral route and passes from the anterior chamber between spaces between muscle bundles, bypassing the canal of Schlemm (Bill 1977; Smith, Kincaid et al. 1999).

1.1.5. BLOOD SUPPLY

As discussed previously, certain structure in the eye require a high level of perfusion to maintain their function, whereas other structure can function without a direct supply of blood into the tissue. Blood enters the eye via the ophthalmic artery, which branches from the large internal carotid vessel. On entry into the eye, the ophthalmic artery branches into the central retinal artery, the posterior ciliary artery and various other ciliary arteries (Figure 1-6). The central retinal artery divides into four major vessels and these vessels supply each quadrant of the inner retina, the optic nerve and the choroid. The posterior ciliary artery on the other hand, branches into two subtypes, the short and the long ciliary arteries. The short ciliary arteries supply the posterior choroid and anterior optic nerve, whereas the long ciliary arteries supply the iris, ciliary body and anterior choroid. Blood supplied to the choroid then goes on to supply the outer retina. Finally, the anterior part of the uvea obtains its blood supply from the anterior ciliary artery. Drainage of blood depends

on tissue positioning within the globe, blood is removed from the retina and optic nerve mainly by the central retinal vein, whereas blood is drained from the uvea and choroid via the vortex veins, which empty into the superior and inferior ophthalmic veins (Smith, Kincaid et al. 1999; Cioffi, Granstam et al. 2003).

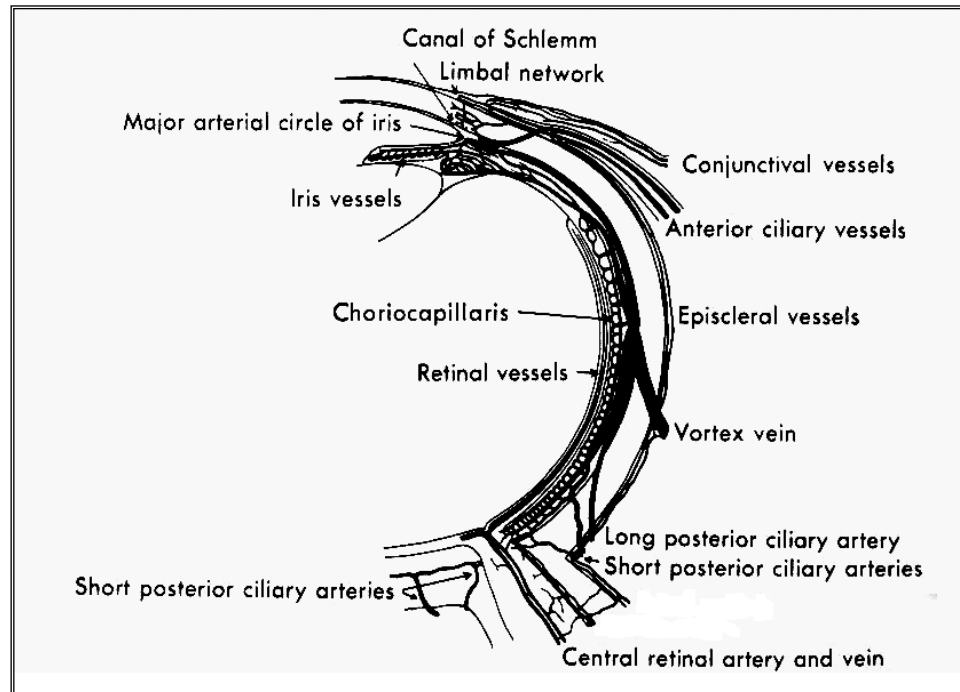


Figure 1-6 Perfusion network of the eye (Cioffi, Granstam et al. 2003).

1.2. POSTERIOR EYE DISEASE AND TREATMENT

As a result of the complex and intricate design of the eye, it can be affected by a multitude of different diseases. Anterior eye disease has been at the forefront of ophthalmic research, with the understanding of conditions such as conjunctivitis, dry eye and cataract improving greatly over recent years. This has led to the establishment of effective treatment, such as topical antibacterial agents and ocular lubricants, entering the worldwide market. Alongside this, the understanding of posterior eye disease has also greatly expanded and the design of effective treatment options available is now beginning to accelerate. However for some posterior conditions treatment options are still minimal due to the problem that the posterior section is particularly difficult to treat. Problems such as access difficulties and the inability to maintain effective therapeutic concentrations, for a suitable time period,

create a significant challenge when designing effective treatment options. This said it is not a lost cause, with conditions such as increased intraocular pressure associated with glaucoma and cytomegalovirus retinitis having relatively established drug therapy. Problems lie within the treatment of age-related macular degeneration and diabetic retinopathy and this research will focus on these areas.

1.2.1. GLAUCOMA

Glaucoma is the second leading cause of blindness and affects greater than 2% of the population of the USA (Reddy and Bodor 1994; Weinreb and Khaw 2004). Glaucoma refers to a group of optic diseases can be divided into open angle and closed angle glaucoma. Closed angle glaucoma is often a medical emergency, whereas open angle glaucoma is more common and is progressive in nature, with the onset often in later life (Reddy and Bodor 1994). Glaucoma is characterised by an increase in intra-ocular pressure (IOP) normally above a value of 22 mmHg and this ultimately leads to retinal ganglion cell death and irreversible blindness (Reddy and Bodor 1994; Weinreb and Khaw 2004).

Since the prevalence of glaucoma is so high, it is fortunate there are many pharmacological agents approved to reduce IOP in glaucoma sufferers. Treatment can involve the use of beta-adrenoreceptor antagonists, alpha-adrenoreceptor agonists, prostaglandin analogues and topical carbonic anhydrase inhibitors, enabling an alternative method to be used when initial treatment is unsuccessful (Reddy and Bodor 1994; Slamovits and Dutton 2002).

1.2.2. RETINITIS PIGMENTOSA

Retinitis Pigmentosa (RP) affects 1 in 4000 people and is typified as a hereditary disease (Hartong, Berson et al. 2006). The majority of cases are inherited and examples of causes include X chromosome linkage and dominant mechanism, where one of the parents only is affected. It also can occur in patients when no other family member is affected and this accounts for approximately 40% of reported cases (Baumgartner 2000). The disease is characterised by degeneration of the rod and cone photoreceptor cells of the eye and symptoms tend to vary between patients. Often the disease initially manifests as impaired adaptation to light and dark, coupled

with night blindness. As the disease progresses, tunnel vision can begin to develop and in the final stages central vision is lost (Baumgartner 2000; Hartong, Berson et al. 2006).

Unfortunately, treatment options in RP are currently limited. However, there is some element of hope, with dietary modification and reduction in light exposure thought to delay disease progression. Dietary modification often includes the addition of nutritional supplements including vitamin A, vitamin E and omega-3 fatty acids. Research into treatment for RP in the future includes gene therapy and retinal tissue transplant (Hartong, Berson et al. 2006) however, treatment can be complex and it is often necessary to explore various routes of drug administration.

1.2.3. CYTOMEGALOVIRUS RETINITIS

Cytomegalovirus (CMV) is a member of the viral family herpesviridae and can cause major problems in immunocompromised patients, especially patients suffering from Acquired Immunodeficiency Syndrome (AIDS) (Nichols and Boeckh 2000). CMV can infect anyone with no notable effects however, CMV in AIDS patients can often result in the development of CMV retinitis. CMV retinitis posed a greater a problem before the discovery and initiation of highly active antiretroviral therapy (HAART), with up to 85% of AIDS patients developing retinitis. Even following the initiation of HAART, this disease still affects 20-30% of AIDS patients (Pollard 1996; Nichols and Boeckh 2000). The development of retinitis occurs with the reduction in CD4 cell count and, if left untreated, can result in irreversible blindness (Jouan and Katlama 1999).

Treatment of CMV retinitis involves high dose antiretroviral drugs to treat the initial infection and reduce the viral load. This is followed by a maintenance dose to prevent the viral load increasing again. The antiretroviral drugs ganciclovir, foscarnet and cidofovir are commonly used and can be administered by a variety of routes including the oral, the intravenous and the intraocular route. Ganciclovir has also been developed in an intraocular implant which releases the drug in a controlled manner over a period of several months (Jouan and Katlama 1999). Antiretroviral therapy in this case is useful; however, it is associated with the development of drug resistance. This problem is worsened when these drugs are inappropriately

administered - for example when used for long courses, intermittent therapy and sub-therapeutic dose regimens (Nichols and Boeckh 2000).

1.2.4. AGE-RELATED MACULAR DEGENERATION

1.2.4.1. PATHOPHYSIOLOGY OF DISEASE

Age Related Macular Degeneration (AMD) is an extremely serious disease affecting the posterior eye and, according to a report issued by the World Health Organisation in 2002, has become one of the most common causes of irreversible blindness in the developed world. AMD is a very complex disease and this makes it particularly difficult to treat. Various risk factors are thought to be involved in the development of AMD, amongst them include smoking, diet, genetics and age. The disease is progressive, involving multiple structures in the eye. The photoreceptors of the RPE, the Bruch's membrane and the choriocapillaries are all affected with progressive visual loss occurring in the later stages due to degeneration of the photoreceptors and thinning of the retina (Ding, Patel et al. 2008).

Two forms of the disease exist, known as non-exudative and exudative, however these forms are more commonly referred to as dry and wet, respectively. The dry form of the disease is more common and characterised by the development of drusen and pigment epithelial atrophy (Figure 1-7). Yellow deposits appear on the retina and the pigmented epithelium begins to degenerate, resulting in subsequent photoreceptor loss and visual impairment. The wet form on the other hand is less common, yet visual impairment tends to be more severe and blindness is more likely to occur (Figure 1-7). In this instance, choroidal neovascularisation occurs and is characterized by the abnormal growth of blood vessels underneath the retina and these vessels can leak and scar. They also overlay the retina, reducing vision (Stokkermans 2000; Gohel, Mandava et al. 2008).

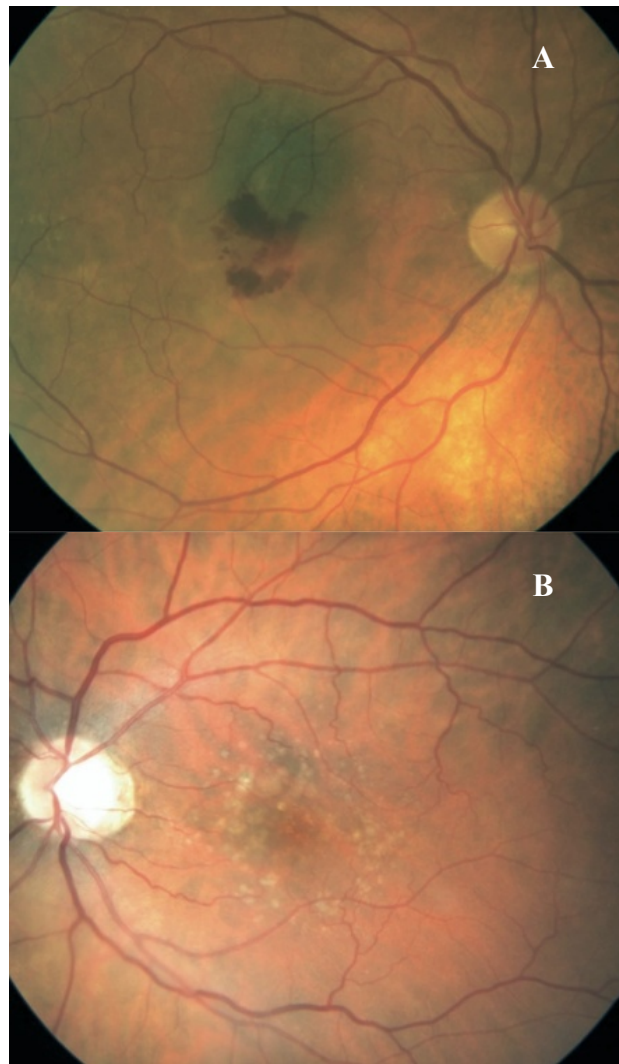


Figure 1-7 Wet Macular Degeneration with neovascularization is illustrated by A, whilst B shows the dry form with drusen and pigment epithelial atrophy (Gohel, Mandava et al. 2008).

1.2.4.2. CURRENT TREATMENT

In the past, treatment options for AMD have been extremely limited and prevention of disease progression has been the main concern. In the case of dry AMD, prevention of disease progression still predominates typical treatment regimens and nutritional supplementation is seen as very important. In the case of most patients supplementation of their diet with vitamin C, vitamin E, zinc oxide and beta-carotene is advisable. Following progressive worsening of the disease and progression into the wet form of the disease, traditional treatment involves laser photo-coagulation, submacular surgery, radiation therapy or the use of an

angiogenesis inhibitor, such as a steroid (Stokkermans 2000). In recent times, a newer class of pharmacological agents has become available for the treatment of AMD, and these drugs exert their action through the inhibition of the effects of vascular endothelial growth factor (VEGF). The binding of VEGF results in inhibition of neovascularisation and for this reason this class of drugs are predominantly used in treating the wet form of the disease. Anti-VEGF agents are normally administered via intravitreal injection and pegaptanib (MACUGEN®) was the first anti-VEGF agent to be successfully used in AMD. Following the success of MACUGEN, the anticancer agent bevacizumab (AVASTIN®) was next utilised and patients showed improvement in their visual acuity following treatment. This led to the development of ranibizumab (LUCENTIS®), an FDA approved treatment effective in maintaining and improving vision in AMD (Chen, Wong et al. 2007; Optometry 2009). The long term safety of these medicines is yet to be established, but an increased cardiovascular risk is thought to be associated (Wong, Liew et al. 2007).

1.2.5. DIABETIC RETINOPATHY

1.2.5.1. THE DISEASE

Diabetic Retinopathy (DR) is another leading cause of blindness and can affect patients suffering from both type I and type II diabetes. In fact, it is estimated that approximately 39% of patients diagnosed with type II diabetes have some form of retinopathy at the time of initial diagnosis (SIGN 2001; Barber 2003). The disease is progressive and is characterised by capillary closure, increased permeability of vessel walls and breakdown of the blood-retinal-barrier. Two forms of the disease exist: non-proliferative and proliferative. In non-proliferative diabetic retinopathy (NPDR), initially capillary microhaemorrhages occur, appearing as small dots on the retina, before progression into larger haemorrhages. Proliferative diabetic retinopathy (PDR) again results in haemorrhage but differs in that new vessels begin to grow in the posterior eye and often massive vitreal haemorrhages occur during the night (Porta and Allione 2004).

1.2.5.2. CURRENT MANAGEMENT

Due to the complex nature of DR it is often difficult to treat and therefore the primary aim is disease prevention and progression. In order to prevent DR, it is essential that the blood glucose levels are tightly controlled and it is recommended that all diabetic patients undergo periodic screening for retinopathy (SIGN 2001). Controlling blood pressure can also prevent disease progression and will often include treatment with anti-diabetic agents and cardiovascular medication. When prevention is unsuccessful and the disease progresses, treatment specifically for DR is required to be initiated. When the disease is advanced and sight is threatened, treatment with laser photocoagulation is indicated. Laser photocoagulation aims to prevent leakage, improve retinal metabolism and oxygenation and additional treatment with steroids may help by reducing inflammation (Gardner, Antonette et al. 2002). If vitreal haemorrhage is persistent, treatment will often need to advance to vitrectomy (removal of the vitreous) and vitreal replacement. The availability of suitable pharmacological agents to treat DR is limited, with focus aimed on prevention rather than cure. More recently anti-VEGF agents, indicated in AMD, have been utilised and have demonstrated an ability to cause regression in neovascularisation (Mason, Nixon et al. 2006).

1.3. PHARMACOKINETICS

In order to improve treatment in AMD and DR, it is important to understand the pharmacokinetics of drug movement within the eye. An understanding of pharmacokinetics can help determine the feasibility of drug treatment and maintaining safe and effective concentrations in the eye for a significant time period.

1.3.1. BASIC PRINCIPLES

The importance of pharmacokinetics in medical research is highlighted by the dependence on pharmacokinetic (PK) data; not only in clinical practice but in the drug discovery and development process (Welling 1997). PK data can provide vital information concerning drug movement within the body and also information about the drug concentrations required to elicit a therapeutic response. It also aids in determining a drugs assigned therapeutic index, by providing insight into drug

concentrations that can lead to toxicity. PK studies are also desirable at the very early stages of pharmaceutical drug development, as studies can determine whether a new drug candidate will obtain a suitable concentration at the desired site of action in order to cause the desired response.

Pharmacokinetics has been described as ‘the process determining drug concentrations and metabolism in the body’ and encompasses the principles of absorption, distribution, metabolism and excretion (Hladky 1990). Drug absorption can be described as the process of drug movement from the site of administration to the site of measurement within the body, with the complexity of absorption dependent on the route of administration. Following absorption, distribution describes the reversible transfer of drug into various tissues and organs. Distribution is influenced by various parameters including the ability of the drug to diffuse through biological membranes, the rate of blood supply and the extent of protein binding which either can enhance or hinder the distribution process. The final steps in the PK process involve drug metabolism and irreversible elimination from the body (Rowland and Tozer 1980; Schoenwald 2002).

Typically changes in drug concentration follow either linear or non-linear pharmacokinetics. In the majority of cases, changes in drug concentration can be described by linear pharmacokinetics where the rate of change in drug level (dC/dt) is directly proportional to the concentration of drug in the body (C) and dependent on the elimination rate (k_{el}) $dC/dt = -k_{el}C$ [Equation 1]. In more complex cases changes in drug concentration are not always linear, often commencing with linear changes then progressing to non-linear changes. In this case, non-linear pharmacokinetics applies and is often as a result of saturation of carrier-mediated systems involved in the drugs pharmacokinetics. The elimination rate is dose dependent and is described by the Michaelis Menten equation, in which V_m represents the maximum elimination occurring and K_m is the Michaelis Menten constant (Schoenwald 2002).

$$\frac{dC}{dt} = -k_{el}C \quad \text{[Equation 1]}$$

$$\frac{dC}{dt} = \frac{V_m C}{K_m + C} \quad \text{[Equation 2]}$$

Pharmacokinetics of drug movement in the body can be complex and can involve multiple calculation steps. For this reason, various PK models have been developed in an attempt to describe the processes involved in drug movement. Models developed to describe pharmacokinetic movements in the body are based on either a non-compartmental or compartmental system.

1.3.2. PHARMACOKINETIC MODELLING SYSTEMS

1.3.2.1. NON COMPARTMENTAL MODEL`

The simplest and most general PK model is described by the non-compartmental model. In the non-compartmental model the movement of the drug within the investigated structure is not considered. The main interest is the therapeutic response to the pharmaceutical agent or the drug concentration obtained in the whole structure, and not the relationship between therapeutic response and movement of drug within the structure. In this type of model it is assumed that the drug is distributed in a random fashion, normally by diffusion and connective flow (Schoenwald 2002). This limits the use of this type of model to simple dose response relationships; for example measuring a physiological change such as blood pressure in response to drug plasma concentration. Non-compartmental models, sometimes referred to as regression analysis, are based on statistical moments and involve area under the curve (AUC) measurements. Data obtained experimentally is plotted as log concentration versus time and AUC is calculated using the trapezoidal rule, to determine the definite integral. Initially the AUC is calculated for the available data based on the concentrations (C) obtained at various time points (t), using Equation 3. The data is then extrapolated to infinity using Equation 4, where C_x represents the concentration measured at the final time point and λ is the terminal elimination slope, and both AUC measurements are then added to give the total AUC (Ritschel and Kearns 2004). AUC measurements can then be used to describe various parameters including drug clearance of an injected dose (Equation 5) (Gabrielsson and Weiner 1998).

$$AUC_0^{tx} = \sum \left(\frac{C_n + C_{n+1}}{2} \right) (t_{n+1} - t_n) \quad [\text{Equation 3}]$$

$$AUC_0^{tx} = \frac{C_x}{\lambda_2} \quad [\text{Equation 4}]$$

$$Cl = \frac{D_{IV}}{AUC_0^\infty} \quad [\text{Equation 5}]$$

Non-compartmental modelling reliability is dependent on the in vivo sampling procedure. When only a small number of samples are taken at widespread time points, the use of the trapezoidal rule can lead to vast over and underestimations of the total AUC measure (Figure 1-8). Whereas, when regular samples are taken at short time intervals under and over estimations will be minor and AUC measurements are more useful (Figure 1-9) (Gabrielsson and Weiner 1998).

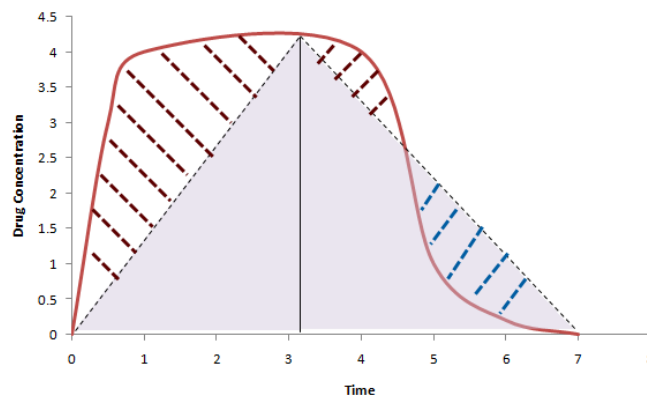


Figure 1-8 Graph representing AUC measurements using trapezoidal rule. In vivo sampling taken at time 0, 3.25 and 7, bulk represents AUC measurement obtained, dashed lines represent periods of under and overestimation.

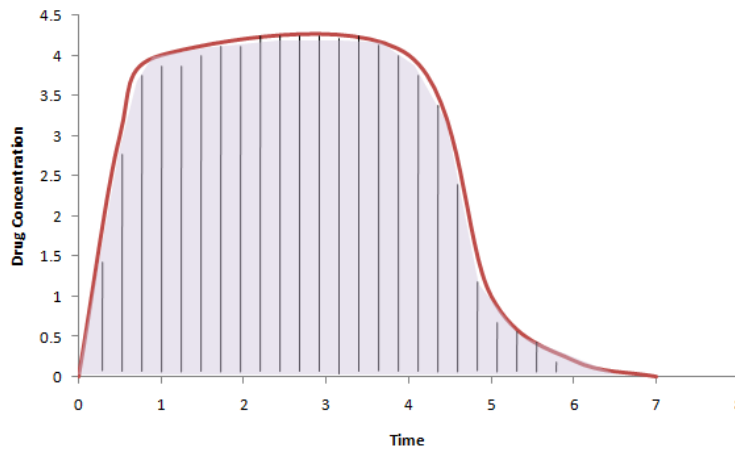


Figure 1-9 Graph representing AUC measurements using trapezoidal rule. In vivo sampling taken frequently, bulk represents AUC measurement obtained, periods of under and overestimation minimal.

1.3.2.2. COMPARTMENTAL MODELS

Compartmental models encompass more complex ideas and can be subdivided into single compartmental models, multi-compartmental models and physiological based models, based on their complexity. Single compartmental models suggest drug is distributed, after absorption, into one single compartment with assigned dimensions (Figure 1-10). The drug is then eliminated from this compartment via a first order process, where the rate of elimination is proportional to the concentration of drug present (Gabrielsson and Weiner 1998). Compartmental models differ from non-compartmental as they take into account the volume of drug distribution within a tissue compartment (V_d). For first order processes, the rate of elimination is described by an elimination rate constant (k) which is established from the slope of the line obtained from a log concentration versus time plot or the drugs half life (Equation 5). The k_{el} can then be used to determine drug concentrations (C) at various time points (t), using the initial drug concentration (C_0) (Equation 6). AUC and clearance can also be calculated (Equation 7, 8 and 9) (Gibaldi 1984; Ritschel and Kearns 2004). This type of model is commonly used when the drug is distributed within the compartment imminently, or at least within a very short time

period and assumes kinetic homogeneity within the tissue. (Rowland and Tozer 1980; Welling 1997)



Figure 1-10 Drug distribution into a single compartment followed by first order elimination, denoted by elimination rate constant k_{el} .

$$t_{\frac{1}{2}} = \frac{0.693}{k} \quad \text{[Equation 5]}$$

$$C = C_0 e^{-kt} \quad \text{[Equation 6]}$$

$$AUC_0^{\infty} = \int_0^{\infty} C_0 e^{-kt} \quad \text{[Equation 7]}$$

$$k = \frac{Cl}{V_d} \quad \text{[Equation 8]}$$

$$Cl = \frac{Dose}{AUC} \quad \text{[Equation 9]}$$

On the other hand, multi-compartmental modelling can be used when the drug distribution within some tissues is not immediate and it takes longer to reach equilibrium between tissues within the whole structure. This type of modelling is more commonly used and encompasses a series of compartments connected via first order rate constants to describe the rate of drug movement through the system. In order to use this type of model effectively, the fluid volumes within each of the compartments must be known and various other parameters that may affect drug concentration within each compartment must be considered. Factors commonly limiting the rate of drug movement within a structure include perfusion of the

structure, diffusion coefficient within the structure and extent of protein binding, especially albumin binding. However, alongside this carrier mediated transport and drug metabolism should also be considered (Welling 1997). The reliability of the model increases when these factors are included in the model, painting a bigger picture of the actual processes occurring.

The simplest of the multi-compartmental model is the two compartment model, which is used to represent blood plasma distribution (compartment 1) and tissue distribution (compartment 2) (Figure 1-11). In this instance elimination is bi-exponential and the concentration at various time points calculated using Equation 10. A, represents the initial concentration and B, represents the concentration at the beginning of the second elimination phase with α , corresponding to the initial elimination rate and β , to the subsequent elimination rate. The elimination rates correspond to the slope of the line of a log concentration versus time plot or can be calculated using Equations 13 and 14 (Gabrielsson and Weiner 1998; Ritschel and Kearns 2004). Models can be expanded to include individual tissue concentrations and involve a series of compartments connected via rate constants (Figure 1-12).

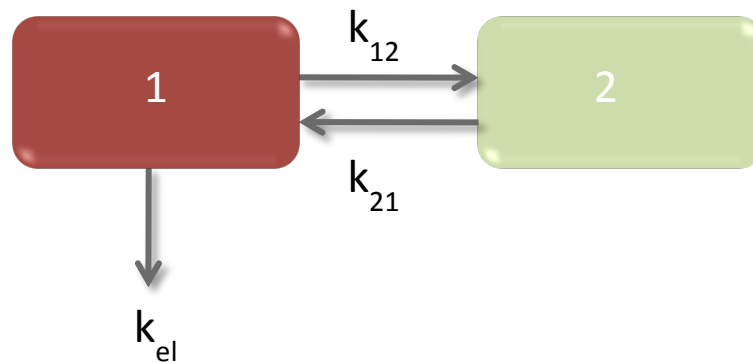


Figure 1-11 Drug distribution in a two compartment model, with elimination occurring from the central compartment.

$$C = Ae^{-\alpha t} + Be^{-\beta t} \quad \text{[Equation 10]}$$

$$A = \frac{D(\alpha - k_{21})}{V(\alpha - \beta)} \quad \text{[Equation 11]}$$

$$B = \frac{D(\beta - k_{21})}{V(\beta - \alpha)} \quad \text{[Equation 12]}$$

$$\alpha = \frac{k_{21}k_{10}}{\beta} \quad \text{[Equation 13]}$$

$$\beta = \frac{1}{2} [(k_{12} + k_{21} + k_{10}) - \sqrt{(k_{12} + k_{21} + k_{10})^2 - 4k_{21}k_{10}}] \quad \text{[Equation 14]}$$

Complexity increases again when using a physiological based model. The physiological based model is essentially an extension of the multi-compartmental model, however compartments are based on the true volume of the region in vivo and can involved sub-compartments with main compartments. This type of model is useful when focus of the study is mainly on drug disposition within each tissue contained with the structure (Schoenwald 2002). Although a model of increased complexity will be more similar to processes occurring in vivo, it is difficult to account for and measure every process occurring. Therefore, certain assumptions often need to be made which can compromise the integrity of the model. A particular assumption that has to be made is that within a compartment the drug concentration is homogenous, which is often not the case.

The selection of a particular modelling system should be based on the number of tissues analysed, the number of elimination pathways measured, and after plotting the data, the rate at which the drug is eliminated (Gabrielsson and Weiner 1998). However, once the model has been created it should be quite clear whether the selection was appropriate or not.

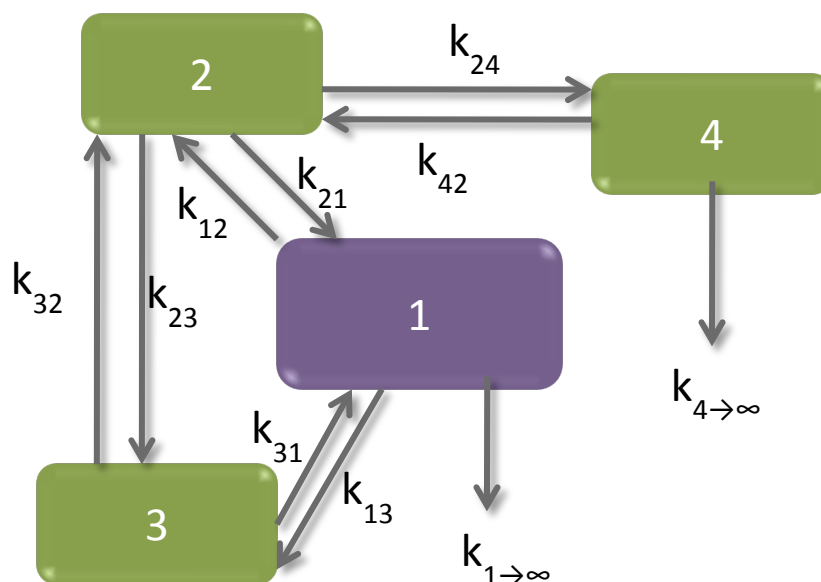


Figure 1-12: Drug distribution within multiple compartments by first order processes denoted by k .

1.3.2.3. OCULAR PHARMACOKINETIC MODELLING

PK modelling of drug movement within the eye is by no means easy and many modelling systems have been employed from non-compartmental to compartmental to more complex mathematic models, such as finite element modelling. The difficulty with describing pharmacokinetics mainly arises from the fact that it is not just a matter of taking a simple blood sample from the specimen at various time points and using this data to obtain a concentration versus time profile. In the fluid based ocular structure, namely the aqueous and vitreous humor, it is possible to sample a very small volume of fluid without the need for total eye enucleation. However this technique cannot be applied to the remaining tissues present in the eye. Therefore, in order to obtain information regarding the movement of substances within the eye, many animals are required to cover a significant time range and each tissue has to be subjected to analysis.

Non-compartmental modelling has been commonly used when single tissues of the ocular system have been investigated. The technique has been used Fu et al (2008) in order to describe the clearance of *S(-)* satropane, administered in-situ gel formulation, from the aqueous humor. Using the linear trapezoidal method,

extrapolated to ∞ , the AUC was calculated and the half life of the drug calculated using the terminal rate constant obtained by a concentration versus time profile. Non-compartmental modelling has also been used to describe movement in more than one ocular tissue. Anand et al (2004) selected this technique to describe the movement of fluorescein in the vitreous humor and plasma following systemic and intravitreal administration. Similarly Claro et al (2009) adopted the same technique to understand clearance patterns of focarnet from the vitreous and retina. From these studies it appears that non-compartmental modelling is useful when determining the rate of drug clearance from a particular ocular tissue. However, this type of system has limited ability to correlate clearance and movement from one ocular tissue into another, which is a common desired outcome in a PK study of the eye.

The compartmental modelling approach has frequently been favoured as a means of describing drug PK in ocular tissues. As discussed previously, the eye is a very intricate organ, comprising various structures. These structure, for the main part, are non-continuous with one and other, making them relatively simple to separate into individual ocular structure; to the point where fluorescent markers can be seen moving from one ocular structure to another in the living eye (Maurice and Mishima 1984). The appearance of various compartments in the eye makes compartmental modelling a desirable approach. Although compartmental modelling introduces assumptions into the model, it can provide a more accurate description of the complex movement of drug substances within the various ocular tissues of the eye. A simple one-compartmental modelling approach has been useful in describing antimicrobial penetration into the aqueous humor of the eye following topical administration (Fukuda and Sasaki 2002), but when describing movement within the structure of the eye, a multi-compartmental approach seems more suitable. The simplest form of the multi-compartmental model in ocular tissues, is the two-compartmental model used to describe drug movement in the aqueous and vitreous humors. In previous models by Beer et al (2003) and Kim et al (2006), following intravitreal injection, the vitreous is seen as the central compartment from which drug distributes and is eliminated (Figure 1-13). This model is useful in understanding movement from vitreous to aqueous; however, due to its simplicity it

lacks important information, including elimination from vitreous via the retinal route, reverse movement of drug from aqueous to vitreous and any drug loss from retraction through injection site. In addition, this type of model also assumes the tissue is a well stirred compartment. In other cases the multi-compartmental model has been used to describe drug pharmacokinetics in other compartments such as systemic circulation, iris, retina and sclera (Hu, Le et al. 2007; Tzepe, Vergados et al. 2009). In these cases the complex process occurring are clearer, however the models could still be expanded further in an attempt to further increase clarity.

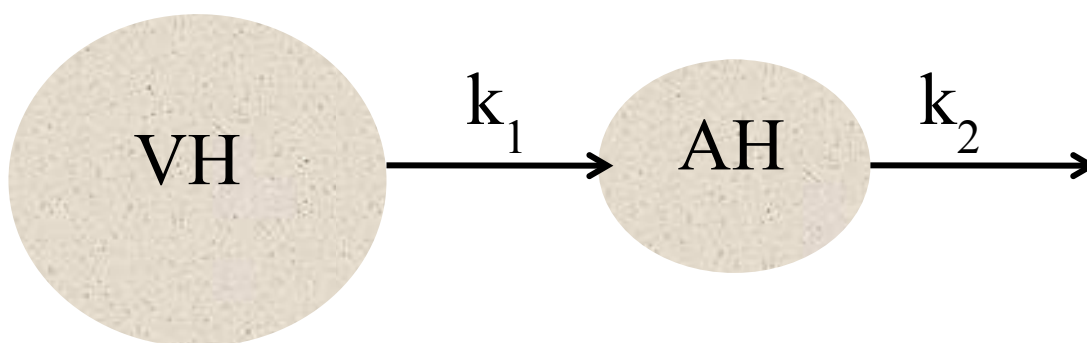


Figure 1-13 A two-compartmental model of drug movement from vitreous (VH) to aqueous (AH). Rate constant for movement from VH to AH denoted by k_1 and elimination from AH denoted by k_2 (Kim, Csaky et al. 2006).

The physiological based model has also been utilised in ocular PK studies. Physiological based models are mathematically more complex but can factor in additional information relevant to drug PK. Using a physiological approach topical drug PK models have been developed to factor in aspects such as permeation of beta blockers through the cornea and clearance in tear fluid (Ranta and Urtti 2006). Other models have also considered flow via diffusion through structure (Francoeur, Sitek et al. 1985) In an attempt to describe the physiological base model, finite element modelling has been utilised due to its application in solving integral PK equations. Finite element modelling is based on compartmental dimensions and has proved useful in modelling diffusion and connective flow through the compartments of the eye (Friedrich, Cheng et al. 1997b; Balachandran and Barocas 2008).

From the various PK modelling systems that have been used to describe and predict drug PK within ocular tissues, it is difficult to decide which systems is most suitable for routine use. An ideal PK model, whilst being able to predict data, should first conform and fit the original experimental data. It should also aid understanding of the organ under study and the processes occurring in vivo (Bonate 2005). All of the systems used previously have the potential to do just this; therefore, when selecting an ocular PK model it appears the best place to start is finding a model which best fits the original data and expanding the model from there.

1.3.3. DRUG DISPOSITION IN EYE

Once a suitable modelling system has been established, it can be used to gain understanding of drug positioning and concentration with respect to time. This is beneficial in ocular research and is a key point within ocular PK studies, due to the difficulty in maintaining suitable drug concentrations in the posterior eye.

Drug disposition describes the processes occurring after the drug is absorbed, namely distribution, metabolism and excretion. Interest in drug disposition in posterior eye disease has increased, especially when treating certain disease states, such as DR and AMD, where effective treatment is currently limited. Understanding the factors which influence drug disposition can potentially improve treatment options in these conditions by enabling improved drug targeting to the desired site of action and prediction of toxicity problems. Intravitreal drug administration currently appears to be the best option in achieving therapeutic drug concentrations in the posterior segment. However once the drug has been administered, problems still arise in maintaining effective drug concentrations at the retina. In order to understand how drugs move following intravitreal administration, it is important to understand the flow processes and clearance patterns, which ultimately govern movement.

1.3.4. FLOW WITHIN THE VITREOUS

In earlier ophthalmic research, flow within the vitreous humor was thought to be determined by diffusion alone (Maurice 1957; Moseley, Foulds et al. 1984). Diffusion can be defined as a 'random molecular motion that leads to complete

mixing' and can be characterised using Fick's law of diffusion (Equation 15) (Cussler 2009). Diffusional flux (J) is dependent upon the diffusion coefficient of the drug molecule (D), concentration (c) and path distance (z). Diffusion occurs when a sample contains differences in concentrations of drug, causing the drug to move from an area of high concentration to low concentration.

$$-J = D \frac{dc}{dz} \quad \text{[Equation 15]}$$

As research progressed and moved on, researchers began to consider the role of convection in the movement of drugs within the vitreous. Convection describes movement in a fluid initiated through an applied force, for example due to pressure gradients or temperature differences. In the vitreous humor convection is thought to arise through a pressure drop between the anterior and posterior eye from a steady permeating flow and by active transport in the retina (Tsuboi and Pederson 1988). Early work considering the impact of both diffusion and convection on flow within the vitreous considered both experimental data and mathematical modelling (Fatt 1975; Fatt 1977; Maurice 1987; Xu, Heys et al. 2000). Work carried out by Fatt (1975) used experimental data obtained from a Na^+ tracer to create a mathematical model tracer movement within the vitreous. Using this model, he was able to demonstrate that both diffusion and convection played a role in the movement of the marker. Although the presence of convection was noted, convective processes appeared to have less of an impact in determining tracer distribution, with diffusion having an 8 fold greater control over tracer movement. Progressing on from this work, a diffusion cell was used to demonstrate hydraulic flow conductivity and lead to the observation that hydraulic conductivity was greater in the bovine vitreous, when compared to the rabbit vitreous (Fatt 1977). More recently, the diffusion cell has again been used to consider the movement of a drug marker, acid orange 8. Using the diffusion cell the diffusion coefficient of acid orange 8 in bovine vitreous and water were shown to differ (3.4×10^{-6} and $6.5 \times 10^{-6} \text{ cm}^2/\text{s}$ respectively). Using the data obtained, the hydraulic conductivity of bovine vitreous was determined to be $8.4 \pm 4.5 \times 10^{-7} \text{ cm}^2/\text{Pas}$, suggesting the convection would play a role in the movement of acid orange 8 in bovine vitreous (Xu, Heys et al. 2000).

More recently, computational modelling systems have been used to investigate the role of diffusion and convection in intravitreal delivery. Using finite element modelling, Missel created a 3D model of hydraulic flow within the eye (Missel 2002). In order to study the effect of convection on different molecular weight intravitreal drug substitutes, the model included data derived using different molecular weight dextrans. When the model was set up to disregard hydraulic flow, the elimination rate of the high molecular weight dextran (157 kDa) was reduced to below the elimination rate expected for a dextran of this size. No notable effect was seen for the lower molecular weight dextrans, leading the author to the conclusion that convection appeared to be important in drug movement within the eye, but only for larger molecular weight molecules. Leading on from this work, a 3D finite element model of the human eye was created, incorporating hydraulic flow conductivity measurements derived from bovine eye (Stay, Xu et al. 2002). Two model compounds were inserted into the model to represent small and large drug molecules, using diffusion coefficients of 5×10^{-6} and 1×10^{-7} cm^2/s respectively. When studying the movement of the small molecule, diffusion appeared to be the main driving force for movement; whereas, for the larger molecule convective flow appeared to have an influence, agreeing with the work of Missel. Coinciding with this data, 3D finite element model of drug movement within the rabbit eye lead to similar conclusions (Park, Bungay et al. 2005). Using a high diffusivity (1×10^{-5} cm^2/s) to represent compounds with an approximate MW of less than 100 Da, when convective flow was altered by increasing vitreous outflow, little effect on time of accumulation at the retina was seen and concentration at the retina increased by about 10 % only. This suggested that convection would have little influence on the pharmacokinetic movement of the drug. On the other hand, when using a low diffusivity for represent larger macromolecules with a molecular weight of greater than 40 kDa, the rate of diffusion is slow and convection appeared to have a more obvious role, with increased vitreous outflow causing a 4 fold increase in accumulation at the retina after 50 hours.

Data obtained from experimental studies has also been incorporated into modelling systems in order to understand the effect of convection on flow. Experimental MRI has been used in a 3D computational model, in a similar manner

to Missel, to investigate the effect of reducing convective flow within the model to zero, on the pharmacokinetic movement of drug surrogate Gd-DPTA (9388 Daltons) (Kim, Lozak et al. 2005). Using the model, it was found that changes in Gd-DPTA concentrations were insignificant when convective flow was initially present and later removed. This suggested that diffusion is more important in determining the disposition of this particular marker, underscoring previous conclusions, that for low molecular weight compounds convective flow is not important (Fatt 1975; Fatt 1977; Xu, Heys et al. 2000).

Recent progression in the diffusion versus convective flow debate has considered the effect of varying vitreous substitute on drug movement within the vitreous. Again using a 3D computation model of the human eye, silicon oil and water were modelled into the systems as different vitreous substitutes (Kathawate and Acharya 2008). Using 3 different diffusion coefficients within the model to represent different drug sizes (6×10^{-10} m²/s for small, 3.9×10^{-11} for large, 1×10^{-11} for very large, eg antibody), the study showed that when the larger diffusion coefficient is incorporated into the system, convection begins to play a role in movement and for the very large molecule movement is directed towards to retina. Looking at the effect of different vitreous substitutes, when water was selected, peak concentrations for the larger molecules were noted closer to the retina than for silicon oil, suggesting that convective flow played a greater role when water was used as the substitute. Data obtained was used to calculate the Peclet numbers (Pe) (Equation 16) as a function of velocity across the vitreous chamber (v), length of path (d) and diffusivity in the vitreous (D). A Peclet number of greater than one suggests that transport by pressure induced convective flow is important. For the very large molecule, when water was used as the vitreous substitute Pe was calculated to be 12.54, compared to 0.012 which was calculated when silicon oil was used. This supports the argument that convective flow is important in the case of a vitreous composed of water whereas diffusion flow was more important in the case of silicon oil.

$$Pe = \frac{v}{dD} \quad \text{[Equation 16]}$$

From the studies evaluated, it appears that drug movement around the eye is controlled by both diffusion and convective flow. Diffusion will have an important role in drug movement regardless; however, the impact and extent of convective flow will alter in relation to the molecular size of the drug molecule. For small molecular weight drugs, convective flow can be disregarded and movement will be controlled mainly by diffusion. For larger molecular weight compounds, convective flow will have an impact on the distribution of the drug within the eye and must be taken into account.

1.3.5. CLEARANCE FROM THE VITREOUS

Drugs are thought to be eliminated from the vitreous by two main mechanisms: aqueous clearance and retinal clearance (Figure 1-14). Aqueous clearance is thought to involve initial drug diffusion over the hyloid membrane in to the anterior segment, followed by removal by the aqueous drainage system and the uveal blood flow. On the other hand, retinal clearance is thought to remove drugs from the posterior eye via drug diffusion over the retina and across the blood retinal barrier. Due to the difficulty in transversing the blood retinal barrier only small, lipophilic drugs should be removed by retina clearance. This leaves large, hydrophilic molecule to be removed by the aqueous system (Atluri and Mitra 2003; Urtti 2006). Various pharmacokinetic studies have considered mechanisms of drug clearance following administration via intravitreal injection.

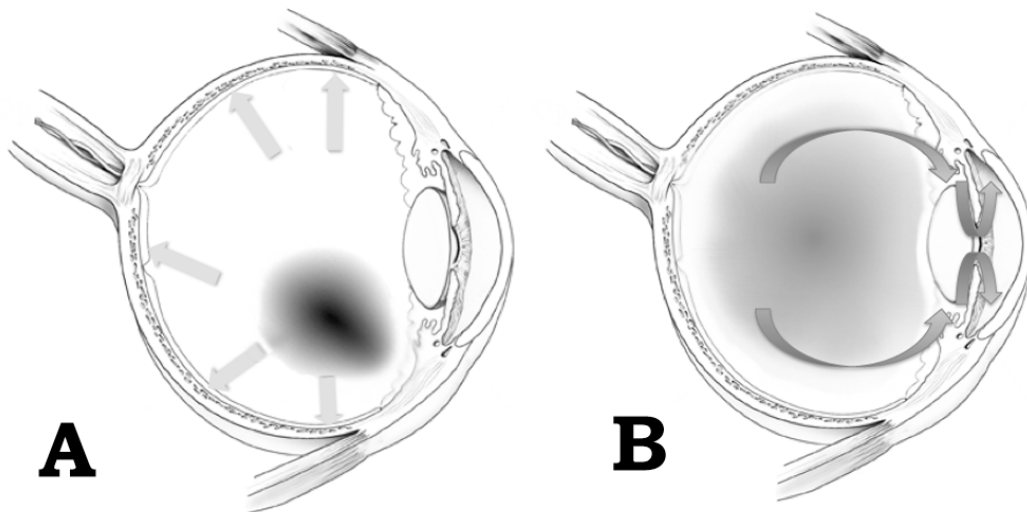


Figure 1-14 Structure A depicts clearance points via the retinal route whilst B depicts aqueous clearance.

1.3.5.1. AQUEOUS CLEARANCE

In agreement with the theory, small hydrophilic molecules fluorescein and fluorescein glucuronide have both been suggested to be subject to elimination through the anterior chamber. These more hydrophilic derivatives of fluorescein, were found to have a steep concentration gradient from the vitreous to the posterior chamber and flux through the retina was small, indicating loss through the aqueous route (Araie and Maurice 1991). In addition, a small study human study, involving samples taken from the aqueous humor, demonstrated that the anterior elimination pathway is important for intravitreal clearance of the steroid, triamcinolone (Beer, Bakri et al. 2003).

Data obtained from pharmacokinetic studies of larger biopharmaceuticals has also demonstrated consistency between theory and experimental data. A relatively small biopharmaceutical, an oligonucleotide with an approximate molecular weight of 7 kDa, also exhibited rapid anterior clearance following intravitreal injection, with less than 7 % remaining after 7 days (Dvorhik and Marquis 2000). A study of a larger sized biopharmaceutical, rituximab, carried out in rabbits, suggested that clearance of rituximab was likely to occur via the aqueous, anterior route. Rituximab was thought to diffuse through the vitreous, between the lens and ciliary body, into the anterior chamber for removal (Kim, Csaky et al. 2006). Similarly, removal via

aqueous humor was thought to represent the predominant clearance pathway of bevacizumab, from intravitreal administration in man (Krohne, Eter et al. 2008).

1.3.5.2. RETINAL CLEARANCE

Following intravitreal drug administration, pharmacokinetic studies have also illustrated retinal drug clearance. An early study by Mosley and Foulds (Moseley, Foulds et al. 1984) characterised the movement of radioisotope Xenon-133. By linking experimental data with samples taken from the vortex vein and along with mathematic modelling, they came to the conclusion that the radioisotope was cleared from the vitreous, to the retina and into the choroid circulation. Atluri and Mitra have demonstrated the theory that lipophilic compounds should exhibit retinal clearance. Using different molecular weight alcohols, they were able to show differences between the alcohols in vitreal half life. Interestingly, heptanol (the most lipophilic alcohol studied) was not found in detectable levels in the anterior chamber, suggestive of retinal elimination. Similarly, the clearance of a less hydrophilic derivative of fluorescein, fluorescein dextran, has been suggested to be retinal.

Retinal clearance has also been shown for small drug molecules used in ophthalmic applications. A pharmacokinetic model of data from an *in vivo* rabbit study, suggested the antiviral used in the treatment of cytomegalovirus retinitis, ganciclovir, is eliminated across the retinal surface (Tojo, Nakagawa et al. 1999). In addition, the elimination of memantine, a drug used in the treatment of glaucoma, has been investigated. Following intravitreal administration of memantine, high concentrations were found in the choroid and RPE, leading the author to consider the likelihood of posterior elimination (Koeberle, Hughes et al. 2003).

Studies considering elimination of drugs from the eye, following intravitreal injection, have demonstrated that certain hydrophilic and large compounds are eliminated anteriorly; whereas, certain lipophilic and small molecules show posterior elimination. This suggests that larger sized molecules could improve drug targeting to the retina and that exploitation of drugs lipophilicity, could also improve drug concentrations at the retina.

1.3.5.3. INFLUENCE OF DEVICE POSITIONING ON CLEARANCE

Aside from the physiochemical properties of the drug, aspects of the drug delivery systems, such as position and volume, could influence drug disposition after intravitreal injection. Using a modelling system of the eye, initial intravitreal injection positioning has been shown to influence distribution of fluorescein and, in particular, permeability at the retina. Different injection sites (including behind the lens, at the hyaloid membrane, central injection and injection next to the retina) were found to change the retinal permeability of fluorescein from 1.94×10^{-5} up to 3.50×10^{-5} cm/s, influencing the distribution of fluorescein in the vitreous (Friedrich, Cheng et al. 1997b). Using a similar modelling system, the highest concentrations of fluorescein and FG were found at the injection site, with peak concentrations in various sections of the vitreous dependent on injection site. In this system volume of the delivery system and its influence on disposition was considered. Two volumes of 100 μ l and 15 μ l were used and it was found that the 15 μ l injection was more rapidly eliminated from the vitreous than the 100 μ l injection, if placed at the compounds site of elimination; whereas, the 100 μ l injection was more rapidly eliminated from the vitreous than the 15 μ l when the compound was placed away from its site of elimination (Friedrich, Cheng et al. 1997a).

Initial positioning of intravitreal injection and volume can influence distribution of drug in the vitreous and should be considered along with the drugs physiochemical properties when studying disposition. Injecting more closely to the retina could increase drug exposure to the retina, improving the treatment of posterior eye disease. The influence of injection volume on drug clearance could also be exploited to increase drug concentration at the target site for the longest possible time period.

1.4. THE ROLE OF TRANSPORTERS IN DRUG DISPOSITION

1.4.1. THE ROLE OF THE BLOOD-RETINAL BARRIER

Passive penetration of substances into the retina is restricted by the blood retinal barrier (BRB). The BRB prevents free movement of substrates from the blood supply into the retinal cells and can be divided into the inner and outer BRB. The inner BRB, positioned at the inner section of the retina, is closest to the vitreous and is formed by capillary endothelial cells, connected via tight junctions. The outer BRB consists of the melanin-rich retinal pigmented epithelium (RPE). Blood is supplied to the initial two thirds of the retina, closest to the vitreous, via the inner BRB and the rest is nourished by the choriocapillaris via the outer BRB (Tomi and Hosoya 2008). Both the inner and outer BRB play a role in drug movement into the retina.

The outer BRB plays a key role in drug penetration from the systemic circulation into the retinal cells. The RPE positioning within the retina is in contact with the Bruch's membrane, separating it from the choriocapillaris. The RPE creates a barrier between the systemic circulation and the retina preventing the free movement of molecules from the systemic circulation to the retina via tight junctions between cells (Leblanc, Jezequel et al. 1998). The active transport systems operating within the RPE enable transfer of materials from the vascular supply, alongside several ion transport systems which transfer ions from the retina to the choroid (Smith, Kincaid et al. 1999; Wilson, Semenera et al. 2007).

The inner BRB is of interest in intraocular drug delivery and in particular intravitreal delivery. Capillary endothelial cells surrounding the vessel lie within a network of neurons, astrocytes and Müller cells and control movement between the retina and blood supply (Gardner, Antonetti et al. 2000). This movement is controlled mainly via influx and efflux transporters. Various influx transporters operate and ensure the retina receives a rich energy supply of glucose, lactate and creatine, alongside antioxidants; including vitamin C and cysteine and amino acids; leucine and taurine. Influx and efflux transporters are also responsible for controlling the transport of organic anions in and out of the retina (Hosoya and Tachikawa 2009). The apparent magnitude of the role transporters play in ensuring

the retina receives its physiological requirements has fuelled interest in the role transporters play in drug delivery to the retina, following intravitreal administration. Understanding the involvement of transporters in maintaining drug concentrations at the retina could improve drug targeting and therapeutic options in treatment of posterior eye disease.

1.4.2. ROLE OF TRANSPORTERS IN DRUG ADMINISTRATION

Various studies considering the involvement of transporters within the inner BRB have been reviewed extensively by Mannermaa et al (Mannermaa, Vellonen et al. 2006). Recently, more studies focussing on the role transporters play with respect to retinal drug delivery have been carried out. Interest has also extended to the role of transporters in movement from vitreous to retina.

1.4.2.1. AMINO ACID TRANSPORT

Although not specifically drug transport, the mechanisms of amino acid transport from vitreous to retina could have potential application in drug delivery. Ocular amino acid transport research has included various transporter studies, with research initially focussing on ocular amino acid transporters in ocular cell cultures (Hosoya, Kondo et al. 2001). In addition, consideration has also been given to understanding the mechanisms involved in amino acid movement from vitreous to retina. Using microdialysis, the role of large neutral amino acid transporter (LAT) on retinal uptake of L-phenylalanine (L-Phe) has been investigated. L-Phe was administered to rabbit eyes via intravitreal injection in isolation and also in the presence of known LAT inhibitors. Retinal uptake of L-Phe was shown to be inhibited following administration of the known inhibitors, demonstrating the role of LAT in amino acid movement from vitreous to retina (Atluri, Talluri et al. 2008). Additionally, the involvement of amino acid transporter system A has been demonstrated in vitreous to retina movement of proline in rat studies. The rate of vitreous elimination of proline was shown to differ from bulk flow marker and was indicative of active transport movement (Yoneyama, Shinozaki et al. 2010). Both LAT and system A could have potential application in drug movement from vitreous

to retina and it is possible that various other amino acid transport systems could also prove useful from a drug delivery perspective. Alongside amino acid movement from vitreous to retina, studies have also investigated the impact of transporter systems on drug movement from vitreous to retina. Studies have considered the role of various transporters including; P-glycoprotein, organic cation transporters and organic anion transporters.

1.4.2.2. P-GLYCOPROTEIN

The multidrug transporter P-glycoprotein (P-gp), is a member of the ATP-binding cassette (ABC) family of transporters and is involved in various functions including: cell signalling, ion transport, nutrient uptake and efflux of undesirable compounds. A number of isoforms of P-gp exist with multidrug resistant 1 (MDR1) and multidrug resistant 2 (MDR2) shown to be expressed in human cell lines (Hennessy and Spiers 2007).

Earlier ocular studies involving MDR, investigated the role of multidrug resistant pump on the uptake of fluorescein sodium (FS) and benzylamine phenyl sulfonylglycine (BAPSG) into human RPE cells. BAPSG is a selective aldosterone reductase inhibitor, considered for its potential role in the treatment of diabetic retinopathy. Indomethacin, verapamil and probenecid were co-administered alongside FS and BAPSG as known MDR inhibitors. Both indomethacin and probenecid were shown to increase FS accumulation in cells, with no significant effect demonstrated by verapamil. BAPSG accumulation also increased in the presence of indomethacin and probenecid but also verapamil when the concentration of inhibitor was increased to 10 μ M. Efflux of BAPSG from RPE cells was also shown to be significantly higher when the inhibitors were not present (Aukunuru, Sunkara et al. 2001). Moving on from this work, using PCR, the presence of P-gp efflux transporter in retinal cells was demonstrated. Using various RPE cells lines, the penetration of rhodamine 123, a known P-gp substrate, into cells was investigated. In one cell line, the presence of P-gp inhibitor, verapamil, resulted in an increased uptake of rhodamine 123 by approximately 13 fold. Little effect was noted on the other cell lines studies, reportedly due to poor expression of P-gp (Constable, Lawrenson et al. 2006). Continuing on from this, in 2003, using an inner

blood-retinal-barrier cell line (TR-iBRB) transfected with P-gp, uptake studies of rhodamine 123 were carried out. Uptake studies were performed in the presence and absence of a series of test compounds; AGN 194716, AGN 195127, AGN 197075, acebutolol, alprenolol, atenolol, brimonidine, carbamazepine epoxide (CBZ-E), metoprolol, nadolol, and sotalol, to identify potential P-gp inhibitors. Using TR-iBRB cell lines, rhodamine 123 uptake identified only AGN 197075 as an inhibitor of P-gp-mediated efflux of rhodamine 123 from compounds studied (Shen, Cross et al. 2003).

Continuing on with P-gp transporter studies in cell lines, Steuer et al used retinal cells isolated from the pig to show both P-gp and multidrug resistant protein (MRP) expression in the outer BRB. In vitro studies also extended on to in vivo work, carried out by administration via interperonial injections of model compounds into mice. Verapamil and rhodamine 123 were applied to both the choroid and retina independently and a higher cell permeability of both compounds into cells was demonstrated when the compounds were applied to the retinal side of the outer BRB. Increases in permeability were 3.5-fold for verapamil and 2.6-fold for rhodamine, leading to the conclusion that P-gp expression in the outer BRB must be greater at the choroidal side. The authors also investigated the penetration of FS from retina to choroid in the presence and absence of MRP inhibitor, probenecid. FS permeability increased 11 fold following addition of the inhibitor (Steuer, Jaworski et al. 2005).

Although the majority of this work was carried out in vitro, using isolated cell lines, the extent of P-gp role in drug delivery is obvious. The work completed illustrated nicely the impact of blocking efflux transporters on drug accumulation in retinal cells. Co-administration of an efflux blocking agent at the time of intravitreal drug administration could be of potential benefit in increasing drug retinal concentrations of drugs subject to P-gp. This could help to maintain therapeutic drug concentrations at the retina, whilst reducing the frequency of administration required. However the pharmacological actions of the inhibitor would need to be considered, as they may be undesirable or detrimental to the patient's treatment.

1.4.2.3. ORGANIC CATIONIC TRANSPORTERS

Organic cationic transporters (Oct) are members of the solute carrier transporter gene family and are involved in the transport of small organic cations and hydrophilic compounds (Kusuhara and Sugiyama 2004). Known substrates of Oct include tetraethylammonium and monoamine neurotransmitters (Tsuji 2005). Organic cationic transporter (Oct) has been shown to be expressed in mouse RPE (Rajan, Kekuda et al. 2000) and its involvement in retinal drug transport was demonstrated by Han et al in 2001. (Han, Sweet et al. 2001) Using human RPE cell lines, RPE/Hu and ARPE-19, the uptake of verapamil into RPE was shown to be a saturable process, with an apparent K_m equal to 7.2 μM . The rate of verapamil uptake decreased in the presence of metabolic inhibitors, when the temperature was reduced, and in the presence of some organic cations: including quinidine, pyrilamine, quinacrine, and diphenhydramine. Uptake was also inhibited by the cationic drugs - diltiazem, timolol, and propranolol - commonly used in the treatment of glaucoma. However, no change in uptake rate was seen in the presence of other organic cations, including tetraethylammonium and cimetidine. Leading the author to conclude that a new organic cationic transporter subtype had been discovered and was involved in verapamil transport.

1.4.2.4. ORGANIC ANION TRANSPORTERS

Alongside cationic transporters, the role of anion transporters in intravitreal drug delivery has previously been considered. Organic anion transporters (Oat) are also members of a family of solute carrier transporters and involved in energy independent efflux transport (Brasnjevic, Steinbusch et al. 2009). Using polymerase chain reaction (PCR), rOat3 (rat organic anion transporter) expression was found in the retina and retinal endothelial cells of rats. Following on from this, a series of radio labelled drug candidates were administered via intravitreal injection and concentration changes measured by microdialysis. *P*-aminohippuric acid, benzylpenicillin and 6-mercaptopurine were all subject to biexponential elimination from the vitreous. The elimination rate of all three was reduced in the presence of rOat3 inhibitor, probenecid, demonstrating the role of rOat3 in drug efflux (Hosoya, Makihara et al. 2009).

Another compound that was investigated for Oat involvement in transport was labelled [³H]Estradiol 17-beta glucuronide ([³H]E17bG). The study was performed in vivo using the rat and microdialysis was used to measure changes in vitreous concentrations. Radio labelled [¹⁴C]D-mannitol was also administered as a marker of bulk flow movement. Elimination of both compounds from the vitreous followed the pattern of biexponential elimination. In the initial phases of drug elimination from the vitreous, elimination rate was more or less the same in the both compounds. However, the second phase of decline differed, with elimination of [³H]E17bG shown to be significantly greater than of [¹⁴C]D-mannitol, with elimination constants of $9.0 \times 10^{-3} \text{ min}^{-1}$ for [³H]E17bG and $5.0 \times 10^{-3} \text{ min}^{-1}$ for [¹⁴C]D-mannitol. The author suggested that the first decline shows the drug diffusing across the whole of the vitreous whereas the second declines drug elimination out of the vitreous. In the presence of probenacid, the rate of elimination of [³H]E17bG was reduced to that of [¹⁴C]D-mannitol, leading to the conclusion that [³H]E17bG undergoes efflux transport via a probenacid sensitive organic anion transport process, likely to take place at the BRB (Hosoya, Ohshima et al. 2003).

Both Oat and Oct transporters will have an important role in drug delivery to the retina. Increasing understanding of the extent of ocular Oat and Oct transporters and their substrates could be of potential benefit in drug design. The potential to select drug candidates based on their presence of cationic and anion functional groups could be used to improve penetration into the retina.

1.4.2.5. OTHER TRANSPORTERS

Similarity to the probenacid sensitive Oat transporter, a probenacid-sensitive transport process was also speculated to be involved in fluorescein elimination. Early work investigating the rate of fluorescein elimination from rabbit vitreous, demonstrated an elimination rate of fluorescein of 0.22 h^{-1} within 8 hours of administration. After addition of probenacid, the rate of fluorescein loss was reduced to 0.13 h^{-1} with little effect on the rate of metabolite, fluorescein monoglucuronide. Since fluorescein is eliminated via the posterior route, a probenacid-sensitive transport process was suggested to be involved in fluorescein transport from vitreous

to retina (Kitano and Nagataki 1986) and could potentially be affiliated to Oat and Oct transporters discussed previously.

Moving on from this, a different system entirely has been suggested to be involved in drug movement. Microdialysis was selected as a means to investigate the involvement of an oligopeptide transporter system on the distribution of a model labelled peptide [³H] glycylsarcosine. At steady state, the area under the curve (AUC) detailing the penetration rate of the peptide from vitreous to plasma was shown to be 1.61 +/- 0.49. After the addition of peptide transporter substrates, glucylproline, carnosine and captopril, the uptake of the model peptide was inhibited. In addition, when non peptide transporter substrates were added, no effect on uptake rate was noted (Atluri, Anand et al. 2003).

Another unrelated transport system that has been considered in ocular studies is P2Y₂ mediated receptor transport. P2Y₂ is a G protein coupled receptor known to have involvement in transfer of extracellular nucleotides. In order to investigate the impact of this transporter system on drug movement, P2Y₂ receptor agonists, UTP and INS542, were administered via intravitreal injection to rabbits alongside FS. Both drugs had a different impact on FS levels reaching the retina. UTP had no effect on FS levels, leading the author to conclude that it was likely UTP was degraded in the vitreous before exerting an effect on the receptor. INS542, on the other hand, significantly reduced fluorescein to metabolite fluorescein glucuronide ratios in the vitreous, when compared to eyes dosed with phosphate buffered saline instead of agonist. Therefore, a larger proportion of the administered fluorescein was transferred out of the vitreous into the retina after administration of the agonist. This increase in transport is likely due to P2Y₂ receptor activation (Takahashi, Hikichi et al. 2004). Finally, a different study has identified the role of a retinal transporter in the movement of other drugs from vitreous to retina, including bevacizumab; however, this work did not record the specific mechanisms involved but did link vitreous elimination of drug to a transporter system (Heiduschka, Fietz et al. 2007).

From the studies considered, it is apparent that drug transporters will play a key role in intravitreal drug delivery with an aim to treat the retina. Various different transport systems have been shown to operate, controlling the movement of a variety of drugs. Although the understanding of transporters involved in treating the retina

has increased dramatically over the last decade, their involvement in ocular drug movement is still not fully understood. Understanding the extent of the effect of specific transporter subgroups on specific ocular treatments could markedly improve drug targeting to the retina, improving therapeutic options and disease prognosis.

1.5. AIMS AND OBJECTIVES OF THE THESIS

In order to research ocular drug distribution, this project will consider a wide spectrum of experimental investigations, using traditional means of determining pharmacokinetics and also developing alternative means of carrying out these investigations. The main aim of this project is to investigate the impact of physicochemical properties and physiological clearance mechanisms on ocular drug distribution and to understand the process of drug penetration to the retina.

The key project objectives are as follows:

1. The development of a suitable analytical method to enable the quantification of a drug series in ocular tissues.
2. Using the analytical method developed, illustrate the ocular pharmacokinetic movement of each of the drug compounds, with respect to their physicochemical properties
3. The development of an alternative analytical method to enable a clearer picture of ocular drug distribution to be created
4. To collaborate with model builders in the US to construct predictive models for mapping pharmacokinetic movement through the eye.

CHAPTER 2. DEVELOPMENT AND VALIDATION OF A LIQUID CHROMATOGRAPHY MASS SPECTROMETRY METHOD FOR THE SIMULTANEOUS QUANTIFICATION OF A DRUG SERIES IN OCULAR TISSUES

2.1. INTRODUCTION

2.1.1. Cassette dosing

Drug movement through the interior structure of the eye follows diffusive and convective processes, coupled with active uptake into tissues. Specific compartment volumes, blood flow, binding and active transport generate a complex model of disposition (Koeberle, Hughes et al. 2006). Since the eye provides many different types of environment, with widely different composition and metabolic rates, a large number of samples are needed to map drug disposition and generating pharmacokinetic (PK) data, in order to understand patterns of drug movement, is a time-consuming process, especially in ocular studies. Measuring drug concentrations in ocular tissues is not a simple process, as it does not involve sampling blood from the animal at predetermined time points and measuring the concentration of drug present in each sample. Determining concentrations within individual ocular tissues

requires each individual ocular tissue to be removed from the eye and the tissue is then subjected to destructive processing, in order to extract and determine the concentration of drug contained within. This leads to distribution studies having very large animal requirements, as for each time point, an animal has to be sacrificed and the tissues removed. In addition to this, is the problem of inter-animal variability and statistical reliability of the results, with normally four to six animals required at each time point, in order to achieve statistically sound results (Eckelman, Kilbourn et al. 2007).

In order to overcome this problem and reduce the number of animals required per PK study, microdialysis has been utilised in ocular studies as a suitable tissue sampling technique (Macha and Mitra 2001; Anand, Atluri et al. 2004). In microdialysis studies a small volume of the aqueous humor and/or the vitreous humor is sampled continuously and the concentration of drug contained over a timed collection quantified, to enable characterisation of drug movement from the anterior to the posterior eye, or vice versa. This technique is easily applied in liquids; however for solid tissues ocular tissues this method of sampling is unsuitable, as intimate contact is not achieved. As a consequence, although undoubtedly useful, a complete PK picture of drug movement through the eye cannot be generated by this methodology. In an attempt to overcome the problems associated with the high animal requirements and variability associated with PK studies, the pharmaceutical industry has developed the idea of using a cassette in which drugs are simultaneously administered as a single dose (Manitpisitkul and White 2004). This technique has been used in various animal models, including rat and mice, to investigate the pharmacokinetics of a variety of drug compounds, from bile acid transport inhibitors to specific enzyme inhibitors (Watanabe, Schulz et al. 2006; Wolf, Vora et al. 2010). Commonly, a small cassette of drugs is used, containing a minimum of two up to a maximum of approximately ten compounds. Within each cassette, the concentration of each compound is kept to a minimum, at a low dose of up to about 1mg/kg/compound for systemic studies. It is assumed that the drugs will behave independently, without complex physical or metabolic interactions, however a reference standard of known pharmacokinetics is often administered within the cassette as a control substance, with the theory that any impact that cassette dosing

has on changing the pharmacokinetics of the drugs within the series, would be easily identified from changes in the pharmacokinetics of the standard (Ackermann 2004; Maniṭpiskitkul and White 2004). The benefits of cassette dosing over traditional PK studies include; reduced animal usage, reduced animal variability and in addition reduced analytical time, especially during the method development process.

The benefits associated with using cassette dosing are clear however, the obvious concern is the potential for drug interactions between compounds contained within the drug mixture. Possible sources of drug interactions which affect the interpretation of pharmacokinetic constants include competition for clearance pathways and protein binding, activation of certain clearance pathways, effects on blood flow and enzyme induction (White and Maniṭpiskitkul 2001). Other potential issues include problems with solubility and development of an analytical technique, as sample preparation can often be difficult when using a set of diverse compounds (Frick, Adkison et al. 1998). In order to maintain the reliability of the study, it is important to minimise the potential problems that are associated with cassette dosing. The strategy of eliminating known inhibitors of drug metabolism from the mixture, using a small dose of each compound and using a small cassette series of up to a maximum of about 5 compounds, may reducing the risk of such effects. Another approach includes administering each compound on two separate occasions, either in a new cassette series or as a single compound (White and Maniṭpiskitkul 2001). However, the increase the experimental time predicates that a reference standard within the cassette is a more feasible option.

The concept of using cassette dosing in ocular studies is relatively novel, with few reports to previous use in published ocular PK studies in the literature. Notably, the development of an analytical technique to test the feasibility of measuring a cassette of compounds in ocular tissue was described in a recent study (Kadam and Kompella 2009). In this work an LCMS method to quantify a range of beta blocking compounds in bovine sclera, choroid, retina and vitreous tissues was designed and validated. Since this work, a cassette study of drug distribution using the rat model has been completed (Kadam and Kompella 2010). In addition to these studies, ocular drug distribution of five compounds has been completed in rabbits dosed with a cassette and with individual compounds. In this study, some variability between

the PK of the drugs administered in a cassette compared to the PK of each individual drug when dosed alone was demonstrated, however the differences were minimal and the results achieved were still regarded as an adequate representation of PK for use in screening (Proksch and Ward 2007).

Cassette dosing has the potential for use as a fast and effective screening tool to identify compounds of interest in ocular PK studies. In order to improve the reliability of the data obtained, it seems sensible to keep the size of the cassette low and use a low dose of each drug.

2.1.2. Ultra performance liquid chromatography

In cassette dosing, multiple analytes are simultaneously detected from the same sample and as a result efficient, high quality analysis is essential. Multiple analyte analysis, especially involving compounds which are chemically diverse, can often lead to prolonged run times when using traditional analytical methods commonly used in PK studies, such as high performance liquid chromatography (HPLC). In the last decade, traditional HPLC equipment and methodology has dramatically improved, with the development of ultra performance liquid chromatography (UPLC). UPLC involves the use of smaller particle sized packing materials within UPLC columns, in order to reduce the diffusional path of the analyte and therefore reduce the time required for compound elution from the column. As a result of using smaller sized particles and increasing the speed of travel with the column, the pressure of the system is increased to well above the maximum pressure a traditional HPLC system can accommodate of approximately 400 bar. In order to solve this issue, new equipment was developed to withstand much higher system pressures of up to 4100 bar (MacNair, Lewis et al. 1997). This system was then further improved, leading to the development of a UPLC system which combined the benefits of improved chromatographic resolution, alongside reduced analytical time when using 1µm sized particles (MacNair, Lewis et al. 1997; MacNair, Patel et al. 1999). Since this initial work was completed, UPLC systems are now commonly used in pharmacokinetic analysis within the pharmaceutical industry and have been designed to withstand pressures in excess of 7000 bar. Direct comparisons between UPLC and HPLC using higher flow rates and shorter column lengths have

demonstrated vast improvements in compound analysis, with compound elution speed shown to increase by approximately 4 fold when compared to 5 μ m particle traditional HPLC system, without any resultant impact on efficiency (Villiers, Lestremau et al. 2006).

In this work ultra performance liquid chromatography-tandem mass spectrometry (UPLC-MS/MS) was selected as a suitable analytical method. UPLC-MS/MS is a highly sensitive technique and can enable simultaneous detection of a number of compounds from ocular tissue samples. The use of tandem MS reduces signal to noise ratio and ensure high selectivity during PK studies (Hoffmann and Stroobant 2002). Using this technique, analytes are initially separated via UPLC before subsequent detection via MS. In this chapter an effective and efficient UPLC-MS/MS method was developed and then validated to enable the simultaneous quantification of atenolol, timolol and propranolol in ovine ocular tissue, in the view to combining both cassette dosing and isolated perfused eye methodology to rapidly generate ocular PK data.

2.2. MATERIALS AND METHODS

2.2.1. Chemicals

Drug samples atenolol hydrochloride (purity \geq 98 %), timolol maleate (purity \geq 98%) and propranolol hydrochloride (purity \geq 99%) along with ammonium hydroxide solution (28%), sodium hydroxide, ammonium acetate and formic acid were all purchased from Sigma-Aldrich (St Louis, MO, USA). Levobunolol hydrochloride was kindly provided by Allergan (Irvine, CA, USA). HPLC grade methanol, ethylacetate, acetonitrile and hexane were purchased from Fisher Scientific (Fair Lawn, NJ, USA)

2.2.2. Instrumentation

UPLC-MS/MS was performed on a Thermo TSQ Quantum Ultra equipped with HFSI-II heated electrospray ionisation probe (Thermo Scientific) and autosampler. The XCalibur data system was used for system control and also data processing.

2.2.3. Chromatographic conditions

Analyte separations were performed on an Acquity, BEH UPLC C₁₈ column (100mm length, 2.1mm internal diameter) with 1.7µm particle size, equipped with guard column. Column temperature was maintained at 60°C throughout. Mobile phase was composed of 0.1% v/v formic acid in HPLC grade water (A) and 0.1% v/v formic acid in methanol (B) at an initial ratio of 95:5 (A:B). Before introduction into the UPLC-MS/MS apparatus, mobile phase was filtered through a 0.45 µm membrane filter and the autosampler temperature was maintained at 4°C. UV absorbance data was collected at 270nm with a bandwidth of 10nm.

A gradient method was selected for compound separation using the following ratios of mobile phase: 95% A for 0.5 minutes decreased to 0% using a linear gradient over 0.5 minutes and held for 1 minute. Mobile phase ratio was then restored to starting 95% A and maintained for 0.9 minutes before next injection. A flow rate of 500µl/minute was used and the injection volume selected was 10µl.

2.2.4. Mass Spectrometry conditions

Nitrogen was used as the gas source and samples were analysed using positive ion mode. For the detector conditions ion spray voltage was set to 3000eV, capillary temperature to 350°C, sheath gas flow rate to 60 units and auxillary gas flow rate to 50 units. Selective ion monitoring mode was selected to detect the daughter ion of each of the compounds and the internal standard in the first instance and progressed on to utilise selected reaction monitoring when the method was refined.

2.2.5. Sample Preparation

2.2.5.1. Dissection procedure

Ovine eyes were collected from a local abattoir, normally within an hour to a maximum of two hours of slaughter. Initially, a 30G needle was inserted into the anterior chamber of the eye and the aqueous humor was removed and stored until further processing. Before dissecting the eye for tissue processing, the adnexal tissue and the extraorbital muscle was removed from the globe and discarded. In order to

dissect each ocular tissue from the eye with minimal cross contamination between tissues, the perfused eye was snap frozen by slowly dipping the eye into liquid nitrogen repeatedly, until the eye was completely frozen. Immediately after freezing, the eye was transferred to a petri-dish and dissected. Initially the optic nerve was cut away at the base of the eye and the eye was then divided into the anterior and the posterior section.

2.2.5.2. Anterior Eye Dissection

The anterior section was removed by creating a small incision into the sclera, approximately 3mm from the edge of the cornea. Using the incision created as a positional marker, the anterior eye was then cut away in a circular dissection, at a constant distance of approximately 3mm from the edge of the cornea. The anterior section was then removed and placed corneal side down in the dish. The lens was lifted away from the iris and ciliary body and stored. The iris and ciliary body was then removed from the sclera by tweezing the tissue off the sclera and stored in a centrifuge tube.

2.2.5.3. Posterior eye Dissection

In order to remove the whole vitreous, the eye was sliced at four positions from the anterior section to the posterior section (Figure 2.1). This method then enabled the vitreous to be carefully removed from the globe. The retina and RPE were removed from the back of the eye by gently lifting it away from the head of the optic nerve and was stored in a centrifuge tube. The RPE was treated as a part of the retina through this work. Following removal of the retinal, the choroid was also gently lifted away from the sclera and placed into a centrifuge tube. Once all of the ocular tissues to be investigated were removed, all of the tissues were weighed individually and stored at -20°C until preparation for analytical processing. Before the tissue standards were prepared, all of the ocular tissues were homogenised using an Ika DI-18 basic homogeniser equip with dispersing element S18N-10G at a speed of 3500 rpm. To the choroid, the iris and ciliary body, the lens and the retina, 1ml of deionised water was added before carrying out the homogenisation process, the

aqueous humor and the vitreous were homogenised without the addition of water. The tissues were homogenised on ice in order to minimise heat damage to the tissues.

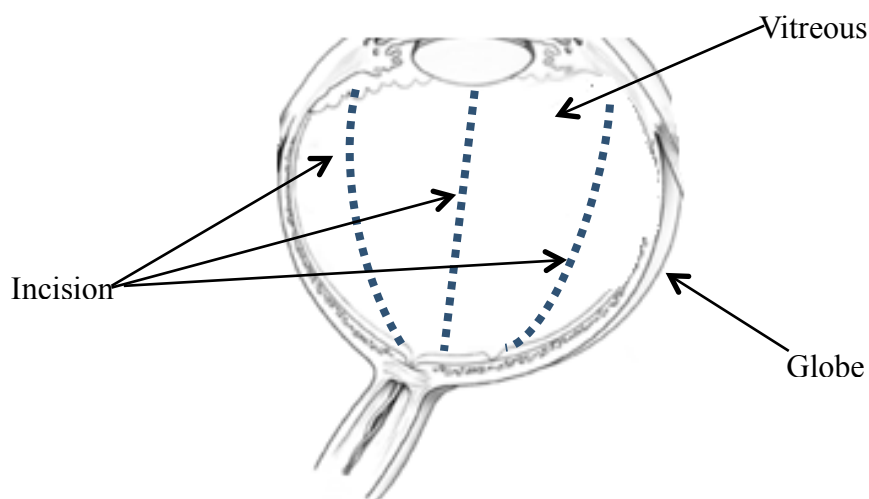


Figure 2.1 Posterior section of eye showing positioning of incisions from posterior section to anterior section. Fourth incision posited at the back of the globe.

2.2.5.4. Standard Preparation

Standard solutions were prepared from a stock solution containing each of the three compounds; atenolol, timolol and propranolol, at a concentration of 1mg/ml prepared in deionised water. A stock solution of internal standard was also prepared at a concentration of 1mg/ml in deionised water and diluted to obtain a working stock solution of 10ng/ml. Standard solutions of the compound mixture were diluted in deionised water to obtain the following concentrations; 60, 30, 20, 7.5 and 5 ng/ml.

2.2.6. Tissue Extraction study

2.2.6.1. Strong cation solid phase extraction

Solid phase extraction (SPE) was the first method selected to extract all three compounds and internal standard from tissue sample. Reverse phase, Strata X-C 33u polymeric strong cation exchange cartridges (Phenomenex, Macclesfield, UK) were selected based on the basic nature of the majority of the compound (Table 2.1). During the extraction, the compounds pass through the cartridge through the column

and bind onto the stationary phase. The sorbent in the Strata XC[®] is a polymeric sorbent based on aliphatic sulfonic groups, which are negatively charged in an aqueous environment. Positively charged cations will be retained onto the column and are then eluted using a suitable solvent. Before SPE, tissue samples were spiked with the drug compounds and internal standard. A tissue sample of 200µl was added to a sample vial and, to this, 1ml of each compound spiking solution was added along with 1ml of internal standard working solution. The sample was then placed on a vortex for 3 minutes before starting the SPE procedure. The initial phase of the SPE procedure involved conditioning the Strata[®] column with 3ml methanol, 3ml of deionised water and 3ml of 0.1% formic acid in succession. Following this the tissue sample was added and eluted slowly from the column. The column was then washed with 1ml of formic acid followed by 1ml of methanol and left to dry for 1 minute. Finally the sample was eluted using 3ml of 1M methanolic ammonium hydroxide and the solvent evaporated under a stream of nitrogen at 40°C. The compounds were then reconstituted in 1ml of mobile phase before injection into the UPLC-MS/MS.

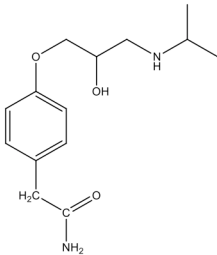
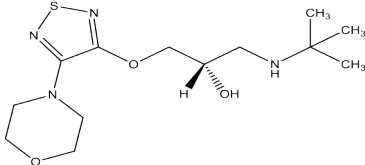
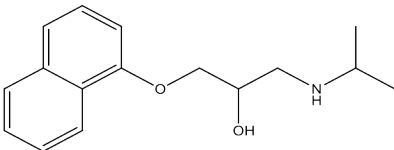
Beta adrenoreceptor antagonist	pKa	LogP	Structure
Atenolol	9.5	0.16	
Timolol	9.2	1.8	
Propranolol	9.3	2.4	

Table 2.1 Physiochemical properties of the drugs studied.

2.2.6.2. Liquid-Liquid extraction

A liquid-liquid extraction technique was selected as the second extraction method used to attempt to isolate all three drugs and internal standard from the tissue sample. This technique was a relatively simple and straightforward technique with the added bonus that it is inexpensive.

Initially 500µl of homogenised vitreous tissue sample was spiked with 1µg of each compound and 0.1µg of internal standard. This sample was gently mixed before adding 500µl of 1M sodium hydroxide and placed on a vortex for 30 seconds. Drug compounds were then extracted with 2ml of ethyl acetate and hexane in a 1:1 ratio and the upper layer removed. Solvent was then removed from the upper layer under a stream of nitrogen and the resultant residue reconstituted in 500µl of mobile

phase (60 A: 40 B). Samples were then filtered through a 0.22 μ m pore membrane before injection into the UPLC-MS/MS for analysis.

2.2.6.3. Weak cation solid phase extraction

The third extraction technique used was another SPE method. This time a weak cation exchange resin was used, in the form of reverse phase, Strata X-CW 33u polymeric strong cation cartridges (Phenomenex, Macclesfield, UK). Before performing the weak cation SPE, tissue samples were spiked with the drug compounds and internal standard. A tissue sample of 200 μ l was added to a sample vial and, to this, 1ml of each compound spiking solution was added along with 1ml of internal standard working solution. The sample was then placed on a vortex for 3 minutes before starting the SPE procedure. The initial phase of the SPE procedure involved conditioning the Strata[®] column with methanol (3ml) and deionised water (3ml) in succession. Following this, the tissue sample was added and eluted slowly from the column. The column was then washed with 25mM ammonium acetate pH 6.5 (1ml) followed by methanol (1ml) and left to dry for 1 minute. Finally the sample was eluted using 2% formic acid prepared in 20:80 methanol to acetonitrile (3ml) and the solvent was evaporated off under a stream of nitrogen at 40°C. The compounds were then reconstituted in 1ml of mobile phase before injection into the UPLC-MS/MS.

2.2.6.4. Protein Precipitation

The final technique selected was a protein precipitation (PP) method. PP was selected as it was regarded as a fast and relatively inexpensive method of extracting the drug compounds and internal standard from tissue samples. Vitreous and aqueous tissue were homogenised alone whereas to the retina, lens and iris and CB, 1ml of deionised water was added before homogenisation. Samples were then spiked with 1ml of drug compound series and 1ml of internal standard. Following this samples were vortexed for 3 minutes. To samples three times the sample volume of methanol was added and samples were ultrasonicated for 2 minutes. Following this samples were centrifuged for 20 minutes at a speed of 3000 rpm and finally, 100 μ L

of the supernatant was added to 900 μ L of 0.1% v/v formic acid in methanol before injection into the UPLC-MS/MS.

2.2.6.5. Validation

A calibration series of drug mixture in each ocular tissue was prepared to contain the following concentrations 100, 60, 30, 15, 10, 7.5, 5ng/ml to assess for linearity. Spiked samples of each tissue were prepared at concentrations of 100, 30, 5ng/ml and used to determine accuracy, precision and recovery. For intra-day precision, 5 sample measurements were taken on the same day and for inter-day precision, 5 sample measurements were taken on the following day. Recovery was determined by comparing the mean spiked sample concentration to standard drug mixture solutions prepared in deionised water.

2.3. RESULTS AND DISCUSSION

2.3.1. UPLC-MS Compound separation

In the first instance, a method to enable separation of all three compounds and IS was developed. Levobunolol was selected as a suitable internal standard due to its similarity to the three beta adrenoreceptor antagonists under investigation (Figure 2.2).

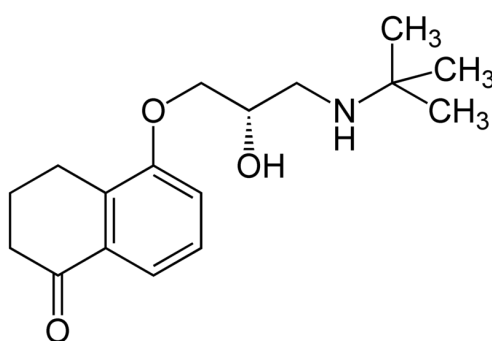


Figure 2.2 Chemical structure of levobunolol

The initial method developed enabled all 4 compounds to be detected on the UPLC-MS, in selective ion monitoring (SIM) mode. All compounds were detected using SIM at their respective molecular weights, 260.2 for propranolol, 267.2 for

atenolol, 292.2 for levobunolol and 317.2 for propranolol. All compounds were successfully detected with good compound retention times in a short sample run time of 3 minutes. An example of the chromatographs of all three drugs and IS at a concentration of 2.5ng/ml are shown in Figure 2-3 **Error! Reference source not found.**

Once a useful UPLC-MS method was in place it was decided to first develop an effective method to enable extraction of compounds from each ocular tissue before completing UPLC-MS method validation.

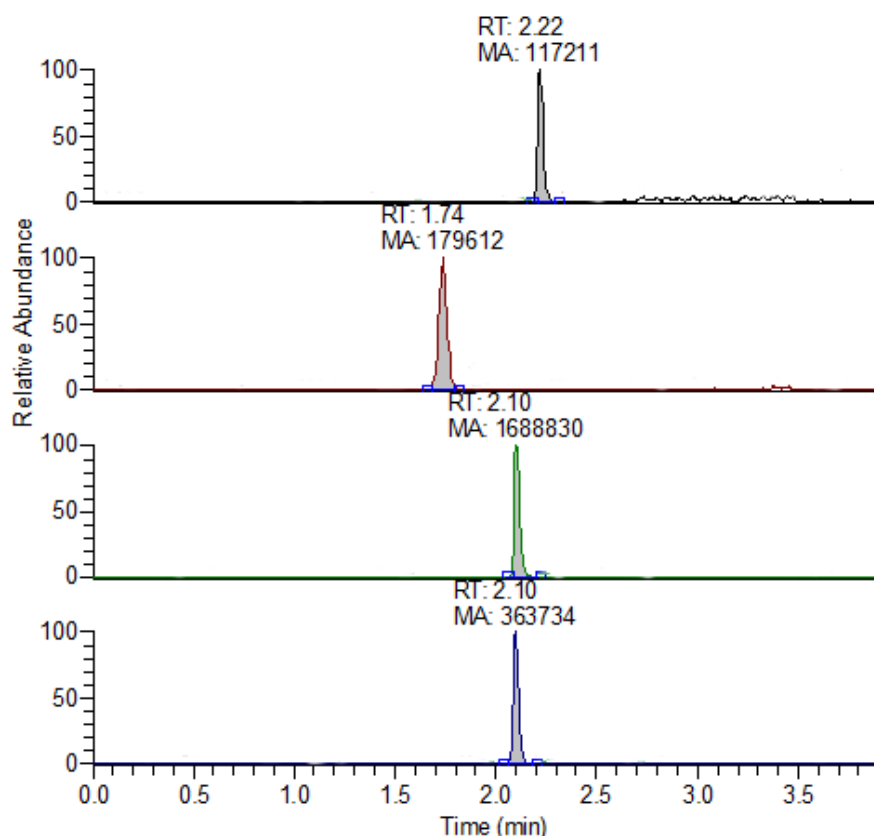


Figure 2-3 Chromatograph showing peaks obtained for propranolol, atenolol, levobunolol and timolol in descending order using SIM, prepared in mobile phase.

2.3.1.1. Strong cation Solid phase extraction

The first extraction method selected was a solid phase extraction method, using strong cation SPE cartridges detailed previously. For the majority of the ocular tissues tested, problems arose with high variability in the peak intensity recorded for

the internal standard. Although the concentration of internal standard was maintained across the calibration range and ocular tissue subtypes, during the extraction procedure the isolation of IS was not consistent, varying by approximately 32 fold from 960395 ng/ml up to 30609090 ng/ml (Table 2.2).

	Levobunolol peak area				
Tissue	Lens	Retina	Vitreous	Aqueous	Iris/CB
Concentration (ng/ml)					
60	960395	2384301	3941893	1618479	1314818
30	22229606	2344550	2253654	1332748	3030337
20	21087937	1951183		26768344	20679628
7.5	23078957	23214746	28096596	21715900	22733818
2.5	1829457	23942071	30609090	25999069	15419274

Table 2.2 Peak areas obtained for levobunolol in various ocular tissues at different analyte concentrations (n=1).

As a result of the poor reproducibility experienced when isolating the IS from ocular tissues, difficulty was experienced in achieving linearity with the three analytes to be used within the cassette. Across the range of different ocular tissues, different problems were noted with different analytes, when the ratio of peak area of analyte recorded to peak area of IS was plotted. The test calibration curves generated in each ocular tissue using strong solid phase extraction technique experienced poor linearity and can be seen Appendix 1 (Figure A2.1, A2.2, A2.3, A2.4 and A2.5). For the aqueous and lens tissues poor linearity was experienced by all three analytes and was especially poor for propranolol. For the retinal and vitreous tissues, poor linearity was also noted, with an improvement on propranolol linearity achieved. For the iris and ciliary body tissue, the results were more promising, with a relatively linear response achieved for all three analytes and R^2 of greater than 0.9 recorded. Although the linearity for the iris and ciliary body was demonstrated for all three analytes, when the ratio of response was visualised, focussing on the peak area alone

demonstrated that the linearity was poor and suggested variability within the extraction method (peak areas are contained in Table A2.1 in Appendix 1).

Strata strong cation SPE tubes are designed to strongly retain basic compounds. In the first instance, analytes are eluted through the column in the charged form using an appropriate mobile phase. The charged compounds then bind to the positively charged anions on the stationary phase of the column by electrostatic attractions. After a washing phase, compounds are eluted by either neutralising functional groups on the stationary phase of the cartridge or by neutralising or displacing the absorbed cation (Sigma-Aldrich 1998). All three compounds selected were weak bases, with pKa values of 9.6 for atenolol, 9.2 for timolol, 9.3 for propranolol and 9.5 for levobunolol (Table 2-1). It is possible that the variability in analyte extraction was due to analyte removal from the column during the washing phase or alternatively, the analyte was strongly retained and during the elution step the analyte was incompletely displaced.

2.3.1.2. Liquid-liquid extraction

Due to the poor linearity experienced using the strong cation SPE method, the method was deemed inappropriate and interest progressed onto using a liquid-liquid extraction (LLE) method as an alternative. In the first instance the LLE method was performed on a small concentration range of each analyte prepared in vitreous tissue as a test based on a method detailed by Kadam and colleagues (Kadam and Kompella 2009). Poor linearity was achieved for atenolol and for propranolol, however for timolol the result was much better (the test calibration can be seen in Appendix 1, Figure A2.6). This differs from results detailed by Kadam et al, where good linearity was achieved for all three drugs. This is perhaps due to the choice of internal standard selected and its impact on the peak area ratio. In addition, in the previous study different ocular tissues were under investigation and again this could impact on the peak area ratio. This being said, when compared to the strong cation SPE method, the reproducibility of the internal standard extraction was much more consistent, however this was tested over a reduced number of samples (details contained in Table A2.2 in Appendix 1).

During LLE, the first step of the extraction involved increasing the alkaline content of the tissue. This was to ensure that lipophilic groups were converted into the non-ionised form. The compounds are then able to partition from the hydrophilic tissue layer into the organic layer. Two organic solvents were used, a more polar solvent ethyl acetate and a non-polar solvent hexane, to ensure all analytes would partition into the organic layer. Atenolol has a low partition coefficient, when compared to the other analytes, of 0.16 (Table 2.1) and it is possible that due to the polarity of atenolol the analyte did not partition as easily into the organic layer. For propranolol the cause of poor linearity is unclear; propranolol is relatively lipophilic, therefore extraction of this analyte into the organic phase was expected to be successful. Perhaps the differences existing in partition coefficients across the range of analytes is too problematic for a LLE, which relies on partitioning into an organic layer. For this reason liquid-liquid extraction would be more beneficial for a group of compounds with similar partition coefficients rather than a variable mixture.

2.3.1.3. Weak cation solid phase extraction

Following on from the disappointing result obtained from the LLE method and the difficulties in isolating different compounds with differing partition coefficients, it was decided to revisit SPE and attempt a similar method using an alternative kind of SPE cartridge. The weak cation solid phase extraction method was performed on three different concentrations of drug cassette prepared in vitreous tissue to test the extraction method for linearity. Weak cation SPE cartridges were used in this set of experiments to determine the effect of using an alternative type of SPE cartridge, to that used previously, on improving analyte linearity. In this instance, for atenolol and timolol the results were very promising, with R^2 values achieved both drugs greater than 0.97, however for propranolol, the linearity of the extraction method was poor (Figure A2.7 in Appendix 1).

Differing from the strong cation cartridges used previously, weak cation SPE cartridges are described by the manufacturer as being particularly useful in the retention of quaternary amines. Although none of the drug structure investigated contain quaternary amines, comparing propranolol to timolol, timolol contains three cyclic tertiary amines whereas propranolol only contains one secondary amine. As

a result, timolol was more specific in binding to the weak cation SPE cartridges and achieved excellent linearity (R^2 0.9919) compared to atenolol (R^2 0.0023). Due to the very poor extraction of propranolol, the weak cation SPE method was deemed unsuccessful and as a result this method was not suitable for use in the study.

2.3.1.4. Protein precipitation

The final method attempted in this study, was a protein precipitation method (PP). The selected PP method involved the addition of an organic solvent to tissue to precipitate the proteins contained within the tissue, to remove any contaminants from the sample. The purpose of this step was to ensure that the analyte could be easily detected, without significant interference from organic compounds present in the various types of ocular tissue samples. When compared to the LLE method and both SPE extraction methods used, the protein precipitation method (PP) appeared more successful and allowed all four compounds to be successfully extracted with only a slight change in retention time from the standards prepared in mobile phase (example chromatograph show in Figure A2.8 in Appendix 1).

In order to test for linearity, for each tissue subtype a small calibration curve was prepared, again using three different analyte concentrations. The test calibration curves generated in each ocular tissue using the protein precipitation technique experienced improved linearity when compared to the other methods and can be seen in Appendix 1 (Figure A2.9, A2.10, A2.11, A2.12, A2.13 and Table A2.3). For the lens and aqueous tissue, good linearity was produced for all three analytes. For the vitreous and iris/CB good linearity was obtained for timolol and propranolol however, for atenolol the linearity was less than adequate. For the retinal tissue good linearity was seen for atenolol and propranolol; however this was less successful for timolol. From all four techniques investigated, this technique has proven to be the most useful method for extracting all three drugs and the internal standard from all of the ocular tissues to be investigated. Although in some tissues and for certain analytes the method required refinement, in these initial tests only a small calibration range was investigated. A refinement was then planned using a full calibration range. This method seems a more reasonable choice when the drug series utilised differ in

their physicochemical properties, as it does not carry the problems associated with other methods due to variable partitioning coefficients and differences in basicity.

2.3.2. Validation of UPLC-MS/MS method

2.3.2.1. Specificity and Chromatographic separations

Following determination of a suitable drug extraction method, the UPLC-MS was refined and an UPLC-MS/MS method developed in selected reaction monitoring (SRM) mode to detect all four analytes. The method was then validated, to enable quantification of atenolol, timolol and propranolol in ocular tissues. Selected reaction monitoring mode (SRM) of the most prominent MS² fragments for each of the analytes was selected as a suitable means of compound detection. For propranolol fragments were monitored at m/z of 155.03-155.13 and 182.96-183.06. For timolol fragments were monitored at m/z of 243.9-244.0 and 260.92-261.02 For atenolol fragments were monitored at m/z of 145.010-145.110 and 189.97-190.07. The internal standard, Levobunolol, was detected by monitoring a single fragment only, at m/z of 235.95-236.05. The method was selective for all of the three drugs under investigation and also for the internal standard, with limited background interference from the tissue matrix. This is illustrated by Figure 2-4 which shows representative chromatograms of a sample of the aqueous based vitreous humor spiked with 10ng/ml of atenolol, timolol, propranolol and the internal standard, levobunolol, Figure 2-5 which shows a representative spectra of the spiked vitreous humor and Figure 2-6 which shows a representative chromatogram of the vitreous humor without drug. In addition, this is also illustrated for a more lipophilic based tissue by Figure 2-7 which shows representative chromatograms of a sample of the aqueous based choroid spiked with 10ng/ml of atenolol, timolol, propranolol and the internal standard, levobunolol, Figure 2-8 which shows a representative spectra of the spiked choroid and **Error! Reference source not found.** Figure 2-9 which shows a representative chromatogram of the choroid without drug. All four drugs were eluted from the chromatographic column efficiently within 2 minutes of commencement of the run. The compounds were eluted from the column with increasing logP. Atenolol, the most polar compound with a logP of 0.16, was eluted first in just less than one minute, immediately before the mobile phase reached 100% 0.1% formic

acid in methanol. Subsequently, timolol (logP of 1.8) and then propranolol (logP of 2.4) were eluted one after the other due to structural similarities, a minute and a half into the run time. Finally, the most lipophilic compound investigated, propranolol with a logP of 3.56, was eluted just less than two minutes into the run. The total run time of the method was efficient, lasting just 3 minutes when compared to the method validated by Kadam et al in bovine tissue, where the total run time lasted 13 minutes (Kadam and Kompella 2009). Very slight shifts in retention time were noted when the ocular tissues matrix varied due to the differences in the physiological composition of each individual tissue (Figures 2-10-2-13).

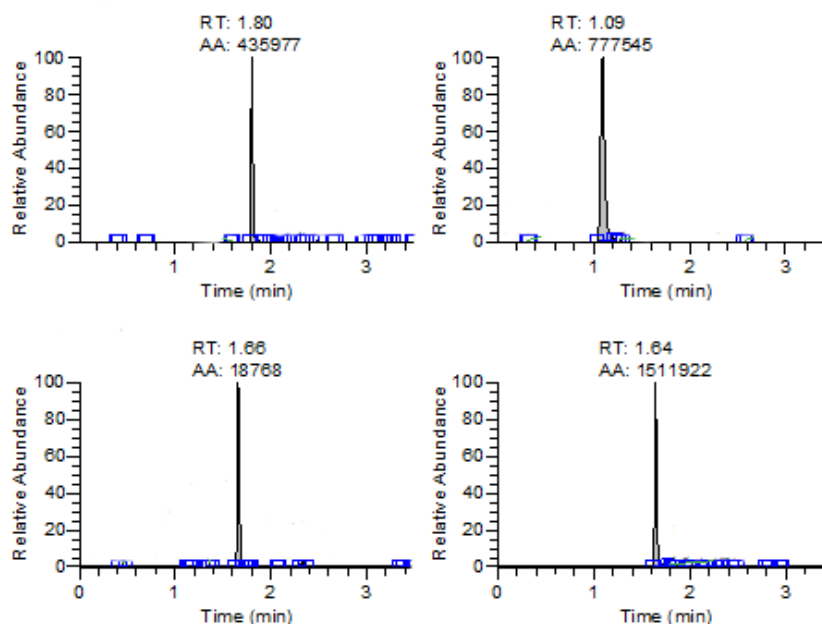


Figure 2-4 Representative UPLC-MS/MS chromatogram of timolol, atenolol, levobunolol and propranolol at a concentration of 10ng/ml in the aqueous based vitreous humor, at m/z of 260.92-261.02 for timolol, m/z of 145.010-145.110 and 189.97-190.07 for atenolol, 235.95-236.05 for levobunolol and 155.03-155.13 and 182.96-183.06 for propranolol, 243.9-244.0.

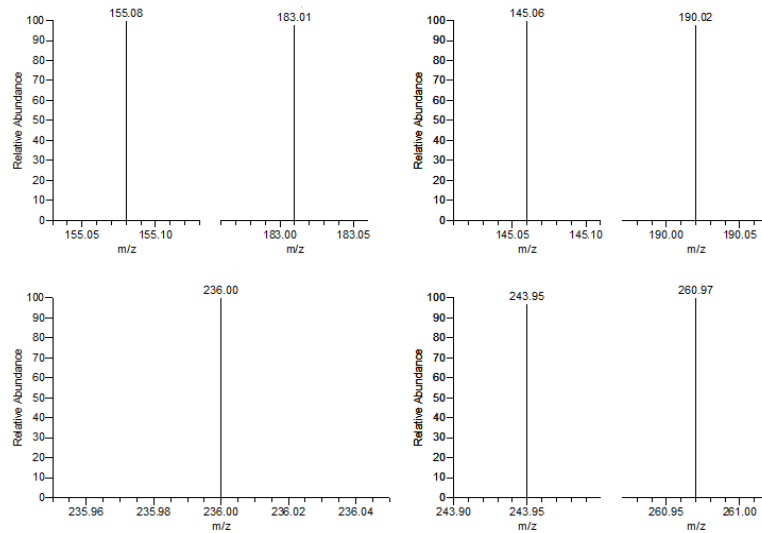


Figure 2-5 Representative UPLC-MS/MS spectra of timolol, atenolol, levobunolol and propranolol at a concentration of 10ng/ml in the aqueous based vitreous humor, at m/z of 260.92-261.02 for timolol, m/z of 145.010-145.110 and 189.97-190.07 for atenolol, 235.95-236.05 for levobunolol and 155.03-155.13 and 182.96-183.06 for propranolol, 243.9-244.0.

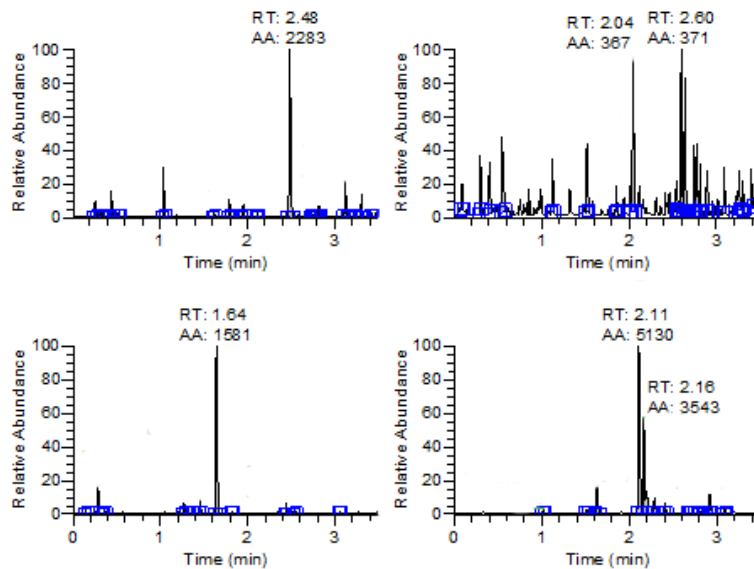


Figure 2-6 Representative UPLC-MS/MS chromatogram of blank sample of the aqueous based vitreous humor

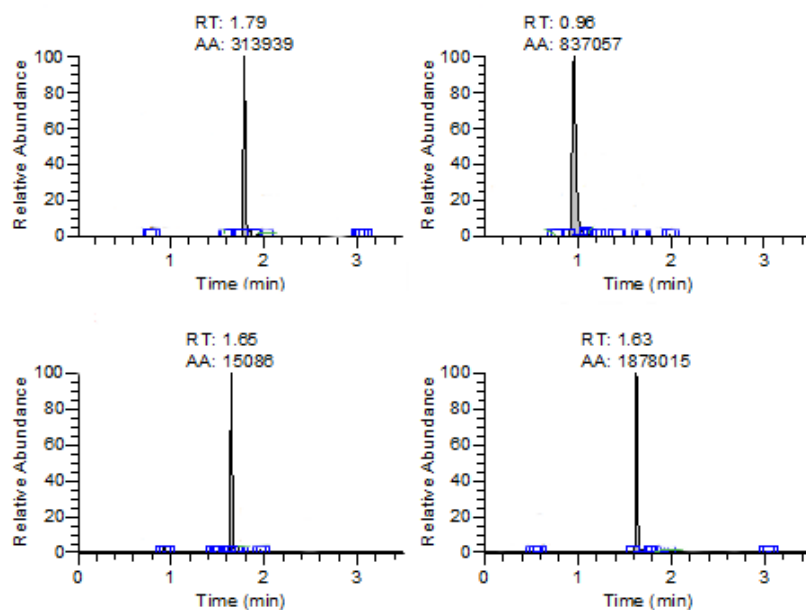


Figure 2-7 Representative UPLC-MS/MS chromatogram of timolol, atenolol, levobunolol and propranolol at a concentration of 10ng/ml in the lipophilic based choroid tissue, at m/z of 260.92-261.02 for timolol, m/z of 145.010-145.110 and 189.97-190.07 for atenolol, 235.95-236.05 for levobunolol and 155.03-155.13 and 182.96-183.06 for propranolol, 243.9-244.0.

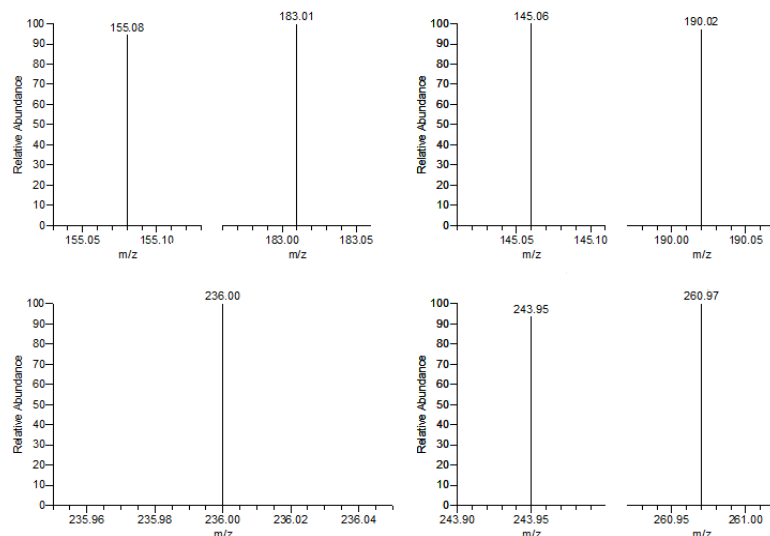


Figure 2.8 Representative UPLC-MS/MS spectra of timolol, atenolol, levobunolol and propranolol at a concentration of 10ng/ml in the lipophilic based choroid tissue, at m/z of 260.92-261.02 for timolol, m/z of 145.010-145.110 and 189.97-190.07 for atenolol, 235.95-236.05 for levobunolol and 155.03-155.13 and 182.96-183.06 for propranolol, 243.9-244.0.

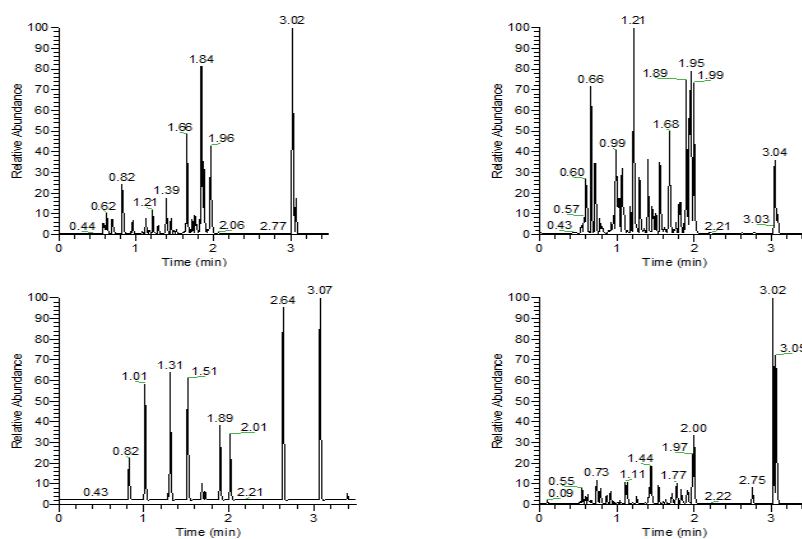


Figure 2-9 Representative UPLC-MS/MS chromatogram of blank sample of the lipophilic based choroid tissue.

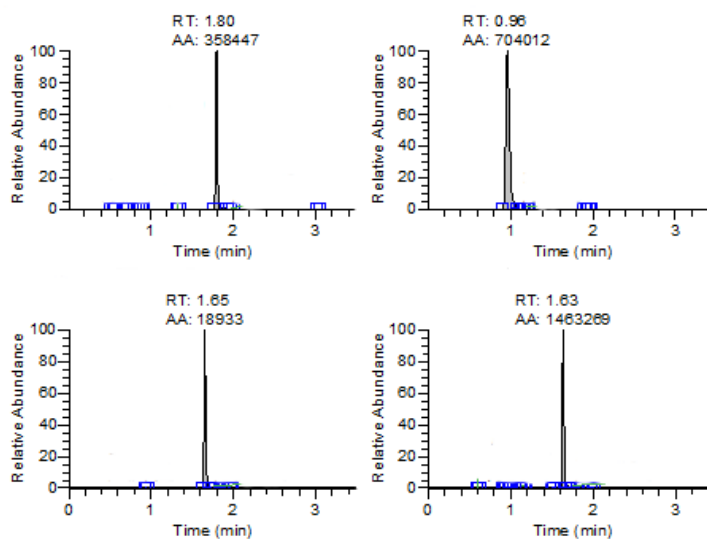


Figure 2.10 Representative UPLC-MS/MS chromatogram of timolol, atenolol, levobunolol and propranolol at a concentration of 10ng/ml in the retina, at m/z of 260.92-261.02 for timolol, m/z of 145.010-145.110 and 189.97-190.07 for atenolol, 235.95-236.05 for levobunolol and 155.03-155.13 and 182.96-183.06 for propranolol, 243.9-244.0.

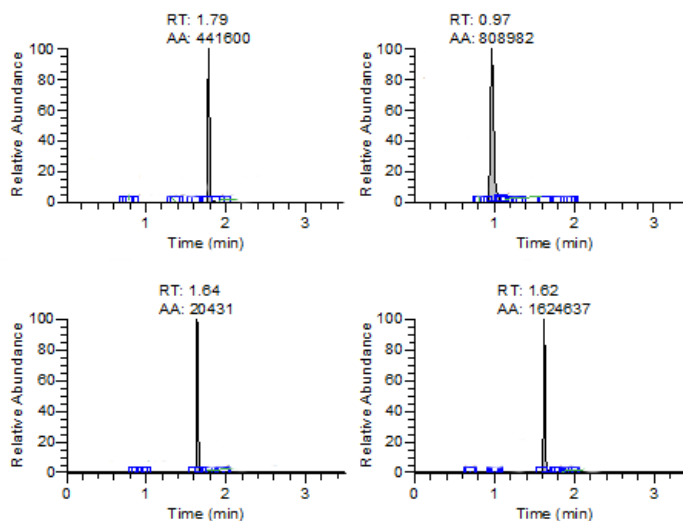


Figure 2-11 Representative UPLC-MS/MS chromatogram of timolol, atenolol, levobunolol and propranolol at a concentration of 10ng/ml in the aqueous humor, at m/z of 260.92-261.02 for timolol, m/z of 145.010-145.110 and 189.97-190.07 for

atenolol, 235.95-236.05 for levobunolol and 155.03-155.13 and 182.96-183.06 for propranolol, 243.9-244.0.

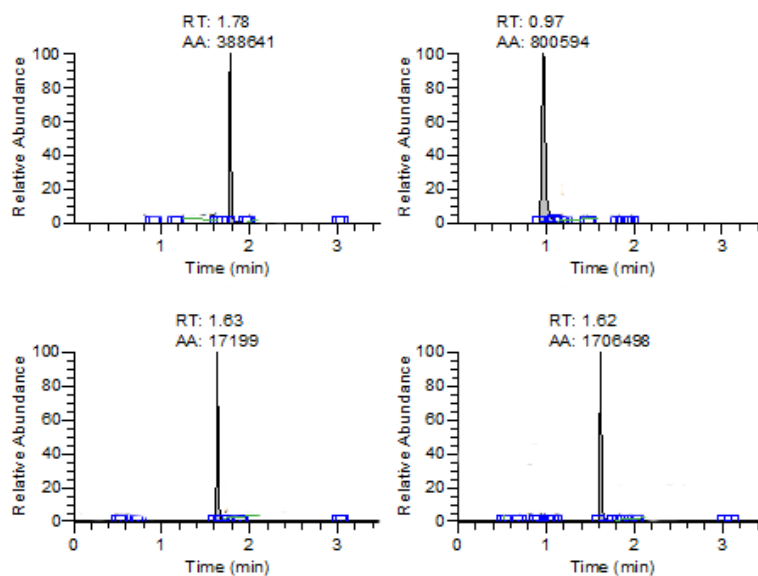


Figure 2-12 Representative UPLC-MS/MS chromatogram of timolol, atenolol, levobunolol and propranolol at a concentration of 10ng/ml in the lens, at m/z of 260.92-261.02 for timolol, m/z of 145.010-145.110 and 189.97-190.07 for atenolol, 235.95-236.05 for levobunolol and 155.03-155.13 and 182.96-183.06 for propranolol, 243.9-244.0.

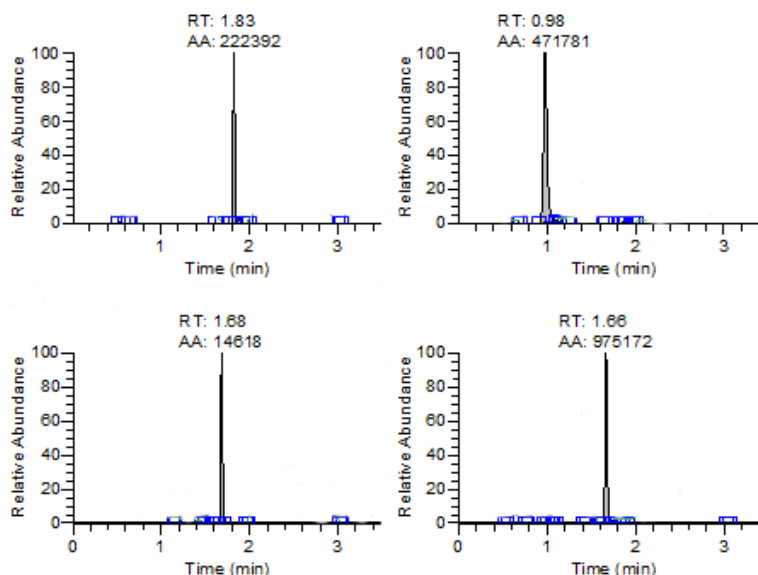


Figure 2-13 Representative UPLC-MS/MS chromatogram of timolol, atenolol, levobunolol and propranolol at a concentration of 10ng/ml in the iris and ciliary

body, at m/z of 260.92-261.02 for timolol, m/z of 145.010-145.110 and 189.97-190.07 for atenolol, 235.95-236.05 for levobunolol and 155.03-155.13 and 182.96-183.06 for propranolol, 243.9-244.0.

2.3.2.2. Method Linearity

A calibration curve was prepared for atenolol, propranolol and timolol individually, to determine linearity. The method was calibrated over the concentration range of 5-100ng/ml for each individual ocular tissue. To prepare the curve, the ratio of the peak area obtained for the drug compound to the peak area obtained for the internal standard was plotted (Table 2-3). Weighted linear regression of $1/x^2$ was selected as a suitable method for calibration, as this method applies focus to data points with lower variance in the calculation and as a result, has less dependence on data associated with high variance. This often makes weighted linear regression more valuable for use than a simple ordinary linear regression. Using ordinary linear regression, deviations at higher concentrations tend to have a greater an impact on the shape of the calibration curve than deviations at lower concentrations (Singtoroj, Tarning et al. 2006). It is often the case that when calibrating LCMS methods, standard deviation increases proportionally with increasing concentration and through the use of weighted regression, in particular $1/x^2$, concentrations at the lower end of the spectrum are more effectively estimated than in non weighted models (Nagaraja, Paliwal et al. 1999; Almeida, Castel-Branco et al. 2002). Using weighted linear regression, good correlation coefficients were obtained for all three drugs in the vitreous, retina, aqueous and lens tissues (>0.97). In the choroid sensitivity was lost at the lowest concentration in the calibration range and as a result, the calibration curve in this tissue was prepared in the range of 7.5-100ng/ml. The correlation coefficient obtained in the choroid tissue was good for atenolol however, for timolol and propranolol a slightly lower value was obtained. Similarly, for the iris and ciliary body tissue, good correlation coefficients were obtained for timolol and propranolol however, for atenolol a slightly lower value was obtained. Both the choroid and iris and ciliary body are thick, melanin rich tissues and as a result, the homogenisation process was more challenging than for the other

ocular tissues. The homogenate formed during tissue preparation was thick and not as clean as the other samples, which may account for the slight reduction in correlation coefficients obtained. In addition to this, basic drugs have been shown to bind well to melanin rich tissues, especially timolol (Leblanc, Jezequel et al. 1998; Koeberle, Hughes et al. 2003). It is possible that a proportion of each drug remained on the tissue and was not dislodged during the extraction process into methanol, accounting for the lower values obtained. Although the values obtained were reduced, values were still greater than the predetermined target of 0.96 and therefore calibration was deemed acceptable.

		Linear regression equation (n=2)	Correlation Coefficient (n=2)
Vitreous	Atenolol	$y=2.71162+3.4073*X$	0.9817
	Timolol	$y=7.81981+6.59161*X$	0.9791
	Propranolol	$y=0.796035+2.06723*X$	0.977
Retina	Atenolol	$y=-4.27061+4.73952*X$	0.9751
	Timolol	$y=-4.69802+8.65143*X$	0.976
	Propranolol	$y=-3.10002+2.47833*X$	0.9749
Aqueous	Atenolol	$y=4.39514+3.08618*X$	0.9837
	Timolol	$y=-1.6378+7.72167*X$	0.9758
	Propranolol	$y=-0.248882+2.0713*X$	0.9701
Choroid	Atenolol	$y=17.6048+2.79882*X$	0.974
	Timolol	$y=39.4333+6.26605*X$	0.9674
	Propranolol	$y=4.31751+1.44896*X$	0.9657
Iris and CB	Atenolol	$y=0.110765+4.31724*X$	0.9687
	Timolol	$y=1.18322+8.32138*X$	0.9795
	Propranolol	$y=-1.0003+1.9678*X$	0.9759
Lens	Atenolol	$y=3.98389+3.6281*X$	0.9789
	Timolol	$y=10.1346+7.29054*X$	0.9759
	Propranolol	$y=1.08502+1.83764*X$	0.9824

Table 2-3 Linear regression and correlation coefficient results of calibration of individual ocular tissues over a concentration range of 5-100ng/ml (n=2).

2.3.2.3. Precision and Accuracy determination

The accuracy and precision of the method was determined for each drug in each ocular tissue at 5, 30 and 100ng/ml, apart from in the choroid tissue where the 5ng/ml sample was excluded, due to complexity of the matrix. The percentage accuracy values were obtained by dividing the mean experimentally determined sample concentration by the expected drug concentration and are detailed in Table 2-

4. Precision was determined using the coefficient of variation by dividing the sample standard deviation by the mean sample concentration and multiplying by 100, the precision values obtained are detailed in Table 2-5 and 2-6. Acceptable accuracy was determined as a less than 20% deviation from the ideal value. For the vitreous, retina, aqueous, lens and iris and ciliary body, good method accuracy was achieved. For the choroid good accuracy was obtained at a concentration of 30ng/ml however, for atenolol the deviation in accuracy was slightly greater than 20% and for propranolol the deviation was 33%.

Intraday precision values were determined on the same day and interday precision values determined the following day. Acceptability of the precision values obtained was determined by the relative standard deviation (RSD) calculated for each drug at a concentration of 5, 30 and 100ng/ml in each ocular tissue. Good intraday precision was obtained for all three drugs at all three concentrations for the vitreous, retina, aqueous and choroid. For the iris and ciliary body slightly higher RSD values were obtained for atenolol at 5ng/ml and 30ng/ml and for timolol at a concentration of 5ng/ml. In the lens tissues, slightly higher RSD values were obtained for all three drugs at 100ng/ml and for atenolol at 30ng/ml. For the interday precision RSD values, again good results were obtained for all three drugs at all three concentrations for the vitreous, retina and aqueous. In the iris and ciliary body and lens tissues, although good values were obtained for all three drugs at 5 and 30ng/ml, slightly higher RSD values were measured at 100ng/ml. In the choroid tissue, acceptable values were obtained for all drugs with the exception of timolol at 30ng/ml, where the RSD was much greater than the rest.

As discussed previously, the nature of the choroid makes it a more difficult tissue to work with, in comparison to other ocular tissues. A key difficulty in the application of LCMS to analyse and quantify drug concentrations in biological tissue is the problem of matrix effects (Matuszewski, Constanzer et al. 1998; Matuszewski 2006). Matrix phenomena is an effect on the signal generated by the investigated analyte, due to either ion enhancement or ion suppression caused by the matrix the analyte is prepared in and this tends to occur at the lower end of the concentration range (Xu, Fan et al. 2007). The choroid differs greatly in chemical physiology from more hydrophilic ocular tissues, such as the vitreous humor and the aqueous humor,

which are water based tissues, and different tissues experience differences in the extent of matrix phenomena (Dams, Huestis et al. 2003). Previously, it has been demonstrated that matrix lipophilicity can have an impact on the extent of matrix effects experienced, with the application of a LCMS method in the quantification of a variety of antipsychotic drugs, validated in plasma tissue, shown to be subject to increased matrix effects when the method was applied to a more lipophilic tissue, the brain (Zhang, Terry Jr et al. 2007). In addition to increased effect with increasing lipophilicity, the selected sample preparation method also can influence the extent of matrix effects generated within the tissue and protein precipitation methods are often regarded as having the greatest risk of matrix effects due to the presence of residual tissue components in the sample (Dams, Huestis et al. 2003). The combination of both of these factors makes it extremely challenging to develop a suitable extraction method and an effective analytical method that will suit tissues of varying properties and a drug series of varying physicochemical properties. In this study six different ocular tissues with very different biological and chemical characteristics were under investigation and in addition, four drugs with distinct physicochemical differences were extracted from the tissues simultaneously. In light of this, for the accuracy and precision measurements, since outlying data was minimal and occurred in only the choroid tissue at the lower end of the concentration range, where greater variance can be tolerated, the accuracy and precision of the selected procedure was accepted. It was argued that outlying values would have minimal impact on the performance of the designed method for its intended purpose.

		ACCURACY (%)		
		5	30	100
VITREOUS	Atenolol	83.0	110.8	86.6
	Timolol	77.7	111.1	90.2
	Propranolol	79.4	108.1	86.8
RETINA	Atenolol	78.0	89.5	74.4
	Timolol	79.6	106.7	102.2
	Propranolol	80.8	94.6	96.0
AQUEOUS	Atenolol	110.4	95.5	99.6
	Timolol	109.5	87.1	88.8
	Propranolol	110.6	96.0	100.4
CHOROID	Atenolol		111.2	120.9
	Timolol		104.9	113.9
	Propranolol		102.0	132.8
IRIS AND CB	Atenolol	104.6	103.6	89.9
	Timolol	95.5	104.0	98.0
	Propranolol	102.3	102.1	109.2
LENS	Atenolol	82.4	93.5	93.5
	Timolol	82.5	96.3	95.8
	Propranolol	91.6	103.4	100.5

Table 0-1 Individual tissues results of accuracy of spiked ocular tissues at three concentrations (n=5).

		INTRADAY PRECISION	Concentration (ng/ml)			INTERDAY PRECISION	Concentration (ng/ml)		
			5	30	100		5	30	100
VITREOUS	Atenolol	Mean (n=5)	4.2	33.2	86.6	Mean (n=5)	4.1	32.0	89.0
		St Dev	0.5	5.4	9.9	St Dev	0.4	4.3	11.5
		RSD	12.2	16.2	11.4	RSD	9.1	13.5	12.9
	Timolol	Mean (n=5)	3.9	33.3	90.2	Mean (n=5)	3.8	32.9	93.9
		St Dev	0.6	5.0	11.5	St Dev	0.4	4.2	14.6
		RSD	15.0	15.0	12.7	RSD	11.0	12.8	15.6
	Propranolol	Mean (n=5)	4.0	32.4	86.8	Mean (n=5)	3.4	31.9	90.4
		St Dev	0.4	4.6	12.3	St Dev	0.4	3.8	15.2
		RSD	10.2	14.1	14.2	RSD	10.1	12.0	16.8
RETINA	Atenolol	Mean (n=5)	3.9	26.9	74.4	Mean (n=5)	3.7	26.8	75.5
		St Dev	0.4	5.0	10.6	St Dev	0.7	4.6	8.7
		RSD	9.7	18.6	14.2	RSD	18.5	17.0	11.5
	Timolol	Mean (n=5)	4.0	29.2	89.5	Mean (n=5)	4.3	28.6	86.6
		St Dev	0.5	4.7	13.8	St Dev	0.8	4.8	10.8
		RSD	12.2	16.2	15.4	RSD	18.7	16.9	12.4
	Propranolol	Mean (n=5)	4.0	27.5	86.2	Mean (n=5)	4.1	26.1	81.1
		St Dev	0.4	3.7	10.9	St Dev	0.6	4.1	10.8
		RSD	10.0	13.7	12.6	RSD	14.5	16.0	13.4
AQUEOUS	Atenolol	Mean (n=5)	5.5	28.7	99.6	Mean (n=5)	5.0	31.7	93.5
		St Dev	0.6	4.2	6.9	St Dev	0.8	5.3	12.6
		RSD	10.5	14.6	6.9	RSD	15.5	16.8	13.4
	Timolol	Mean (n=5)	5.5	26.1	88.8	Mean (n=5)	5.3	27.9	83.0
		St Dev	0.6	3.7	6.6	St Dev	0.5	4.0	11.3
		RSD	10.2	14.0	7.5	RSD	10.0	14.4	13.6
	Propranolol	Mean (n=5)	5.5	28.8	100.4	Mean (n=5)	5.4	30.6	93.5
		St Dev	0.7	4.4	6.6	St Dev	0.6	4.8	13.6
		RSD	13.0	15.3	6.6	RSD	12.3	15.7	14.6

Table 0-2 Individual tissues results of precision of spiked vitreous, retina and aqueous tissues (n=5).

		INTRADAY PRECISION	Concentration (ng/ml)			INTERDAY PRECISION	Concentration (ng/ml)		
			5	30	100		5	30	100
CHOROID	Atenolol	Mean (n=5)		33.4	120.9	Mean (n=5)		29.9	114.4
		St Dev		6.1	9.9	St Dev		5.9	14.2
		RSD		18.3	8.2	RSD		19.7	12.4
	Timolol	Mean (n=5)		31.5	113.9	Mean (n=5)		25.5	108.0
		St Dev		5.7	8.5	St Dev		11.2	13.0
		RSD		12.1	7.5	RSD		43.8	12.0
	Propranolol	Mean (n=5)		30.6	132.8	Mean (n=5)		30.6	132.8
		St Dev		5.7	13.8	St Dev		5.7	13.8
		RSD		18.5	10.4	RSD		18.5	10.4
IRIS/CB	Atenolol	Mean (n=5)	5.2	31.1	89.9	Mean (n=5)	5.5	31.6	85.0
		St Dev	1.3	3.6	19.1	St Dev	1.0	5.0	20.8
		RSD	25.1	11.6	21.3	RSD	19.5	15.7	24.5
	Timolol	Mean (n=5)	4.8	31.2	98.0	Mean (n=5)	5.0	31.8	91.4
		St Dev	1.4	3.8	20.4	St Dev	1.1	4.7	22.5
		RSD	30.0	12.2	20.8	RSD	21.6	14.7	24.6
	Propranolol	Mean (n=5)	5.1	32.8	109.2	Mean (n=5)	5.5	32.5	100.9
		St Dev	0.9	3.6	22.0	St Dev	1.0	3.8	26.1
		RSD	18.6	10.9	20.1	RSD	17.4	11.8	25.9
LENS	Atenolol	Mean (n=5)	4.1	28.1	93.5	Mean (n=5)	4.3	25.4	94.1
		St Dev	0.5	6.0	27.6	St Dev	0.7	5.4	21.5
		RSD	12.8	21.5	29.5	RSD	16.1	21.4	22.8
	Timolol	Mean (n=5)	4.1	28.9	95.8	Mean (n=5)	4.1	26.6	96.8
		St Dev	0.8	5.9	28.2	St Dev	0.8	5.2	22.0
		RSD	19.5	20.4	29.5	RSD	19.1	19.5	22.8
	Propranolol	Mean (n=5)	4.6	31.0	100.5	Mean (n=5)	5.2	30.8	101.3
		St Dev	0.7	2.4	28.9	St Dev	1.0	3.7	22.7
		RSD	14.8	7.8	28.7	RSD	18.3	11.9	22.4

Table 0-3 Individual tissues results of precision of spiked choroid, iris and ciliary body and lens tissues (n=5).

2.3.2.4. Recovery

Sample recovery was determined by dividing the mean sample concentration in each tissue standard by the mean concentration determined for the standard prepared in deionised water, the results of the recovery obtained for atenolol, timolol and propranolol from each tissue are detailed in Table 2-7. For all drugs prepared in all tissues, the deviation from 100% recovery was within acceptable limits. Slight ion enhancement effects were noted in some tissues, due to matrix effects. It has been noted previously, that analysing multiple compounds by mass spectrometry simultaneously, has been shown to result in a reduction in the ion intensity of the desired analyte and the extent of intensity reduction has been shown to be dependent on the chemical structure of the co-analyte (Tang and Kebarle 1993). The intensity of the ion detected can become both suppressed and enhanced and is dependent on the environment the analyte is contained within. (Taylor 2005) It is likely that both ion suppression and ion enhancement were a contributing factor in the recovery obtained for each analyte, with the recovery achieved was less than 100% for some samples, whereas for others recovery was greater than 100%. The extent of ion suppression can be influenced by the sample preparation method and also the chemical composition of the analyte. In the case of this experimental work, a simple protein precipitation method was selected as a fast and effective extraction method. Protein precipitation methods have been shown previously to experience greater problems with ion suppression effects when compared to certain solid phase extraction methods however, the use of a solid phase extraction method in this work would be extremely time consuming due to the sheer volume of individual tissue samples requiring preparation before subsequent analysis (Bonfiglio, King et al. 1999; Muller, Schafer et al. 2002). Although the extraction method can have an effect on ion suppression, the chemical structure of the analytes involved often has a much greater influence on suppression, with more polar compounds experiencing greater sensitivity to loss (Bonfiglio, King et al. 1999). In this instance there appears to be no distinct relationship between analyte polarity and ion suppression effects. Atenolol is the more polar of the drug series and in some samples showed ion suppression, but in others experienced ion enhancement. Often in validation, tissue

samples from various animals are pooled and homogenised for use in sample spiking, resulting in all samples having the same matrix effects (Taylor 2005). This was not the case in the present study, as for each tissue sample a different animal was used, perhaps leading a more pronounced effect on ion intensity. The differing matrix from sample to sample helps to explain the lack of pattern in ion effects across individual tissues. Although from a method validation point of view, having the same matrix effect across all tissues would be simpler, this would not be the case during a pharmacokinetic study where an individual animal is required for each time point. Using different tissue samples from different animals introduced the problem of intra-animal variability and as a result, differing matrix effects between samples of the same tissue subtype, thus making the present validation more realistic and relevant to the study in which it will be utilised.

			RECOVERY (%)		
			5	30	100
VITREOUS	Atenolol	Mean (n=5)	111.3	143.5	91.9
	Timolol	Mean (n=5)	98.8	122.5	79.2
	Propranolol	Mean (n=5)	92.9	130.1	83.2
LENS	Atenolol	Mean (n=5)	138.6	145.5	99.2
	Timolol	Mean (n=5)	131.0	133.9	91.0
	Propranolol	Mean (n=5)	111.1	123.1	96.1
RETINA	Atenolol	Mean (n=5)	93.9	148.1	107.6
	Timolol	Mean (n=5)	92.8	139.0	108.0
	Propranolol	Mean (n=5)	77.0	122.9	97.3
AQUEOUS	Atenolol	Mean (n=5)	154.5	114.5	96.2
	Timolol	Mean (n=5)	123.6	143.1	96.0
	Propranolol	Mean (n=5)	115.9	83.4	95.9
CHOROID	Atenolol	Mean (n=5)		144.7	92.7
	Timolol	Mean (n=5)		143.2	89.4
	Propranolol	Mean (n=5)		83.4	58.4
IRIS/CB	Atenolol	Mean (n=5)	101.9	129.0	126.6
	Timolol	Mean (n=5)	128.3	142.9	142.7
	Propranolol	Mean (n=5)	56.8	87.9	92.1

Table 2-7 Individual tissues results of recovery of spiked ocular tissues at three concentrations, determined from solutions of concentrations prepared in aqueous.

2.4. CONCLUSIONS

In this work a rapid UPLC-MS/MS method has been developed and validated for the quantification of atenolol, timolol and propranolol in the aqueous humor, the lens, the iris/ciliary body, the vitreous humor, the choroid and the retina. Although another method for quantifying this drug series in bovine tissue has previously been reported, this method has been validated in ovine tissue and offers the advantages of reduced sample run time, simpler drug extraction from tissue and therefore reduced sample preparation time. In addition this method can be used in a wide range of ocular tissues and will be extremely useful in the investigation of the pharmacokinetic movement of beta adrenoreceptor antagonists through both the anterior and the posterior eye.

CHAPTER 3. PHARMACOKINETIC STUDY OF A DRUG SERIES IN THE ISOLATED PERFUSED OVINE EYE

3.1. INTRODUCTION

The isolated perfused eye methodology was first developed by Gouras and Hoff, as a means of examining retinal function, ex-vivo, whilst maintaining arterial circulation and nutritional status within the eye (Gouras and Hoff 1970). Progressing on from this initial work, the isolated perfused eye has been used extensively in various animal models, including cat, rat, bull, horse, dog and frog, to monitor retinal changes and blood flow within the eye (Friedman and Marchese 1981; Ripps, Mehaffey et al. 1989; Su, Yu et al. 1995; Wiederholt, Bielka et al. 1995; Shiels, Sanderson et al. 1999). Sections of human eyes and whole human eyes have also been perfused and used to investigate the effects of prostaglandin analogues and TGF- β 2 on aqueous flow (Dijkstra, Schneemann et al. 1999; Gottanka, Chan et al. 2004). More recently, the isolated perfused eye has been utilised in pharmacokinetic (PK) studies as an alternative to performing ocular drug distribution studies on full animals. In the case of PK studies, the isolated perfused bovine eye appears to be the animal model of choice in most experiments. The bovine eye is frequently used for

perfusion studies due to its large size; this enables ease of handling and also makes the catheterisation procedure relatively straightforward. Studies on the isolated perfused bovine eye have shown tazarotenic acid penetration into the bovine sclera of perfused eye from polymer films and also memantine accumulation in the posterior section following topical drug application to the perfused eye (Koeberle 2002; Kek, Foulds et al. 2010). The isolated perfused eye offers several advantages when compared to using a full animal during a PK study. Advantages include the following: no anaesthetic requirements or concern over animal comfort, control over the physiological environment in which the eye exists in especially the temperature the eye is exposed to, reduced animal usage as waste eyes from the food industry can be utilised, controlled drug administration and a lack of movement of substances from systemic circulation into the ocular system (Niemeyer 2001). These advantages make the isolated model a useful alternative technique of measuring drug distribution within ocular systems. Alongside these advantages come the possible limitations of the model. Limitations include; a loss of neural control of the eye and also some differences between perfusion parameters selected and conditions typically experienced in vivo, are bound to occur (Yu, Su et al. 2003). It is important to keep these limitations to a minimum throughout the isolated perfused eye experiment by having tight control over factors such as the temperature of the eye, the positioning of the eye on the perfusion apparatus and the rate of arterial perfusion of the eye.

The isolated eye can be perfused using two methods; the constant arterial perfusion pressure method or alternatively the constant perfusion flow rate method. In the constant arterial perfusion pressure method, the arterial perfusion pressure (APP) is maintained at a set value and changes in the perfusion pressure are accommodated by adjusting the flow rate accordingly. The constant perfusion flow rate method is more straightforward and the eye is perfused at a predetermined flow rate throughout the entire experiment. A previous investigation carried out to investigate the impact of the selected method on the intraocular pressure (IOP) has been performed using the isolated bovine eye. The constant flow method was demonstrated to be more favourable, with the constant flow rate method adopting a better starting IOP of approximately 7 mmHg and having better stability in IOP readings throughout the experiment. On the other hand, the constant pressure

method had a higher starting IOP of approximately 9 mmHg and showed greater variability during the experiment (Wilson, Shahidullah et al. 1993). The requirement to adjust the APP during the perfusion experiment in order to accommodate changes in IOP is more challenging than simply maintaining a constant flow rate. In addition to this, increasing the perfusion pressure in the anterior bovine perfused eye model over the course of the experiment has been shown to have an effect on aqueous outflow. Increasing the perfusion pressure stepwise from 5 mmHg to 50 mmHg, increased aqueous outflow from 5 μ l/min to a peak of approximately 37 μ l/min, achieved at a perfusion pressure of 40 mmHg (Wiederholt, Bielka et al. 1995). Changes in aqueous humor outflow could potentially affect the flow and distribution of the investigated compounds around the eye, increasing the variability in the pharmacokinetics of the drugs. Therefore, taking these factors in to account, in this work the constant flow rate method was selected as a suitable means of perfusing the isolated eyes.

In this work, in a deviation from the norm of using bovine eyes, the isolated perfused ovine eye model was used. Ovine eyes have been used previously in isolated perfused eye experiments, to investigate physiological factors. Perfused ovine sclera stroma preparations have been used to investigate the effect of pH on the corneal stroma and have demonstrated that perfusion at acidic pH can cause corneal compaction (Doughty 2008). In addition to this, the isolated sheep choroid has been perfused to demonstrate carrier mediated uptake of neutral amino acids into the choroid across the blood-retinal barrier (Preston, Segal et al. 1989). The relative similarity of the ovine eye size and shape to human eyes, compared to the bovine and rabbit eye, make it a useful model in drug distribution studies. Ovine eyes are easy to handle and since the ciliary artery wraps clearly around the optic nerve, the artery is straight forward to isolate and the cannulation procedure uncomplicated. Our group has previously demonstrated the use of the isolated perfused ovine eye model, through the investigation of fluorescent microparticle distribution in the vitreous and drug distribution using time-of-flight secondary ion mass spectrometry (Mains, Wilson et al. ; Tan 2010). In this chapter, the isolated perfused ovine eye combined with the method of cassette dosing as a suitable means of generating ocular PK data, is presented for the first time, reducing both the number of animals required to be

utilised during the experimental work and analytical time. It has also been shown that drug lipophilicity plays an important role in the extent of ocular drug distribution, following drug administration via an intravitreal injection.

3.2. METHODS

3.2.1. Chemicals and reagents

Minimum essential medium eagle (M4655), sodium bicarbonate, atropine sulphate, ethylenediamine-tetra acetic acid (EDTA, free acid), penicillin G sodium salt, streptomycin, gentamycin free base, insulin from bovine pancreas, bovine holo-transferrin (siderophilin) iron saturated, sodium selenite, sodium hydroxide pellets and hydrochloric acid were all obtained from Sigma-Aldrich (Dorset, UK). Lactate dehydrogenase in vitro assay kit, lactate dehydrogenase, glucose solution, formic acid, atenolol, timolol maleate and propranolol hydrochloride were also all purchased from Sigma-Aldrich. Levobunolol was kindly provided by Allergan (Irvine, CA, USA). HPLC grade methanol was purchased from Fischer Scientific (Loughborough, UK).

3.2.2. Perfusion materials

A peristaltic cassette pump was obtained from Watson Marlow (Cornwall, UK). A waterbath to maintain a temperature of 37°C was purchased from Grant (Cambridge, UK). Quickfit coil condenser was purchased from Sigma-Aldrich (Dorset, UK). A perfusion chamber to hold eye was custom made from ACE glass incorporation (Vineland N.J) with an internal diameter 80 mm, depth of 120 mm and 13 mm opening at the bottom. Propylene filter funnel (65 mm mouth diameter) was purchased from Fisher (Loughborough, UK) A metal mesh holder to hold the eye was made in house. Nylon membrane filters (0.22 µm pore size, 25 mm diameter) were used to filter perfusion fluid before entry into eye and were purchased from Millex (Cork, Ireland). Tubings were used to circulate water from the water bath around the system and deliver perfusion fluid. Silcon tubings (9.5 mm, 0.76 mm and 1.6 mm inner diameter) were purchased from Portex (Dorset, UK), PVC tubing (5 mm inner diameter) was purchased from Fisher (Loughborough, UK) and tygon tubing (1.6 mm inner diameter) was purchased from Watson Marlow (Cornwall,

UK). 95% Oxygen /5% Carbon dioxide was purchased from Boc Medical (Manchester, UK). A pressure recording system was used to monitor intraocular pressure (IOP) and perfusion pressure and was composed of the following: pressure transducer and connecting cable (Medex, Dublin, OH, USA), signal conditioners CM015 10V bridge, adapters CM002 ADC16, data logger ADC16 and data logging software Picolog (Picotech, St Neots, UK). Finally, 23G needles were obtained from Neolus (Terumo, Surrey, UK).

3.2.3. Perfusion system design

An illustration of the design of the perfusion system is shown in Figure 3-1 and the perfusion system set up is shown in Figure 3-2. Throughout the experiment, a gas mixture of 95% oxygen and 5% carbon dioxide was bubbled through the perfusion fluid to maintain oxygen and carbon dioxide saturation. To ensure the perfusion fluid remained uniform, a magnetic stirrer was added to the beaker containing the perfusion fluid and was stirred throughout the experiment at a constant rate of approximately 500 rpm, using a magnetic stirrer plate. A water bath was used to maintain the eye at physiological temperature of 37°C and to also warm the perfusion fluid before entry into the eye, by circulating water from the bath through a quickfit coil condenser and then through the custom made perfusion chamber, before returning back into the water bath. The perfusion fluid was then pumped through tygon tubing at the desired rate from the beaker using a peristaltic pump. The perfusion fluid was then passed through the quickfit coil condenser to a 0.22 µm nylon filter membrane before entering the isolated ovine eye. Connected to the filter via a three way stopcock, was a bubble trap and pressure transducer. This was used to monitor the APP.

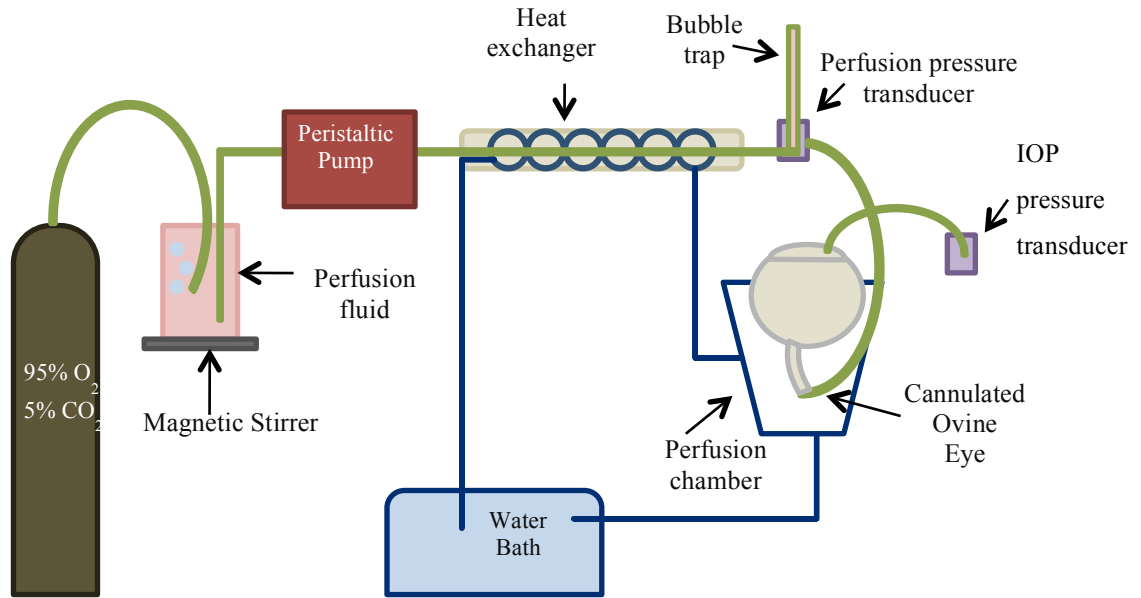


Figure 3-1 An illustration of the set up and design of the isolated ovine eye perfusion system.

The custom-made perfusion chamber was used to accommodate the isolated ovine eye and was fitted with a wire mesh moulded over the top of the chamber to hold the eye in place. Directly under the mesh, a filter funnel (65 mm mouth diameter) was placed within the chamber to collect the venous perfusate draining from the eye. Identical perfusion systems were aligned in triplicate in order to perform three perfusion experiments simultaneously.

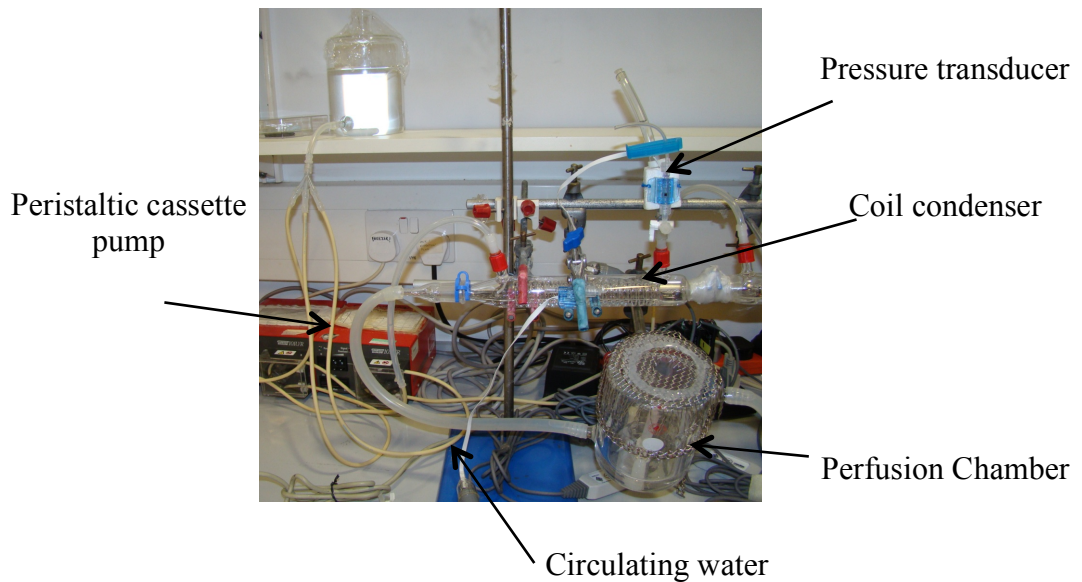


Figure 3-2 Photograph detailing the isolated ovine eye perfusion system in the laboratory.

3.2.4. Perfusion Fluid

The perfusion fluid was prepared based on a method detailed previously by Koeberle et al and originally based on a method developed for perfusion studies using the isolated bovine eye by Coo et al (Coo, Zonnenberg et al. 1993; Koeberle, Hughes et al. 2006). Using serum-free minimal essential culture medium as the main building block of the perfusion fluid, Coo et al supplemented the culture medium with various additives and showed that isolated bovine eyes could remain viable for up to 9 days on delivery of the perfusion fluid into the ciliary artery of the bovine eye (Coo, Zonnenberg et al. 1993). The composition of the perfusion fluid is detailed in Table 3-1 and lists the composition of the original serum-free minimal essential culture medium and the additional additives that were used to supplement and enhance the medium. Antibiotics were added in order to reduce the risk of a bacterial growth and contamination in both the medium and the perfused eyes. Ethylenediamine-tetraacetic acid, insulin, holo-transferin and sodium selenite were added in order to maintain regular cell function and to ensure perfused eyes remained viable over the course of the study. Following addition of the additives and in order to oxygenate the perfusion fluid, the perfusion fluid was saturated with a gas mixture of 95% oxygen and 5% carbon dioxide for 45 minutes prior to use. The pH of the

perfusion fluid was then adjusted to pH 7.4 using a 1M solution of sodium hydroxide to mimic physiological pH. The complete perfusion fluid was then stored at 2-8°C for a maximum of 2 days before utilisation.

Chemical	Concentration	Physiological Role
Inorganic salts (g/l)		
CaCl ₂	0.2	Plasma electrolyte
MgSO ₄	0.09767	Plasma electrolyte
KCl	0.4	Plasma electrolyte
NaHCO ₃	2.2	Plasma electrolyte
NaCl	6.8	Plasma electrolyte
NaH ₂ PO ₄	0.122	Plasma electrolyte
Amino acids (g/l)		
L-Alanyl-L-Glutamine	0.4344	Protein metabolism
L-Arginine	0.126	Protein metabolism
L-Cystine	0.0313	Protein metabolism
L-Glutamine	0.292	Protein metabolism/Neurotransmitter
L-Histidine	0.042	Protein metabolism
L-Isoleucine	0.052	Protein metabolism
L-Leucine	0.052	Protein metabolism
L-Lysine	0.0725	Protein metabolism
L-Methionine	0.015	Protein metabolism
L-Phenylalanine	0.032	Protein metabolism
L-Threonine	0.048	Protein metabolism
L-Tryptophan	0.01	Protein metabolism
L-Tyrosine	0.0519	Protein metabolism
L-Valine	0.046	Protein metabolism
Vitamins (g/l)		
Choline chloride	0.001	Neurotransmitter synthesis
Folic acid	0.001	DNA synthesis
myo-Inositol	0.002	Cell signalling
Niacinamide	0.001	ATP synthesis
D-Pantothenic acid	0.001	Coenzyme-A synthesis/metabolism
Pyridoxal	0.001	Amino acid metabolism
Riboflavin	0.0001	Metabolism
Additives		
Sodium bicarbonate	2.2 g/l	Buffer/Plasma electrolyte
Atropine sulphate	0.005 g/l	Anticholinergic/Mydriatic
Ethylenediamine-tetraacetic acid	0.2922 g/l	Anticoagulant/vasodilator
Penicillin G	100 kU/l	Antibiotic
Streptomycin	75.6 kU/l	Antibiotic
Gentamycin	0.08 g/l	Antibiotic
Insulin Bovine	50 U/l	Glucose regulation
Bovine holo-transferin	0.0025g/l	Iron binding and transfer
Sodium Selenite	2.4 µg/l	Essential element

Table 3-1 Perfusion media composition.

3.2.5. Ovine eye cannulation procedure

Ovine eyes were collected on ice from a local abattoir, within an hour to a maximum of two hours of slaughter. On arrival into the laboratory, eyes were warmed to room temperature. Each eye was then inspected for suitability with each eye requiring corneal transparency, general eyeball turgidity and aqueous chamber turgidity. Any eyes with visible ocular infection, ocular damage or poor corneal transparency were immediately excluded and discarded. Suitable eyes were then placed on petri-dishes and washed to remove excess blood with approximately 5 ml of the perfusion fluid. Initially any remaining parts of the animal's eye lids were removed using dissection scissors and the extraorbital muscles and excess extraorbital tissue cut away and discarded. One of the long ciliary arteries which typically wrap around the optic nerve was identified and isolated from the optic nerve. One long posterior ciliary artery was cannulated, as within the eye, the lateral and medial ciliary arteries merge. It has previously been reported that no difference in ocular blood flow occurred when both arteries were perfused, when compared to the perfusion of one artery only (Shiels, Sanderson et al. 1999). In the ovine eye, the long posterior arteries supply the iris, ciliary body and anterior choroid and also branch out to form the short posterior arteries, which supply the posterior choroid (Cioffi, Granstam et al. 2003). The long posterior ciliary arteries also provide a reinforcing branch to the choroidoretinal artery and this vessel supplies the choroid and the retina via the retinal arterioles, which branch out from the choroidoretinal artery (Simoens and Ghoshal 1981). In previous ocular perfusion studies, perfusion of one of the ciliary arteries has been shown to maintain the viability of the eye over a prolonged time period with slow deterioration of Bruch's membrane (Coo, Zonnenberg et al. 1993; Wilson, Shahidullah et al. 1993) and maintenance of oxygen and glucose consumption, indicating retinal tissue perfusion. Excess tissue around the ciliary artery was trimmed away to make the artery itself more accessible and the ciliary artery was then straightened out. The ciliary artery was then secured using braided silk wax surgical suture and the suture pulled taught, stretching out the artery. A small incision was made in the ciliary artery, in order to facilitate cannula insertion. A small piece of plastic tubing was used as a flexible cannula and was narrowed at both ends before attachment to a longer piece of flexible tubing. The

cannula and tubing were filled with perfusion fluid before being inserted into the eye, to ensure no air bubbles were introduced into the eye via the ciliary artery on delivery of the perfusion fluid. Air bubbles entering the eye could potentially result in the formation of an embolism in the blood vessels and as a result, render the eye unusable. The cannula was then inserted into the ciliary artery at the point in incision and gently pushed approximately 20 mm into the artery (Figure 3-3). To complete the cannulation process, the cannula was finally secured by tying a small piece of suture around the inserted cannula. This process was repeated twice, to ensure the cannula was tightly secured in the ciliary artery.

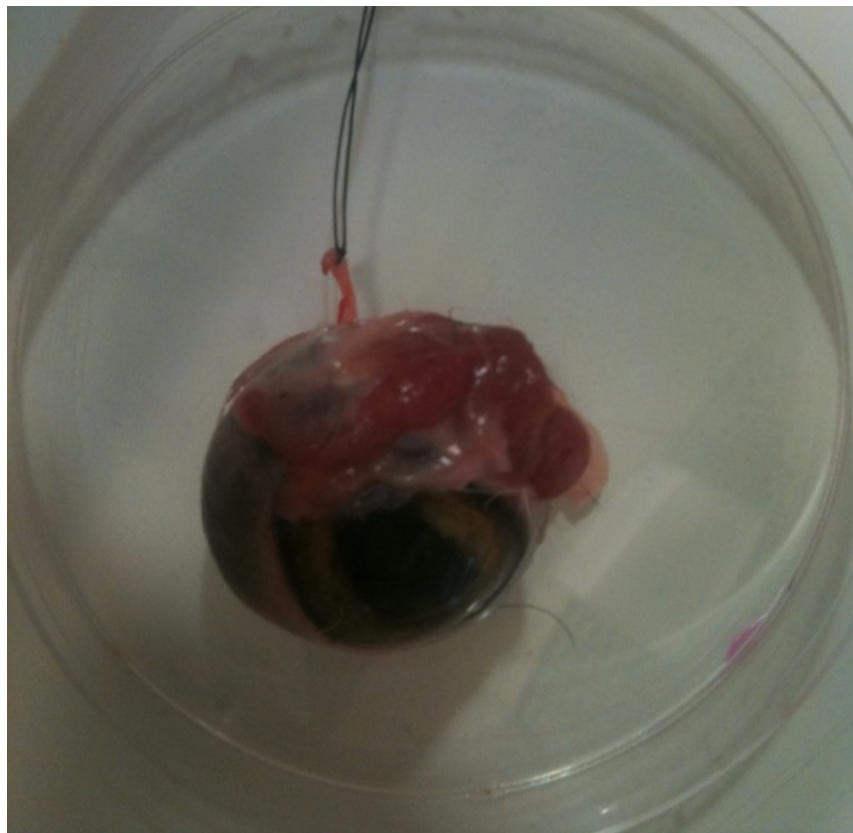


Figure 3-3 The isolated ovine eye with separated ciliary artery for cannulation.

3.2.6. Perfusion procedure

The eye was placed on the stage of the perfusion system on its side, with the cornea facing outwards, to mimic typical in vivo eye positioning. The cannula and the tubing were then attached to the filter of the perfusion fluid port. (Figure 3-4). The eye was then washed a second time with approximately 5 ml of the perfusion

fluid. In order to prevent the eye dehydrating during the course of the experiment and to help maintain the temperature of the eye at 37°C, a piece of polyethylene film (cling film) was used to cover the ovine eye, creating a seal around the perfusion chamber. The perfusion process was then initiated by starting the peristaltic pump, to deliver the perfusion fluid at an initial rate of approximately 0.2 ml/minute. At this point the isolated ovine eye was inspected for ocular flow, by checking the vortex veins for exit of the perfusion fluid from the eye. Occasionally no flow was detected from the vortex vein and this was typically due to a blockage in vein caused by blood clotting. In this instance it was necessary to make a small incision in the vortex vein in an attempt to stimulate flow. After the incision had been made, if flow was still not detected, the eye was deemed unsuitable and disposed of. The flow rate of the perfusion fluid was then steadily and gradually increased over the course of a 30 minute period to the maximum flow rate of 1 ml/minute.



Figure 3-4 Photograph of the perfusion system in operation using an isolated ovine eye.

3.2.7. Viability Parameters

During the perfusion procedure, certain viability parameters were monitored to ensure the eye was successfully perfused and maintained flow throughout the course of the experiment. The parameters monitored throughout were the arterial perfusion pressure, the intraocular pressure (IOP), glucose consumption and lactate dehydrogenase (LDH) activity.

APP is the pressure at which blood flows into the eye via the artery. In the isolated perfused eye, the APP gives an indication of resistance to flow of the perfusion fluid through the eye. The APP can also indicate damage to the blood-aqueous barrier and blood retinal barrier (Raviola 1977). For this reason, APP must be maintained at a minimum level to ensure ocular flow systems are in operation, without reaching too high an APP which could potentially damage the eye and render the perfusion procedure unsuccessful. Increases in APP can also be indicative of a blockage in either the cannula, inserted into the artery, or in the artery supplying the eye and again this would compromise the effectiveness of the perfusion procedure. As a result of this information, in order for a perfused ovine eye to be deemed viable, following the equilibration period where the maximum perfusion flow rate was achieved, arterial perfusion pressure had to be maintained below 60 mmHg throughout the experiment, with a maximum drift in pressure of 6 mmHg at any time.

IOP is created by the pressure exerted from the generation and the drainage of the fluid based structure of the eye, the aqueous humor and the vitreous humor. Aqueous humor drainage occurs through the trabecular meshwork, with a constant IOP suggesting effective drainage. It has been shown that aqueous outflow could be maintained in an isolated perfused eye, without significant disruption over a period of several hours. However, on increasing IOP the aqueous outflow was reduced, demonstrating that IOP is an effective method of determining normal aqueous humor function (Erickson-Lamy, Rohen et al. 1988). In light of this and in order for a perfused eye to be deemed viable, effective drainage of the aqueous humor had to occur. Following the equilibration period where the maximum perfusion flow rate

was achieved, for the perfusion of the eye to be successful the intraocular pressure had to remain below 10 mmHg throughout the experiment

Glucose is a simple sugar formed in breakdown of complex carbohydrates and is used as a key source of energy in the body. Glucose uptake into cells is controlled by both facilitated diffusion, through several glucose transporters, and also by active transport (Widmaier, Raff et al. 2004). Changes in glucose consumption in response to tissue damage are trivial and it is only when the tissue becomes severely damaged that changes in glucose levels become detectable. Therefore, throughout the perfusion study, glucose consumption was not regarded as a marker of cell death but rather as a measure of perfusion effectiveness (Koeberle 2002). In some cases, during the initial cannulation procedure, the cannula may not be fully inserted into the ciliary artery and pierce through the artery into the surrounding tissue, resulting in incomplete fluid flow within the eye. This can be difficult to visualise and may not be obvious from the other viability measurements. The perfusion procedure was regarded as effective if the glucose concentration in the venous perfusate was lower than the concentration measured in the perfusion media, indicating glucose uptake into cells.

LDH is a cytoplasmic enzyme, involved in the metabolic generation of adenosine triphosphate (ATP) from nutrients. Specifically, LDH is involved in the catalytic conversion of pyruvate to lactate under anaerobic conditions. LDH is typically found in the intracellular environment however, upon cell lysis LDH is released into the extracellular environment and for this reason, extracellular LDH activity is often used as an indicator of tissue damage. LDH is a widespread enzyme in body and for this reason, increased levels of LDH activity represents a non specific indicator of cell death. LDH has been used as a marker of cell integrity in the bovine cornea and it has been shown that LDH activity can change and be detected after damage (Doughty 1997). Monitoring changes in LDH activity in the isolated perfused eye can indicate if the perfusion procedure has been successful, as high levels of LDH leakage, in response to tissue damage, can be detected even from a small mass of tissue (Drent, Cobben et al. 1996). During the initial stages of preparing the isolated eye for perfusion, a large increase in LDH activity would be expected in response to the cannulation procedure, however following on from this,

the LDH levels should begin to decline. Levels of LDH measured in the perfusate should be considered relatively in each individual eye and not to an absolute value. Therefore, the perfusion procedure was deemed to be successful if LDH levels measured in the perfusate were lower than those measured in the initial stages of the perfusion (Dijkstra, Schneemann et al. 1999). If two consecutive LDH readings were larger than the LDH value determined at the start of the perfusion, the eye was discarded.

3.2.7.1. Arterial Perfusion pressure

In order to monitor the arterial perfusion pressure in the isolated ovine eye, a pressure transducer was connected to a three-way stop clock, which was then attached to the cannulated ovine eye via plastic tubing. At the opposite end of the transducer, plastic tubing filled with perfusion medium and free of air bubbles was attached to create a seal. The pressure transducer was connected to a laptop and pressure was monitored using the Picolog data-logging system (Picotech, St Neots, UK). The arterial perfusion pressure was monitored and recorded every second from the moment the cannulated ovine eye was connected to the perfusion kit to the completion time point of the experiment.

3.2.7.2. Intraocular pressure

To measure intraocular pressure, a 23 gauge needle was attached to 150 mm length of plastic tubing and filled with perfusion medium, free from air bubbles. The plastic tubing was attached to a pressure transducer and a plastic stopper was inserted into the opposite end of the pressure transducer to create a tight seal. The pressure transducer was connected to a laptop and pressure was monitored using the Picolog data-logging system (Picotech, St Neots, UK). After perfusion of the isolated ovine eye had commenced and 40% of the maximum perfusion flow rate had been achieved, the needle was inserted into the centre of the anterior chamber through the outer edge of the cornea (Figure 3-5). In order to avoid siphoning effects and prevent differences in the accuracy of intraocular pressure measurements between experiments, the pressure transducer was positioned at the same height, in parallel to the isolated ovine eye. The intraocular pressure was monitored and recorded every

second from the moment of needle insertion into the anterior chamber to the completion time point of the experiment.



Figure 3-5 An isolated ovine eye in operation on the perfusion system illustrating the needle inserted into the anterior chamber to monitor intraocular pressure.

3.2.7.3. Glucose Consumption

The concentration of glucose contained within the venous perfusate of the isolated ovine eye was measured using a glucometer. Before determining glucose concentrations in the perfusate, the glucometer was calibrated in triplicate using glucose standard solutions in the concentration range of 0.6 g/L to 1 g/L. Glucose standard solutions were prepared by adding the required volume of glucose standard solution (Sigma-Aldrich, UK) to 900 μ l of fresh perfusion medium to create a final

standard volume of 1000µl. Using a fresh glucose test strip (Medisense Optium Plus test strips, Abbott, UK) for each measurement, 5 µl of calibration solution was placed on the end of the test strip and the glucose reading was measured and recorded. During each perfusion experiment, the venous perfusate was collected every 30 minutes and the glucose concentration in the perfusate was determined.

3.2.7.4. Lactate Dehydrogenase activity

The LDH activity in the venous perfusate of the isolated perfused ovine eye was measured using an LDH based in vitro assay kit (TOX7, Sigma-Aldrich, UK) and measured using ultraviolet-visible (UV) spectroscopy. In order to prepare the LDH assay kit for analysis, initially the LDH assay cofactor was prepared by adding 25 ml of deionised water to the lyophilized cofactor provided in the assay kit. The LDH assay mixture was then prepared by mixing equal volumes of the LDH assay cofactor solution with the LDH assay substrate solution and the LDH assay dye solution. Before determining LDH activity in the perfusate, the UV spectrometer was calibrated in triplicate, using LDH standard solutions in the concentration range of 0.3 to 1 U/ml. LDH standard solutions were prepared by adding 25 µl of the required volume of LDH standard solution (Sigma-Aldrich, UK), prepared to the required concentration in fresh perfusion medium, to 75 µl of the prepared LDH assay kit and then diluted in 750 µl of fresh perfusion medium. The prepared solution was then covered in aluminium foil, to prevent any light degradation, and incubated for 20 minutes. Following the incubation period, in order to terminate the reaction, 85 µl of 1M HCl was added to the solution. Standard solutions were then analysed by measuring the UV absorption of the solution at 490 nm. During each perfusion experiment, the venous perfusate was collected every 60 minutes to determine the LDH activity. Venous perfusate samples were prepared and UV absorbance was measured using the same method used for the calibration solutions and subsequently, LDH concentration in the venous perfusate was determined.

3.2.8. Intravitreal injection

To investigate the impact of physicochemical properties on drug disposition following intravitreal administration, three different beta adrenoreceptor antagonists

were used (Table 2.1). All three beta adrenoreceptor antagonists were administered to the eye in a cassette. A solution containing atenolol, timolol and propranolol each at a concentration of 5 mg/ml was prepared by weighing 25 mg of each drug and dissolving them in 1 ml of deionised water. The three 1ml solutions were then combined and deionised water was added, to create a final solution volume of 5ml. The solution was then passed through a 0.22 µm syringe filter to remove any particulates. Once the eye had reached maximum perfusion rate and APP and IOP was maintained, the drug cassette was administered into the vitreous. The dose delivered to the eye was 500 µg of each of the three drugs in a total injection volume of 100 µl. The injection was performed using a 1ml syringe and 23G needle, inserted 5 mm into the vitreous approximately 3 to 4 mm from the limbus in the posterior direction. Following injection, the needle was drawn very slowly from the eye in order to minimise leakage from the injection site.

3.2.9. Study Design and tissue processing

In this study, a 100 µl intravitreal injection was performed on twenty five isolated perfused eyes. At 1, 2, 3, 5 and 7 hours post dose, perfusion was terminated and the aqueous humor collected from the eye for analysis. Following removal of the aqueous humor from the eye it was immediately frozen in liquid nitrogen. Whilst frozen the lens, iris and ciliary body, vitreous humor, retina and choroid were collected, using the method detailed in chapter two of this thesis.

The weight of each tissue was recorded and all tissues were transferred into 16mm screw top plastic vials. Tissues were then homogenised and prepared for analysis using the method detailed in chapter two of this thesis. Tissue concentrations were determined also using the method detailed in chapter two of this thesis. From this the mean concentration at each time point was calculated, along with the standard deviation and the relative standard deviation. In order to test for statistically relevant changes in tissue drug concentrations with time, one-way analysis of variance (ANOVA) was performed on the data using Minitab Statistical Software version 16. Differences in tissue concentrations were considered significant when the p value obtained was less than 0.05 ($p < 0.05$).

3.3. RESULTS AND DISCUSSION

3.3.1. Number of successfully perfused eyes

In order for an eye to be successfully perfused, all of the viability criteria detailed in section 3.2.7 had to be met. In order for a pharmacokinetic study to produce reliable results, the number of animals used should be sufficient enough to account for population variability and typically for small animal studies, 3-4 animals are required per time point (FDA 2000). Defining the actual number of animals required is often based on achieving a set target goal of statistical significance (normally $p < 0.05$) and in most cases, a minimum of 5 animals per time point are required (Eckelman, Kilbourn et al. 2007). In the case of the isolated perfused eye, the successfulness of the perfusion procedure depended on the perfused eye meeting the strict viability conditions and as a result, successfully perfusing a larger number of eyes can become quite a challenging and time consuming process. In light of this, it was decided that the PK study would include 5 time points, with a minimum of three eyes per time point; however it was desirable the five eyes were successfully perfused per time point. The number of eyes perfused per time point is summarised in Table 3-3. Five eyes were successfully perfused per time point, improving the statistical reliability of the results. Using the perfusion method, it was demonstrated that ovine eyes can be successfully perfused and remain viable over a period of one to seven hours. During the perfusion experiment only eyes that met the predetermined viability criteria were utilised and as a result, numerous eyes had to be discarded after the perfusion procedure had commenced, due to the viability conditions not being achieved. The main viability parameter resulting in the perfusion procedure to fail was the APP. On numerous occasions the APP was initially greater than 50 mmHg, at the starting low flow rate. On increasing flow rate, the APP increased to above the defined limits, most likely due to a blockage in one of the blood vessels, and the perfusion procedure had to be terminated and the eye discarded. Although a less frequent cause of perfusion failure, the IOP was also a factor in the successfulness of the perfusion. During the course of the perfusion experiments, some eyes had to be discarded due to the IOP of the eye increasing to greater than 10 mmHg.

Perfusion time (hours)	Number of eyes successfully perfused
1	5
2	5
3	5
5	5
7	5
Total	25

Table 3-2 Number of successfully perfused eye for each time point investigated within the study

3.3.2. Tissue weights

The mean weights of each tissue for each time point (n=5) and the average overall weight of each tissue (n=25) are summarised in Table 3-4. For some tissues the differences in weight across the eyes samples were relatively consistent, whereas for other tissues the difference in weight was large. Differences in tissue weights across the eye samples are due to both inter-animal variability and the dissection procedure. For tissues with a well defined outer perimeter, the vitreous and the lens, the weights were consistent and the relative standard deviation (RSD) was less than 9%. These tissues are obvious compartments and large in size, therefore they are easy to separate. For less well defined tissues, the choroid, the retina and the iris and ciliary body, the RSD was higher. In these tissues the dissection procedure can be more challenging and as a result the relative standard deviation measured was higher, sitting between 20% and 30%.

For the aqueous tissue, the tissue weights measured were significantly less consistent and a much higher RSD of approximately 48% was recorded. The high RSD achieved is unlikely to be mainly due to inter-animal variability and is most likely due to leakage of the aqueous humor from the needle inserted into the anterior chamber to monitor IOP. During the experiment, leakage of the aqueous humor from the needle insertion site was not obvious visually and the stability of the IOP measurements suggests that the aqueous humor did not escape from the aqueous chamber during the course of the experiment. In the initial few perfusion experiments carried out, the needle measuring the IOP was first removed and immediately following on from this, the needle used to extract the aqueous humor was inserted and the aqueous humor was removed. Using this method, it was noted

that the volume of aqueous humor removed from the anterior chamber was low and on removal of the needle inserted to measure IOP, the aqueous humor began to seep out of the hole in the cornea created by the needle, and therefore, it was decided at this point to alter the method of aqueous humor removal. As a slight modification, the needle inserted to extract the aqueous humor was first inserted into the anterior chamber and the aqueous humor was removed before removing the needle measuring the IOP. This slight alteration in the method was beneficial, preventing aqueous humor leakage and as a result, larger volumes of aqueous humor were extracted from the remaining eyes.

Although the individual tissue weights varied between eyes and as a result, the total weight of each eye differed, it was decided that a standard injection of 500 µg of each of the three drugs in 100 µl of deionised water would be given and weight adjustment relative to each individual eye would not be carried out. The main reason for deciding to conduct the experiment in this manner was due to issues with timings. In order to provide the greatest chance of successful eye perfusion, if possible, three eyes were simultaneously perfused and it was essential that the eyes were perfused as quickly as possible following slaughter. Weighing each individual eye and correspondingly adjusting the dose of drug mixture to be administered would have delayed the perfusion process and would have impacted on the number of eyes successfully perfused. It was often the case that, on perfusion, several eyes would fail to meet the criteria and have to be discarded. Therefore, it was essential that on failure the eye was removed as soon as possible and a replacement eye perfused quickly, without the need for having to reweigh the new eye and calculate a suitable dose. Due to slight differences in tissue weights across the animals used in this work and the administration of a standard dose, differences in tissue concentrations measured were inevitable. However, it was anticipated that the magnitude of this difference would be minimal. As a result, in order to make the results of each individual drug in each tissue comparable, results are reported in terms of concentration per gram of tissue.

Tissue	Time point		Standard	
	(hours)	Mean	Deviation	% RSD
Vitreous	1	4.456	0.620	13.920
	2	4.562	0.182	3.984
	3	4.408	0.489	11.097
	5	4.283	0.237	5.531
	7	4.254	0.323	7.602
	Sum	4.393	0.387	8.808
Aqueous	1	0.474	0.228	48.179
	2	0.251	0.200	79.648
	3	0.399	0.221	55.245
	5	0.477	0.152	31.914
	7	0.577	0.156	27.006
	Sum	0.436	0.209	47.907
Lens	1	0.853	0.039	4.522
	2	0.785	0.081	10.372
	3	0.869	0.064	7.345
	5	0.885	0.035	3.902
	7	0.921	0.064	6.906
	Sum	0.863	0.071	8.206
Retina	1	0.906	0.296	32.683
	2	0.926	0.142	15.301
	3	1.322	0.364	27.520
	5	1.358	0.202	14.855
	7	1.408	0.247	17.526
	Sum	1.184	0.328	27.719
Iris and Ciliary Body	1	0.714	0.054	7.523
	2	0.741	0.196	26.414
	3	0.817	0.063	7.756
	5	0.583	0.138	23.610
	7	0.612	0.092	14.980
	Sum	0.693	0.141	20.283
Choroid	1	0.313	0.118	37.755
	2	0.379	0.074	19.516
	3	0.353	0.090	25.402
	5	0.372	0.068	18.380
	7	0.329	0.074	22.517
	Sum	0.349	0.083	23.823

Table 3-3 Mean tissue weights in grams (n=5), standard deviation and relative standard deviation of each ocular tissue at each of the time points investigated.

3.3.3. Viability Parameters

For each perfused eye that was subjected to sample analysis and was included in the pharmacokinetic study, all four viability parameter requirements; APP, IOP, glucose consumption and LDH activity were met. The APP of all samples was consistent, with only minor fluctuations occurring and existed within the range of 20 – 45 mmHg, ensuring that successful perfusion fluid movement around the eye occurred without damaging the barriers created by the eye. The measured IOP of the isolated eyes were typically within the range of 2 – 9 mmHg and IOP remained relatively constant after the initial equilibration period, ensuring that effective aqueous humor drainage had occurred. A representative graph of APP and IOP measurements recorded over the time course of one perfusion can be seen in Figure 3-6 and Figure 3-7 respectively.

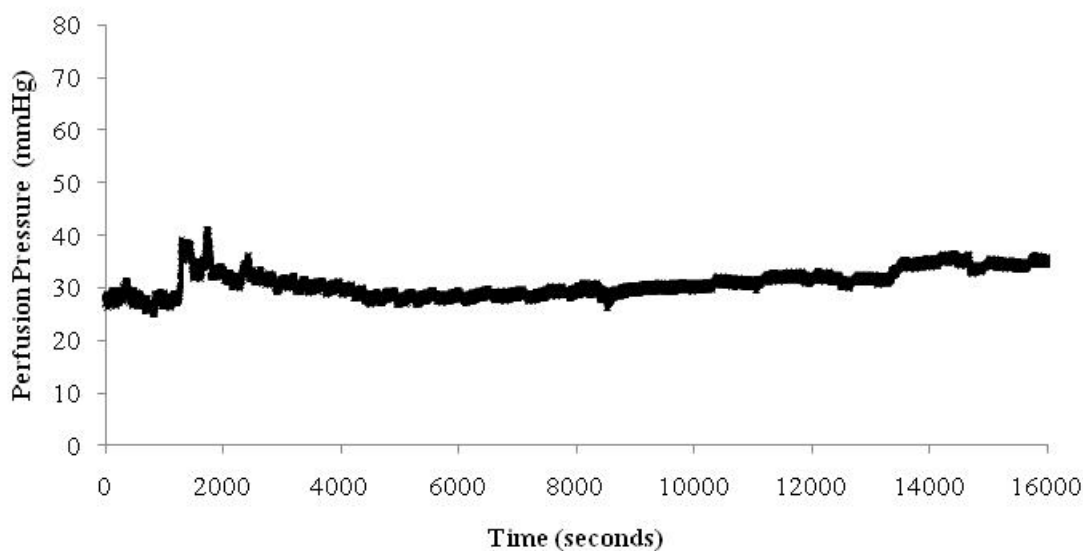


Figure 3-6 Representative graph of perfusion pressure generated during an isolated ovine eye perfusion.

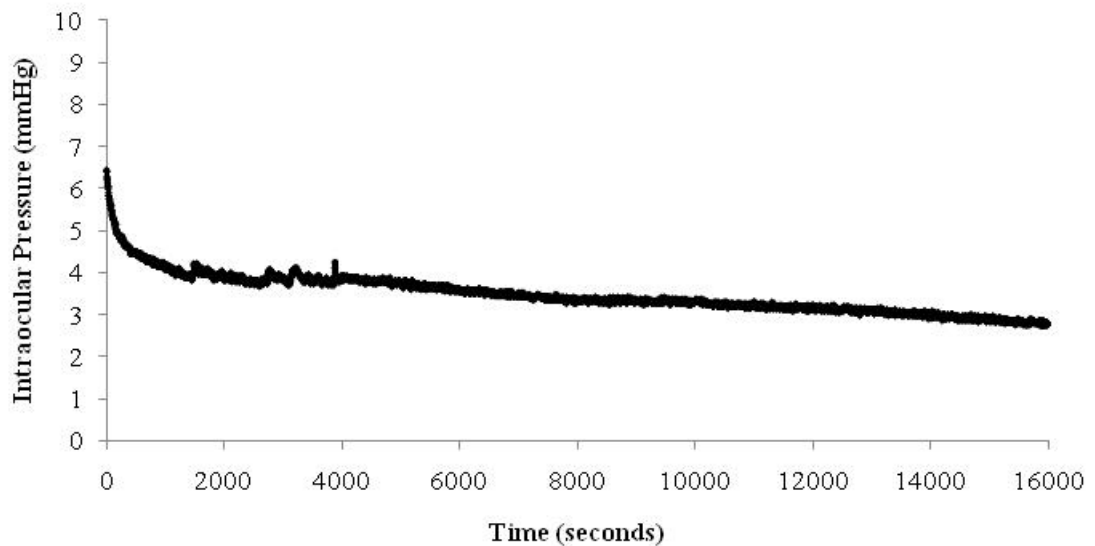


Figure 3-7 Representative graph of intraocular pressure generated during an isolated ovine eye perfusion.

Glucose consumption was obvious in each eye perfusion, with the glucose concentration measured in the venous perfusate lower than the concentration measured in the perfusion fluid, demonstrating that the perfusion procedure had been successful. An example graph of glucose concentrations recorded in the venous perfusate is illustrated in Figure 3-8 and shows relatively consistent glucose measurements over the time course of the experiment. LDH measurements were considered in each eye individually, with the LDH activity recorded at the initiation of the experiment consistently higher than the LDH activity recorded throughout the remainder of the experiment. This showed that the perfusion procedure was successful over the set perfusion time of each experiment and that normal eye function was maintained during the perfusion. A representative graph of LDH activity measured during a perfused eye experiment can be seen in Figure 3-8 and shows a drop in LDH activity from the start of the perfusion procedure over the first two hours of perfusion, followed by minor fluctuations in activity for the remainder of the experiment.

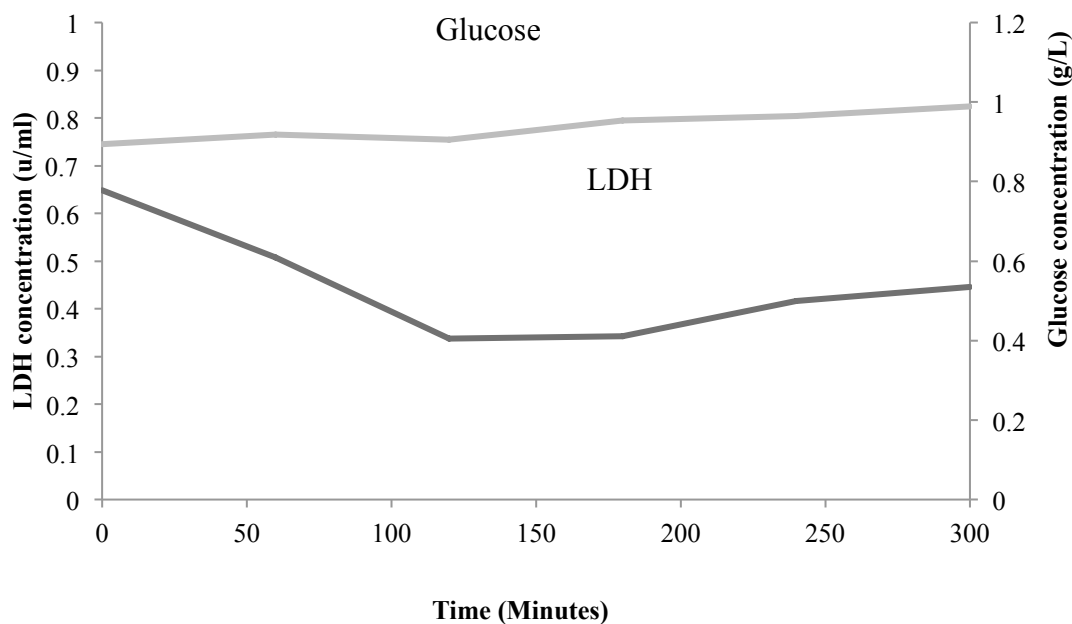


Figure 3-8 Representative graph of glucose concentrations and lactate dehydrogenase concentrations recorded in the venous perfusate during an isolated ovine eye perfusion.

3.3.4. Effect of physicochemical properties on drug distribution

Three beta adrenoreceptor antagonists (atenolol, timolol and propranolol) were selected for investigation in this study due to their individual physicochemical properties (see Table 2-1 for values). All three drugs had similar molecular weights (267 a.m.u., 316 a.m.u. and 260 a.m.u. respectively) removing molecular weight influences on drug distribution within the eye (Fatt 1975; Kathawate and Acharya 2008). All three drugs were basic compounds and had very similar pKa values, since all three drugs were positively charged at physiological pH, pKa would have had little influence on the distribution of each drug. Where a distinct difference did occur in the physicochemical properties of each of the drug compounds, was in their partition coefficients. Partition coefficient has been shown to have a large influence on the distribution of drugs within ocular tissues, with hydrophilic molecules thought to distribute and be cleared from the anterior section of the eye and lipophilic molecules thought to distribute and be cleared from the posterior section of the eye

(Atluri and Mitra 2003). An intravitreal cassette dosing study performed previously in rabbits failed to show clear differences in the impact of partition coefficient on drug distribution within ocular tissues (Proksch and Ward 2007). However, within the drug series selected, all of the drugs were very lipophilic molecules and this would have accounted for the lack of correlation in drug distribution and partition coefficient. Previous work investigating the impact of beta adrenoreceptor antagonist lipophilicity on drug distribution following systemic administration in the rat, demonstrated that increased tissue accumulation occurred with increasing drug lipophilicity (Rodgers, Leahy et al. 2005). In this study, atenolol was selected due to its low logP and is the most hydrophilic of the three compounds with a logP of 0.16. Propranolol was selected to be the most lipophilic molecule, with a logP much greater than atenolol at 2.4. Finally, timolol was selected as an intermediate compound with a logP equal to 1.8 sitting between the logP of other two compounds, but leaning more towards the more lipophilic region of the scale.

Following intravitreal drug administration, the corresponding concentration maxima of drug within tissue (C_{Max}) and the time required to reach C_{Max} (T_{Max}) of all three drug molecules in each individual tissue was obtained (see table 3 for details and table A2.4 for all raw data). The highest concentration of atenolol measured in the vitreous was 2489 $\mu\text{g/g}$ and was recorded in the first hour. Atenolol then appears to move quickly into the iris and ciliary body with C_{Max} recorded to be 5649 $\mu\text{g/g}$ at 2 hours post dosing. Maximal concentrations in the choroid and in the retina were noted simultaneously at 3 hours post dosing and were 2237 and 1014 $\mu\text{g/g}$ respectively, whereas the C_{Max} of the aqueous humor and the lens were seen at 5 hours post dosing and measured to be 426 and 3255 $\mu\text{g/g}$ respectively. In contrast to the data for atenolol, the C_{Max} of timolol was measured in the vitreous humor occurred at the 3 hour time point, post drug administration. However, only at a concentration of 2672 $\mu\text{g/g}$ which is only slightly higher than the concentration of 2664 $\mu\text{g/g}$ seen at 1 hour post dosing. In a similar manner to atenolol, timolol moved quickly into the iris and ciliary body with T_{Max} occurring at 2 hours after drug administration, with a corresponding C_{Max} of 7086 $\mu\text{g/g}$. Peak concentrations in the aqueous humor and the lens again occur at 5 hours post dosing, with C_{Max} recorded to be 300 and 4000 $\mu\text{g/g}$ respectively. In this instance, the retina mirrors vitreous

humor and not the choroid, with a maximum concentration of 1118 $\mu\text{g/g}$ recorded in the retina at the 3 hour time point. The choroid, in contrast to atenolol, reaches a concentration of 3391 $\mu\text{g/g}$ towards the end of the experiment at a T_{Max} of 7 hours. With propranolol, again high concentrations were detected in the vitreous in the initial phase of the experiment, with a C_{Max} of 2341 $\mu\text{g/g}$ occurring at 1 hour post administration. In the anterior segment of the eye the peak aqueous humor concentration occurred at 5 hour post dosing, although concentrations of propranolol in the aqueous humor were generally low throughout the experiment and C_{Max} was determined to be only 108 $\mu\text{g/g}$. As with the other drugs, peak levels of propranolol in the iris and ciliary body occurred at the 2 hour time point and peak levels of propranolol in the lens occurred at 5 hours. C_{Max} for both tissues were very similar and were determined to be 5478 $\mu\text{g/g}$ and 5555 $\mu\text{g/g}$ respectively. In similarity to timolol, a peak level in the retina of 1240 $\mu\text{g/g}$ occurred 3 hours post dosing and in the choroid, a peak level of 4975 $\mu\text{g/g}$ was seen at 7 hours after drug administration.

Atenolol		
Tissue	C_{max} ($\mu\text{g/g}$)	T_{max} (hours)
Aqueous	426.32	5
Iris and Ciliary Body	5648.98	2
Lens	3254.83	5
Vitreous	2488.78	1
Retina	1014.08	3
Choroid	2237.10	3

Timolol		
Tissue	C_{max} ($\mu\text{g/g}$)	T_{max} (hours)
Aqueous	299.86	5
Iris and Ciliary Body	7086.28	2
Lens	3999.93	5
Vitreous	2672.32	3
Retina	1117.88	3
Choroid	3391.22	7

Propranolol		
Tissue	C_{max} ($\mu\text{g/g}$)	T_{max} (hours)
Aqueous	59.48	1
Iris and Ciliary Body	5477.54	2
Lens	5555.18	5
Vitreous	2341.12	1
Retina	1239.80	3
Choroid	4975.08	7

Table 3-4 C_{Max} and T_{Max} obtained for atenolol, timolol and propranolol in each individual ocular tissue.

Focusing on the concentration versus time profile for each tissue obtained for each individual drug. For atenolol, there is an initial dip in the vitreous concentration at 2 hours where the drug appears to move quite quickly into the iris and ciliary body (Figure 3.9). At this point it was noted that the drug began to move into the aqueous humor. At 3 hours post dosing, a slight increase in the concentration measured in the vitreous was noted before the concentration again reduced and began to level off at 5 hours post dosing. Corresponding to the vitreous concentration increase, noted at 3 hours, there was a dip in the concentration measured in the iris and ciliary body. The iris and ciliary body appeared to act as a reservoir, taking up a high concentration of drug initially before releasing drug back into vitreous when the concentration in the vitreous fell however, since the changes in the concentration of atenolol in the both

the vitreous and the iris and ciliary body with time were shown to have no statistical significance (ANOVA $p>0.05$), it is unlikely that this is a true effect of the drug moving off of the iris and ciliary body. At the three hour time point, the vitreous supplies the posterior tissues and increases in choroid and retina concentrations also occurred. Atenolol appeared to accumulate on the choroid was the changes in concentration with increasing time demonstrated to be statistically significant (ANOVA, $p<0.05$). The concentration time profiles of the choroid and the retina appear to mirror each other, suggesting steady state exchange of drug between the two tissues, however changes in drug concentration in the retina were not shown to be statistically significant (ANOVA, $p>0.05$). Another larger dip in the iris and ciliary body concentration occurred after 5 hours, where atenolol could have moved out of the iris and ciliary body and into the other anterior tissues, the aqueous humor and the lens.

Focusing on the concentration versus time profiles generated for timolol (Figure 3.10), a similar pattern of drug distribution to atenolol was seen, with differences in concentration profile occurring in the retina and in the choroid. Initially timolol moved quickly out from the vitreous humor and into the iris and ciliary body within the first 2 hours of the experiment. Differing from atenolol, at the 2 hour time point we also seen rapid movement of timolol from the vitreous humor and into the retina, with concentrations in the retina rising steadily over the first 3 hours as drug began to move in the posterior direction, however again, these changes were not shown to be statistically significant and this could be due to the large inter-animal variations experienced throughout the experiment (ANOVA, $p>0.05$). At 3 hours post administration, like atenolol again timolol appeared to move back from the iris and ciliary body into the vitreous, which, at the point, feeds the posterior retina and choroid tissues. However again this change with time was not shown to be statistically relevant (ANOVA $p>0.05$) and is unlikely the drug moved in this fashion. Increases in drug movement into the anterior chamber occurred again at 5 hours post dosing, with increases in aqueous and lens concentrations in response to a corresponding dip in the concentration achieved in the iris and ciliary body, however again due to the large intra-animal variations, this effect was not statistically significant (ANOVA $p>0.05$). Finally, towards the end of the experiment, drug

began to accumulate in the choroid, which facilitated rising concentrations in the retina.

Propranolol moved in the anterior direction from the vitreous to the iris and ciliary body in the first 2 hours, but again the drug also moved in the posterior direction and the levels in the retina began to rise too (see Figure 3-11). Propranolol was then appeared to become dislodged from the iris and ciliary body at 3 hours post administration, and moved back into the vitreous tissue, with simultaneous increases in concentrations detected in the retina and in the choroid. However, as with the other two drugs, the changes in concentration of propranolol in the iris and ciliary body showed no statistical significance (ANOVA, $p>0.05$) and therefore, this apparent effect unlikely to be true. Although the changes in the concentrations shown in the iris and ciliary body were not statistically significant, changes in the concentration of propranolol with time in the vitreous and the choroid, were shown to be statistically significant (ANOVA, $p<0.05$), demonstrating propranolol movement through the vitreous and into the choroid. The effect on the iris and ciliary body was seen across all three drugs and it is also possible that the increased vitreous concentrations could have been due to drug movement through the lens into the vitreous humor. *Tan et al.* has noted from the ocular fluorophotometry in live rabbit eyes that intravitreally injected sodium fluorescein penetrated the lens at 2 hours after dosing but the substance did not continue a forward diffusion into the anterior chamber but unloaded the absorbed fluorescein back into the vitreous humour 3 hours later (Tan, Orilla et al. 2011). This coincides with the study by Stepanova and colleagues, who showed that when fluorescein was initially placed in the central section of the lens, it rapidly moved towards the posterior pole of the lens and out into the vitreous humor, with no fluorescein shown to move in the anterior direction (Stepanova, Marchenko et al. 2005). In this case, it was postulated that fluorescein movement was caused by a vectorial fluid flow in the lens that opposes diffusion, most likely mediated by the transport system present in the lens epithelium. After 5 hours another fall in the iris and ciliary body concentration occurred, corresponding to an increase in the concentration of propranolol in the lens. At the end of the experiment, as with timolol, a spike in the concentration of propranolol detected in the choroid occurred and fed the retina with a rich supply of

drug. However, the concentration of propranolol bound to the choroid was much greater than the concentration of timolol measured.

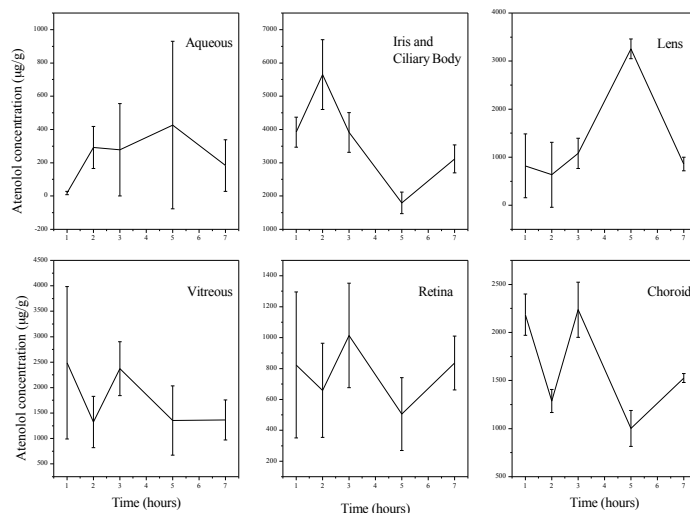


Figure 3-9 Mean concentration (n=5) versus time profile obtained for atenolol in each individual ocular tissue. Error bars show standard deviation from the mean.

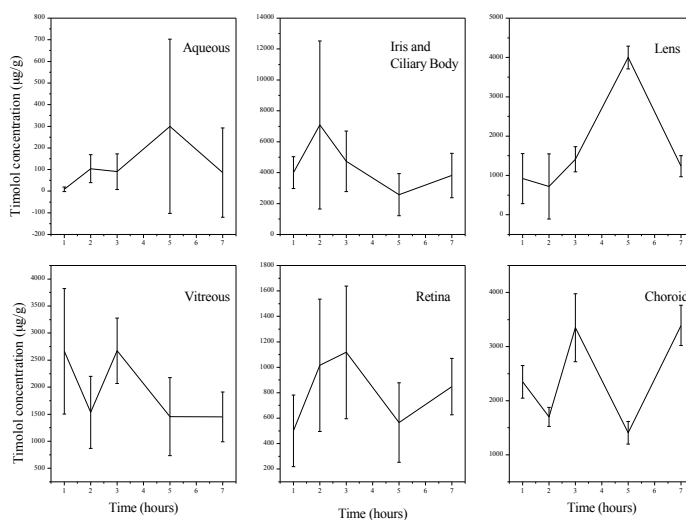


Figure 3-10 Mean concentration (n=5) versus time profile obtained for timolol in each individual ocular tissue. Error bars show standard deviation from the mean.

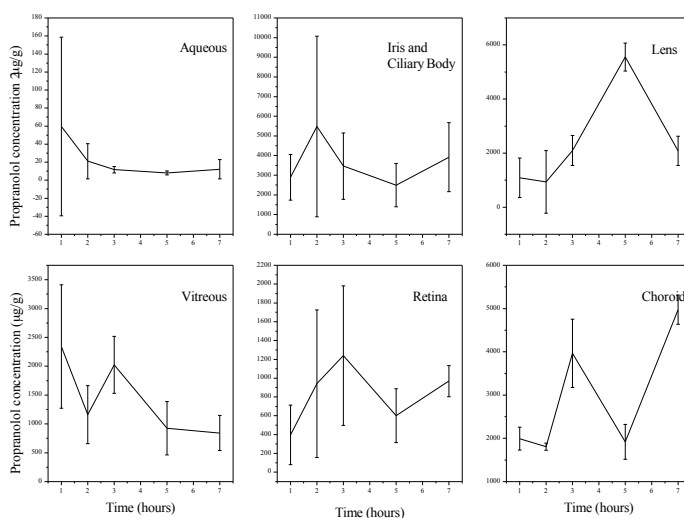


Figure 3-11 Mean concentration (n=5) versus time profile obtained for propranolol in each individual ocular tissue. Error bars show standard deviation from the mean.

Directly comparing the C_{Max} achieved for each of the three beta adrenoreceptor antagonists used, shows key differences in drug distribution patterns (see Figure 3-12). In the anterior segment of the eye, differences in C_{Max} occurred in all three tissues investigated, the aqueous humor, the lens and the iris and ciliary body. In the aqueous humor the highest C_{Max} was achieved by the most hydrophilic molecule, atenolol, followed by a reduction in C_{Max} according to decreasing hydrophilicity, with timolol higher than propranolol. More hydrophilic compounds have been shown to penetrate and have greater disposition within the water based aqueous humor than more lipophilic drug compounds (Atluri and Mitra 2003). Therefore, an increase in the aqueous humor C_{Max} of the three beta blocking compounds with decreasing logP was due to an increase in the ease of drug diffusion into the aqueous humor because of drug hydrophilicity. More hydrophilic compounds are also subject to removal through the aqueous clearance system and will migrate from the vitreous into the anterior section of the eye before removal (Araie and Maurice 1991; Beer, Bakri et al. 2003). Therefore, a higher concentration of the more hydrophilic drug, atenolol, moved in the anterior direction than the other

two more lipophilic drugs. In contrast to a previous study where T_{Max} in the aqueous humor was shown to increase with increasing logP, no significant difference between the compounds was recorded for T_{Max} , with T_{Max} determined to be 5 hours post dosing for atenolol and timolol, and 1 hour for propranolol (Atluri and Mitra 2003). The difference in trends in T_{Max} could be related to the molecular size of the compounds used in the previously study, as the logP of the compounds corresponded to a progressive increase in molecular size, whereas in this study no such relationship between size and partition coefficient existed. Significant differences in C_{Max} were noted in the iris and ciliary body with timolol showing the greatest binding to this tissue followed by atenolol and then closely followed by propranolol, with a difference between the two of 200 $\mu\text{g/g}$. For the lens, a progressive increase in penetration into this tissue was seen with increasing drug lipophilicity. Movement of compounds within the lens has previously been investigated using fluorescein as a drug marker (Kaiser and Maurice 1964; Stepanova, Marchenko et al. 2005). In the rabbit eye it was demonstrated that fluorescein penetrated into the lens at both the anterior side and the posterior side, with little resistance created by the lens capsule. resistance to fluorescein entry into the lens was however caused by the lens epithelium. For this reason, compounds with a higher partition coefficient will more readily penetrate the epithelial barrier than more hydrophilic drugs, explaining the rank order in drug penetration into the lens tissue with increasing lipophilicity (Kaiser and Maurice 1964).

In the posterior segment, and at the site of initial drug administration, little difference in the C_{Max} measured in the vitreous humor across the drug series was noted. The C_{Max} of timolol appeared to be the greatest, but the difference was small with a large variance. A difference in T_{Max} also occurred across the tissues, with the T_{Max} of atenolol and propranolol recorded at 1 hour and the T_{Max} of timolol determined to be 3 hours. The vitreous has been shown to experience an initial drug diffusion stage over the first hour following administration, followed by a gradual drug elimination phase, explaining the T_{Max} of one hour obtained for atenolol and propranolol (Atluri and Mitra 2003; Hu, Le et al. 2007). As discussed previously, all three drugs also show an increase in measured drug levels at three hours, due to drug displacement from the iris and ciliary body and re-equilibrating through the lens back

into the vitreous. As a result, for all three drugs similar drug levels were obtained at both one hour and three hours post dosing. For timolol, the level obtained at three hours was just slightly greater than the level obtained at one hour, accounting for the apparent difference in T_{Max} compared to the other drugs in the series. In the remaining posterior tissues, the retina and the choroid, a pattern in the extent of drug movement was seen. In the retina, a stepwise increase was noted with increasing lipophilicity, with atenolol having the lowest C_{Max} , followed by timolol and then by propranolol with the greatest C_{Max} . The retina mirrored the choroid with a progressive increase in C_{Max} with increasing lipophilicity. The increase in choroid levels with increasing lipophilicity is in keeping with previous observations from the rat eye following a trans-scleral injection of a beta blocker drug series (Kadam and Kompella 2010). However, in this case the choroid did not mirror the retina as retinal levels decreased with increasing lipophilicity. The lack of correlation could be explained by the difference in route of administration, as following trans-scleral injection, the beta blocker drug mix would reach the choroid before penetrating into the vitreous. The more lipophilic drugs would have bound to the choroidal melanin and as a result less drug would be free to move into the vitreous. Lipophilic drugs are subject to retinal clearance and will migrate towards the posterior pole before subsequent elimination (Koeberle 2002; Atluri and Mitra 2003). As a result a progressive increase in drug levels in the posterior eye with increasing lipophilicity is seen, as more hydrophilic drugs tend to move towards the anterior section of the eye. T_{Max} differed also in the choroid, with C_{Max} occurring much earlier for atenolol at 3 hours post dosing, whereas drug accumulation on the choroid with time occurred for timolol and propranolol, with C_{Max} determined at the end of the experiment at 7 hours post dosing, had the experiment continued longer the concentration at the choroid may have continued to rise and the time for C_{Max} to be achieved increased. The delay in reaching C_{Max} was probably caused by progressive drug accumulation on the melanin contained in the choroid over the course of the perfusion. Beta adrenoreceptor antagonists have previously been shown to bind to melanin of the choroid/RPE (retinal pigmented epithelium) with a high percentage of the available drug accumulating on the melanin (Pitkanen, Ranta et al. 2007). It has been reported that all drugs known to bind to melanin are basic or have some element of basicity in

their structure and, in addition to this; all drugs were known to have a positive logP and therefore a degree of lipophilicity (Leblanc, Jezequel et al. 1998). All three drugs used in this study were basic compounds, with varying levels of lipophilicity. It is interesting that the extent of drug accumulation to the choroid tissue increased with increasing drug lipophilicity. This differs from the results obtained in the iris and ciliary body where a step wise increase in drug tissue binding with increasing lipophilicity was not demonstrated and timolol had the highest C_{Max} out of the three drugs investigated. This difference may be influenced by the clearance mechanisms operating within the eye, as propranolol is very lipophilic and subject to retinal clearance, less propranolol would be available in the anterior section of the eye than the less lipophilic timolol, accounting for the reduced levels experienced on the iris and ciliary body. In addition, although a higher concentration of atenolol would have migrated towards the anterior eye, the more hydrophilic nature of atenolol may have reduced the extent of atenolol binding to the melanin of the iris and ciliary body. Although the iris and ciliary body and the retina are both melanin rich tissues, the melanin structure within these tissues is slightly different. The uveal tract is known to contain two types of melanin; pheomelanin and eumelanin, whereas the choroid is thought to contain mainly eumelanin. Pheomelanin is a lighter coloured pigment and the content of pheomelanin varies between eyes with a higher ratio of pheomelanin/eumelanin existing in lighter coloured eyes (Prota, Hu et al. 1998). The pheomelanin content of the iris, choroid and RPE has been previously shown to be low for all three tissues, however distinct differences in content existed across the tissue range with 1% pheomelanin content in the iris, 0.1-0.5% in the RPE and a negligible amount in the choroid (Liu, Hong et al. 2005). The basic melanin composition between the tissues also differs, with differences in the elemental composition of melanin contained in the iris, the choroid and the RPE previously demonstrated (Dryja, O-Neil-Dryja et al. 1979). In the human eye, differences in eumelanin content of the melanocytes of the iris and the melanocytes of the choroid were apparent. Although not statistically significant, eumelanin content in the choroidal melanocytes was shown to be greater in the melanocytes of the choroid compared to the melanocytes of the iris (Wakamatsu, Hu et al. 2007). In the bovine eye differences in the amino acid content of melanin containing tissues was apparent,

with amino acid content higher in the choroid than the iris and the RPE (Liu, Hong et al. 2005). It is likely that the structural differences in the varying types of melanin played a role in the differences in the extent drug accumulation in the choroid, however, investigations directly comparing drug binding to the different melanin binding tissues of the eye are limited. Although a potential relationship in drug accumulation on melanin rich tissues has been shown further work is still required to directly assess the extent of melanin binding of atenolol, timolol and propranolol in melanin isolated from the choroid and the iris of the ovine eye in order to determine the importance of both melanin biochemistry and melanin composition within ocular tissues.

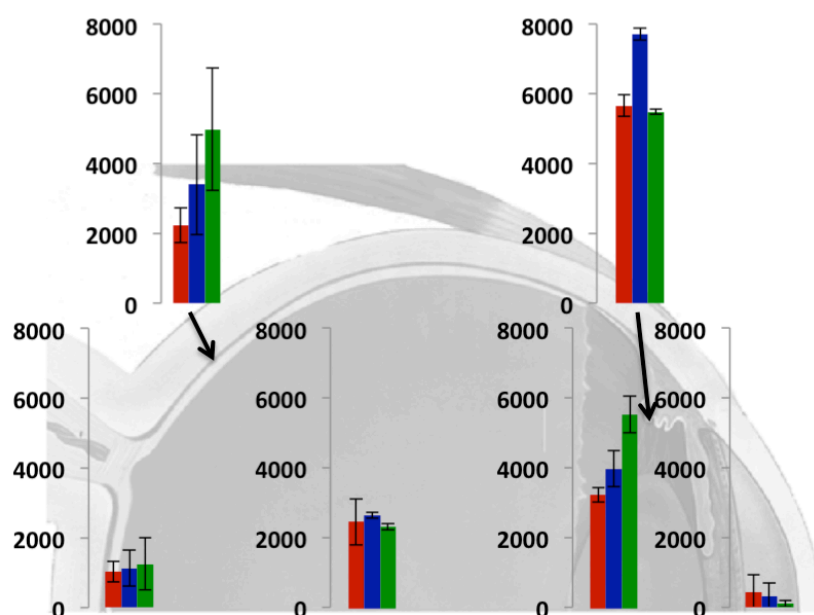


Figure 3-12 C_{Max} (y axis in µg/g) obtained for atenolol (red column), timolol (blue column) and propranolol (green column) in each ocular tissue shown at the position of the tissue within the eye. Moving from left to right; retina, choroid, vitreous, lens, iris and ciliary body and finally aqueous humor.

In addition to melanin binding phenomena, drug transporter systems are thought to have a key role in the transfer of materials at the RPE and therefore drug movement from the vitreous to the retina and the choroid (Smith, Kincaid et al. 1999; Wilson, Semenera et al. 2007). Various drug transporter systems have previously

been shown to play a role in drug distribution in the posterior eye, including P-glycoprotein, organic cation transports and organic anion transporters (Han, Sweet et al. 2001; Hosoya, Ohshima et al. 2003; Steuer, Jaworski et al. 2005). Although the involvement of drug transport systems in the extent of drug penetration of the drug series into the retina and the choroid was out with the scope of this study and remains unclear, the impact of drug lipophilicity on drug levels with the retina and choroid has been demonstrated. The potential involvement of drug transport systems cannot be disregarded and therefore should be taken into consideration when interpreting the results.

3.4. CONCLUSION

In summary, this work has demonstrated that cassette dosing using the isolated perfused ovine eye is a suitable means of carrying out drug distribution studies, significantly reducing both the number of animals utilised during the experimental work as well as analytical time. The results reported here have clearly shown that drug lipophilicity plays an important role in the extent of ocular drug distribution following drug administration via an intravitreal injection. Drugs with greater lipophilicity will penetrate to the posterior eye, Residing in the retina and the choroid at greater levels than those seen for more hydrophilic drugs. This will impact on the drug candidate selection process for the treatment of posterior eye diseases such as age-related macular degeneration and diabetic retinopathy where the desire is to penetrate to the back of the eye at desirable drug concentrations.

CHAPTER 4. TOF-SIMS ANALYSIS OF OCULAR TISSUES TO REVEAL BIOCHEMICAL DIFFERENTIATION AND DRUG DISTRIBUTION

4.1. INTRODUCTION

Time of flight secondary ion mass spectrometry (ToF-SIMS) is an extremely surface sensitive spectrometric technique that can provide detailed chemical information of a wide variety of systems, including biological tissue (Börner, Nygren et al. 2006; Wu, Lu et al. 2007), drug formulations (Belu, Davies et al. 2000; Davies, Head et al. 2008) and polymers (Shard, Davies et al. 1997; Urquhart, Taylor et al. 2007). In ToF-SIMS analysis, a monoatomic (Conlan, Gilmore et al. 2006) or cluster ion source (Davies, Weibel et al. 2003) is focused onto a sample's surface generating sample specific secondary ions and neutral fragments from the resulting direct ion collisions and indirect atomic/molecular knock on collisions (commonly referred to as the collision cascade). Sample specific secondary ions are focused and accelerated to the time-of-flight detector. Time-of-flight detectors rely upon the principle that ions with the same kinetic energies have different velocities depending on their mass (i.e. different flight times). In ToF-SIMS an electrostatic field is used to accelerate secondary ions to a common kinetic energy with low mass ions reaching the detector before heavier ions. The technique has a depth analysis of 1-2

nm and like many surface analytical techniques is performed under ultra high vacuum conditions (UHV) (Urquhart, Taylor et al. 2007). Cluster (polyatomic) ion sources offer numerous advantages over traditional monoatomic ion sources and have since become more favourable in ToF-SIMS analysis. Cluster ion sources enhance the yield of secondary ions generated and have been shown to be useful when high sample sensitivity is essential (Appelhans and Delmore 1989; Gillen and Roberson 1998). In addition, cluster ion sources can enhance secondary ion yield at low energies, resulting in the reduced beam damage of organic samples and improvement in depth resolution (Gillen and Roberson 1998; Gillen and Walker 1999).

The technique of ToF-SIMS has previously been successfully applied to ocular tissues, however studies have been limited and mainly focused on physiological composition of retina tissue from a specific animal model (Amemiya, Gong et al. 2003; Gong, Amemiya et al. 2003; Kishikawa, Gong et al. 2003; Amemiya, Tozu et al. 2004; Kishikawa, Suematsu et al. 2005; Kim, Kim et al. 2008). Work by Amemiya *et al* demonstrated the presence of vitamin A and E in cross sections of rat retina as well as differences in counts obtained in response to light stimulus (Amemiya, Gong et al. 2003). Using the same model the group also showed differences in retina expression of fatty acids (maleic, palmitic, oleic, stearic, arachidonic and docosahexaenoic acid) with the highest ion counts obtained for maleic acid (Amemiya, Tozu et al. 2004). In addition, expression of oleic acid differed depending on rat age, with higher ion counts noted in an 18 month old rat when compared to a 4 month old rat (Gong, Amemiya et al. 2003). The ability of ToF-SIMS to spatially map sample cross sections was not exploited in this retinal work as in each case work focussed on total ion counts measured for the whole tissue cross section. Total ion count is often not an ideal method of direct comparison between samples due to matrix effects, where the ion count achieved can vary depending on the chemical environment of the sample (Jung, Foston et al. 2010). Following on from this work, a study by Kim *et al* moved on to demonstrate spatial distribution in ocular tissue by mapping the distribution of Na^+ , K^+ , Mg^{2+} and Ca^{2+} in the mouse retina (Kim, Kim et al. 2008). ToF-SIMS was also used on the tissue samples to demonstrate differences in Ca^{2+} ion distribution in the ischemic retina

when compared to a normal retina. Another ocular tissue, which has been investigated using ToF-SIMS, is the lens. The lens is an oval shaped, transparent tissue positioned immediately behind the anterior section of the eye. It has an important role in the generation of vision as it is responsible for focussing light onto the retina before it is detected and transmitted. Protein content in the lens is high, with the lens synthesizing its own unique proteins known as the crystallins (Rafferty 1985). Very limited work has been carried out on lens tissue using the technique of ToF-SIMS with only one study reporting use of this technique. Kinoshita *et al* used the rat model to demonstrate that concentration differences of Ca^{2+} , Fe^{2+} , Mg^{2+} and Na^{+} existed in 4 month old rats when compared to 15 month old rats (Kinoshita, Gong et al. 2003). Similarly to the lens, limited studies have been performed on the vitreous tissue of the eye. Unlike the retina and the lens, the vitreous tissue of the eye can be difficult to prepare for ToF-SIMS analysis. The vitreous humor is the largest structure in the eye and is responsible for the support and the protection of the retina and the lens. It also acts as a barrier to diffusion of molecules between the anterior and posterior eye and ensure light can pass through the posterior eye unrestricted. It has also been described as a 'sink' for some proteins and solutes which are unable to cross over the blood-retinal-barrier (Bito 1977). The vitreous humor is composed of approximately 99% water but owes it viscoelastic properties to other components contained in the vitreous; including collagen, hyaluronic acid and proteoglycans (Balazs and Denlinger 1984). The vitreous is an extremely important tissue in the treatment of posterior eye disease, as drug formulations are often administered into the vitreous via direct intravitreal injection. Although the vitreous is an extremely interesting ocular tissue, the structure of the vitreous, mainly water, makes it a difficult tissue to prepare and analyse, perhaps explaining the previous lack of use of the ToF-SIMS technique in this tissue. Only one previous study, by Kishikawa *et al*, has been performed on vitreous tissue, looking at the distribution of various elements, fatty acids and vitamins A and E in patients with diabetic retinopathy and vitreoretinopathy (Kishikawa, Gong et al. 2003). The vitreous in this case was subjected to a washing stage to facilitate salt removal and was treated as a mass of tissue, analysing the outer layer of the tissue mass rather than a cross section through the tissue. Although ToF-SIMS has been used to

consider organic substance distribution within some ocular tissues, ocular tissues have not previously been investigated as a collective to reveal any important physiological differences between tissues. In addition to this, the potential of ToF-SIMS to map drug distribution within ocular tissues has not previously been explored. Interest in mapping drug distribution within ocular tissues has increased recently, especially when treating certain posterior eye disease states, such as diabetic retinopathy (Porta and Allione 2004; Mason, Nixon et al. 2006) and age-related macular degeneration (Wong, Liew et al. 2007; Ding, Patel et al. 2008), where effective treatment is currently limited. Understanding the factors which influence drug distribution can potentially improve treatment options in these conditions, by enabling improved drug targeting to the desired site of action and prediction of toxicity problems. At the present moment, intravitreal drug administration appears to be the best option in achieving therapeutic drug concentrations in the posterior eye (Edelhauser, Rowe-Rendleman et al. 2010), however the process of generating ocular drug distribution data can be time-consuming and requires the eye to be separated into its various ocular tissues. The eye can be divided into four sections: the outer coat, the middle coat, the inner coat and the periocular structure. Following separation and ocular tissue extraction, the tissues are subjected to destructive processing. Typically ocular tissues are homogenised before the drug is extracted from the tissue, providing no spatial awareness of the drug location within the tissue. The ability to detect drug concentrations directly from a cross section of ocular tissue using ToF-SIMS, without the need for an extraction method could provide useful distribution information.

Analysis of ToF-SIMS mass spectra data can be seriously challenging with a simple sample, such as a homopolymer, producing thousands of secondary ion mass peaks (Davies, Lynn et al. 1995). This challenge is increased in magnitude for biological tissue due to the biochemical complexity and composition (from small molecules to kiloDalton weight proteins and polysaccharides) of tissue. It is now commonplace with analytical chemistry to utilise data mining techniques to fully explore large data sets. In the field of ToF-SIMS both principle component analysis (PCA) (Urquhart, Taylor et al. 2007; Lee, Gilmore et al. 2008) and partial least

square regression (PLS) (Taylor, Urquhart et al. 2009) are extensively used and have established rules for data pre-processing and processing (Lee, Gilmore et al. 2008). PCA is used to establish variance with a data set and determine where the direction of this variance originates. Through the use of PCA chemically distinct regions in ToF-SIMS data can be identified and key peaks associated with image features selected, in both biological and non-biological samples (Tyler 2003; Wagner, Graham et al. 2004; Graham, Wagner et al. 2006). Multivariate statistical analysis (MVA) has been previously performed in ocular tissue, mainly in ocular surgery to investigate surgical risks and preoperative and postoperative effects on tissues of the eye (Borderie, Scheer et al. 1998; Capeans, Lorenzo et al. 1998; Sonoda, Sakamoto et al. 2004). In particular, PCA has been used to compare responses of the retina to light stimulus and to investigate the effects of UV-A (Ultraviolet) and UV-B rays on the metabolic profile of the aqueous humor (Heynen and Van Norren 1985; Tessem, Bathen et al. 2005). Although PCA has been performed on tissue of the eye, PCA has not been used to show relationships between ToF-SIMS data obtained from ocular tissue samples. Prior to carrying out MVA it is important to select an appropriate means of scaling, as the method selected is widely known to have a major influence on extracting the most useful information from the data set. The use of various data scaling methods have been shown to aid the ability to identify chemical information governing differences within data sets, however there appears to be no clear guidance on which method is most effective (Keenan and Kotula 2004; Vaidyanathan, Fletcher et al. 2008). As a pre-processing step, normalisation is often carried out first before the selected scaling method is applied and PCA carried out. Various types of pre-processing include mean centring, root mean scaling, auto-scaling, filter scaling and shift variance scaling. In this study, we show for the first time how PCA can be successfully applied to both positive ToF-SIMS data in order to highlight similarities and differences within the physiological chemistries of the lens, vitreous and retinal ocular tissues. We also present the first use of the ToF-SIMS technique to identify the presence of a model drug compound within these ocular tissues.

4.2. MATERIALS AND METHODS

4.2.1. Ocular tissue preparation

Using the perfused eye method detailed in Chapter 3 of this thesis, once arterial perfusion pressure was maintained, an intravitreal injection of model drug amitriptyline (Figure 4-1) was administered to both eyes. Amitriptyline was identified as a suitable representation of a routinely administered small, generic, biologically active drug molecule. Amitriptyline was selected due to similarities in its basicity, molecular weight and partition coefficient to small drug molecules typically used in the treatment of ocular disease. Intravitreal injections of model drug amitriptyline hydrochloride (Sigma-Aldrich Dorset, UK) were prepared at two concentrations in 100 μ l of deionised water. A low dose and a high dose injection were prepared, containing 250 μ g and 2000 μ g of drug respectively. The injection was performed using a 1ml syringe and 23G needle, inserted 1mm into the vitreous approximately 3 to 4 mm from the limbus in the posterior direction. Non-perfused eyes, with and without drug administration were used as controls. To non-perfused eyes with drug administration, intravitreal injection was performed using the same method as perfused eyes. Following exposure for 2 hours, the perfusion procedure was ended and perfused eyes were removed from the perfusion kit. All eyes were immediately frozen in liquid nitrogen and the lens, retina and vitreous were removed. The anterior eye was then cut away in a circular manner and the lens removed. In order to achieve cross sections of the vitreous and the retina, the eye was sliced at four positions from the anterior to the posterior section. The vitreous was removed and the sclera was pressed back for cryosectioning. All tissues were stored at -80°C prior to sectioning. The lens, vitreous and retina from each eye were mounted onto a cryostat chuck using Shandon M-1 embedding matrix (Thermo-Scientific, Chesire). 20 μ m thick sections were cut through the centre of the tissue on a Leica CM1850 Cryostat (Leica Microsystems, Milton Keynes, UK). Tissue sections were mounted directly onto 1x1cm silicon wafers that were previously cleaned with isopropyl alcohol.

4.2.2. ToF-SIMS analysis

Time of flight-secondary ion mass spectrometry was performed on a an Ion-TOF ToF-SIMS IV instrument (IONTOF, GmbH, Munster, Germany) using a Bi³⁺ cluster source and a single-stage reflectron analyzer. A primary ion energy of 25 kV along with a pulsed target current of approximately 1 pA and postacceleration energy of 10 kV were employed throughout the analysis. The primary ion dose density was maintained at less than 10¹² ions per cm² throughout to ensure static conditions. Spectra were acquired in both positive and negative mode by rastering the stage under the primary ion beam over a sample area of 500 x 500 µm. Low energy electrons (20 eV) were delivered to the sample surface to compensate for positive primary ion beam induced surface charging, a common insulating effect of biological surfaces. Data processing was performed using IonSpec and IonImage software (version 4.0), for spectroscopy and image analysis.

4.2.3. Multivariate Statistics

Statistical analysis was performed using SIMCA-P version 11 (Umetrics, Sweden). Data was exported from IonSpec into Microsoft Excel and divided into three groups; complete sample data, low drug dose data and high drug dose data. The low and high dose data sets each contained data for all three tissues from a dosed perfused eye section, a dosed non-perfused eye section and a non-dosed control. Normalisation was carried out as a pre-processing step by dividing total ion count of individual mass peaks obtained for each sample by the total ion count of all peaks calculated for the sample. Following this, mean centering was utilised as an appropriate data scaling method and principle component analysis performed (Lee, Gilmore et al. 2008).

4.3. RESULTS AND DISCUSSION

In order to analyse lens, retina and vitreous samples by ToF-SIMS, both positive and negative spectra were obtained for all samples. For each of the tissue subtypes and tissue samples, dosed and controls, analysis was performed on three replicates of each sample. Mass spectra obtained for each sample contained

numerous peaks with m/z ranging from 1 to 800. Peaks at the lower end of the mass spectra dominated, with greater peak intensities achieved in the m/z range of 1 to 200 (Figure 4-1). A peak list was generated using a method detailed previously by Urquhart *et al* (Urquhart, Taylor et al. 2007). From the spectra obtained, poor sample separation was observed with the negative ion spectra whereas strong sample separation was shown using the positive ion spectra. It is often the case that with negative spectra, poor sample separation is observed and information obtained using the negative spectrum can often be less specific (Pasche, De Paul et al. 2003; Urquhart, Taylor et al. 2007). The positive ion spectra were used in this study, as they enabled a more interesting and in-depth peak list to be generated and applied to the data. In the positive spectra, 774 ion peaks were selected and added to produce a peak list. After applying the generated peak list to every sample spectrum, the spectra were normalised, before carrying out data processing. To investigate model drug location on the sample surface and identify key model drug peaks, PCA was performed on the positive ion data sets obtained after scaling each of the data sets. It appears selection of a suitable pre-processing method can often depend on the individual data set, with only small differences noted when comparing scaling methods, however it is noted that PCA of scaled data is a vast improvement on PCA of unscaled data (Tyler, Rayal et al. 2007). During the data processing step of this work we explored the use of mean centring, root mean scaling and autoscaling. Mean centring revealed the greatest information from the data and as a result became the focus of this work. Principle components (PC) 1, 2 and 3 demonstrated the best discrimination between tissue subtypes, separating out clearly the lens, retina and vitreous samples, whilst covering 94% of the cumulative variance.

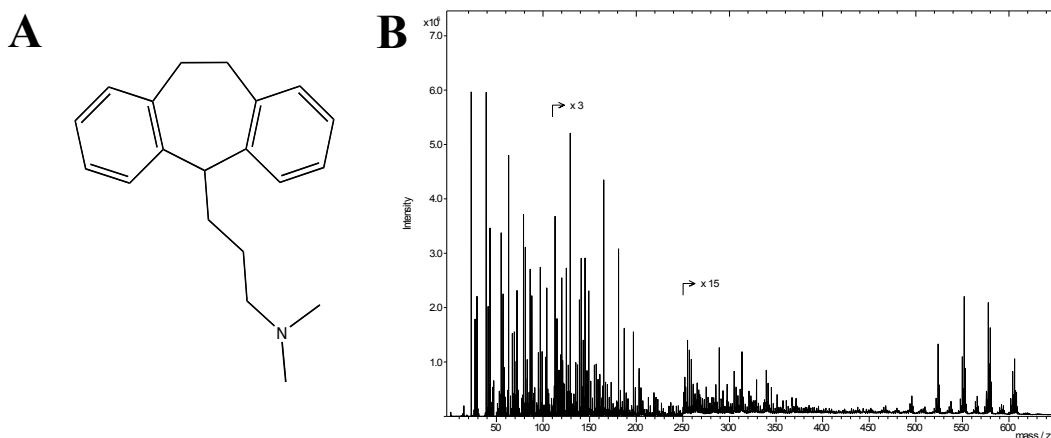


Figure 4-1 A schematic showing the structure of amitriptyline. B) An example of a positive ion spectrum obtained from a vitreous tissue sample.

4.3.1. Principle Component 1 versus Principle Component 2

Figure 4-2A shows the scores plot obtained for the first two PC's for the positive ion spectra of all tissue samples and Figure 4-2B shows the scores plot obtained for the control samples of each tissue only. From both plots, it is clear that the three ocular tissue subtypes; the lens, retina and vitreous, group together as three distinct groups, reflecting the physiological differences between the tissues. Often in the analysis of biological samples, in the first instance, a salt washing step is employed during sample preparation to reduce the salt concentration, as often salts present within the sample surface are associated with the induction of peak suppression (Piwowar, Lockyer et al. 2009). Salt washing has been shown previously to counteract some effects associated with salt suppression however, the removal effect of the washing phase reduces the secondary ion yield generated which can result in the loss of important biological information (Piwowar, Lockyer et al. 2009). In this work no salt washing step was utilized, as in this case salts were not viewed as contaminations but as biologically important tissue determinants. Good sample clustering was obtained for all three tissue types without the need for a salt washing step (Figure 4-2A). The loadings plot of PC 1 and 2 (Figure 4-4A) contains the mass peak data used to create the score plot. Suggested structural ion assignments detailing relevant peaks to PC 1, 2 and 3 are detailed in Table 2 and show that salt peaks were important in determining biological differences between

tissue types. Mass peaks controlling sample distribution on the scores plot of PC 1 and 2 fell within the mass region of 22 to 185 m/z.

Interesting biochemical information and chemical physiological determinants of ocular subtypes were identified. Positive PC 1 values were strongly associated with physiological salts, with $m/z = 23$ and 39 corresponding to Na^+ and K^+ respectively (Figure 4-2A and Table 4-1). On PC 2 from Figure 4-4A, positive PC 2 values were associated with Na^+ ($m/z = 23$) and negative PC 2 values are associated with K^+ ($m/z = 39$). The vitreous tissue lies on the positive region of PC 1 demonstrating that this structure is almost completely dominated by Na^+ and K^+ ions. This is in keeping with the known alkali metal composition of the vitreous (Balazs and Denlinger 1984; Nickerson, Park et al. 2008). Other physiological components of the vitreous are likely not to be seen, due to the sheer magnitude of the salt peaks obtained overshadowing any other biochemical peaks obtained. The vitreous tissue has much higher concentrations of Na^+ and K^+ when compared to the lens and the retina, as both of these tissues sit on the negative region of PC 1. The lens and the retina tissues are predominantly separated on PC 2 by differences in Na^+ and K^+ ion concentration. The lens tissue, sits within the negative region of PC 2, demonstrating a high K^+ concentration ($m/z = 39$) rather than a high Na^+ concentration ($m/z = 23$). The lens is known to contain Na^+ , K^+ and Ca^{2+} with these ions thought to control fluid circulation and nutrient movement (Beebe 2003). It is extremely interesting that the ovine lens appears to be a richer source of K^+ than Na^+ , as previously the human lens has been reported to contain Na^+ concentrations twice that of K^+ (Dilsiz, Olcucu et al. 2000). The difference in K^+ prevalence between the human lens and ovine lens represents an interesting species variation in lens tissue electrolyte composition. The bovine lens has also been shown to have a higher K^+ concentration than Na^+ (Amoore, Bartley et al. 1958), highlighting differences between human ocular tissues and animal models typically used in pharmacokinetic studies. The retinal tissue sits within the positive region of PC 2, demonstrating that the retina is very different to the lens in the sense that it is dominated by the Na^+ ions rather than the K^+ ions. Again this shows a distinct species variation in ion distribution with the frog retina reported to contain higher concentrations of K^+ than Na^+ (Duncan and Weeks 1972). Differences in Na^+ and K^+ concentrations between the lens and retina have not been

previously reported and this shows an interesting difference in ion importance within these tissues.

m/z	Positive Ion Structure
22.9930	Na ⁺
29.0409	C ₂ H ₅ ⁺
30.0378	CH ₄ N ⁺
38.9687	K ⁺
40.9660	Ca ⁺
43.0565	CH ₃ CO ⁺
44.0529	C ₂ H ₆ N ⁺
55.0568	Fe ⁺
63.0214	C ₅ H ₃ ⁺
70.0728	C ₄ H ₈ N ⁺
71.9842	FeO ⁺
72.0860	C ₅ H ₁₂ N ⁺
86.1090	C ₄ H ₈ NO ⁺ or C ₅ H ₁₂ N ⁺
94.9363	C ₇ H ₁₀ ⁺
104.1218	C ₅ H ₁₄ NO ⁺
147.0273	C ₂ H ₅ O ₄ P Na ⁺
184.1090	C ₅ H ₁₅ NPO ₄ ⁺

Table 4-1 Ion Fragments (m/z) and Structural Assignment for Positive Ion Spectra.

In addition to Na⁺ and K⁺, Ca²⁺ ions (m/z = 41) were also detected in the tissue samples however, two ion peaks of m/z = 41 were obtained, one of which represented Ca²⁺ and the other representing an organic hydrocarbon peak (Wu, Lu et al. 2007). The first peak at 41 was associated with a positive value on PC 1 whereas the second peak at 41 sat the on the negative region of PC 1. On PC 2, positive directionality was associated with the first peak at 41 and negative values associated the second m/z of 41. The retina sat within the negative region of PC 1 and the position region on PC 2, with positioning influenced by the second m/z of 41. The presence of Ca²⁺ in the retina is already well established with the presence of Ca²⁺ in the retina of mice demonstrated previously using ToF-SIMS (Kim, Kim et al. 2008). Although Ca²⁺ is also present in the lens and vitreous, the Ca²⁺ content in the retina is high (Hess 1975), due to the essential role of Ca²⁺ in the visual process (Akopian and

Witkovsky 2002), therefore, the second peak with m/z 41 in Figure 4-2B represented Ca^{2+} .

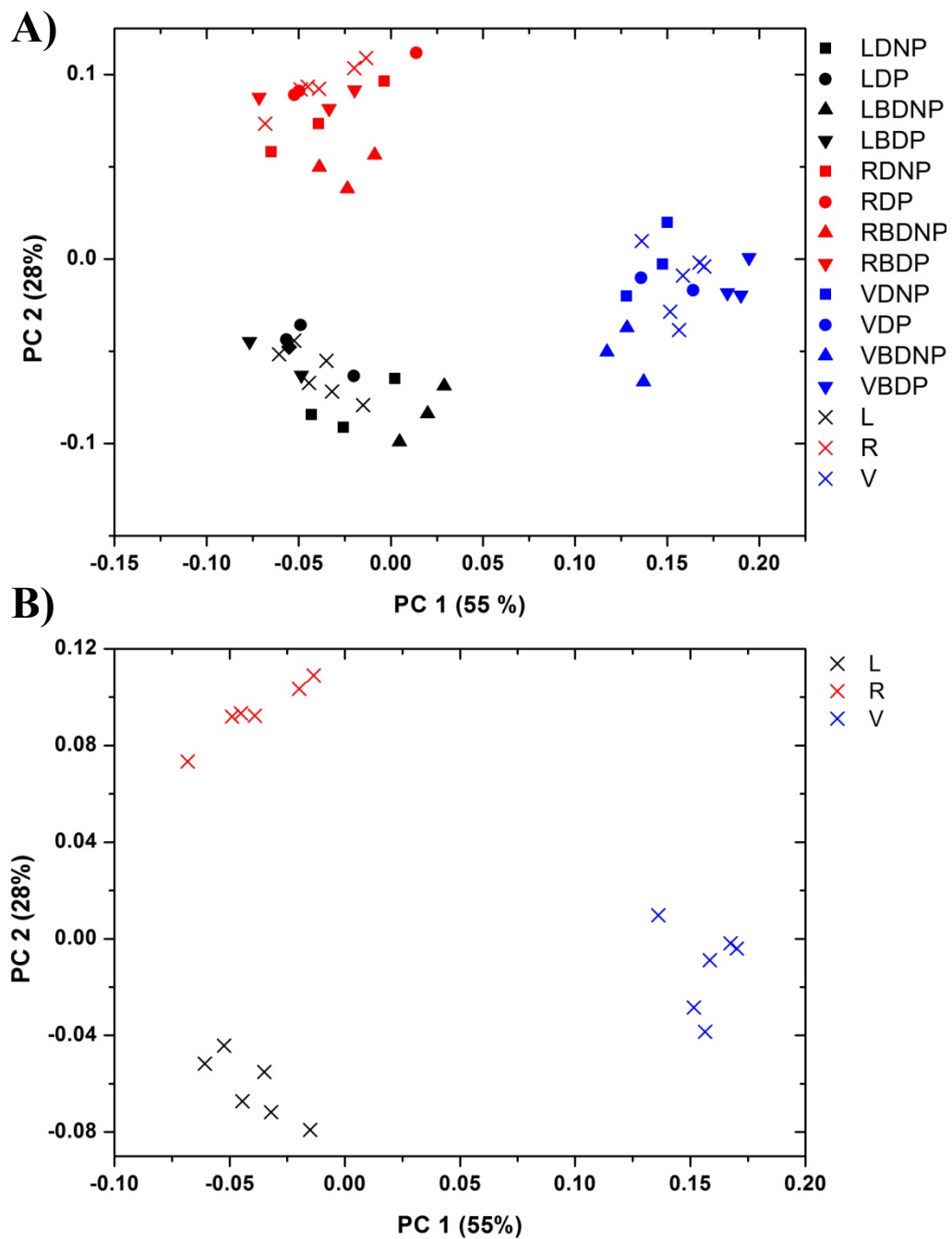


Figure 4-2 A) The scores plot for PC 1 versus PC 2 using positive ion spectra obtained for all ocular tissues samples. L corresponds to lens, V to vitreous and R to retina. DNP corresponds to low dosed non-perfused controls and BDNP to high dosed non-perfused. DP corresponds to low dosed perfused samples and BDP to high dosed perfused samples. B) The scores plot for PC 1 versus 2 using positive ion

spectra obtained control tissue samples. L corresponds to lens, V to vitreous and R to retina.

A peak of $m/z = 63$ was also detected and was associated with positive directionality on PC 1 and also positive directionality on PC 2. A positive value on both PC 1 and PC 2 was associated with the vitreous tissue. Copper ($m/z = 63$, Cu^{2+}) is known to reside in the human vitreous and levels are often found to be increased during vitreoretinal diseases such as diabetic retinopathy (Konerirajapuram, Coral et al. 2004). The ocular tissues used in this work come from healthy ovine eyes sacrificed at a young age, therefore it is unlikely the ocular tissues investigated would have increased Cu^{2+} levels. In addition the positioning of ion $m/z = 63$ on Figure 4-4A, shows only a weak pull in the positive direction, therefore it is likely this peak is commonly found in all three ocular tissues investigated and relates to a typical hydrocarbon species C_5H_3^+ , commonly seen in positive ion spectra and likely deriving from phenylalanine, tryptophan and tyrosine, which contain aromatic ring structure (Eynde and Bertrand 2000; Zhou, Chan et al. 2002).

Using ToF-SIMS we were not only able to detect small molecules, but interestingly we were able to detect smaller fragments of larger molecules found in ocular tissues. Phosphocholine fragments, including the phosphocholine head group $\text{C}_5\text{H}_{15}\text{NPO}_4^+$ with m/z 184, were shown to be present in the ocular tissue samples. (Figure 4-4A and Table 4-1) (Gazi, Dwyer et al. 2003; Jones, Lockyer et al. 2007). Negative PC 1 values were strongly associated with $\text{C}_5\text{H}_{15}\text{NPO}_4^+$, however another ocular constituent, vitamin A is also known to fragment and produce ions with a corresponding m/z of 184 (Amemiya, Gong et al. 2003; Gazi, Dwyer et al. 2003). The lens tissue, sits within the negative regions of PC 1 and 2 and is dominated by the peak at a m/z of 184. The lens is well known to contain vitamin C (Berman 1991) however, vitamin A content of the lens is unclear. On the other hand, the retinal content of vitamin A (Amemiya, Gong et al. 2003) is well established due to the essential role of vitamin A in the visual process (Quadro, Blaner et al. 1999). If the peak at $m/z = 184$ was induced by a fragment of vitamin A, it would feature on the positive side of PC 2, where the retina samples lie and not where the lens samples sit. The lens is composed of fibre cells, which are surrounded by a phospholipid

bilayer and as a result phosphocholine concentrations are likely to be high. Due to the position and importance of mass peak of $m/z = 184$ in the distribution of the lens samples, m/z of 184 represents $C_5H_{15}NPO_4^+$ (Figure 4-3). In addition to the phospholipid fragment identified, other potential fragments of larger molecules were also detected. A negative pull on PC 1, where the retina samples are positioned, was associated with a mass peak of $m/z = 86$ and represents either another phosphocholine fragment or the amino acid leucine (Aranyosiova, Michalka et al. 2008). Two amino acid transport systems are known to operate in the retina, namely the large neutral amino acid transporter (LAT) (Atluri, Talluri et al. 2008) and system A transporter (Yoneyama, Shinozaki et al. 2010). These transport systems transport amino acids in and out of the retina at the retinal pigmented epithelial layer, suggesting that the peak at 86 could be related to the amino acid leucine. However, the retina also contains phospholipids in the form of the retinal pigmented epithelial layer of cells. For this reason, although we have interestingly detected another fragment from a larger molecule, further investigation is required to determine whether this fragment is in fact a component of leucine or a component of phosphocholine.

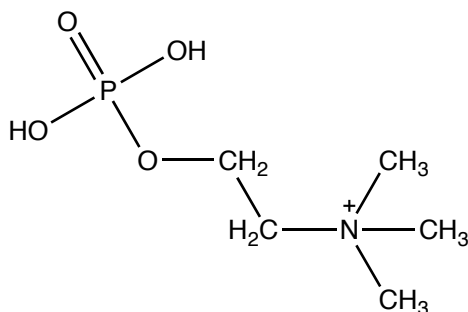


Figure 4-3 Potential chemical structure of fragment $m/z = 184$

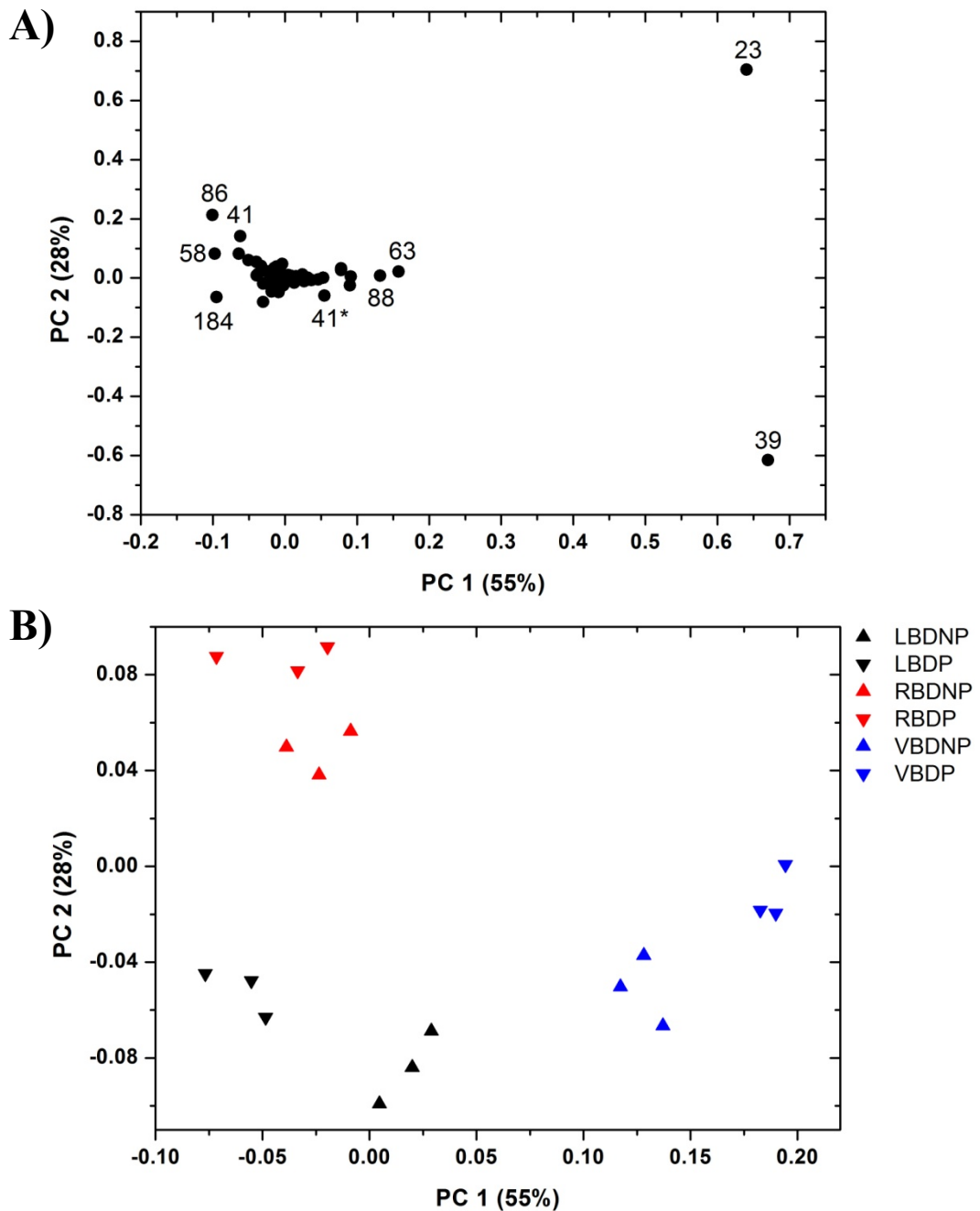


Figure 4-4 A) The loadings plot for PC 1 versus PC 2 demonstrating ion fragments controlling sample discrimination for positive ion spectra. B) The scores plot for PC 1 versus 2 using positive ion spectra obtained high dosed tissue samples. B represents the scores plot for PC 1 versus 2 using positive ion spectra obtained for all ocular tissues samples. L corresponds to lens, V to vitreous and R to retina. DNP corresponds to low dosed non-perfused controls and BDNP to high dosed non-

perfused. DP corresponds to low dosed perfused samples and BDP to high dosed perfused samples.

In addition to the identification of physiological ocular constituents on PC 1 and PC 2, information about the location of amitriptyline is also evident on these components. Within each of the tissue subtypes, sample grouping of model drug treated samples and untreated samples is evident. In the vitreous tissue samples, both the high dosed perfused samples and the high dosed non-perfused samples group together. Within the lens and the retina samples, grouping is present within samples treated with a high dose of drug, but only within samples that were dosed and non-perfused (**Figure 4-4B**). The model drug was administered directly into the vitreous of treated eyes that were either perfused or non-perfused. In the non-perfused eye, drug movement through the eye occurred by diffusion alone, resulting in drug not being cleared out of the eye due to the lack of blood flow. Therefore, highest drug concentrations would likely be seen in non-perfused, treated eyes where the total dose remained in the eye and was not cleared. This explains the grouping together of the non-perfused treated eye samples within the tissue groups for all three ocular tissues. In perfused eye samples, ocular flow systems were enabled, resulting in drug movement through the eye by both diffusion and convection processes, in addition to this, drug clearance from the vortex veins was also in operation (Moseley, Foulds et al. 1984; Tsuboi and Pederson 1988). For the treated perfused eye samples, it is likely that within the 2 hour perfusion period, some of the drug was cleared from the eye reducing the concentration present in relation to the non-perfused eye. This accounts for the lack of grouping between perfused treated eye samples of the lens and retina. For the vitreous, the grouping together of perfused treated samples suggests that a significant drug concentration still remained present within the vitreous. As the vitreous is an avascular structure, movement within the vitreous will often remain slow, even whilst flow systems are in operation within the eye. For this reason, a significant drug concentration remained within the vitreous, explaining the grouping in this tissue. Although the presence of the drug molecule is evident in PC 1 versus PC 2 (**Figure 4-2A**), the biochemical composition of the individual ocular tissue dominates the multivariate analysis and has overshadowed peaks related

to the model drug. For this reason, it is difficult to determine key ion peaks deriving only from drug fragmentation. Two peaks remain undetermined on PC 1 and PC 2, m/z of 58 and m/z of 88, and are possible fragments of the model drug (**Figure 4-4A**). The difficulty in identifying drug peaks could be related to the dose of drug administered to the eye and further work is required to investigate if specific drug fragments would be more apparent at a higher concentration within the tissue. Although this drug is a good representation of small drug molecules administered to the eye, the similarity of the drug structure to organic tissue constituents also make the process of identifying and assigning drug peaks more complex. Through the sample grouping, the presence of the drug is evident on PC 1 and PC 2 and is a highly promising result.

4.3.2. Principle Component 2 versus Principle Component 3

Considering PC 2 compared to PC 3 increases the complexity of the story, with new peaks controlling the directionality of the sample data. **Figure 4-6** shows the scores plot obtained for the PC 2 and 3 for the positive ion spectra of all tissue samples. As with PC 1 and 2, the data separates into the three distinct regions by ocular tissue subtype. The loadings plot of PC 2 and 3 (**Figure 4-6B**) contains the mass peak data used to create the score plot. Similarly with PC 1 and 2, the mass peaks controlling sample distribution on the scores plot of PC 2 and 3 fell within the mass region of 22 to 185 m/z , with additional mass peak involvement in determination of the scores plot, revealing added information about the physiological basis of the tissues.

From **Figure 4B**, iron (Fe^{2+} , $m/z = 55$) was identified and associated with a positive result on both PC 2 and PC 3 in the direction of the retinal samples. The retina is a vascular structure and, unlike the lens and vitreous, receives a rich blood supply, accounting for the influence of Fe^{2+} on the positioning of the retinal samples on PC 2 versus PC 3. A mass peak of 43 sat in a similar position to the Fe^{2+} peak on the positive side of both PC2 and PC3 and represents CH_3CO^+ , a smaller fragment of a larger biochemical structure of the eye. The fragment CH_3CO^+ could represent either hyaluronic acid (Shard, Davies et al. 1997) or a fragment of cholesterol (Nygren, Boerner et al. 2006). Hyaluronic acid is well known to be an important

constituent of the vitreous tissue however, it is also an important component of the retina, causing difficulty in identifying which of these fragments m/z of 43 relates to. (Gross-Jendroska, Lui et al. 1992) Another interesting peak identified by PC 2 and 3, most likely due to a fragment of a larger molecule, was m/z 70. This mass peak fell on the negative region of PC 2 and the positive region of PC 3 and is likely to be due to a fragment of the model drug ($C_4H_8N^+$) or the amino acid proline ($C_4H_8N^+$) (Dambach, Fartmann et al. 2003; Aranyosiova, Michalka et al. 2008). It is difficult to determine the identity of this fragment as proline is a known component of collagen which is present throughout the eye. However, sample grouping in high dose non-perfused samples remains for all three tissues on PC 2 and 3 (**Figure 4-6A**), with grouping only lost in the high dose perfused vitreous samples. Therefore, even on the second and third PC, the model drug is having an influence on the positioning of the samples within the matrix and it is possible m/z of 70 is a fragment of drug (**Figure 4-6**).

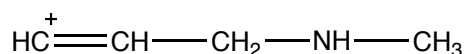


Figure 4-5 A potential fragment of amitriptyline with m/z of 70.

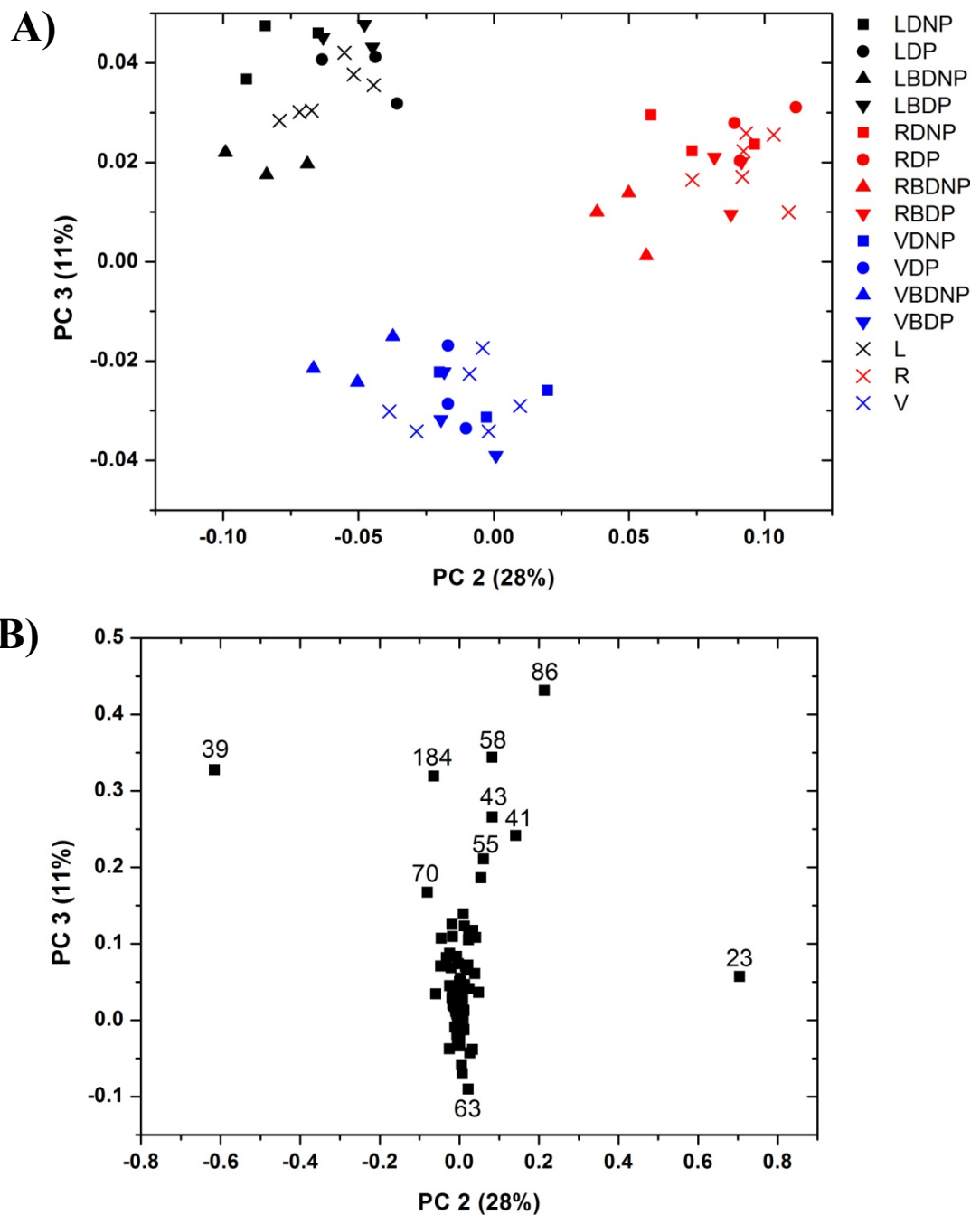


Figure 4-6 A) The scores plot for PC 2 versus PC 3 using positive ion spectra obtained for all ocular tissues samples. L corresponds to lens, V to vitreous and R to retina. DNP corresponds to low dosed non-perfused controls and BDNP to high dosed non-perfused. DP corresponds to low dosed perfused samples and BDP to high dosed perfused samples. B) The loadings plot for PC 2 versus PC 3

demonstrating ion fragments controlling sample discrimination for positive ion spectra.

4.4. CONCLUSIONS

This work has demonstrated that PCA can be applied to ToF-SIMS data in order to gain key physiological chemical information of ocular tissues and identify important physiological differences between ocular subtypes. The ability to detect and identify physiological constituents holds significant value in adding to the understanding of the structural components of the lens, vitreous and retinal tissues. PCA has also successfully detected model drug presence within ocular tissues, showing differences between ocular tissues treated with model drug and control ocular tissues. Although challenges arose in identifying specific drug fragments, this preliminary piece of work shows good promise in the use of the ToF-SIMS technique to identify drug location within ocular tissues. However, further work is still required in order to progress the use of ToF-SIMS in identifying drug distribution in ocular tissues. Studies focusing on a drug containing distinct chemical groups not typically seen in the ocular tissues analysed, such as a fluorinated compound, is of interest and would aid the identification of specific drug fragments.

CHAPTER 5. TOF-SIMS ANALYSIS OF DEXAMETHASONE DISTRIBUTION - IN THE ISOLATED PERFUSED EYE

5.1. INTRODUCTION

Dexamethasone (see Figure 1 for chemical structure) is a glucocorticoid drug currently used in the treatment of various inflammatory disease states, including inflammatory conditions of the eye such as uveitis and conjunctivitis. Dexamethasone has been administered to the eye using various routes of administration including, topical, systemic and intravitreal injection. Using the topical route of administration, dexamethasone has been shown to be of benefit as an inhibitor of inflammation following the ocular surgical procedures such as the vitrectomy or the lensectomy. It has also been used topically in combination with antibiotics to reduce anterior eye inflammation (Notivol, Bertin et al. 2004). Although dexamethasone has been shown to be useful in the treatment of anterior eye inflammation, following topical administration dexamethasone experiences poor penetration into the vitreous and posterior eye tissues (Weijtens, Schoemaker et al. 1998), as a result of this, topical treatment will have little effect in the treatment of posterior eye inflammatory conditions. The systemic route of dexamethasone administration has also been shown to be no better than the topical route with only

0.1% of the injected dose penetrating into the eye (Weijtens, Schoemaker et al. 1998). In order to penetrate to the back of the eye and treat posterior eye inflammation, the intravitreal route of administration is a more feasible option. Using the intravitreal route, dexamethasone has been shown to reduce inflammation and lessen the breakdown of the blood-ocular barrier (Barcia, Herrero-Vanrell et al. 2009; Earla, Boddu et al. 2010) and more recently, a dexamethasone implant has been shown to improve vision in patients suffering from macular edema (Haller, Bandello et al. 2010). Although dexamethasone administration via the intravitreal route has been shown to benefit patients suffering from macular edema, it has been associated with numerous adverse events (Armaly 1965; Williams, Haller et al. 2009; Haller, Kuppermann et al. 2010), with the two principal side-effects reported to be cataract formation (Williams, Haller et al. 2009) and increased intraocular pressure (Armaly 1965; Haller, Kuppermann et al. 2010).

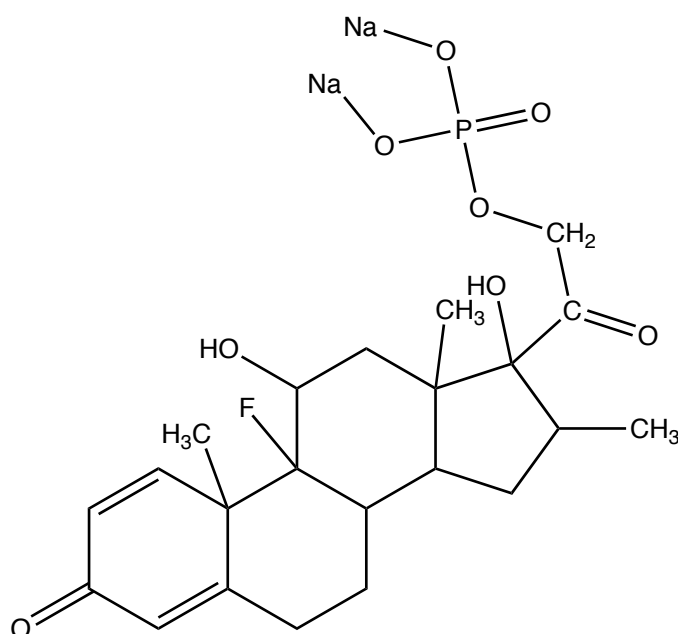


Figure 5-1 The chemical structure of dexamethasone. Note the Fluorine atom bonded to the 9th Carbon atom in the tetracyclic ring, which provides a unique chemical label for the drug.

Determining the extent of dexamethasone drug distribution within ocular tissues has involved the utilisation of various different analytical techniques. Standard analytical methods often used in determining ocular pharmacokinetics, including HPLC (Kwak and D'Amico 1995; Eljarrat-Binstock, Raiskup et al. 2005) and LCMS (Earla, Boddu et al. 2010), have been developed and used previously in the rabbit eye. In addition to these methods, tracking the movement of radiolabelled dexamethasone has also been performed (Attia, Kassem et al. 1988). In order to prepare ocular tissues for analysis via these commonly used methods, each ocular tissue is typically extracted and then is homogenized before performing a method of drug extraction from the tissue. The destructive nature of the standard analytical techniques has led to the desire to investigate alternative routes of measuring drug distribution within ocular structure and has included the development of a fluorescence polarization immunoassay method (Baeyens, Kaltsatos et al. 1998) and also a nuclear magnetic resonance imaging (NMR) method (Midelfart, Dybdahl et al. 1998). Using ^1H and ^{19}F NMR, Midelfart and colleagues were able to demonstrate the presence of dexamethasone and various amino acids in the aqueous humor of the rabbit eye, without the need for the lengthy drug extraction techniques required when performing standard analytical techniques on ocular tissue samples. Although this technique was shown to be a useful alternative technique in detecting drug presence within the aqueous humor, drug detection may not be as straight forward in one of the more complicated tissues of the eye such as the lens and the retina. In addition to this, NMR provided no spatial information on the drug location within the tissue. Interest in mapping drug distribution within ocular tissues has increased recently, especially when the target site of action is the posterior eye, which is particularly difficult to reach. Posterior eye conditions such as diabetic retinopathy (Porta and Allione 2004; Mason, Nixon et al. 2006) and age-related macular degeneration (Wong, Liew et al. 2007; Ding, Patel et al. 2008), have limited effective treatment options available and understanding spatial drug distribution patterns in ocular tissues could potentially improve treatment options in these conditions.

ToF-SIMS of samples requires no sample modification, unlike a similar but well used technique of matrix-assisted laser desorption/ionization time of flight mass spectrometry (MALDI-ToF) (Marko-Varga, Fehniger et al. 2011), which requires the

sample to be coated with a matrix. In ToF-SIMS measurements a primary ion beam is fired at the surface of the sample of interest. The primary ions then collide with the sample causing sample fragmentation and the generation of secondary ions. The secondary ions generated are then accelerated to the detector with a known kinetic energy, enabling an accurate ion mass to be determined from the flight time required by the ion (Benninghoven, Hagenhoff et al. 1993). The potential of ToF-SIMS to map drug distribution within ocular tissue, without the need for prior drug extraction, has previously been demonstrated in our group, using amitriptyline as a model basic drug (Mains, Wilson et al.). Using ToF-SIMS and the multivariate analytical technique, principle component analysis (PCA), key physiological differences between ocular subtypes were identified and in addition to this, presence of the model drug in drug treated tissue samples was demonstrated. However, this study focused on the use of PCA to data mine mass spectra from specific ocular tissue types to determine drug distribution, rather than utilize key mass fragments to build ion maps to determine drug distribution. In this study, we present for the first time how the technique of ToF-SIMS can be successfully utilised to image as well as spatially determine drug distribution in the lens, vitreous and retinal ocular tissues, following intravitreal drug administration. In addition, we also demonstrate key differences in the movement and distribution of dexamethasone phosphate disodium within the vitreous humor, the lens and retina of the living eye and the non-living eye.

5.2. MATERIALS AND METHODS

5.2.1. Chemicals

Dexamethasone phosphate disodium salt (purity \geq 98%) was purchased from Sigma-Aldrich (Dorset, UK). Isopropyl alcohol that was used to clean silicon wafers before sample mounting was obtained from Fischer Scientific (Loughborough, UK).

5.2.2. Isolated ovine eye preparation

Ovine eyes were prepared and perfused using the isolated perfused ovine eye technique detailed in chapter three of this thesis. The non-perfused ovine eyes were prepared by removing any remaining parts of the animal's eye lids, extraorbital

muscles and excess extraorbital tissue using dissection scissors. Following this, the non-perfused eyes were first gently washed using a small volume of the perfusion fluid (composition detailed in chapter three) and were then placed into 50 mm tissue lined petri dishes. Finally, the ovine eyes were then washed and moistened again with a small volume of the perfusion fluid.

5.2.3. Intravitreal administration of dexamethasone phosphate disodium

To investigate the distribution of dexamethasone phosphate disodium within the ovine eye following intravitreal administration using the technique of ToF-SIMS, a solution containing dexamethasone at a concentration of 100mg/ml was prepared by weighing 100mg of dexamethasone phosphate disodium and dissolving in 1ml of deionised water. The solution was then passed through a 0.22 μm syringe filter to remove any particulates. For the isolated perfused ovine eyes, once the eye had reached maximum perfusion rate and arterial perfusion pressure and IOP was maintained, the intravitreal injection was performed. The dose delivered to the eye was 10 mg of dexamethasone phosphate disodium in a total injection volume of 100 μl . The injection was performed using a 1ml syringe and 23G needle, inserted 5mm into the vitreous approximately 3 to 4 mm from the limbus in the posterior direction. Following injection the needle was drawn very slowly from the eye in order to minimise leakage from the injection site. For the isolated non-perfused ovine eyes the injection was performed as soon as the ovine eye had been prepared and used the same injection method adopted for the isolated perfused ovine eye.

5.2.4. Tissue preparation

One hour following the intravitreal injection, for the isolated perfused ovine eyes, the perfusion procedure was terminated and the perfused eyes were removed from the perfusion kit. Both the perfused eyes and the non-perfused eyes were then immediately frozen in liquid nitrogen before the tissue dissection procedure was performed. Using the same technique detailed in chapter four of this thesis, the anterior eye was then cut away in a circular manner and the lens removed. In order to achieve cross sections of the vitreous and the retina, the eye was sliced at four

positions from the anterior to the posterior section. The vitreous was removed and the sclera was pressed back for cryosectioning. All tissues were stored at -80°C prior to sectioning. The lens, vitreous and retina from each eye were mounted onto a cryostat chuck using Shandon M-1 embedding matrix (Thermo-Scientific, Chesire). $20\ \mu\text{m}$ thick sections were cut through the centre of the tissue on a Leica CM1850 Cryostat (Leica Microsystems, Milton Keynes, UK). Tissue sections were mounted directly onto $1\times 1\text{cm}$ silicon wafers, which were previously cleaned with isopropyl alcohol.

5.2.5. Drug sample preparation

In order to understand the drug fragmentation patterns of the pure drug substance alone, without the presence of physiological chemical fragments from the ocular tissue samples, a solution containing dexamethasone phosphate disodium at a concentration of 100mg/ml was prepared by weighing 100mg of dexamethasone phosphate disodium and dissolving in 1ml of deionised water. $100\ \mu\text{l}$ of the dexamethasone phosphate disodium solution was then applied to a silicon wafer and left to dry in a fume hood overnight before subsequent analysis was performed.

5.2.6. ToF-SIMS analysis

An Ion-TOF ToF-SIMS IV instrument (IONTOF, GmbH, Munster, Germany) using a Bi^{3+} cluster source and a single-stage reflectron analyzer was used to perform time of flight-secondary ion mass spectrometry. Spectra were acquired in both positive and negative by rastering a primary ion energy of $25\ \text{kV}$ along with a pulsed target current of approximately $1\ \text{pA}$ and postacceleration energy of $10\ \text{kV}$ across the sample surface. Analysis was performed on a sample area of $500\times 500\ \mu\text{m}$ of each tissue. The primary ion dose density was maintained at less than 10^{12} ions per cm^2 throughout to ensure static conditions. A common insulating effect of biological surfaces is positive primary ion beam induced surface charging. In order to account for this low energy electrons ($20\ \text{eV}$) were delivered to the sample surface throughout the analysis. Data processing was performed using SurfaceLab 6 Image software (IONTOF, GmbH, Munster, Germany), for spectroscopy and image analysis

5.3. RESULTS AND DISCUSSION

5.3.1. ToF-SIMS spectra analysis

Dexamethasone phosphate disodium was selected for investigation in this work due its anti-inflammatory effect in both the anterior and the posterior eye and also its structural chemistry. Dexamethasone phosphate disodium is relatively large, slightly lipophilic drug molecule, with a molecular weight of 516.45 and a log P of 0.56 (

Figure 5-1). The presence of the fluorine group makes it an ideal candidate for studying distribution using ToF-SIMS, as fluorine based anions tend to dominate ToF-SIMS negative ion spectra due to the stability of the fluorine anion (Feng, Chan et al. 2000; Huang, Goh et al. 2004)

In order to analyse lens, retina and vitreous samples by ToF-SIMS, both positive and negative spectra were obtained for all samples. For each of the tissue subtypes and tissue samples, perfused eye samples and non-perfused eye samples, analysis was performed on three replicates of each sample. ToF-SIMS analysis was also performed on a sample of dexamethasone phosphate disodium alone. In ToF-SIMS analysis, the ion beam is rastered across the sample surface and a complete mass spectrum is obtained for each point on the sample hit. From the mass spectra produced, key ions of interest can then be selected and an image of the distribution pattern of the ion in the sample generated. Mass spectra obtained for each sample contained numerous peaks with m/z ranging from 1 to 870. Peaks at the lower end of the mass spectra dominated, with greater peak intensities achieved in the m/z range of 1 to 200, a common occurrence in ToF-SIMS (Urquhart, Taylor et al. 2007). A peak list was generated for both the positive and negative spectra, using a method detailed previously by Urquhart et al (Urquhart, Taylor et al. 2007). Peak lists were initially generated using the pure drug substance sample. Using the positive spectra obtained for the drug and tissue samples, 172 ion peaks were selected and added to form the peak list. In the negative pure drug spectra, 292 ion peaks were selected and added to form the peak list. The positive and negative ion peak lists generated were then applied to each of the tissue samples. Positive spectra obtained from a perfused eye lens sample and a non-perfused lens sample were then directly

compared to the positive spectra obtained for the pure drug sample. Using all three spectrums, key drug peaks present in the lens samples were identified. This process was repeated for both the retina and the vitreous tissue samples and used to generate a list of fundamental drug ion fragments to be imaged across the samples. Example positive spectra obtained from the lens, retina and vitreous tissues are shown in Figure 5-2 to Figure 5-4. Across the samples in the positive spectra, four significant dexamethasone fragments were identified due to their presence in the spectra obtained for the drug, the lens, the vitreous and the retina samples (m/z 63, 109, 187, 289).

As with the positive spectra, key drug peaks present in the perfused eye and non-perfused eye samples were identified by directly comparing the negative spectra of samples with the negative spectra obtained for the pure drug samples. Again following this, the process was repeated for both the retina and vitreous to generate a complete list of crucial drug ion fragments to be imaged across the sample. Across the samples in the negative spectra, just one critical dexamethasone phosphate disodium fragment ($m/z = 19$) was identified due to its presence in the spectra obtained for the drug, the lens, the vitreous and the retina samples.

The four drug peaks identified in the positive ion spectra represent molecular fragments of dexamethasone phosphate disodium (**Figure 5-1**). The peak at $m/z = 63$ represents $C_5H_3^+$, a commonly encountered hydrocarbon species in positive ToF-SIMS spectra of molecules containing aromatic ring structure (Gazi, Dwyer et al. 2003). It is possible that $m/z = 63$ could be a fragment of an amino acid, such as phenylalanine, tryptophan or tyrosine, however due to the uneven distribution within the vitreous of the non-perfused eye, $m/z = 63$ represents a single ring fragment of the drug. Mass peak $m/z = 109$ represents $C_7H_9O^+$, which represents another single ring based structure, arising typically in mass spectrometry of steroid drug structure (Williams, Kind et al. 1999). The peak at $m/z = 187$ remains unassigned however the similarity in distribution of this ion peak to the other drug peaks suggest it is likely to represent a bicyclic ring fragment of the drug. The final drug peak identified in the positive spectra at $m/z = 289$ represents $C_{18}H_{25}O_3^+$, a tricyclic ring fragment generated from the dexamethasone phosphate disodium (Calza, Pelizzetti et al. 2001). In the positive spectra, there is a potential chance that a proportion of the

ion intensity measured for each molecular ion fragment could be influenced by the signal generated by molecular ions emitted from biological molecules released from the tissue surface. In the case of the negative spectra, the ion intensity signal of the characteristic fluorine ion of the drug was high and is highly unlikely to be influenced by the secondary ions generated from the tissue sample. For this reason, $m/z = 19$ (F^-) was also selected to monitor drug distribution through the eye and to validate the patterns of drug distribution recorded for key drug peaks obtained in the positive spectrum.

m/z	Spectra	Ion Structure
63	Positive	$C_5H_3^+$
107	Positive	$C_7H_9O^+$
187	Positive	Unassigned
289	Positive	$C_{18}H_{25}O_3^+$
19	Negative	F^-

Table 5-1 Selected drug ion fragments (m/z) and structural assignment for positive and negative ion spectra.

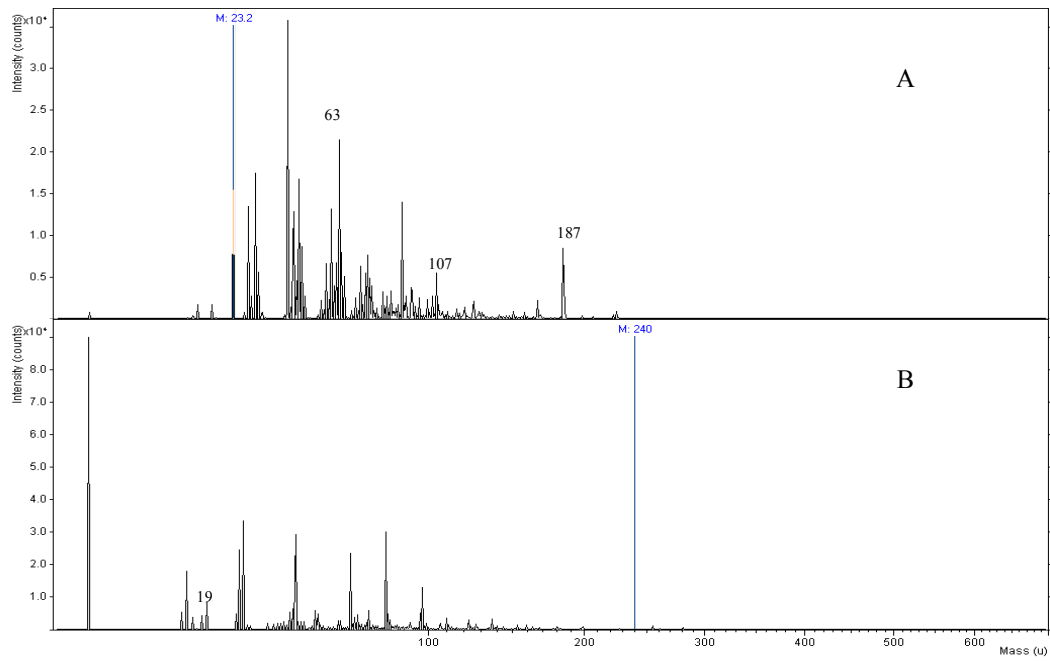


Figure 5-2 Example ToF-SIMS spectra of the Retina, A represents the positive spectra and B represents the negative spectra.

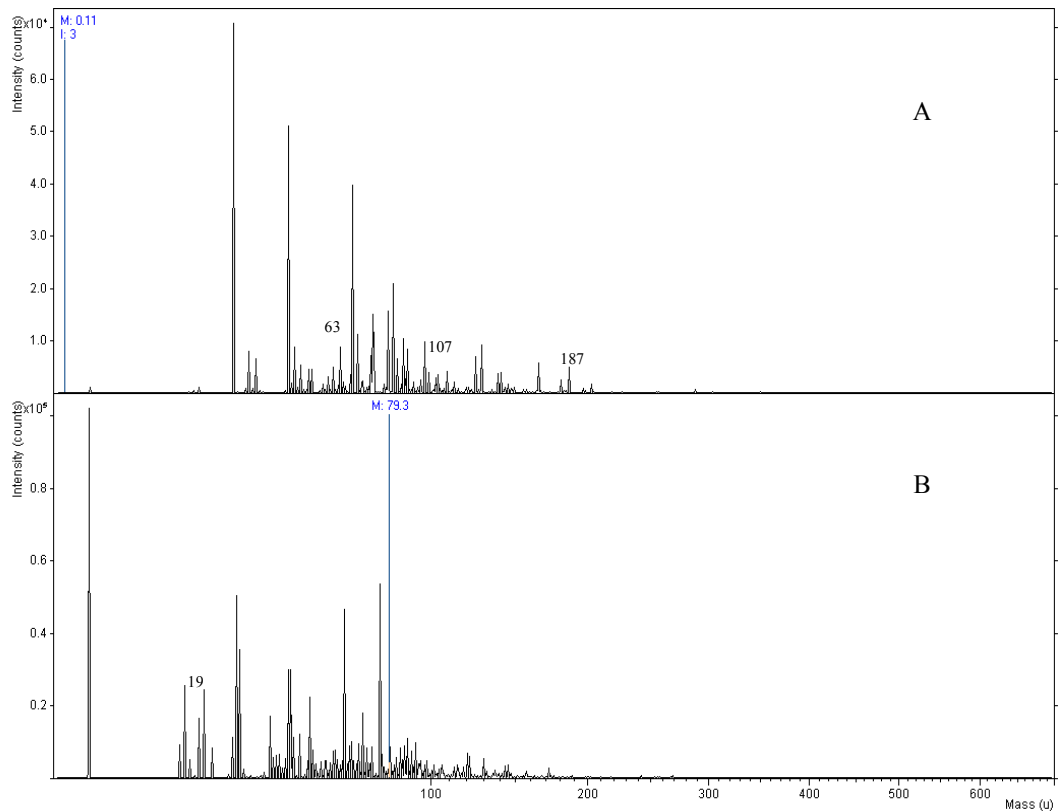


Figure 5-3 Example ToF-SIMS spectra of the Lens, A represents the positive spectra and B represents the negative spectra.

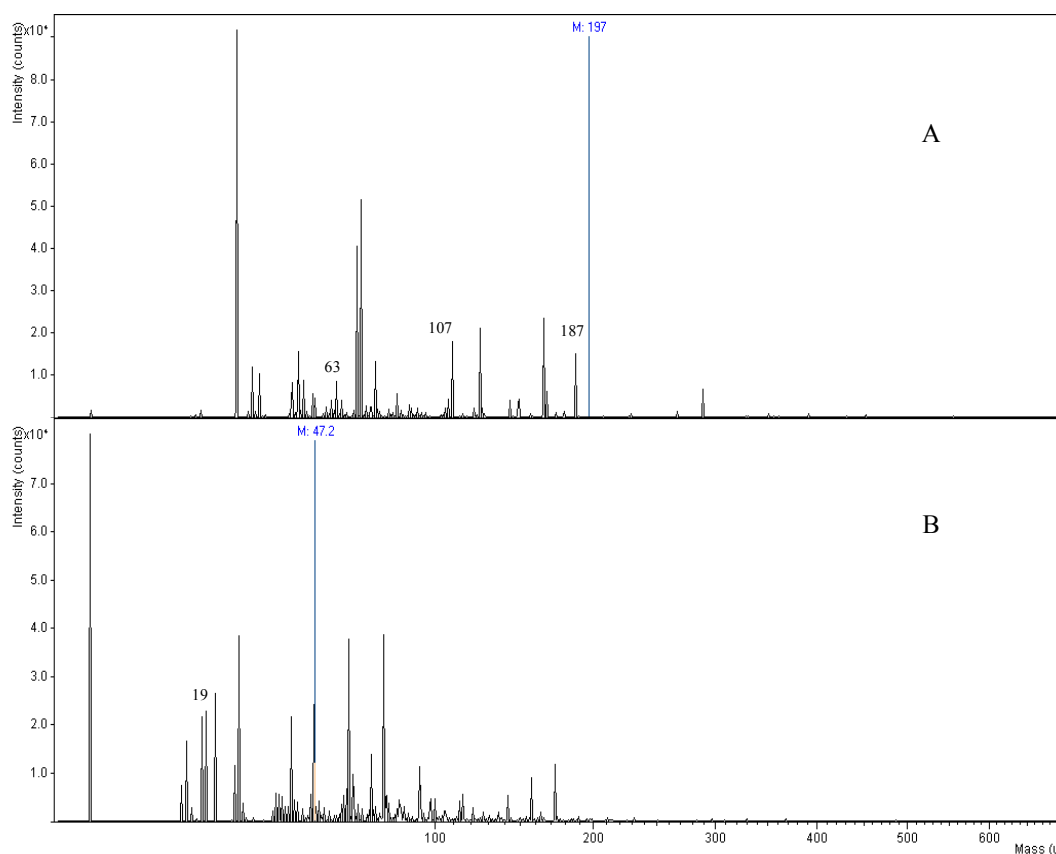


Figure 5-4 Example ToF-SIMS spectra of the Vitreous, A represents the positive spectra and B represents the negative spectra.

5.3.2. Dexamethasone phosphate disodium distribution in the non-perfused eye

Images of the distribution of the significant positive ion drug peaks in the non-perfused eye treated with dexamethasone phosphate disodium are shown in Figure 5.5. A high signal intensity was obtained for drug peak $m/z = 63$ in the vitreous samples. Similar signal intensities were achieved at the front and the middle of the vitreous, with the greatest signal intensity recorded in the back section of the vitreous towards the retina. A high signal intensity was also seen at the front of the retina, with intensity decreasing in the middle of the retina and becoming extremely low at the back of the retina. In the lens samples, the presence of the molecular ion $m/z = 63$ was negligible. The remaining three chosen drug peaks ($m/z = 109, 187,$

289) showed similar intensities in the non-perfused eye. Signals were detectable in the vitreous samples with low intensity at the front and in the middle of the vitreous but increasing in intensity at the back of the vitreous. In the retina, although signal intensity was low, the intensity decreased moving through the retina, with the highest signal intensity detected at the front of the retina, next to the vitreous, and the lowest at the back. Again in the lens samples, the presence of all three drug peaks was insignificant.

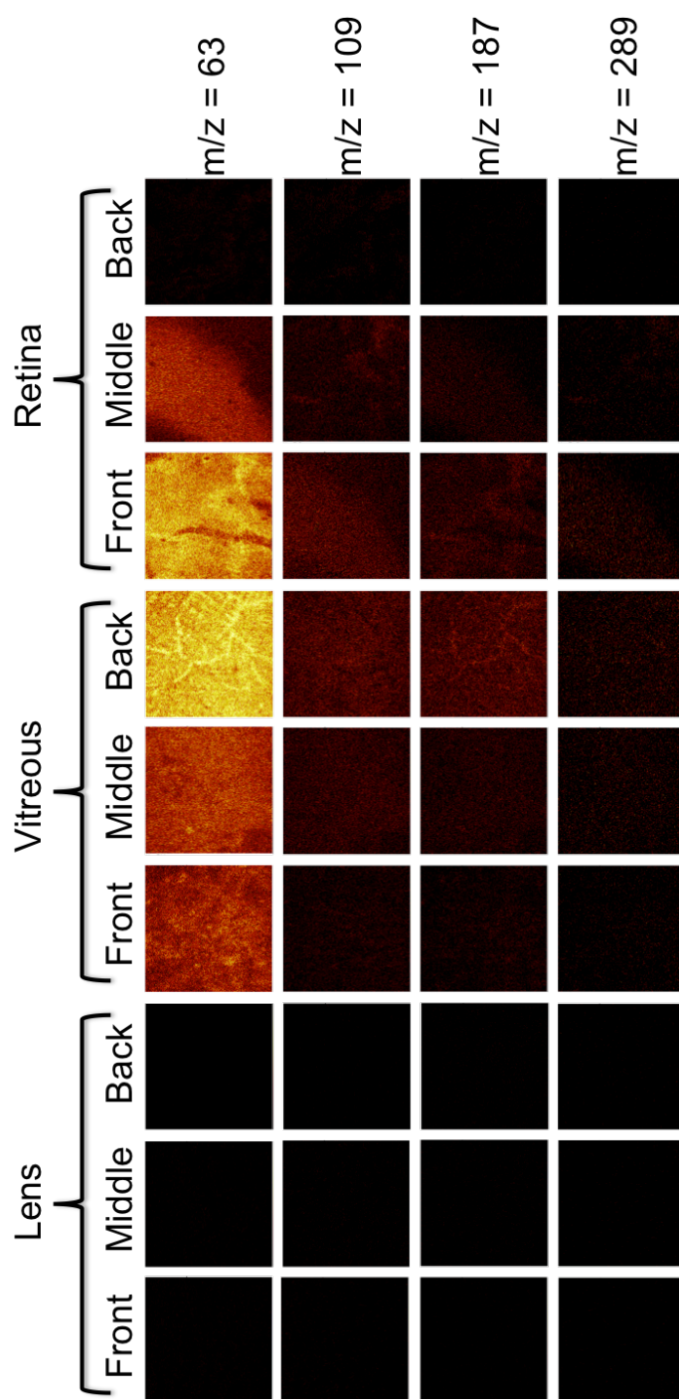


Figure 5-5 ToF-SIMS images showing the spatial distribution of drug specific dexamethasone phosphate disodium drug fragments detailed by the drug fragments m/z (mass to charge ratio) in the front, middle and back sections of the lens, the vitreous humor and the retina. The 500 x 500 μm images were obtained from

measurements of positive secondary ions and show images obtained for non-perfused eye tissue sections.

The distribution of the $m/z = 19$ drug fragment in the non-perfused eye samples treated is shown in Figure 5-6A. In the non-perfused eye, fluorine signal intensity was low at the front of the vitreous but high in the middle and in the back vitreous samples. Interestingly, a spot of very high signal intensity was seen in the middle vitreous and also in the front of the retina. At the front of the retina, significant peak intensity was recorded and again a small area of larger signal intensity was seen. In the remaining retina samples, lower intensities were seen in the middle and at the back of the retina. Peak intensity in the lens samples was marginal.

The non-perfused eye was selected as an initial means of determining the feasibility of imaging drug location within the ocular tissue cross sections. In the non-perfused eye, flow and circulation within the isolated eye are redundant and as a result drug movement will occur by diffusion alone. There is also no clearance systems operating within the non-perfused eye, therefore no drug would have been removed from the eye during the course of the experiment and drug concentrations would have remained high in the vitreous. In the vitreous of the non-perfused eye, drug fragment distribution was successfully imaged and drug diffusion from the front section of the vitreous to the middle and back sections was evident. In the non-perfused eye a differential concentration gradient is present in the vitreous, providing a motive force, which drives drug movement through the vitreous to the retina and this is shown by the presence of drug in the positive spectrum in the front section of the retina only (Figure 5-5). This is confirmed by the generation of a much greater signal intensity of F⁻ in the front section of the retina, compared to the middle and back sections, in the negative spectrum (Figure 5.6A). As the drug solution was injected into the back of the vitreous, the lack of uniformity in drug distribution across the vitreous (from front to back) is likely to reflect vitreal structure. The vitreous is a fluid based structure composed of approximately 99% water. However, although composed of predominantly water, the vitreous has a gel like structure owing its viscoelastic properties to collagen, hyaluronic acid and proteoglycans

which are contained within (Balazs and Denlinger 1984). It has previously been shown that dexamethasone diffusion through the vitreous is 4-5 times slower than its diffusion in water (Gisladdottir, Loftsson et al. 2009). In the non-perfused eye lens images, drug was not shown to be present due to the lack of flow operating in the dead eye and therefore the drug did not penetrate into the ocular lens. In addition we also see a potential element of drug clumping in the vitreous and the retina of the non-perfused eye, this could be due drug localisation on structure contained within these tissues when flow systems are not in operation within the eye.

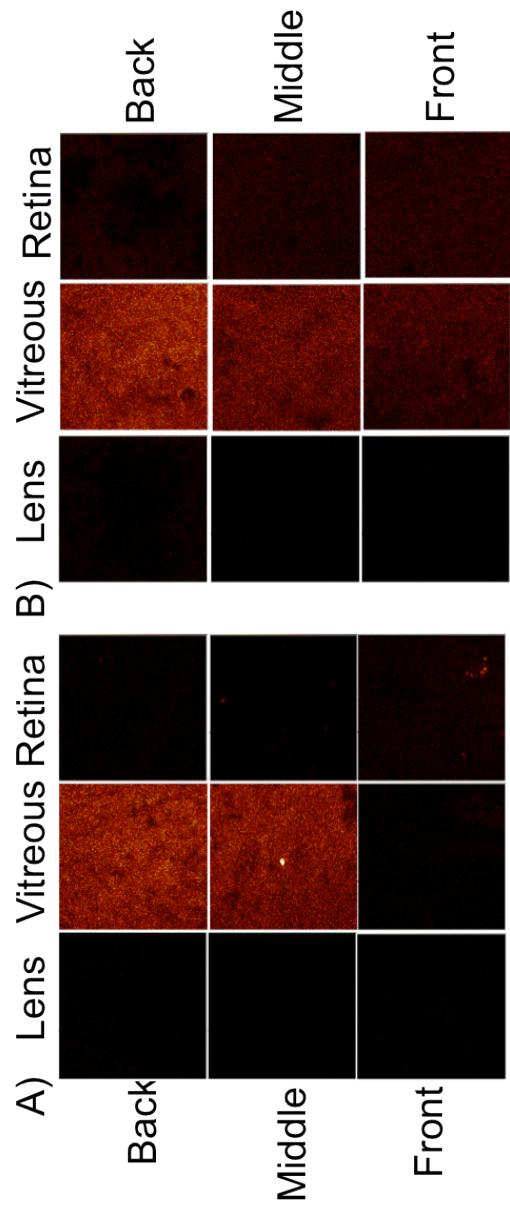


Figure 5-6 A) F^- ion distribution in the non-perfused eye (500 x 500 μm images). B) F^- ion distribution in the perfused eye (500 x 500 μm images).

5.3.3. Dexamethasone phosphate disodium distribution in the perfused eye

The distribution of the significant positive ion drug peaks in the perfused eye samples treated with dexamethasone phosphate disodium are shown in Figure 5.7. For drug peak $m/z = 63$ in the vitreous samples a high signal intensity, similar to that seen in the back of the vitreous of the non-perfused eye samples, was seen across the front, middle and back sections of the vitreous. Signal intensities in the retina of the perfused eye samples were higher than in the non-perfused eye samples. High signal intensities were seen at the front and in the middle sections of the retina, with intensity decreasing at the back of the retina. In the lens samples of the perfused eye, a low intensity of mass peak $m/z = 63$ was detected at the back of the lens (in contact with the vitreous) however, at the front and in the middle of the lens signal intensities were still insignificant. For drug peak $m/z = 109$, significant and relatively equal signal intensity was seen in front vitreous, middle vitreous, front retina and middle retina, with seemingly even distribution across the samples. At the back of the vitreous and the back of the retina, the signal intensity was slightly reduced. In the lens samples, again a low intensity was detected at the back of the lens, with negligible drug detection at the front and in the middle of the vitreous. A similar pattern of intensity was shown for drug peak $m/z = 187$ for the retina and vitreous samples, with the exception for the lens tissue where for all samples front to back, signal intensities were negligible. For drug mass peak $m/z = 289$, a similar pattern of intensity to drug peak $m/z = 187$, was noted across all samples with reduced signal intensity.

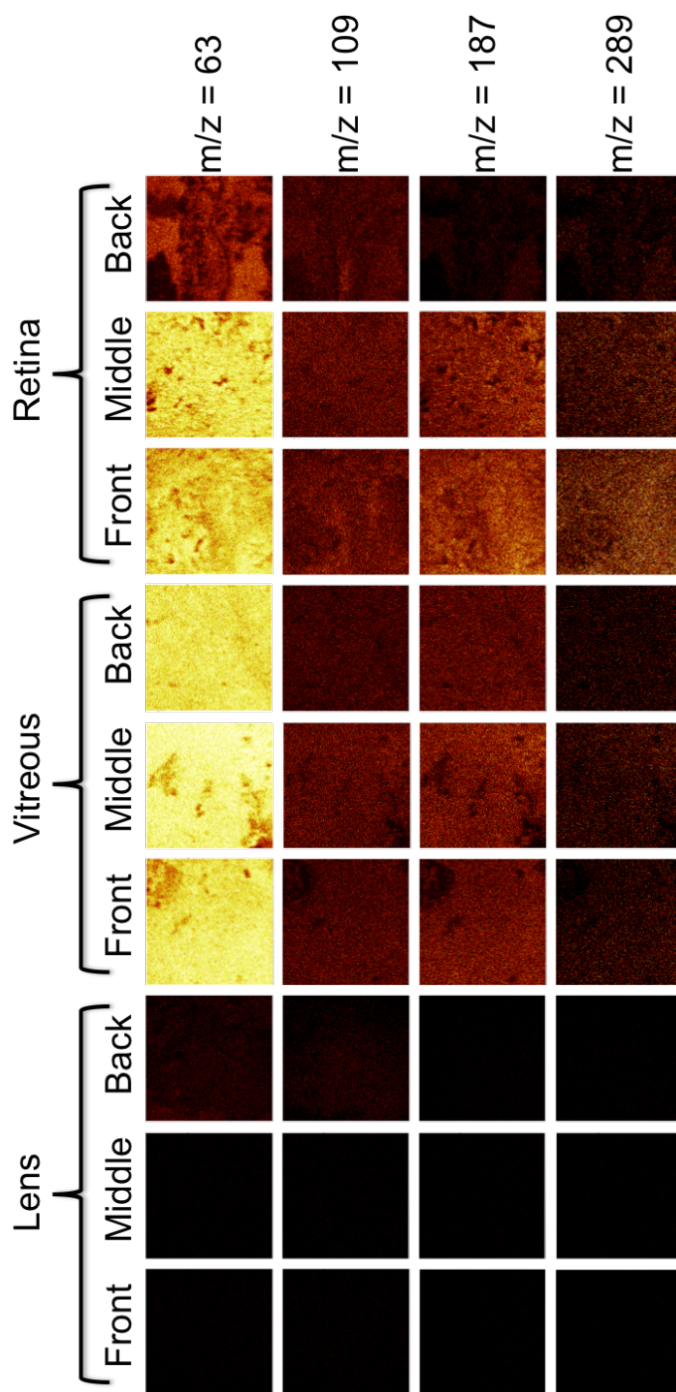


Figure 5-7 ToF-SIMS images showing the spatial distribution of drug specific dexamethasone phosphate disodium drug fragments detailed by the drug fragments m/z (mass to charge ratio) in the front, middle and back sections of the lens, the

vitreous humor and the retina. The 500 x 500 μm images were obtained from measurements of positive secondary ions and show images obtained for perfused eye tissue sections.

The distribution of the $m/z = 19$ drug fragment in the perfused eye samples treated is shown in Figure 5.6B. In the perfused eye greater dexamethasone distribution was apparent. Across the vitreous samples, high, evenly distributed signal intensities were seen from front to back, with slightly greater intensity seen at the back of the vitreous. In the retina samples $m/z = 19$ peak intensity was much greater in the perfused eye compared to the non-perfused eye, with slightly reduced signal intensity at the back of the retina when compared to the front and middle retina samples. Again in the lens samples signal intensities were marginal, with a slightly greater signal intensity noted at the back of the lens (see Figure 5-8 for increased clarity).

All of the positive and negative drug fragments selected to monitor drug distribution in ocular tissue cross sections followed very similar patterns of drug distribution within each of the eye tissue sections, however it is noted that the signal intensities obtained for each individual ion are not the same. As the individual ion fragments are generated from the same parent drug compound, in a simplistic view it would be anticipated that each ion fragment would generate the same signal intensity, as the concentration of the drug contained in the tissue cross section that the ion is generated from is the same. In ToF-SIMS this is not the case as the yield of secondary ions generated is not a simple process and can depend on several factors. Two important factors which experience variability and influence secondary ion generation and therefore signal intensity, are the yield of secondary ions generated per impact of the primary ion beam and also the probability that a given particle will be released from the sample surface as a certain ion (Belu, Graham et al. 2003). In addition, there is also the influence of matrix effect phenomena, where the yield of secondary ions emitted can vary depending on the environment in which they are generated. The sample environment can change during analysis and this again can influence the secondary ion yield, however by employing the spectra pre-

processing steps discussed previously, the impact of this effect can be limited (Tyler, Rayal et al. 2007).

The perfused eye system has been developed as an effective method of investigating properties of the eye, ex-vivo, whilst maintaining arterial flow and nutritional status within the eye (Gouras and Hoff 1970). Advantages of the isolated eye model, in comparison to performing a full animal study, include no anaesthetic requirements or concern over animal welfare, control over the physiological environment, reduced animal usage, controlled drug administration and control of exposure to substances from systemic circulation into the ocular system (Niemeyer 2001), making it an ideal model in which to study drug distribution. In the vitreous samples of the perfused eye, a more even distribution of the drug across the front, the middle and the back of the vitreous was evident, when compared to the non-perfused eye. As flow systems remain operational within the perfused eye, drug movement in the vitreous occurs by both diffusion and convection (Fatt 1975; Xu, Heys et al. 2000). There has been some debate over the role of convection in drug distribution in the vitreous with some suggestion that convection plays a role, although the impact is lesser than that of diffusion (Fatt 1975; Park, Bungay et al. 2005). Whereas other work has suggested that convection will only become important for larger sized molecules (Missel 2002; Stay, Xu et al. 2002). Although dexamethasone phosphate disodium is regarded as a small drug molecule, it is clear from the images that drug movement within the non-perfused and perfused eye differ, with drug movement in the perfused eye occurring not only in the posterior direction but also in the anterior direction, where it was also detected in the back section of the lens. Therefore, in this case drug movement is not caused solely by diffusion but demonstrates the importance of convection on drug movement, even for a small drug molecule. In the perfused eye, the signal intensity in the retina images were much larger than the signal obtained in the non-perfused eye retina images for both the positive drug fragments and the negative drug fragment F⁻. The drug was evident in all retina cross sections, demonstrating that dexamethasone sodium phosphate can penetrate from the vitreous completely through the retina to the posterior retina, which is extremely desirable in the treatment of posterior eye disease. The transfer of materials at the RPE and therefore drug movement from the vitreous to the retina and

the choroid is not only controlled by flow systems operating within the eye but is thought to involve drug transporter systems (Smith, Kincaid et al. 1999; Wilson, Semenera et al. 2007) Previously, the involvement of transporter systems in ocular drug delivery, such as p-glycoprotein, organic cation transports and organic anion transporters, has been demonstrated (Han, Sweet et al. 2001; Hosoya, Ohshima et al. 2003; Steuer, Jaworski et al. 2005). The involvement of drug transporter systems in dexamethasone movement into the retina was out of the scope of this study however, the potential impact of drug transporter systems on dexamethasone phosphate disodium distribution in ocular tissues should be considered when interpreting the results. Although the signal intensity of drug fragments in the lens is extremely low, the presence of drug within the back section of the lens is apparent, suggesting that dexamethasone phosphate disodium will also move towards the anterior eye following intravitreal administration. However, the lack of drug presence in the middle and the front lens sections could suggest that the drug will not move any further forward through the lens and will potentially move back into the vitreous. A similar effect on movement was noted by *Tan et al.* with intravitreally injected sodium fluorescein in the rabbit eye (Tan, Orilla et al. 2011). Using ocular fluorophotometry, it was shown that sodium fluorescein will penetrate into the ocular lens 2 hours after dosing however the substance did not continue a forward diffusion into the anterior chamber but unloaded the absorbed fluorescein back into the vitreous humour 3 hours later. However, due to the short time course of the experiment it is difficult to determine if the drug would penetrate further into the lens and through to the anterior chamber. It would be interesting in the future to extend the perfusion time and image the drug moving through and out of the lens tissue.

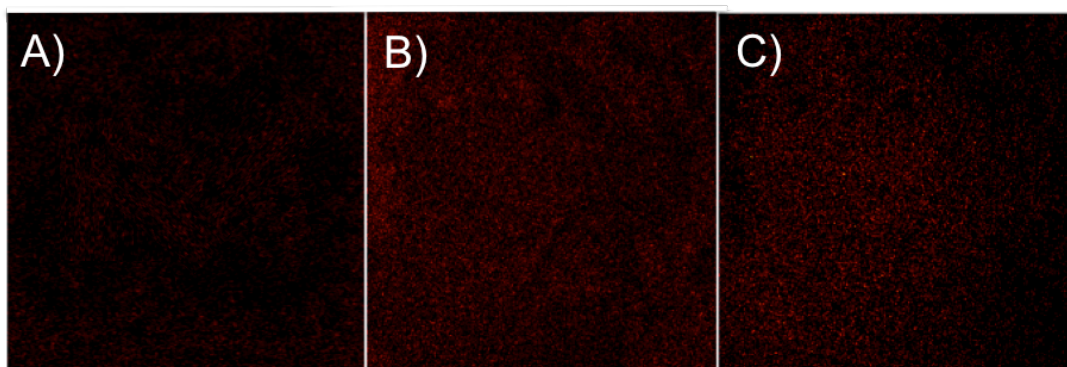


Figure 5-8 Enhanced contrast ToF-SIMS images, from the perfused eye back of the lens sample, altering saturated pixel percentage from 0.4 % to 2.5 % as an aid for clarity. A) $m/z = 19$, B) $m/z = 63$ and C) $m/z = 109$. All images are 500 x 500 μm .

5.4. CONCLUSIONS

Spatial ocular drug distribution is currently not well understood, as standard PK techniques treat individual ocular tissues as well stirred compartments. As such, these techniques are unable to characterise the spatial disposition of drug compounds and understanding drug distribution within a tissue is key for ensuring effective drug development. The results presented in this work illustrate the ability of ToF-SIMS to characterise and provide spatial information about drug distribution within ocular tissues. The capability to characterise drug positioning within an ocular tissue is extremely desirable, as typically when determining ocular drug distribution ocular tissues are homogenised and the drug is then extracted from the tissue, therefore no specific information with regards to the spatial positioning of the drug within the tissue can be determined. The ability to map and image drug positioning within individual ocular tissues holds significant value in adding to the understanding of how we can improve drug treatment options in posterior eye disease. Understanding spatial drug distribution within the target site of action, the retina, is especially useful as drug penetration through the retina is key in treating disease states such as diabetic retinopathy and age-related macular degeneration. In addition, here we have also demonstrated key differences in drug movement through the vitreous humor, towards both the anterior and posterior tissues, in the living eye and the non-living ovine eye, demonstrating that dexamethasone phosphate disodium distribution through the

vitreous is not determined by diffusion alone and will involve the circulatory flow systems operating within the eye and drug transporter systems.

CHAPTER 6. A FINITE ELEMENT MODEL OF BRIMONIDINE DISTRIBUTION IN THE RABBIT EYE

6.1. INTRODUCTION

Alongside the challenges of using intravitreal drug delivery methods to reach the back of the eye, utilizing topical ocular drug delivery methods to target posterior eye disease remains a challenging and difficult task. Typically, when drug delivery vehicles are applied to the cornea in the form of an eye drop, only a small proportion of the drop makes contact with the surface of the eye. This is mainly due to spillage of the drop from the lid onto the face during administration and also precorneal clearance mechanisms operating within the eye (Wilson, Zhu et al. 2001). Alongside these problems, the selectivity of the cornea restricts the free movement of drug compounds into the ocular tissues, by allowing only certain compounds to penetrate through its complex structure (Grass and Robinson 1984). Another physiological factor which prevents topically applied drugs penetrating into the ocular tissues is the tear drainage systems operating within the eye, known as the nasolacrimal drainage system. When applied to the surface of the cornea, drugs are often cleared down the nasolacrimal duct and into the nose, leading to the possibility of nasal drug absorption (Shell 1982; Urtti and Salminen 1993). If nasal drug absorption occurs,

there is potential for the administered drug to enter into the systemic circulation and cause unwanted systemic side effects. In light of these factors, it is estimated that, for the majority of topical drugs applied to the corneal surface, less than 5% of the delivered topical dose will actually penetrate into the anterior eye following administration (Sigurdsson, Stefansson et al. 2005). In addition to this, even if a small proportion of the applied dose manages to penetrate into the anterior eye, the difficult task of reaching the posterior eye remains.

Drugs applied topically to the front of the eye are thought to achieve concentrations in the posterior eye via three main penetrations pathways, through the cornea, through the sclera or via the systemic circulation. The first and most widely recognized penetration route is drug diffusion through the cornea into the aqueous humor (Valeri, Palmery et al. 1985). On reaching the aqueous humor the drug is then able to distribute into vitreous and into various other neighbouring intraocular tissues. More recently, penetration of topical drugs through the sclera has attracted more interest. Early work completed by Maurice and Polgar (Maurice and Polgar 1977) illustrated the ability of a range of compounds of differing molecular size to penetrate through bovine sclera. Further investigations then demonstrated that movement through the sclera involves a similar mechanism to the corneal stroma and that the extent of penetration is dependent on the thickness of the sclera and the surface area available, as well as the molecular weight of the drug in question (Geroski and Edelhauser 2001). The route of topical ocular drug penetration via the anterior scleral route first involves drug penetration across the conjunctiva. On penetrating the conjunctiva, the drug then diffuses through the sclera onto the iris and into the anterior eye or the drug moves in the posterior direction to the choroid (Ahmed and Patton 1985; Mizuno, Koide et al. 2009). Finally the drug can reach the posterior eye via the systemic circulation. On topical drug administration, the drug can penetrate into the systemic circulation by drug movement into the conjunctival vessels or movement into the nasal vessels arising from drainage into the nasolacrimal duct. The circulating drug can then reach the posterior tissues through the choroid, however movement into the retina poses a greater challenge due to the blood-retinal barrier (Leblanc, Jezequel et al. 1998).

Investigating the routes of topical drug penetration can be a challenging and time-consuming process. Typical *in vivo* ocular pharmacokinetic studies involve analytical determination using mass spectrometry and have large animal requirements. Numerous animals are required for each time point in the study due to the destructive nature of the drug quantification process and experimental variability between animals. In addition to this, the destructive nature of the analytical process requires each ocular tissue to be homogenized and treated as a uniform compartment, thus making it difficult to understand how the drug is moving through each tissue. Various experimental techniques have been exploited in an attempt to gain a clearer understanding of the processes involved in drug movement around the eye, including scintillation counting (Acheampong, Shackleton et al. 2002), magnetic resonance imaging (Kim, Csaky et al. 2007) and time-of-flight secondary ion mass spectrometry (Mains, Wilson et al 2011.). Although these techniques provide greater information on the processes involved in drug movement through the eye, clear, live images of drug movement are not yet possible. In an attempt to overcome this, interest has turned to using finite element modelling (FEM) as a suitable means of imaging drug penetration through ocular tissues. FEM has been used to model drug distribution in the vitreous humor in both a rabbit eye model and a human eye model (Friedrich, Cheng et al. 1997a; Friedrich, Cheng et al. 1997b). Using a model of the vitreous only, Friedrich and colleagues were able to visualize fluorescein movement through the vitreous and identify the importance of intravitreal injection positioning on drug distribution. In addition to drug movement, the routes of compound clearance from the vitreous due to diffusion and hydraulic flow have also been successfully studied using FEM and demonstrated that hydraulic flow has little impact on movement of small molecules that are subject to choroidal clearance (Missel 2002). Although drug movement in the vitreous humor has been well characterized using FEM, investigations into drug movement through the eye following topical drug administration using FEM has not been utilized to the same extent.

Brimonidine is a α_2 adrenoreceptor antagonist used in the treatment of various eye diseases, due to its ability to lower intraocular pressure through the reduction of aqueous humor formation. Following topical drug administration,

brimonidine has been shown to penetrate to the posterior tissues of the eye reaching the back of the eye and penetrating into the systemic circulation (Acheampong, Shackleton et al. 1995; Acheampong, Shackleton et al. 2002). Although it has been clearly demonstrated that brimonidine can penetrate through to the back of the eye following topical administration, the precise method of drug penetration is poorly understood. It is thought that penetration into the posterior tissues occurs by a combination of drug transmission through the cornea and through the sclera. In addition to these routes, it has also been suggested that transporters in the retina, specifically organic cation transporters, are thought to be involved in brimonidine distribution within ocular tissues (Hughes, Olejnik et al. 2005). In this study, we present for the first time a finite element model of brimonidine distribution through the rabbit eye following topical drug administration. In addition, we identify the main routes of brimonidine penetration from the delivery site to the retina are through the cornea in to the anterior eye, through the conjunctiva into the sclera and finally through the systemic circulation.

6.2. MATERIALS AND METHODS

6.2.1. Geometry

A 3D FEM model of the rabbit eye was created previously assuming cylindrical symmetry (Figure 6-1) (Damian-Iordache 2010). The rabbit eye geometry and meshing was created in COMSOL multiphysics version 3.5a, in 2D. Boundary conditions and parameter conditions were modified in MATLAB version 7.4.0. Simulations were performed on a fedora system operating out of Linux on a cluster source with 4 processors. The FEM accounted for all ocular tissues present in the rabbit eye and also membranes that existed between the different ocular tissues. Simple compartmental models were also included in the model to account for drainage through the nasolacrimal duct into the nose, drainage via the lymphatic system, the stomach, the gastrointestinal tract and also the systemic circulation.

6.2.2. Conditions

Within the model various parameters were created to control fluid flow and movement around the eye. Between each individual ocular tissue a membrane was

put in place to separate each tissue from and control movement between tissues. If no physiological barrier between the tissues exists, then the membrane was set to pose no barrier to drug movement. Each individual tissue was appointed its own diffusion coefficient and this was uniform across the whole tissue, treating the tissue as a stirred compartment. The potential of drug molecules to bind to ocular melanin in the choroid, the iris, the ciliary body and the retinal pigmented epithelium was accounted for. The fraction of drug binding to each pigmented tissue was treated separately and was kept uniform within the tissue. In addition to melanin binding, the fraction of drug free with respect to drug protein binding was accounted for and again protein binding was uniform within an individual tissue but treated separately in different tissues. The generation of tear film and tear turnover were accounted for, alongside the flow of ocular humor. In the anterior section of the eye, the aqueous humor was generated at a rate of $2.2 \mu\text{l}/\text{minute}$ and cleared from the eye at a rate of $2 \mu\text{l}/\text{minute}$. In the posterior section of the eye, vitreous humor flow was set at a rate of $20 \mu\text{m}/\text{h}$.

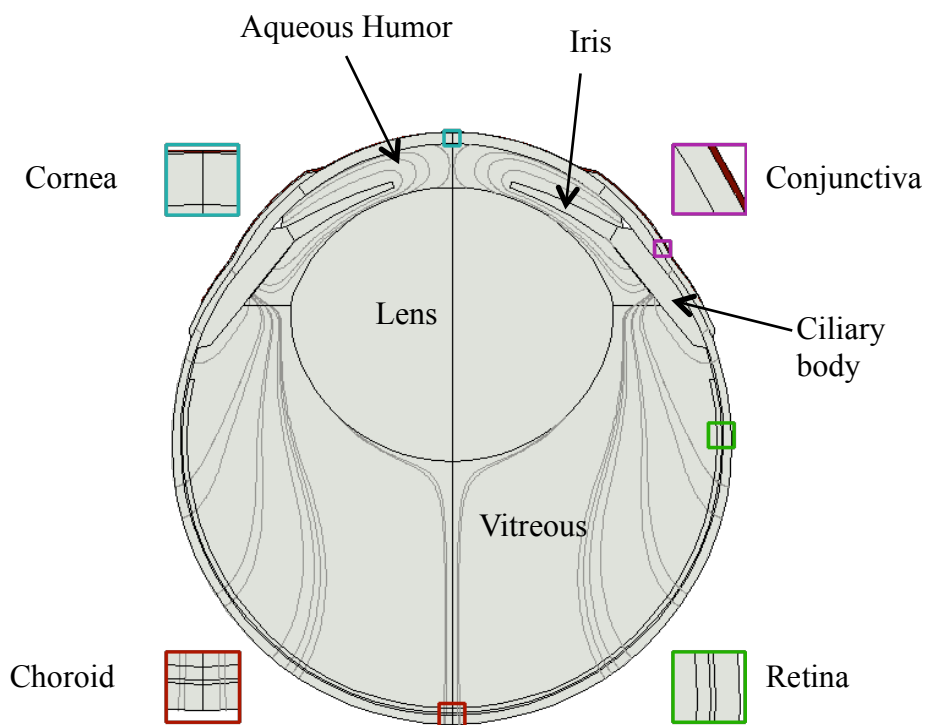


Figure 6-1 3D FEM model of the rabbit eye detailing individual ocular structure.

6.2.3. Brimonidine Pharmacokinetics

Brimonidine tartrate, a topical ocular drug, was selected for investigation. 35 µl of a 0.5% w/v solution of brimonidine was applied to the left eye in the form of a drop and the simulation was performed for 24 hours, following administration. A simulation of brimonidine movement through the eye was then monitored in the eye treated with brimonidine and also in the fellow, non treated eye. Tissue boundary and parameter conditions were modified according to the physicochemical properties of the drug and modified according to published pharmacokinetic data (Acheampong, Shackleton et al. 2002).

6.3. RESULTS AND DISCUSSION

Brimonidine tartrate is commonly administered to the eye in the form of topical drops, for the treatment of various disease states affecting the human eye (Figure 6.2). Brimonidine was selected as a compound of interest for investigation in this study, as it has previously been shown to penetrate to the posterior eye tissues following topical administration, however from clinical studies it is difficult to visualise the mechanisms involved in the complex path brimonidine takes to reach the back of the eye. Drug lipophilicity is thought to influence drug distribution within ocular tissues, with lipophilic drugs experiencing posterior clearance from the eye and hydrophilic drugs experiencing anterior clearance (Atluri and Mitra 2003). Brimonidine has been reported to be slightly lipophilic with a logP of 0.7 and therefore has the potential to move in the posterior direction towards the back of the eye. In addition, brimonidine is classified as small drug molecule, with a molecular weight of 442 a.m.u. for the tartrate salt, and small lipophilic drug molecules have been shown to be subject retinal drug clearance (Koeberle, Hughes et al. 2006).

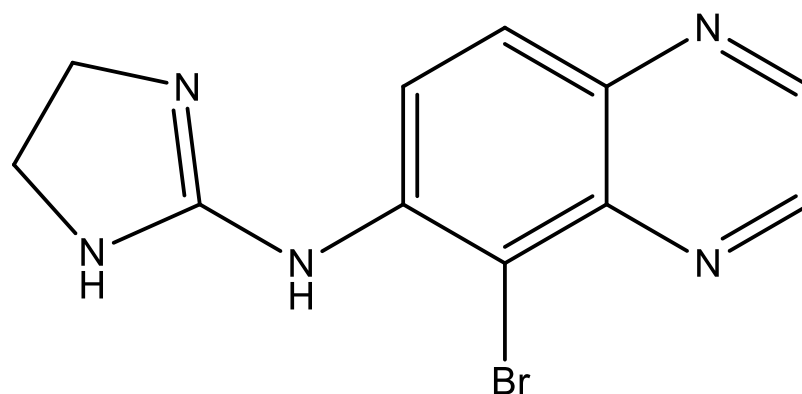


Figure 6-2 The chemical structure of brimonidine.

The model parameters were modified and adjusted in order to match the model predicted pharmacokinetic data to the published in vivo pharmacokinetic data. Adjustment of the model parameters was based on the physicochemical properties of brimonidine and during this process certain parameters were identified as being critical to matching both data sets (listed in Table 6-1). Drug permeability was important in the case of brimonidine movement in and out of the systemic circulation and also in the availability brimonidine contained within the tears at the cornea and conjunctiva. In respect of drug diffusion through tissues, for the aqueous humor and the lens tissue, the rate of drug diffusion was important. The remaining critical parameters identified were all related to the pigmented, melanin rich tissues. The fraction of drug bound to the melanin of the choroid, the ciliary body and the iris were important and relatively similar for each tissue. The clearance rate of the drug in the iris, the ciliary body and the choroid was also essential, with a shorter clearance rate selected in the choroid than the clearance rate selected for the iris and the ciliary body. The final critical set of parameters identified was the half life of drug dissociation off of the melanin rich tissues. In this case the ciliary body differed greatly to the choroid and the iris, with the rate of drug dissociation in the ciliary body determined to be much slower. During model parameter adjustment, it was noted that the permeability of brimonidine movement from the tears into the conjunctiva and cornea was a critical parameter in matching the in vivo data with the model generated data and can essentially be described as the availability of brimonidine in the tears at the cornea and conjunctiva. In both cases, the availability

of brimonidine in tears was maintained at a high level based on the high solubility of brimonidine tartrate in water, reported as 34 mg/ml (Ali, Khatri et al. 2009). The maximum concentration of brimonidine contained within the tears was the only model predicted C_{Max} to experience a poor match to the in vivo pharmacokinetic data. In an in vivo setting, it would be challenging to measure the concentration of drug contained within the tears accurately and this would have accounted for the differences in the model predicted concentrations to the in vivo determined concentrations.

Parameter Name	Parameter Description	Brimonidine treated eye
perm cor_tear	Membrane permeability between the tears and the cornea	$5 \times 10^{-9} \text{ cm}^2/\text{s}$
perm tear_conj	Membrane permeability between the tears and the conjunctiva	$16 \times 10^{-8} \text{ cm}^2/\text{s}$
clear	Permeability of blood vessels	$24 \text{ cm}^2/\text{s}$
dcoeff lens	Diffusion coefficient within the lens	$2.6990 \times 10^{-9} \text{ cm}^2/\text{s}$
dcoeff anterior	Diffusion coefficient within the anterior chamber	$2.0242 \times 10^{-9} \text{ cm}^2/\text{s}$
fb_choroid	Fraction of drug bound to melanin in the choroid	$350 \text{ } \mu\text{mol}/\text{ml}$
fb_cilliary	Fraction of drug bound to melanin in the ciliary body	$300 \text{ } \mu\text{mol}/\text{ml}$
fb_iris	Fraction of drug bound to melanin in the iris	$400 \text{ } \mu\text{mol}/\text{ml}$
tt_choroid	Clearance rate within the choroid	144 minutes
tt_cilliary	Clearance rate within the ciliary body	576 minutes
tt_iris	Clearance rate within the iris	720 minutes
hloff_cilliary	Half life of drug dissociation in ciliary melanin	54000 hours
hloff_choroid	Half life of drug dissociation in choroidal melanin	7200 hours
hloff_iris	Half life of drug dissociation in iris melanin	7200 hours

Table 6-1 Critical model parameters identified in matching FEM generated data to in vivo data.

The FEM presented of the rabbit eye matched the experimental in vivo data well, with Figure 6-3 and Figure 6-4 demonstrating the model predicated concentration versus time profiles of brimonidine in the treated eye. The anterior eye model data produced for the treated eye matched the published experimental data well (**Error! Reference source not found.**). In the initial points of drug contact with the eye, the cornea and the conjunctiva, an excellent match of model data to experimental data was achieved. In the cornea the C_{Max} of brimonidine was equal to 11000 ng/g with T_{Max} occurring within the first 30 minutes of applying the dose of brimonidine and for the conjunctiva, the C_{Max} of brimonidine was equal to 13000 ng/g with T_{Max} again occurring within the first 30 minutes of commencement of the simulation. The drug then penetrated into the anterior eye and into the aqueous humor, in line with the published pharmacokinetic data to achieve a C_{Max} of 1200 ng/g with the T_{Max} occurring slightly earlier than in vivo within the first hour of the study. Brimonidine then favourably moved on the pigmented tissues of the anterior eye, with high brimonidine concentrations measured in the iris and the ciliary body. In the iris, a good match in the T_{Max} of brimonidine to in vivo data was achieved, with T_{Max} occurring 1.5 hours after the dose was applied to the cornea, the C_{Max} achieved was slightly lower than in vivo and determined to be 38000 ng/g. In the ciliary body, T_{Max} was slightly delayed and occurred at approximately 2 hours post dosing. The C_{Max} measured in the ciliary body was also slightly lower than the C_{Max} measured in vivo and determined to be 1250 ng/g. In the lens, the T_{Max} matched the published data well although the model determined C_{Max} was slightly lower than the concentrations seen in vivo and determined to be 85 ng/g. In the anterior eye, the only tissue that achieved a poor match to the experimental data was the C_{Max} measured in the tears, a 2.5 fold increase in the C_{Max} of brimonidine was noted in the model when compared to the in vivo data.

	In Vivo treated eye C_{Max} (ng/g)	FEM treated eye C_{Max} (ng/g)	In Vivo non-treated eye C_{Max} (ng/g) fellow eye	FEM non- treated eye C_{Max} (ng/g)
Tear	195000	4900000	4.34	4900000
Conjunctiva	12900	13000	11	180
Cornea	11500	11000	9.76	1
Aqueous humor	1260	1200	0.763	0.6
Iris	53800	38000	332	275
Ciliary body	19100	12500	445	190
Lens	107	85	0.247	1
Vitreous humor	49.3	30	2.01	1.5
Choroid/retina	3220	2400	124	4.5
Blood	7.89	10.5	10.5	10.5

Table 6-2 C_{Max} obtained for brimonidine in vivo and C_{Max} obtained by the FEM in the treated rabbit eye and the non-treated rabbit eye.

In the posterior eye the model data produced for the treated eye again provided a close match to the experimentally determined data (Table 6-2). In the vitreous humor the predicted T_{Max} occurred within the first 30 minutes of running the simulation and C_{Max} was determined to be slightly lower at 30 ng/g. For the retina and the choroid it was difficult to determine how well the model data matched the experimental data, due to the fact that the retina and choroid were treated as a single compartment in the published pharmacokinetic data. Combining the model data, a good match of C_{Max} to the experimental data was achieved with the combined C_{Max} of the retina and the choroid determined to be slightly lower than the C_{Max} achieved in vivo at approximately 2400 ng/g. Differences however, occurred in the measured T_{Max} , with T_{Max} in the retina matching the experimental data however, in the choroid the T_{Max} was delayed, occurring at 4 hours post dosing. Finally the concentration measured in the model for the systemic circulation was slightly greater by approximately 20% than in the in vivo data at 10.5 ng/g.

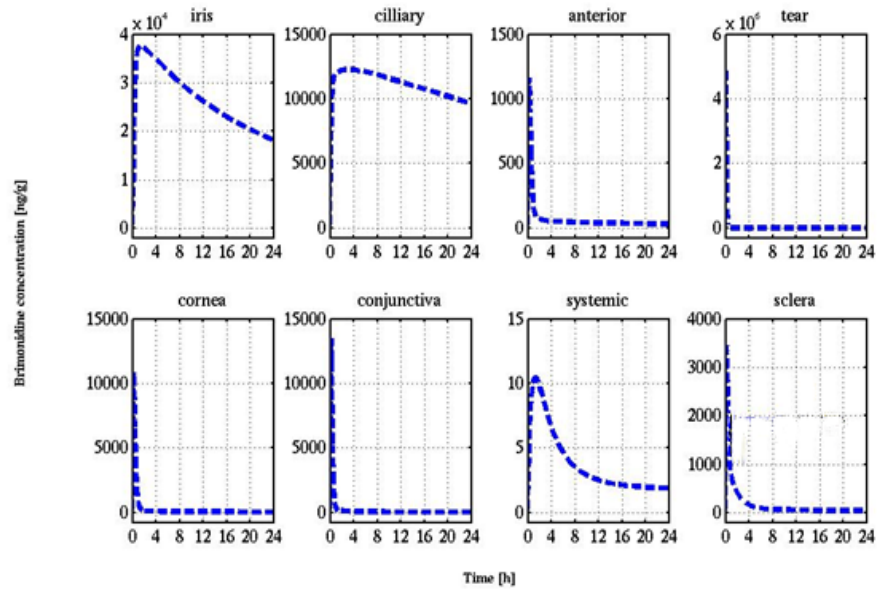


Figure 6-3 Pharmacokinetic data generated in the FEM for the anterior eye tissues of the treated rabbit eye.

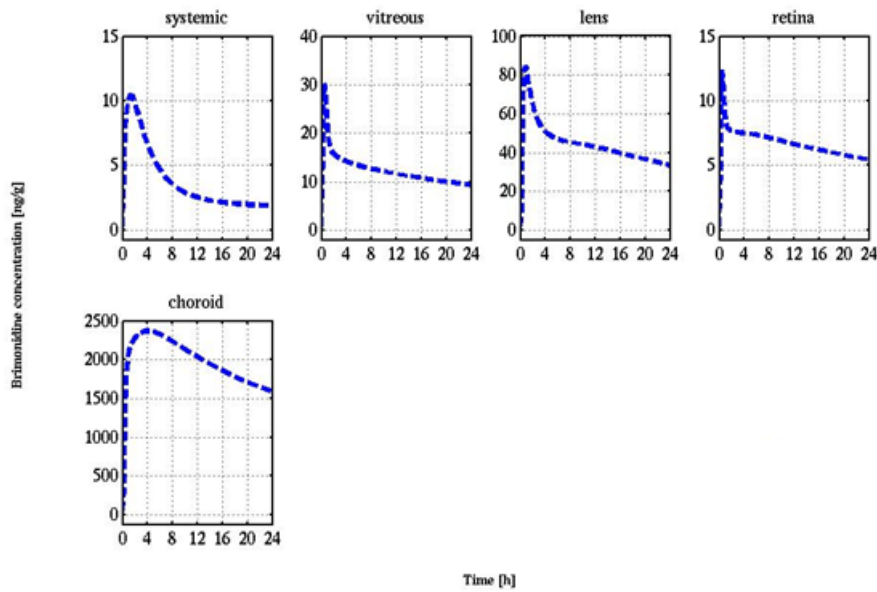


Figure 6-4 Pharmacokinetic data generated in the FEM for the posterior eye tissues of the treated rabbit eye.

Figure 6-5 and Figure 6-6 show the model predicated concentration versus time profiles of brimonidine in the non-treated eye. The drug penetrates into the non-treated eye via absorption into the systemic circulation following administration to the treated eye. In the aqueous humor, although a difference in T_{Max} was noted, a good match was noted in the C_{Max} predicted by the model with the C_{Max} measured to be approximately 0.6 ng/g. A similar pattern was noted in the iris and in the ciliary body where the measured T_{Max} in vivo was recorded at 6 hours, however the model predicted that T_{Max} would occur much later after 24 hours of treatment. For the iris, a much better correlation was achieved with the C_{Max} predicted in the iris reaching approximately 275 ng/g and the C_{Max} in the ciliary body reaching 190 ng/g, at the 24 hour time point. In the conjunctiva and the cornea, concentrations in general for the model and the in vivo data were low, however for both tissues the C_{Max} predicted in the model was lower than those determined in vivo. In the case of the lens, the C_{Max} provided a better match to the in vivo data with the C_{Max} determined to be just over 1 ng/g. Although the C_{Max} provided a good match, the T_{Max} was significantly delayed, occurring at around 10 hours post dosing. In the case of the posterior tissues, for the vitreous again the T_{Max} was delayed however the C_{Max} of the model matched the experimental data well at 1.5 ng/g. Again in the fellow eye, the retina and the choroid were treated as a single compartment and as a result it was difficult to determine how well the model data matched the experimental data. In this case the T_{Max} determined in the retina matched the experimental data however in the choroid the T_{Max} was delayed. Finally, in combining both tissues the C_{Max} predicted by the model was around four times greater than the C_{Max} measured in vivo.

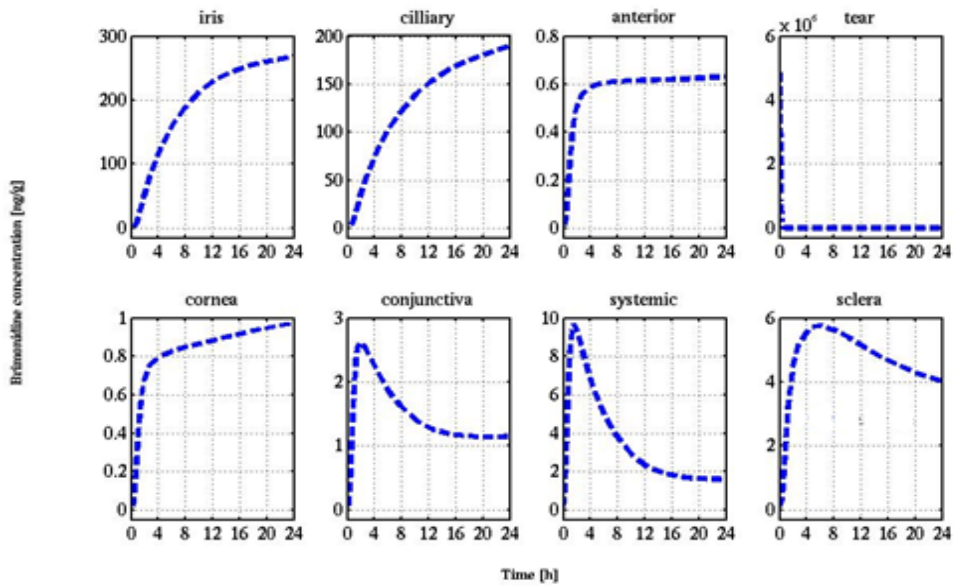


Figure 6-5 Pharmacokinetic data generated in the FEM for the anterior eye tissues of the fellow, non-treated rabbit eye

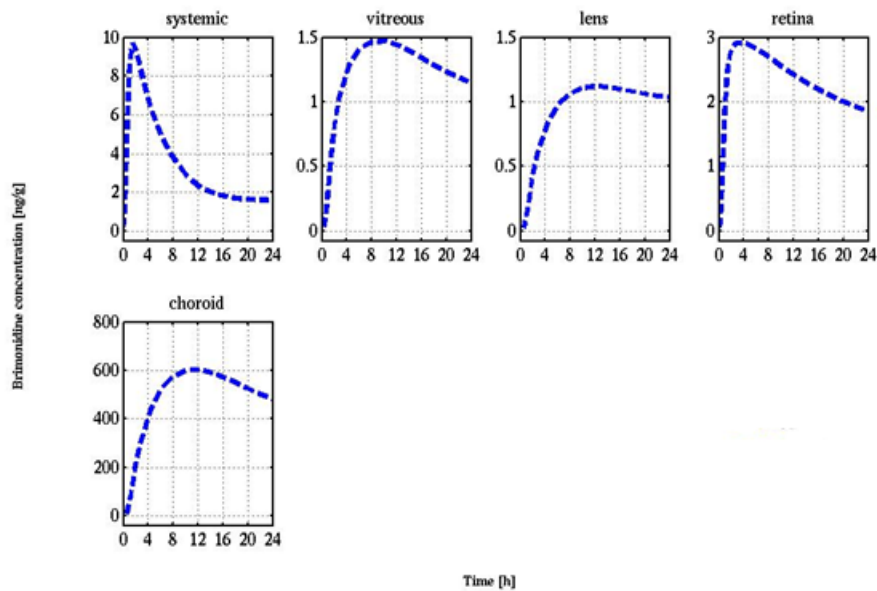


Figure 6-6 Pharmacokinetic data generated in the FEM for the posterior eye tissues of the fellow, non-treated rabbit eye.

In addition to matching the published pharmacokinetic data, the model successfully demonstrated the various routes involved in the penetration of brimonidine to the posterior eye tissues. Figure 6-7 shows the model predicted velocity profiles as a contour plot for the treated eye. In the dosed model eye, the applied brimonidine quickly penetrates through both the cornea and also the conjunctiva. Brimonidine appears to spread onto the conjunctiva and moves through to the anterior section of the eye. Following this, the drug then binds to the iris and the ciliary body at high concentrations. The drug then moves through the cornea, reaches the aqueous humor first and from there it begins to spread onto the iris and, in turn, the ciliary body. After 15 minutes post dosing, brimonidine had penetrated into the lens and moved towards the vitreous humor. In addition, the drug also moved into the vitreous humor from the ciliary body. Interestingly, at this point in time, the drug also distributed through the sclera and migrated to the posterior portion of the sclera, supplying the choroid and the retina with drug. As time progressed, the drug continued to move in the posterior direction through the anterior tissues into the vitreous humor. In addition to this, the drug also moved from the posterior section, from the sclera into the choroid, then into the retina and finally into the posterior vitreous. After six hours post dosing, concentrations of brimonidine in the ocular tissues began to fall, as the drug appeared to be cleared from the eye, although the rate of brimonidine reduction from the pigmented tissues; the iris, the choroid and the retina, was lower.

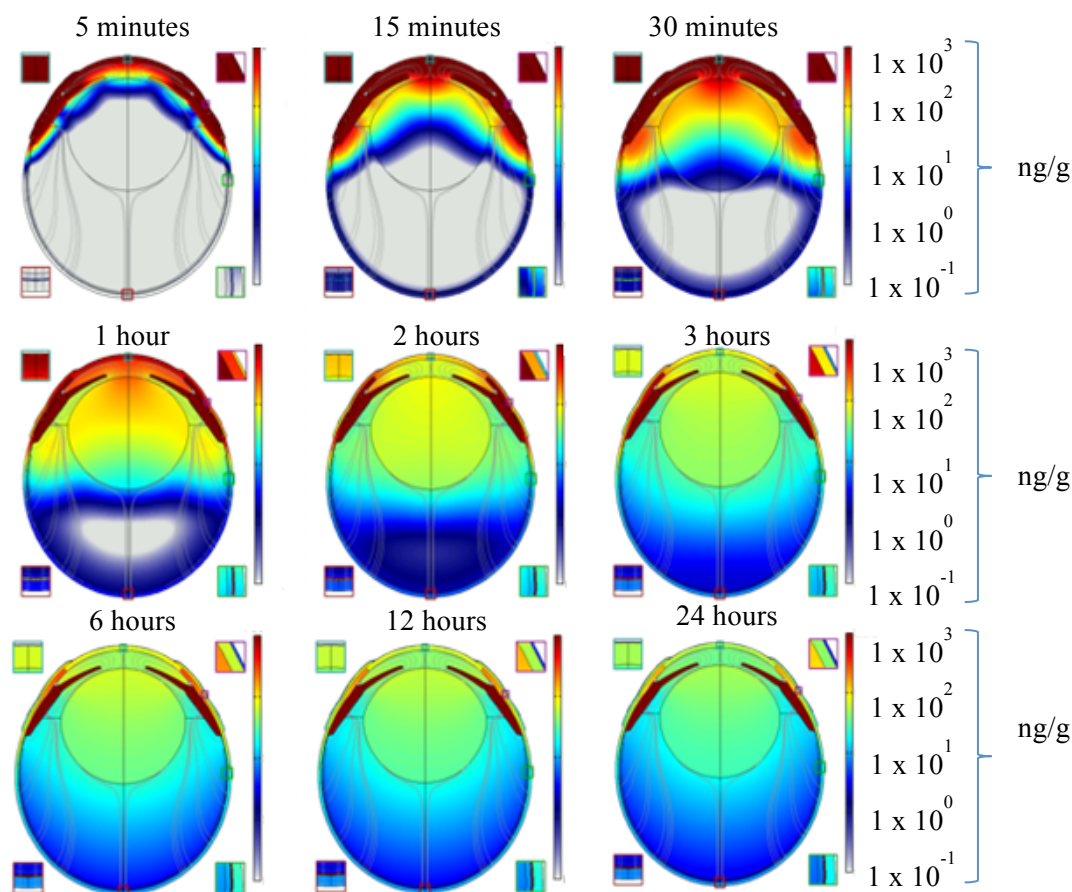


Figure 6-7 Illustrations of the 3D FEM generated to demonstrate brimonidine distribution in the treated rabbit eye at various time points over a period of 24 hours post drug administration. Scale bar shows colour scale corresponding to brimonidine concentration in ng/g,

Figure 6-8 shows the model predicted velocity profiles as a contour plot achieved for the non-treated eye. In the initial phase of the simulation, brimonidine was seen to penetrate into the non-treated eye via the systemic circulation. The drug then appeared to move into the choroid and also into the iris and ciliary body 15 minutes post dosing. From there, brimonidine moved from the iris and ciliary body on the conjunctiva, into the aqueous humor and from the aqueous humor into the lens. The drug also moved from the choroid into the sclera and through the retina into the vitreous humor. Over the course of the next 24 hours, the drug was seen to

move from the systemic circulation and accumulate at the iris, the ciliary body and the choroid, where it supplied the rest of the ocular tissues with brimonidine.

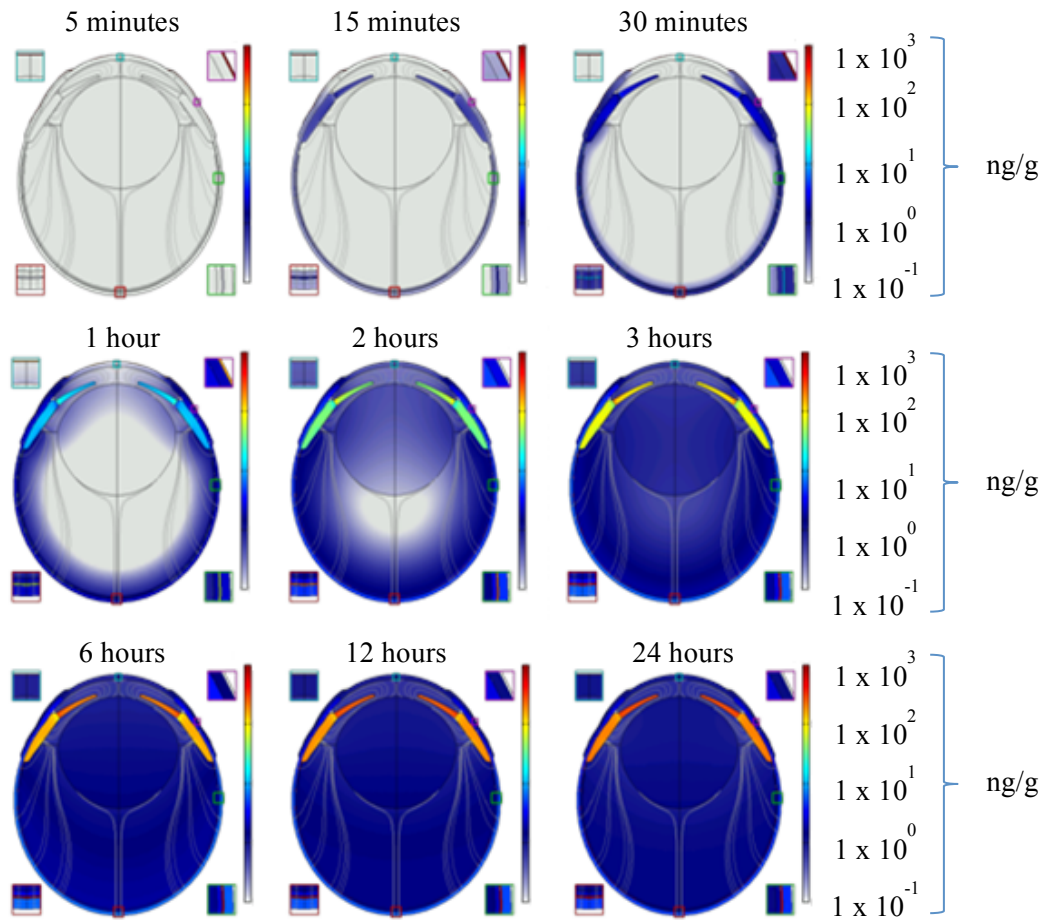


Figure 6-8 Illustrations of the 3D FEM generated to demonstrate brimonidine distribution in the fellow, non-treated rabbit eye at various time points over a period of 24 hours post drug administration. Scale bar shows colour scale corresponding to brimonidine concentration in ng/g,

In the first instance, the model demonstrated that brimonidine was able to penetrate into the anterior section of the eye via both the cornea and the conjunctiva routes, in line with previously published literature (Chien, Hornsy et al. 1990; Acheampong, Shackleton et al. 2002). Drug absorption through the cornea directly fed into the aqueous humor, onto the iris and into the lens. From this route the drug was seen to move in the posterior direction from the iris root into the posterior

aqueous humor. The drug then moved around the lens and into the vitreous and finally, through the lens into the vitreous humor. The model appears to show drug diffusion through the lens from the anterior lens, through the central part of the lens into the posterior segment of the eye. The extent of this movement was likely due to a mathematical artefact, however provided some important information regarding the characteristic movement through the lens into the posterior eye and coincides with previously published data by Stepanova et al, using fluorescein. On placing fluorescein in the central section of the lens, fluorescein did not move in the anterior direction but was shown to favourably move in the posterior direction into the vitreous (Stepanova, Marchenko et al. 2005). Movement in the posterior direction from the lens was also noted by Tan et al. where at two hours post dosing of sodium fluorescein into the vitreous humor of rabbits, sodium fluorescein penetrated the lens and then unloaded back into the vitreous humor after a further 3 hours (Tan, Orilla et al. 2011). It is anticipated that transporter systems are involved in drug movement through the lens however, drug transporter systems were not directly accounted for in the model.

The second route by which brimonidine was able to penetrate to the posterior eye was via the conjunctival route. Conjunctival drug absorption supplied the sclera with brimonidine and in addition, this route also contributed to the movement of the drug into the systemic circulation, via the blood vessels contained in the episclera (Chien, Hornsy et al. 1990). The episclera is positioned on the surface of the sclera and forms an outer layer. The main role of the episclera is to provide vascular nutrition to the sclera and as a result of this function, the episclera is a heavily vascularised structure. Blood is supplied to the sclera via the anterior ciliary arteries and the long posterior ciliary arteries, with also some additional blood supplied from the conjunctival arteries. Two vascular layers exist, the superficial layer and the deep layer. The deep layer forms a rich plexus to the conjunctiva in which blood is supplied from the ciliary arteries and this capillary network is closely applied to the sclera. The vessels of the superficial layer are arranged radially and connect at the limbus with the conjunctival vessels and deep plexus (Okhravi, Odufuwa et al. 2005). In the model the episclera was not modelled as an individual layer, however although a vascular system is not present in the sclera in reality, to account for the

episclera, a blood supply was added into the sclera in the model and in addition, the diffusion rates present in the sclera were designed to account for drug movement within episclera. In the model brimonidine was seen to move through the sclera within the first 15 minutes of the simulation, where it was able to penetrate to the back of the eye due to the drug entering the vascular structure of the episclera.

The final route by which the drug was able to penetrate to the posterior tissues was through entry into the systemic circulation. The permeability of drug movement into the systemic circulation was identified as a critical model parameter, as during the vivo study, brimonidine concentrations were noted in the fellow non-treated rabbit eye following administration into the opposing eye. This parameter was adjusted accordingly to match systemic concentrations in the FEM with concentrations measured in the rabbit systemic circulation in vivo and also to generate drug movement in the non-treated eye model. Drug administered topically can enter into the systemic circulation via two possible routes, through vessels contained in the conjunctiva or via drainage into the nasolacrimal duct (Hughes, Olejnik et al. 2005). The importance of this route on the distribution of brimonidine in the rabbit eye model was demonstrated by the fellow non-dosed eye. In the non dosed eye, brimonidine quickly appeared in some ocular tissues, with brimonidine first appearing in the choroid, the iris and the ciliary body, before it entered into the sclera. In the dosed eye, brimonidine was again seen to reach and bind to the choroid tissue fast and again, this occurred before the drug had reached the sclera. The rate at which brimonidine reached the choroid suggests that drug movement into the choroid occurred not only via the scleral route, but through the systemic circulation also. In the published pharmacokinetic data, this route was dismissed as the concentrations in the non-treated eye were considerably lower than those seen in the treated eye (Acheampong, Shackleton et al. 2002). From the published in vivo data is it difficult to visualize the exact mechanisms of penetration, as all of the ocular tissues are treated as homogenous compartments with brimonidine evenly distributed with each compartment and although this route may not have achieved large concentrations of brimonidine in the posterior eye, it's involvement in brimonidine movement within the model was clear.

In addition to demonstrating the routes of brimonidine penetration into the posterior eye, the importance of brimonidine melanin binding was nicely illustrated by the model. In the anterior eye, brimonidine was clearly shown to accumulate on the iris and on the ciliary body, with the highest anterior drug concentrations recorded in both the treated and non-treated eye measured in these tissues. The importance of melanin in this binding mechanism has been demonstrated by previously by Achaempong et al where the reported C_{Max} of brimonidine following topical dosing in the iris and ciliary body was reported to be four times higher in pigmented rabbits, when compared to albino rabbits without melanin (Acheampong, Shackleton et al. 1995). In the posterior eye, the drug was shown to bind to the melanin rich choroid, with the highest posterior brimonidine concentrations recorded in the treated and the non-treated eye measured within this tissue. Brimonidine binds well to melanin rich structure due to its physicochemical nature. Brimonidine is slightly lipophilic, basic drug with a reported logP of 0.7 and a pKa of 7.22 (Bhagav, Deshpande et al. 2010). Drugs with lipophilic and basic structure have been previously shown to bind well to melanin rich tissues (Tsuchiya, Hayasaka et al. 1987; Leblanc, Jezequel et al. 1998; Pitkanen, Ranta et al. 2007). In the matching the FEM to previously published pharmacokinetic data, the melanin binding parameters incorporated into the model were identified as critical parameters involved in controlling the distribution of brimonidine. The values achieved in the model for the fraction of drug bound to ocular melanin model parameter was similar for the iris, the choroid and for the ciliary body however, where differences arose in the melanin binding parameters was the in the clearance rate off of the melanin based tissues and also the half life of drug dissociation from the melanin of the different tissues. Drug clearance rate from the melanin based tissues was highest in the iris, followed by the ciliary body, followed by the choroid. The differences in the clearance rates selected were due to the differences in surface area occupied by the different tissues. The choroid has the largest surface area and more points of direct contact with other ocular tissues, for this reason the drug should theoretically have the ability to move out of the choroid quicker than the other two tissues. In the model, the iris and the ciliary body clearance rates were more similar, however since the iris occupied the smallest surface area out of the three tissues, the clearance rate

was slightly lower than that of the ciliary body. The half life of drug dissociation was the same for the iris and the choroid, however for the ciliary body the half life of drug dissociation from melanin was almost eight fold greater than for the other two tissues. In the initial stages of developing the model, the half life of drug dissociation from all three tissues was maintained at similar levels, however at lower values the pharmacokinetic profile generated in the ciliary body poorly matched the published in vivo data. A potential explanation for the differences in the half life of drug dissociation of the different tissues could be differences in the melanin composition of the tissues affecting the melanin binding kinetics of the drug. The basic melanin composition of melanin rich tissues has been shown to differ between different ocular tissues previously, with differences demonstrated in the elemental composition of melanins (Dryja, O-Neil-Dryja et al. 1979). In addition to this, two types of melanin are known to be present in the eye, pheomelanin and eumelanin. Distinct differences in the content of each of the types of melanin is known to exist within the melanin rich tissues of the eye (Liu, Hong et al. 2005). Although melanin composition has been shown to differ between tissues, there is limited work directly comparing the differences in the extent of melanin binding in the different tissues of the eye. However, if differences in melanin composition were responsible for the differences in the half life of drug dissociation of melanin in the tissues, it would be expected that all three tissues would have experience different rates of drug removal. Therefore, the large difference in the rate of the half life of drug dissociation is a likely deviation in the model requiring further refinement.

6.4. CONCLUSION

In this work we present the use of a FEM of the rabbit eye to demonstrate the pharmacokinetic distribution of brimonidine to the posterior eye, following topical administration. The results reported in the model demonstrate that brimonidine can penetrate to the posterior eye tissues via the cornea route of penetration, the conjunctival route of penetration and finally through entering into the systemic circulation. The FEM presented aids the understanding of how drugs move within ocular tissues and can be utilized to aid pharmacokinetic studies, with the potential to minimize the number of animals required during in vivo studies. Further work is still

required to refine the melanin binding mechanisms involved within the model, incorporate drug transporter systems into the model and also to extrapolate the model to demonstrate the ocular distribution of different topically applied ophthalmic drugs.

CHAPTER 7. SUMMARY AND FUTURE WORK

7.1. SUMMARY

In this work, the impact of physicochemical properties and physiological clearance mechanisms on ocular drug distribution has been explored using a variety of different techniques. In the initial stages, the development and validation of a rapid UPLC-MS/MS for the purpose of enabling the quantification of a drug series, namely atenolol, timolol and propranolol, was successfully achieved and enabled the quantification of the drug series in the aqueous humor, the lens, the iris/ciliary body, the vitreous humor, the choroid and the retina of the eye. This method was then utilised in the isolated perfused ovine eye model, to generate a pharmacokinetic profile of drug movement of a physicochemical different drug series through the various tissue contained within the eye. Using the isolated perfused ovine eye model significantly reduced both the number of animals utilised during the experimental work, as well as sample preparations and analytical time required. Drug lipophilicity was demonstrated to play an important role in the extent of ocular drug distribution following drug administration via an intravitreal injection, with drugs of greater

lipophilicity shown to penetrate to into the posterior eye and locate preferentially at the retina and the choroid at greater levels than those seen for more hydrophilic drugs.

Another approach investigated in this thesis was the use of an alternative means of determining ocular drug distribution, by using time of flight secondary ion mass spectrometry as a suitable means of spatially mapping drug distribution through different ocular tissues. In the initial development of this concept, challenges arose in identifying specific drug fragments and this led on to the use of the statistical technique, principal component analysis, to identify model drug presence within ocular tissues and show differences between ocular tissues treated with model drug and control ocular tissues. The challenges faced during the development of this technique, due to the physiological basis of the ocular tissues investigated, revealed key physiological chemical information and also identified important physiological differences between ocular subtypes. This added to our understanding of the structural components of the tissues investigated, the lens, the vitreous and the retina.

In order to progress and develop this initial work and aid in the identification of specific drug fragments, it was decided to perform a study focusing on a drug containing distinct chemical groups that were not typically seen in the ocular tissues analysed, for this reason a fluorinated compound was deemed suitable and dexamethasone selected. Key progression of the technique was shown and illustrated the ability of ToF-SIMS to characterise and provide spatial information about drug distribution within ocular tissues. This technique provided more valuable information than the current established techniques typically used, as it removed the need for tissue homogenisation and drug extraction from the tissue, providing specific information with regards to the spatial positioning of the drug within the tissue. This piece of work also demonstrated nicely, key differences in drug movement through the vitreous humor, towards both the anterior and posterior tissues, in the living eye and the non-living ovine eye. Illustrating that dexamethasone sodium phosphate distribution through the vitreous is not determined by diffusion alone and will involve the circulatory flow systems operating within the eye and drug transporter systems.

The work carried out in this thesis then led on to an opportunity to enhance the project and this work formed the final section of this thesis. This work involved an external collaboration with GlaxoSmithKline in the USA, in order to investigate ocular pharmacokinetic drug distribution using a finite element modelling approach. In this instance, the use of topical drug administration to reach the posterior eye tissues became the primary focus. From the literature, brimonidine was identified to penetrate to the posterior tissues following topical administration and was selected to develop the model. The generated model provided valuable information with regards to the pharmacokinetic movement of brimonidine in ocular tissues and showed that brimonidine can penetrate to the posterior eye tissues via various different routes, the cornea route of penetration, the conjunctival route of penetration and finally through entering into the systemic circulation.

The work presented in this thesis holds significant value in adding to the understanding of how we can improve drug treatment options in posterior eye disease. Understanding the impact an individual drug's physicochemical properties has on determining drug distribution through ocular tissues and specifically understanding the spatial distribution of the drug within the target site of action, the retina, is especially useful. This knowledge will impact on the drug candidate selection process for the treatment of posterior eye diseases such as age-related macular degeneration and diabetic retinopathy, where the desire is to penetrate to the back of the eye at therapeutic drug concentrations.

7.2. FUTURE WORK

Following the investigations carried out in this thesis, several potential areas of research have been identified, which should be pursued in the future.

In the first instance it would be beneficial to expand the validated UPLC-MS/MS method to include the remaining ocular tissues contained within the eye, namely the sclera, the conjunctiva and the optic nerve. It would also be of interest to develop a reliable method of separating the iris and the ciliary body for single tissue analysis. This expanded method could be utilised when carrying out pharmacokinetic studies in the isolated perfused eye in order to gain a complete picture of the ocular distribution of the drug series, following intravitreal injection.

As a cassette dosing study approach was used in the work, in order to ensure the reliability of the results was not compromised, the number of drugs administered in the cassette was kept to a minimum and as a result, only three drug of varying lipophilicity were selected. In the future, it would be beneficial to expand the number of drugs in the series to demonstrate the relationship between drug distribution and logP, using a greater range of lipophilicities. It would also be of interest to utilise the experimental set up to investigate the impact of other physicochemical properties, such as molecular weight and pKa, on drug distribution with ocular tissues. Although shown to play a role in drug distribution, the direct impact of melanin binding and drug transporters on movement and penetration in the posterior eye was also not investigated in isolation in this work. It would be of interest to expand this piece of work and include experimental data focussing solely on these principles to gain a greater insight into the factors involved in the distribution of this drug series within ocular tissue.

In addition to this work, a second area of interest could be pursued in order to develop the use of ToF-SIMS to spatially map drug distribution within the eye. Extrapolating the methodology to monitor the distribution of a range of drugs with varying physicochemical properties would be of interest, particularly if the quantification of a drug series could be enabled simultaneously, however due to the complex fragmentation patterns of compounds during ToF-SIMS analysis and the impact of matrix effects, this could prove extremely challenging.

Finally, in the initial planning stages it was anticipated that the FEM developed in Chapter 6 would be developed and then applied to a range of drug compounds with varying physicochemical properties. Unfortunately due to time constraints, this work was not possible. It would be of great interest to perform this work and have the ability to visualise, in real time, how drugs move around the eye with respect to their physicochemical properties.

REFERENCES

- Acheampong, A. A., M. Shackleton, et al. (2002). "Distribution of brimonidine into anterior and posterior tissues of monkey, rabbit, and rat eyes." Drug Metabolism Disposition **30**: 421-9.
- Acheampong, A. A., M. Shackleton, et al. (1995). "Comparative ocular pharmacokinetics of brimonidine after a single dose application to the eyes of albino and pigmented rabbits." Drug Metabolism and Disposition **23**: 708-712.
- Ackermann, B. L. (2004). "Results from a bench marking survey on cassette dosing practices in the pharmaceutical industry." Journal of the American Society for Mass Spectrometry **15**: 1374-1377.
- Ahmed, I. and T. F. Patton (1985). "Importance of the noncorneal absorption route in topical ophthalmic drug delivery." Investigative Ophthalmology and Visual Science **26**: 584-587.
- Akopian, A. and P. Witkovsky (2002). "Calcium and retinal function." Molecular Neurobiology **25**: 113-132.
- Ali, M. S., A. R. Khatri, et al. (2009). "A stability-indicating assay of brimonidine tartrate ophthalmic solution and stress testing using HILIC." Chromatographia **70**: 539-544.
- Almeida, A. M., M. M. Castel-Branco, et al. (2002). "Linear regression for calibration lines revisited: weighting schemes for bioanalytical methods." Journal of Chromatography B **774**: 215-222.
- Amemiya, T., H. Gong, et al. (2003). "Changes of vitamins A and E in the rat retina under light and dark conditions detected with TOF-SIMS." Applied Surface Science **203-204**: 738-741.
- Amemiya, T., M. Tozu, et al. (2004). "Time-of-flight secondary ion mass spectrometry can replace histochemistry demonstration of fatty acids in the retina." Japanese Journal of Ophthalmology **48**: 287-293.
- Amo, E. M. d. and A. Urtti (2008). "Current and future ophthalmic drug delivery systems. A shift to the posterior segment." Drug Discovery Today **13**: 135 - 143.
- Amoore, J. E., W. Bartley, et al. (1958). "Distribution of sodium and potassium within cattle lens." Biochemical Journal **72**: 126-133.

- Anand, B. S., H. Atluri, et al. (2004). "Validation of an ocular microdialysis technique in rabbits with permanently implanted vitreous probes: systemic and intravitreal pharmacokinetics of fluorescein." International Journal of Pharmaceutics **281**: 79-88.
- Appelhans, A. D. and J. E. Delmore (1989). "Comparison of polyatomic and atomic primary beams for secondary ion mass spectrometry of organics." Analytical Chemistry **61**: 1087-1093.
- Araie, M. and D. M. Maurice (1991). "The Loss of Fluorescein, Fluorescein Glucuronide and Fluorescein Isothiocyanate Dextran from the Vitreous by the Anterior and Retinal Pathways." Experimental Eye Research **52**: 27-39.
- Aranyosiova, M., M. Michalka, et al. (2008). "Microscopy and chemical imaging of Behcet brain tissue." Applied Surface Science **255**: 1584-1587.
- Armaly, M. F. (1965). "Statistical attributes of the steroid hypertensive response in the clinically normal eye." Investigative ophthalmology and visual science **4**: 187-197.
- Ashwin, P. T., S. Shah, et al. (2009). "The relationship of Central Corneal Thickness (CCT) to Thinnest Central Cornea (TCC) in healthy adults." Contact Lens and Anterior Eye **32**: 64-67.
- Atluri, H., B. S. Anand, et al. (2003). "Mechanism of a Model Dipeptide Transport Across Blood Ocular Barriers Following Systemic Administration." Experimental Eye Research **78**: 815-822.
- Atluri, H. and A. K. Mitra (2003). "Disposition of short-chain aliphatic alcohols in rabbit vitreous by ocular microdialysis." Experimental Eye Research. **76**: 315-320.
- Atluri, H., R. S. Talluri, et al. (2008). "Functional activity of a large neutral amino acid transporter (LAT) in rabbit retina: A study involving the in vivo retinal uptake and vitreal pharmacokinetics of l-phenyl alanine." International Journal of Pharmaceutics **347**: 23-30.
- Attia, M. A., M. A. Kassem, et al. (1988). "In vivo performance of [3H]dexamethasone ophthalmic film delivery systems in the rabbit eye." International Journal of Pharmaceutics **47**: 21-30.
- Augusteyn, R. C. and A. Stevens (1998). "Macromolecular structure of the eye lens." Progress in Polymer Science **23**: 375-413.
- Aukunuru, J., G. Sunkara, et al. (2001). "Expression of multidrug resistance-associated protein (MRP) in human retinal pigment epithelial cells and its interaction with BAPSG, a novel aldose reductase inhibitor." Pharmaceutical Research **18**: 565-572

- Baeyens, V., V. Kaltsatos, et al. (1998). "Optimized release of dexamethasone and gentamicin from a soluble ocular insert for the treatment of external ophthalmic infections." Journal of Controlled Release **52**: 215-220.
- Balachandran, R. K. and V. H. Barocas (2008). "Computer Modeling of Drug Delivery to the Posterior Eye: Effect of Active Transport and Loss to Choroidal Blood Flow." Pharmaceutical Research **25**: 2685-2696.
- Balazs, E. A. and J. L. Denlinger (1984). The Vitreous. The Eye. H. Daveson, Academic Press. **1a**: 533 - 589.
- Barber, A. J. (2003). "A new view of diabetic retinopathy: a neurodegenerative disease of the eye." Progress in Neuro-Psychopharmacology & Biological Psychiatry **27**: 283-290.
- Barcia, E., R. Herrero-Vanrell, et al. (2009). "Downregulation of endotoxin-induced uveitis by intravitreal injection of polylactic-glycolic acid (PLGA) microspheres loaded with dexamethasone." Experimental Eye Research **89**: 238-245.
- Baumgartner, W. A. (2000). "Etiology, pathogenesis, and experimental treatment of retinitis pigmentosa." Medical Hypotheses **54**: 814-824.
- Beebe, D. C. (2003). Lens. Adler's Physiology of the Eye. P. L. Kaufman and A. Alm. St Louis, Missouri, Mosby Inc: 117-158.
- Beer, P. M., S. J. Bakri, et al. (2003). "Intraocular concentration and pharmacokinetics of triamcinolone acetonide after a single intravitreal injection." Ophthalmology **110**: 681-686.
- Belu, A., D. J. Graham, et al. (2003). "Time-of-flight secondary ion mass spectrometry: techniques and applications for the characterization of biomaterial surfaces." Biomaterials **24**: 3635-3653.
- Belu, A. M., M. C. Davies, et al. (2000). "TOF-SIMS Characterization and Imaging of Controlled-Release Drug Delivery Systems." Analytical Chemistry **72**: 5625-5638.
- Benninghoven, A., B. Hagenhoff, et al. (1993). "Surface MS: Probing Real-World Samples." Analytical Chemistry **65**: 630-640.
- Berman, E. R. (1991). Biochemistry of the eye. New York, Plenum Press.
- Bhagav, P., P. Deshpande, et al. (2010). "Development and validation of stability indicating UV spectrophotometric method for the estimation of brimonidine tartrate in pure form formulations and preformulation studies." Der Pharmacia Lettre **2**: 106-122.

- Bill, A. (1977). "Basic Physiology of the Drainage of Aqueous Humor." Experimental Eye Research **Suppl.**: 291-304.
- Bito, L. Z. (1977). "The Physiology and Pathophysiology of Intraocular Fluids." Experimental Eye Research **Suppl.**: 273-289.
- Bonate, P. (2005). Pharmacokinetic-Pharmacodynamic Modeling and Simulation, Springer.
- Bonfiglio, R., R. C. King, et al. (1999). "The effects of sample preparation methods on the variability of the electrospray ionization response for model drug compounds." Rapid communications in mass spectrometry **13**: 1175-1185.
- Borderie, V. M., S. Scheer, et al. (1998). "Donor organ cultured corneal tissue selection before penetrating keratoplasty." British Journal of Ophthalmology **82**: 382-388.
- Börner, K., H. Nygren, et al. (2006). "Localization of Na⁺ and K⁺ in rat cerebellum with imaging TOF-SIMS." Applied Surface Science **252**: 6777-6781.
- Brasnjevic, I., H. W. M. Steinbusch, et al. (2009). "Delivery of peptide and protein drugs over the blood-brain barrier." Progress in Neurobiology **87**: 212-251.
- Calza, P., E. Pelizzetti, et al. (2001). "Ion trap tandem mass spectrometry study of dexamethasone transformation products on light activated TiO₂ surface." American Society for Mass Spectrometry **12**: 1286-1295.
- Capeans, C., J. Lorenzo, et al. (1998). "Comparative study of incomplete posterior vitreous detachment as a risk factor for proliferative vitreoretinopathy." Graefe's Archive for Clinical and Experimental Ophthalmology **236**: 481-485.
- Chen, C. Y., T. Y. Wong, et al. (2007). "Intravitreal Bevacizumab (Avastin) for Neovascular Age-related Macular Degeneration: A Short-term Study." American Journal of Ophthalmology **143**: 510-512.
- Chien, D. S., J. J. Hornsy, et al. (1990). "Corneal and conjunctival/scleral penetration of p-aminoclonidine, AGN 190342 and clonidine in rabbit eyes." Current Eye Research **9**: 1051-1059.
- Chirlia, T. V., Y. Hong, et al. (1998). "The use of hydrophilic polymers as artificial vitreous." Progress Polymer Science **23**: 475-508.
- Cioffi, G. A., E. Granstam, et al. (2003). Ocular Circulation. Adler's Physiology of the Eye. P. L. Kaufman and A. Alm, Mobsy: 293-319.

- Conlan, X. A., I. S. Gilmore, et al. (2006). "Polyethylene terephthalate (PET) bulk film analysis using C60+, Au3+, and Au+ primary ion beams." Applied Surface Science **252**: 6562-6565.
- Constable, P. A., J. G. Lawrenson, et al. (2006). "P-Glycoprotein exPression in human retinal pigment epithelium cell lines." Experimental Eye Research **83**: 24-30.
- Coo, F. A. M., B. A. Zonnenberg, et al. (1993). "Prolonged normothermic perfusion of the isolated bovine eye: initial results." Current Eye Research **12**: 293-301.
- Coo, F. A. M. d., B. A. Zonnennberg, et al. (1993). "Prolonged normothermic perfusion of the isolated bovine eye: initial results." Current Eye Research **12**: 292-301.
- Cussler, E. L. (2009). Diffusion: Mass transfer in fluid systems. Cambridge.
- Dambach, S., M. Fartmann, et al. (2003). "ToF-SIMS and laser-SNMS analysis of apatite formation in extracellular protein matrix of osteoblasts in vitro." Surface and Interface Analysis **36**: 711-715.
- Damian-Iordache, V. (2010). Physiological based modeling of drug delivery to the back of the eye. 2nd Annual Ocular Disease and Drug Discovery Conference. Boston, MA.
- Dams, R., M. A. Huestis, et al. (2003). "Matrix effect in bio-analysis of illicit drugs with LC-MS/MS: influence of ionization type, sample preparation, and biofluid." Journal of the American Society for Mass Spectrometry **14**: 1290-1294.
- Davies, M. C., R. A. P. Lynn, et al. (1995). "Surface Chemical Characterization Using XPS and TOF-SIMS of Latex Particles Prepared by the Emulsion Copolymerization of Functional Monomers with Methyl Methacrylate and 4-Vinyl Pyridine." Langmuir **11**: 4313-4322.
- Davies, N., D. E. Weibel, et al. (2003). "Development and experimental application of a gold liquid metal ion source." Applied Surface Science **203-204**: 223-227.
- Davies, O. R., L. Head, et al. (2008). "Surface Modification of Microspheres with Steric Stabilizing and Cationic Polymers for Gene Delivery." Langmuir **24**: 7138-7146.
- Davson, H. (1980). The vegetative physiology and biochemistry of the eye. Physiology of the Eye. London, Churchill Livingstone: 1-164.

- Dijkstra, B. G., A. Schneemann, et al. (1999). "Flow after prostaglandin E1 is mediated by receptor-coupled adenylyl cyclase in human anterior segments." Investigative ophthalmology and visual science **40**: 2622-2626.
- Dilsiz, N., A. Olcucu, et al. (2000). "Determination of calcium, sodium, potassium and magnesium concentrations in human senile cataractous lenses." Cell Biochemistry and Function **18**: 269-262.
- Ding, X., M. Patel, et al. (2009). "Molecular Pathology of Age-Related Macular Degeneration." Progress in Retinal and Eye Research **28**: 1-18.
- Donaldson, D. D. (1973). Anterior chamber, iris and ciliary body. Atlas of external diseases of the eye. Saint Louis, The C V Mosby Company. **IV**: 1-325.
- Doughty, M. J. (1997). "Changes in lactate dehydrogenase activity in bovine corneal stroma and epithelium in response to in vitro toxic challenges in the enucleated eye test." Optometry and vision science **1997**: 198-206.
- Doughty, M. J. (2008). "Use of a corneal stroma perfusion technique and transmission electron microscopy to assess ultrastructural changes associated with exposure to slightly acidic pH 5.75 solutions." Current Eye Research **33**: 45-57.
- Drent, M., N. A. M. Cobben, et al. (1996). "Usefulness of lactate dehydrogenase and its isoenzymes as indicators of lung damage or inflammation." European Respiratory Journal **9**: 1736-1742.
- Dryja, T. P., M. O-Neil-Dryja, et al. (1979). "Elemental analysis of melanins from bovine hair, iris, choroid and retinal pigment epithelium " Investigative ophthalmology and visual science **18**: 231-236.
- Duncan, G. and F. I. Weeks (1972). "Distribution and movement of sodium and potassium in the toad retina." Experimental Eye Research **13**: 278-288.
- Dvorhik, B. H. and J. K. Marquis (2000). "Disposition and toxicity of a mixed backbone antisense oligonucleotide, targeted against human cytomegalovirus, after intravitreal injection of escalating single doses in the rabbit " Drug Metabolism and Disposition **28**: 1255-1261.
- Earla, R., S. H. S. Boddu, et al. (2010). "Development and validation of a fast and sensitive bioanalytical method for the quantitative determination of glucocorticoids--Quantitative measurement of dexamethasone in rabbit ocular matrices by liquid chromatography tandem mass spectrometry." Journal of Pharmaceutical and Biomedical Analysis **52**: 525-533.
- Eckelman, W. C., M. R. Kilbourn, et al. (2007). "Justifying the number of animals for each experiment." Nuclear Medicine and Biology **35**: 1-2.

- Edelhauser, H. F., C. L. Rowe-Rendleman, et al. (2010). "Drug delivery systems for retinal diseases." Investigative ophthalmology and visual science **51**: 5403-5420.
- Eljarrat-Binstock, E., F. Raiskup, et al. (2005). "Transcorneal and transscleral iontophoresis of dexamethasone phosphate using drug loaded hydrogel " Journal of Controlled Release **106**: 386-390.
- Erickson-Lamy, K., J. W. Rohen, et al. (1988). "Outflow facility studies in the perfused bovine aqueous outflow pathways." Current Eye Research. **7**: 799-807.
- Eynde, X. V. and P. Bertrand (2000). "Matrix effects in TOF-SIMS analyses of styrene-methyl methacrylate random copolymers." Macromolecules **33**: 5624-5633.
- Fatt, I. (1975). "Flow and diffusion in the vitreous body of the eye." **37**: 85-90.
- Fatt, I. (1977). "Hydraulic flow conductivity of the vitreous." Investigative Ophthalmology and Visual Science **16**: 565-568.
- FDA (2000). Guidance for Industry and Other Stakeholders Toxicological Principles for the Safety Assessment of Food Ingredient. Food: 1-9.
- Feng, J., C.-M. Chan, et al. (2000). "Influence of chain sequence structure of polymers on ToF-SIMS spectra." Polymer **41**: 2695-2699.
- Forester, J. V., A. D. Dick, et al. (2002). Anatomy of the eye and orbit. The eye: Basic sciences in practice, W B Saunders: 1-87.
- Francoeur, M. L., S. J. Sitek, et al. (1985). "Kinetic disposition and distribution of timolol in the rabbit eye. A physiologically based ocular model." International Journal of Pharmaceutics **25**: 275-292.
- Frick, L. W., K. K. Adkison, et al. (1998). "Cassette dosing: rapid in vivo assessment of pharmacokinetics." Pharmaceutical Science & Technology Today **1**(1): 12-18.
- Friedman, A. H. and A. L. Marchese (1981). "The isolated perfused frog eye: a useful preparation for the investigation of drug effects on retinal function." Journal of Pharmacological Methods **5**: 215-234.
- Friedrich, S., Y. Cheng, et al. (1997a). "Drug distribution in the vitreous humor of the human eye: the effects of intravitreal injection position and volume." Current Eye Research. **16**: 663-669.

- Friedrich, S., Y. Cheng, et al. (1997b). "Finite element modelling of drug distribution in the vitreous humor of the rabbit eye." Annals of Biomedical Engineering **25**: 303-314.
- Fukuda, M. and K. Sasaki (2002). "General Purpose Antimicrobial Ophthalmic Solutions Evaluated Using New Pharmacokinetic Parameter of Maximum Drug Concentration in Aqueous." Japanese Journal of Ophthalmology **46**: 384-390.
- Gabrielsson, J. and D. Weiner (1998). Pharmacokinetic and Pharmacodynamic Data Analysis: Concepts and Applications. Stockholm, Apotekarsocieteten.
- Gardner, T. W., D. A. Antonette, et al. (2002). "Diabetic Retinopathy: More than meets the eye." Survey of Ophthalmology **47**: 253-262.
- Gardner, T. W., D. A. Antonetti, et al. (2000). "The molecular structure and function of the inner blood-retinal barrier." Documenta Ophthalmologica **97**: 229-237.
- Gazi, E., J. Dwyer, et al. (2003). "The combined application of FTIR microspectroscopy and ToF-SIMS imaging in the study of prostate cancer." Faraday Discussions **126**: 41-59.
- Geroski, D. H. and H. F. Edelhauser (2001). "Transscleral drug delivery for posterior segment disease." Advanced Drug Delivery Reviews **52**: 37-48.
- Gibaldi, M. (1984). Biopharmaceutics and Clinical Pharmacokinetics. Philadelphia, Lea & Febiger.
- Gillen, G. and S. Roberson (1998). "Preliminary evaluation of an SF5+ polyatomic primary ion beam for analysis of organic thin films by secondary ion mass spectrometry." Rapid Communications in Mass Spectrometry **12**: 1303-1312.
- Gillen, G. and M. Walker (1999). "Use of an SF5+ polyatomic primary ion beam for ultrashallow depth profiling on an ion microscope secondary ion mass spectroscopy instrument." Journal of Vacuum Science and Technology B **18**: 503-508.
- Gisladottir, S., T. Loftsson, et al. (2009). "Diffusion characteristics of the vitreous humour and saline solution follow the Stokes Einstein equation." Graefe's Archive for Clinical and Experimental Ophthalmology **247**: 1677-1684.
- Gohel, P. S., N. Mandava, et al. (2008). "Age-related Macular Degeneration: An Update on Treatment." The American Journal of Medicine **121**: 279-281.
- Gong, H., T. Amemiya, et al. (2003). "Time-of-flight secondary ion mass spectrometry of fatty acids in rat retina." Applied Surface Science **203-204**: 734-737.

- Gottanka, J., D. Chan, et al. (2004). "Effects of TGF-B2." Investigative ophthalmology and visual science **45**: 153-158.
- Gouras, P. and M. Hoff (1970). "Retinal function in an isolated perfused mammalian eye." Investigative ophthalmology and visual science **9**: 388-399.
- Graham, D. J., M. S. Wagner, et al. (2006). "Information from complexity: Challenges of TOF-SIMS data interpretation." Applied Surface Science **252**: 6860-6868.
- Grass, G. M. and J. R. Robinson (1984). "Relationship of chemical structure to corneal penetration and influence of low-viscosity solution on ocular bioavailability " Journal of Pharmaceutical Sciences **73**: 1021-1027.
- Green, K. (1984). "Physiology and Pharmacology of Aqueous Humor Inflow." Survey of Ophthalmology **29**: 208-214.
- Gross-Jendroska, M., G. Lui, et al. (1992). "Retinal pigment epithelium-stromal interactions modulate hyaluronic acid deposition." Investigative ophthalmology and visual science **33**: 3394-3399.
- Haller, J. A., F. Bandello, et al. (2010). "Randomized, hsm-controlled trial of dexamethasone intravitreal implant in patients with macular edema due to retinal vein occlusion." Ophthalmology **117**: 1134-1146.
- Haller, J. A., B. U. Kuppermann, et al. (2010). "Randomized controlled trial of an intravitreal dexamethasone drug delivery system in patients with diabetic macular edema." Archives of Ophthalmology **128**: 289-296.
- Han, Y., D. H. Sweet, et al. (2001). "Characterization of a novel cationic drug transporter in human retinal pigment epithelial cells." The journal of pharmacology and experimental therapeutics **296**: 450-457.
- Hartong, D. T., E. L. Berson, et al. (2006). "Retinitis pigmentosa." The Lancet **368**: 1795-1809.
- Heiduschka, P., H. Fietz, et al. (2007). "Penetration of bevacizumab through the retina after intravitreal injection in the monkey." Investigative Ophthalmology and Visual Science **48**: 2814-2823.
- Hennessy, M. and J. P. Spiers (2007). "A primer on the mechanics of P-glycoprotein the multidrug transporter." Pharmacological Research **55**: 1-15.
- Hess, H. H. (1975). "The high calcium content of retinal pigmented epithelium." Experimental Eye Research **21**: 471-479.

- Heynen, H. and D. Van Norren (1985). "Origin of the electroretinogram in the intact macaque eye--I: Principal component analysis." Vision Research **25**: 697-707.
- Hladky, S. B. (1990). Pharmacokinetics. Manchester Manchester University Press
- Hoffmann, E. d. and V. Stroobant (2002). Mass Spectrometry: Principles and Applications. New Jersey, Wiley.
- Hosoya, K., T. Kondo, et al. (2001). "MCT1-mediated transport of L-lactic acid at the inner blood-retinal barrier: A possible route for delivery of monocarboxylic acid drugs to the retina." Pharmaceutical Research **18**: 1670-1676.
- Hosoya, K., A. Makihara, et al. (2009). "Roles of inner blood-retina barrier organic anion transporter 3 in the vitreous/retina-to-blood efflux transport of p-aminohippuric acid, benzylpenicillin and 6-mercaptopurine." The journal of pharmacology and experimental therapeutics **329**: 87-93.
- Hosoya, K., Y. Ohshima, et al. (2003). "Use of microdialysis to evaluate efflux transport of organic anions across the blood-retinal barrier." AAPS J **5**: 583.
- Hosoya, K. and M. Tachikawa (2009). "Inner blood-retinal barrier transporters: Role of retinal drug delivery." Pharmaceutical Research **26**: 2055-2065.
- Hu, T., Q. Le, et al. (2007). "Determination of doxorubicin in rabbit ocular tissues and pharmacokinetics after intravitreal injection of a single dose of doxorubicin-loaded poly-[beta]-hydroxybutyrate microsphere." Journal of Pharmaceutical and Biomedical Analysis **43**: 263-269.
- Huang, H. L., S. H. Goh, et al. (2004). "ToF-SIMS studies of poly(methyl methacrylate-co-methacrylic acid), poly(2,2,3,3,3-pentafluoropropyl methacrylate-co-4-vinylpyridine) and their blends." Applied Surface Science **227**: 373-382.
- Hughes, P. M., O. Olejnik, et al. (2005). "Topical and systemic drug delivery to the posterior segments." Advanced Drug Delivery Reviews **57**: 2010-2032.
- Jones, E. A., N. P. Lockyer, et al. (2007). "Mass spectral analysis and imaging of tissue by ToF-SIMS - The role of buckminsterfullerene, C₆₀⁺, primary ions." International Journal of Mass Spectrometry **260**: 146-157.
- Jones, R. F. and D. M. Maurice (1966). "New methods of measuring the rate of aqueous flow in man with fluorescein." Experimental Eye Research **5**: 208-220.

- Jouan, M. and C. Katlama (1999). "Management of CMV retinitis in the era of highly active antiretroviral therapy " International Journal of Antimicrobial Agents **13**: 1-7.
- Jung, S., M. Foston, et al. (2010). "Surface Characterization of Dilute Acid Pretreated Populus deltoides by ToF-SIMS." Energy & Fuels **24**: 1347-1357.
- Kadam, R. S. and U. B. Kompella (2009). "Cassette analysis of eight beta-blockers in bovine eye sclera, choroid_RPE, retina and vitreous by liquid chromatography-tandem mass spectrometry." Journal of Chromatography **877**.
- Kadam, R. S. and U. B. Kompella (2010). "Influence of Lipophilicity on Drug Partitioning into Sclera, Choroid-Retinal Pigment Epithelium, Retina, Trabecular Meshwork, and Optic Nerve." The Journal of Pharmacology and Experimental Therapeutics **332**: 1107-1120.
- Kaiser, R. J. and D. M. Maurice (1964). "The diffusion of fluoresecein in the lens." Experimental Eye Research **3**: 156-165.
- Kathawate, J. and S. Acharya (2008). "Computational modeling of intravitreal drug delivery in the vitreous chamber with different vitreous substitutes." International Journal of Heat and Mass Transfer **51**: 5598-5609.
- Kaufman, P. L. and A. Alm (2002). Adler's Physiology of the Eye: Clinical Application, Mosby.
- Kaufman, P. L. and A. Alm (2002). Aqueous Humor Hydrodynamics Adler's Physiology of the Eye: Clinical Application. P. L. Kaufman and A. Alm, Mobsy.
- Keenan, M. R. and P. G. Kotula (2004). "Optimal scaling of TOF-SIMS spectrum-images prior to multivariate statistical analysis." Applied Surface Science **231-232**: 240-244.
- Kek, W. K., W. S. Foulds, et al. (2010). "Two-photon fluorescence excitation microscopy to assess transscleral diffusional pathways in an isolate perfused bovine eye model." Investigative ophthalmology and visual science **51**: 5182-5189.
- Kim, H., K. G. Csaky, et al. (2006). "The pharmacokinetics of rituximab following an intravitreal injection." Experimental Eye Research **82**: 760-766.
- Kim, H., M. J. Lozak, et al. (2005). "Study of ocular transport of drugs released from an intravitreal implant using magnetic resonance imaging." Annals of Biomedical Engineering **33**: 150-164.

- Kim, J. H., J. H. Kim, et al. (2008). "Label-free calcium imaging in ischemic retinal tissue by TOF-SIMS." Biophysical Journal **94**: 4095-4102.
- Kim, S. H., K. G. Csaky, et al. (2007). "Drug elimination kinetics following subconjunctival injection using dynamic contrast-enhanced magnetic resonance imaging." Pharmaceutical Research **25**: 512-520.
- Kinoshita, A., H. Gong, et al. (2003). "Trace elements in lenses of normal Wistar Kyoto rats." Applied Surface Science **203-204**: 742-744.
- Kishikawa, Y., H. Gong, et al. (2003). "Elements and organic substances in epiretinal proliferative tissue excised during vitreous surgery: analysis by time-of-flight secondary-ion mass spectrometry " Japanese Society of Microscopy **52**: 349-354.
- Kishikawa, Y., T. Suematsu, et al. (2005). "Analysis of internal limiting membranes of secondary macular hole and idiopathic macular hole by time-of-flight secondary ion mass spectrometer." Investigative ophthalmology and visual science **46**: 5422.
- Kitano, S. and S. Nagataki (1986). "Transport of fluorescein monoglucuronide out of the vitreous." Investigative Ophthalmology and Visual Science **27**: 998-1001.
- Koeberle, M. (2002). Investigation of factors involved in the disposition and pharmacokinetics of memantine in the isolated bovine eye. Glasgow, University of Strathclyde. **PhD**.
- Koeberle, M. J., P. M. Hughes, et al. (2003). "Binding of memantine to melanin: influence of type of melanin and characteristics." Pharmaceutical Research **20**: 1702-9.
- Koeberle, M. J., P. M. Hughes, et al. (2006). "Pharmacokinetics and disposition of memantine in the arterially perfused bovine eye." Pharmaceutical Research **23**: 2781-2798.
- Konerirajapuram, N. S., K. Coral, et al. (2004). "Trace elements iron, copper and zinc in the vitreous of patients with various vitreoretinal diseases." Indian Journal of Ophthalmology **52**: 145-148.
- Krohne, T. U., N. Eter, et al. (2008). "Intraocular Pharmacokinetics of Bevacizumab After a Single Intravitreal Injection in Humans." American Journal of Ophthalmology **146**: 508-512.
- Kusuhara, H. and Y. Sugiyama (2004). "Efflux transport systems for organic anions and cations at the blood-CSF barrier." Advanced Drug Delivery Reviews **56**: 1741-1763.

- Kwak, H. W. and D. J. D'Amico (1995). "Determination of dexamethasone sodium phosphate in the vitreous by high performance liquid chromatography." Korean Journal of Ophthalmology **9**: 79-83.
- Leblanc, B., S. Jezequel, et al. (1998). "Binding of Drugs to Eye Melanin Is Not Predictive of Ocular Toxicity." Regulatory Toxicology and Pharmacology **28**: 124-132.
- Leblanc, B., S. Jezequel, et al. (1998). "Binding of drugs to eye melanin is not predictive of ocular toxicity." Regulatory Toxicology and Pharmacology **28**: 124-32.
- Lee, J. L. S., I. S. Gilmore, et al. (2008). "Quantification and methodology issues in multivariate analysis of ToF-SIMS data for mixed organic systems." Surface and Interface Analysis **40**: 1-14.
- Liu, Y., L. Hong, et al. (2005). "Comparisons of the structural and chemical properties of melanosomes isolated from retinal pigment epithelium, iris and choroid of newborn and mature bovine eyes." Photochemistry and Photobiology **81**: 510-516.
- Lund-Andersen, H. and B. Sander (2003). The Vitreous. Adler's Physiology of the Eye. P. L. Kaufman and A. Alm, Mosby: 293-314.
- Macha, S. and A. K. Mitra (2001). "Ocular Pharmacokinetics in Rabbits using a Novel Dual Probe Microdialysis Technique." Experimental Eye Research **72**: 289-299.
- MacNair, J. E., K. C. Lewis, et al. (1997). "Ultrahigh-pressure Reversed-Phase Liquid Chromatography in Packed Capillary Columns." Analytical Chemistry **69**: 983-989.
- MacNair, J. E., K. D. Patel, et al. (1999). "Ultrahigh-pressure Reversed-Phase Capillary Liquid Chromatography: Isocratic and Gradient Elution Using Columns Packed with 1.0- μ m Particles." Analytical Chemistry **71**: 700-708.
- Mains, J., C. Wilson, et al. (2011) "ToF-SIMS analysis of ocular tissues reveals biochemical differentiation and drug distribution." European Journal of Pharmaceutics and Biopharmaceutics **79**: 328-333
- Manitpisitkul, P. and R. E. White (2004). "Whatever happened to cassette-dosing pharmacokinetics?" Drug Discovery Today **9**: 652-658.
- Mannermaa, E., K.-S. Vellonen, et al. (2006). "Drug transport in corneal epithelium and blood-retina barrier: Emerging role of transporters in ocular pharmacokinetics." Advanced Drug Delivery Reviews **58**: 1136-1163.

- Marko-Varga, G., T. E. Fehniger, et al. (2011). "Drug localization in different lung cancer phenotypes by MALDI mass spectrometry imaging." Journal of Proteomics **74**: 982-992.
- Mason, J. O., P. A. Nixon, et al. (2006). "Intravitreal Injection of Bevacizumab (Avastin) as Adjunctive Treatment of Proliferative Diabetic Retinopathy." American Journal of Ophthalmology **142**: 685-688.
- Matuszewski, B. K. (2006). "Standard line slopes as a measure of a relative matrix effect in quantitative HPLC-MS bioanalysis." Journal of Chromatography B **830**: 293-300.
- Matuszewski, B. K., M. L. Constanzer, et al. (1998). "Matrix effect in quantitative LC/MS/MS analyses of biological fluids: A method for determination of finasteride in human plasma at picogram per milliliter concentrations." Analytical Chemistry **70**: 882-889.
- Maurice, D. M. (1957). "The exchange of sodium between the vitreous body and the blood and aqueous humor." Journal of Physiology **137**: 110-125.
- Maurice, D. M. (1957). "The exchange of sodium between the vitreous body and the blood and aqueous humour." Journal of Physiology **137**: 110-125.
- Maurice, D. M. (1987). "Flow of water between aqueous and vitreous compartments in the rabbit eye." American Journal of Physiology **252**: F104-F108.
- Maurice, D. M. and S. Mishima (1984). Ocular Pharmacokinetics. Pharmacology of the Eye. M. L. Sears. Berlin, Springer-Verlag.
- Maurice, D. M. and J. Polgar (1977). "Diffusion across the sclera." Experimental Eye Research **25**: 577-582.
- Midelfart, A., A. Dybdahl, et al. (1998). "Dexamethasone and dexamethasone phosphate detected by H and F NMR spectroscopy in the aqueous humour." Experimental Eye Research **66**: 327-337.
- Missel, P. (2002). "Hydraulic flow and vascular clearance influences on intravitreal drug delivery." Pharmaceutical Research **19**: 1636-1647.
- Mizuno, K., T. Koide, et al. (2009). "Route of penetration of topically instilled nipradilol into the ipsilateral posterior retina." Investigative ophthalmology and visual science **50**: 2840-2847.
- Moseley, H., W. S. Foulds, et al. (1984). "Routes of clearance of radioactive water from the rabbit vitreous." British Journal of Ophthalmology **68**: 145-151.

- Muller, C., P. Schafer, et al. (2002). "Ion suppression effects in liquid chromatography-electrospray-ionisation transport-region collision induced dissociation mass spectrometry with different serum extraction methods for systematic toxicological analysis with mass spectra libraries." Journal of Chromatography B **773**: 47-52.
- Nagaraja, N. V., J. K. Paliwal, et al. (1999). "Choosing the calibration model in assay validation." Journal of Pharmaceutical and Biomedical Analysis **20**: 433-438.
- Nichols, W. G. and M. Boeckh (2000). "Recent advances in therapy and prevention of CMV infections." Journal of Clinical Virology **16**: 25-40.
- Nickerson, C. S., J. Park, et al. (2008). "Rheological properties of the vitreous and the role of hyaluronic acid." Journal of Biomechanics **41**: 1840-1846.
- Niemeyer, G. (2001). "Retinal Research using the Perfused Mammalian Eye." Progress in Retinal and Eye Research **20**: 289-318.
- Notivol, R., D. Bertin, et al. (2004). "Comparison of topical tobramycin-dexamethasone with dexamethasone-neomycin-polymyxin and neomycin-polymyxin-gramicidin for the control of inflammation after cataract surgery: results of a multicenter, prospective, three-arm, randomized, double-masked, controlled, parallel-group study." Clinical Therapeutics **26**: 1274-1285.
- Nygren, H., K. Boerner, et al. (2006). "Localization of cholesterol in rat cerebellum with imaging TOF-SIMS. Effect on tissue preparation." Applied Surface Science **252**: 6975-6981.
- Okhravi, N., B. Odufuwa, et al. (2005). "Scleritis." Survey of Ophthalmology **50**: 351-363.
- Olsen, T. W., S. Y. Aaberg, et al. (1998). "Human sclera: Thickness and surface area." American Journal of Ophthalmology **125**: 237-241.
- Optometry (2009). "The rapidly evolving diagnosis and treatment of age-related macular degeneration." Optometry - Journal of the American Optometric Association **80**: 101-106.
- Park, J., P. M. Bungay, et al. (2005). "Evaluation of coupled convective-diffusive transport of drugs administered by intravitreal injection and controlled release implant." Journal of Controlled Release **105**: 279-295.

- Pasche, S. p., S. M. De Paul, et al. (2003). "Poly(l-lysine)-graft-poly(ethylene glycol) Assembled Monolayers on Niobium Oxide Surfaces: A Quantitative Study of the Influence of Polymer Interfacial Architecture on resistance to Protein Adsorption by ToF-SIMS and in Situ OWLS." Langmuir **19**: 9216-9225.
- Pitkanen, L., V. Ranta, et al. (2007). "Binding of betaxolol, metoprolol and oligonucleotides to synthetic and bovine ocular melanin, and prediction of drug binding to melanin in human choroid-retinal pigment epithelium." Pharmaceutical Research **24**: 2063-2070.
- Piwowar, A. M., N. P. Lockyer, et al. (2009). "Salt Effects on Ion Formation in Desorption Mass Spectrometry: An Investigation into the Role of Alkali Chlorides on Peak Suppression in Time-of-Flight-Secondary Ion Mass Spectrometry." Analytical Chemistry **81**: 1040-1048.
- Pollard, R. B. (1996). "CMV retinitis: ganciclovir/monoclonal antibody." Antiviral Research **29**: 73-75.
- Porta, M. and A. Allione (2004). "Current approaches and perspectives in the medical treatment of diabetic retinopathy." Pharmacology & Therapeutics **103**: 167-177.
- Preston, J. E., M. B. Segal, et al. (1989). "Neutral amino acid uptake by the isolated perfused sheep choroid plexus." Journal of Physiology **408**: 31-43.
- Proksch, J. W. and K. W. Ward (2007). "Cassette dosing pharmacokinetic studies for evaluation of ophthalmic drugs for posterior ocular diseases." Journal of Pharmaceutical Sciences **97**: 3411 - 3421
- Prota, G., D.-N. Hu, et al. (1998). "Characterization of Melanins in Human Irides and Cultured Uveal Melanocytes From Eyes of Different Colors." Experimental Eye Research **67**: 293-299.
- Quadro, L., W. S. Blamer, et al. (1999). "Impaired retinal function and vitamin A availability in mice lacking retinol-binding protein." The European Molecular Biology Organisation Journal **18**: 4633-4644.
- Rafferty, N. S. (1985). The Lens Morphology. The Ocular Lens: Structure, Function and Pathology. M. H. New York, Marcel Dekker: 1-60.
- Rajan, P. D., R. Kekuda, et al. (2000). "Expression of the extraneuronal monoamine transporter in RPE and neural retina." Current Eye Research **20**: 195-204.
- Ranta, V.-P. and A. Urtti (2006). "Transscleral drug delivery to the posterior eye: Prospects of pharmacokinetic modeling." Advanced Drug Delivery Reviews **58**: 1164-1181.

- Raviola, G. (1977). "The structural basis of the blood-ocular barriers." Experimental Eye Research **25**(Supplement 1): 27-63.
- Reddy, I. K. and N. S. Bodor (1994). "Novel approaches to design and deliver safe and effective anti-glaucoma agents to the eye." Advanced Drug Delivery Reviews **14**: 251-267.
- Ripps, H., L. Mehaffey, et al. (1989). "Vincristine-induced changes in the retina of the isolated arterially-perfused cat eye." Experimental Eye Research **48**: 771-790.
- Ritschel, W. A. and G. L. Kearns (2004). Handbook of basic pharmacokinetics including clinical applications. Washington DC, American Pharmacists Association.
- Rodgers, T., D. Leahy, et al. (2005). "Tissue distribution of basic drugs: Accounting for enantiomeric, compound and regional differences amongst b-blocking drugs in rat." Journal of Pharmaceutical Sciences **94**: 1237-1248.
- Rosen, A. M., D. B. Denham, et al. (2006). "In vitro dimensions and curvatures of human lenses." Vision Research **46**: 1002-1009.
- Rowland, M. and T. N. Tozer (1980). Concepts. Clinical Pharmacokinetics. Concepts and Applications. Philadelphia, Lea and Febiger.
- Saude, T. (1993). The outer coats of the eye. Ocular anatomy and physiology. London, Blackwell Science Ltd.
- Schoenwald, R. D. (2002). Basic Principles. Pharmacokinetics in drug discovery and development, CRC Press Ltd.
- Sebag, J. and E. A. Balazs (1989). "Morphology and Ultrastructure of Human Vitreous Fibers." Investigative ophthalmology and visual science **30**: 1867-1871.
- Shard, A. G., M. C. Davies, et al. (1997). "X-ray Photoelectron Spectroscopy and Time-of-Flight SIMS Investigations of Hyaluronic Acid Derivatives." Langmuir **13**: 2808-2814.
- Shell, J. W. (1982). "Pharmacokinetics of topically applied ophthalmic drugs." Survey of Ophthalmology **26**: 207-218.
- Shen, J., S. T. Cross, et al. (2003). "Evaluation of an immortalized retinal endothelial cell line as an in vitro model for drug transport studies across the blood-retinal-barrier." Pharmaceutical Research **20**: 1357-1363.
- Shiels, I. A., S. D. Sanderson, et al. (1999). "Arterially perfused eye model of uveitis." Australian Veterinary Journal **2**: 100-104.

- Shiels, I. A., S. D. Sanderson, et al. (1999). "Arterially perfused eye model of uveitis." Australian Veterinary Journal **77**: 100-104.
- Sigma-Aldrich. (1998). "Bulletin 910: Guide to Solid Phase Extraction." Retrieved 17th June, 2009, from <http://www.sigmaaldrich.com/Graphics/Supelco/objects/4600/4538.pdf>.
- SIGN (2001). Management of Diabetes: Quick reference guide, Scottish Intercollegiate Guidelines Network.
- Sigurdsson, H. H., E. Stefansson, et al. (2005). "Cyclodextrin formulation of dorzolamide and its distribution in the eye after topical administration." J. Cont. Rel. **102**: 255-262.
- Simoens, P. and N. G. Ghoshal (1981). "Arterial supply to the optic nerve and the retina of the sheep." Journal of Anatomy **133**: 481-497.
- Singtoroj, T., J. Tarning, et al. (2006). "A new approach to evaluate regression models during validation of bioanalytical assays." Journal of Pharmaceutical and Biomedical Analysis **41**: 219-227.
- Slamovits, T. L. and J. J. Dutton (2002). "Primary Drug Therapy for Glaucoma: Beta-Blockers versus other medication." Survey of Ophthalmology **47**: 63-67.
- Smith, M. E., M. C. Kincaid, et al. (1999). Basic Science, Refraction, and Pathology. The requisites in ophthalmology., Mosby-Year Book Inc.
- Sonoda, K.-H., T. Sakamoto, et al. (2004). "Residual vitreous cortex after surgical posterior vitreous separation visualized by intravitreal triamcinolone acetonide." Ophthalmology **111**: 226-230.
- Stay, M. S., J. Xu, et al. (2002). "Computer simulation of convective and diffusive transport of controlled release drugs in the vitreous humor." Pharmaceutical Research **20**: 96-102.
- Stepanova, L. V., I. Y. Marchenko, et al. (2005). "Direction of fluid transport in the lens." Bulletin of Experimental Biology and Medicine **139**: 50-51.
- Steuer, H., A. Jaworski, et al. (2005). "Functional characterization and comparison of the outer blood-retinal barrier." Investigative Ophthalmology and Visual Science **46**: 1047-1053.
- Stokkermans, T. J. (2000). "Treatment of age-related macular degeneration." Clinical Eye and Vision Care **12**: 15-35.

- Su, E.-N., D.-Y. Yu, et al. (1995). "Altered vasoactivity in the early diabetic eye: Measured in the isolated perfused rat eye." Experimental Eye Research **61**(6): 699-711.
- Summers Rada, J. A., S. Shelton, et al. (2006). "The sclera and myopia." Experimental Eye Research **82**: 185-200.
- Takahashi, J., T. Hikichi, et al. (2004). "Effect of nucleotide P2Y2 receptor agonists on outward active transport of fluorescein across normal blood-retina barrier in rabbit." Experimental Eye Research **78**: 103-108.
- Tan, L. E. (2010). A model of ageing vitreous: Implications for drug delivery. SIPBS. Glasgow, University of Strathclyde. Doctor of Philosophy: 272.
- Tan, L. E., W. Orilla, et al. (2011). "Effects of vitreous liquefaction on intravitreal distribution of sodium fluorescein, fluorescence dextran and fluorescent microparticles." Investigative ophthalmology and visual science **52**: 1111-1118.
- Tang, L. and P. Kebarle (1993). "Dependence of ion intensity in electrospray mass spectrometry on the concentration of the analytes in the electrosprayed solution." Analytical Chemistry **65**: 3654-3668.
- Taylor, M., A. J. Urquhart, et al. (2009). "Partial least square regression as a powerful tool for investigating larger combinatorial polymer libraries." Surface and Interface Analysis **41**: 127-135.
- Taylor, P. j. (2005). "Matrix effects: The achilles heel of quantitative high-performance liquid chromatography-electrospray-tandem mass spectrometry." Clinical Biochemistry **38**: 328-334.
- Tessem, M. B., T. F. Bathen, et al. (2005). "Effect of UVA and UVB irradiation on the metabolic profile of aqueous humor in rabbits analyzed by H NMR spectroscopy." Investigative ophthalmology and visual science **46**: 776-781.
- Tojo, K., K. Nakagawa, et al. (1999). "A pharmacokinetic model of intravitreal delivery of ganciclovir." European Journal of Pharmaceutics and Biopharmaceutics **47**: 99-104.
- Tomi, M. and K. Hosoya (2008). Molecular Mechanisms of the Inner Blood-Retinal Barrier Transporters. Ocular transporters in ophthalmic diseases and drug delivery. J. Tombran-Tink and C. J. Barnstable. Totawa, NJ, Human Press.
- Tripathi, R. C. and B. J. Tripathi (1984). Anatomy of the Human Eye, Orbit and Adnexa. The Eye: Vegetative Physiology and Biochemistry H. Davson. Orlando, Florida, Academic Press Inc. **1a**: 1-88.

- Tsuboi, S. and J. E. Pederson (1988). "Volume flow across the isolated retinal pigmented epithelium of cynomolgus monkey eyes." Investigative ophthalmology and visual science **29**: 1652-1656.
- Tsuchiya, M., S. Hayasaka, et al. (1987). "Affinity of ocular acid-insoluble melanin for drugs in vitro." Investigative ophthalmology and visual science **28**: 822-825.
- Tsuji, A. (2005). "Influx transporters and drug targeting: Application of peptide and cation transporters." International Congress Series **1277**: 75-84.
- Tyler, B. (2003). "Interpretation of TOF-SIMS images: multivariate and univariate approaches to image de-noising, image segmentation and compound identification." Applied Surface Science **203-204**: 825-831.
- Tyler, B. J., G. Rayal, et al. (2007). "Multivariate analysis strategies for processing ToF-SIMS images of biomaterials." Biomaterials **28**: 2412-2423.
- Tzepi, I., I. Vergados, et al. (2009). "Pharmacokinetics of intravenously administered moxifloxacin in eye compartments: an experimental study." International Journal of Antimicrobial Agents **33**: 160-162.
- Urquhart, A. J., M. Taylor, et al. (2007). "TOF-SIMS Analysis of a 576 Micropatterned Copolymer Array To Reveal Surface Moieties That Control Wettability." Analytical Chemistry **80**: 135-142.
- Urtti, A. (2006). "Challenges and obstacles of ocular pharmacokinetics and drug delivery." Advanced Drug Delivery Reviews **58**: 1131 - 1135.
- Urtti, A. and L. Salminen (1993). "Minimizing systemic absorption of topically administered ophthalmic drugs." Survey of Ophthalmology **37**: 435-456.
- Vaidyanathan, S., J. S. Fletcher, et al. (2008). "Exploratory analysis of TOF-SIMS data from biological surfaces." Applied Surface Science **255**: 1599-1602.
- Valeri, P., M. Palmery, et al. (1985). "Investigations on the ocular pharmacokinetics of bendazac in rabbits." Experimental and Molecular Pathology **43**: 283-287.
- Villiers, A. d., F. L. Lestremau, et al. (2006). "Evaluation of ultra performance liquid chromatography. Part I. Possibilities and limitations." Journal of Chromatography **1127**: 60-69.
- Wagner, M. S., D. J. Graham, et al. (2004). "Maximizing information obtained from secondary ion mass spectra of organic thin films using multivariate analysis." Surface Science **570**: 78-97.

- Wakamatsu, K., D. Hu, et al. (2007). "Characterisation of melanin in human iridal and choroidal melanocytes from eyes with various colored irides." Pigment Cell Melanoma Research **21**: 97-105.
- Washington, N., C. Washington, et al. (2001). Physiological Pharmaceuticals: Barries to Drug Absorption, Taylor and Francis.
- Watanabe, T., D. Schulz, et al. (2006). "High-throughput pharmacokinetic method: Cassette dosing in mice associated with minuscule serial bleedings and LC/MS/MS analysis." Analytica Chimica Acta **559**: 37-44.
- Weijtens, O., R. C. Schoemaker, et al. (1998). "Dexamethasone Concentration in Vitreous and Serum After Oral Administration." American Journal of Ophthalmology **125**: 673-679.
- Weinreb, R. N. and P. T. Khaw (2004). "Primary open-angle glaucoma." The Lancet **363**: 1711-1720.
- Welling, P. G. (1997). Drug transport. Pharmacokinetics: Processes, mathematics and applications, American Chemical Society.
- White, R. E. and P. Manitpiskitkul (2001). "Pharmacokinetic theory of cassette dosing in drug discovery screening." Drug Metabolism and Disposition **29**: 957-966.
- WHO (2004). Magnitude and causes of visual impairment. Fact sheet: 282. Geneva, Switzerland, World Health Organisation.
- Widmaier, E. P., H. Raff, et al. (2004). Movement of molecules across cell membranes Human Physiology Boston, McGraw Hill higher education.
- Wiederholt, M., S. Bielka, et al. (1995). "Regulation of outflow rate and resistance in the perfused anterior segment of the bovine eye." Experimental Eye Research **61**: 223-234.
- Williams, G. A., J. A. Haller, et al. (2009). "Dexamethasone Posterior-Segment Drug Delivery System in the Treatment of Macular Edema resulting from Uveitis or Irvine-Gass Syndrome." American Journal of Ophthalmology **147**: 1048-1054.
- Williams, T. M., A. J. Kind, et al. (1999). "Electrospray collision-induced dissociation of testosterone and testosterone hydroxy analogs." Journal of Mass Spectrometry **34**: 206-216.
- Wilson, C. G., E. M. Semenera, et al. (2007). Eye Structure and Physiological Function. Enhancement in Drug Delivery. E. Touitou and B. W. Barry. LLC, Taylor and Francis Group: 473-486.

- Wilson, C. G., Y. P. Zhu, et al. (2001). Ophthalmic Drug Delivery, Taylor and Francis.
- Wilson, W., M. Shahidullah, et al. (1993). "The bovine arterially-perfused eye: an in vitro method for the study of drug mechanisms on IOP, aqueous humour formation and uveal vasculature." Current Eye Research **12**: 609-620.
- Wilson, W. S., M. Shahidullah, et al. (1993). "The bovine arterially-perfused eye: an in vitro method for the study of drug mechanisms on IOP, aqueous humour formation and uveal vasculature." Current Eye Research **12**: 609-620.
- Wolf, K. K., S. Vora, et al. (2010). "Use of cassette dosing in sandwich-cultured rat and human hepatocytes to identify drugs that inhibit bile acid transport." Toxicology in Vitro **24**: 297-309.
- Wong, T. Y., G. Liew, et al. (2007). "Clinical Update: new treatments for age related macular degeneration." The Lancet **370**: 204-206.
- Wu, L., X. Lu, et al. (2007). "Imaging and differentiation of mouse embryo tissues by ToF-SIMS." International Journal of Mass Spectrometry **260**: 137-145.
- Xu, J., J. J. Heys, et al. (2000). "Permeability and diffusion in the vitreous humor: Implications for drug delivery." Pharmaceutical Research **17**: 664-669.
- Xu, R. N., L. Fan, et al. (2007). "Recent advances in high-throughput quantitative bioanalysis by LC-MS/MS." Journal of Pharmaceutical and Biomedical Analysis **44**: 342-355.
- Yoneyama, D., Y. Shinozaki, et al. (2010). "Involvement of system A in the retina-to-blood transport of l-proline across the inner blood-retinal barrier." Experimental Eye Research **90**: 507-513.
- Yu, D.-Y., E.-N. Su, et al. (2003). "Isolated preparations of ocular vasculature and their applications in ophthalmic Research." Progress in Retinal and Eye Research **22**: 135-169.
- Zhang, G., A. V. Terry Jr, et al. (2007). "Sensitive liquid chromatography/tandem mass spectrometry method for the simultaneous determination of olanzapine, risperidone, 9-hydroxyrisperidone, clozapine, haloperidol and ziprasidone in rat brain tissue." Journal of Chromatography B **858**: 276-281.
- Zhou, H., C. M. Chan, et al. (2002). "Relationship between the structure of polymers with well-defined fluorocarbon segmental lengths and the formation of secondary ions in SIMS." Surface and Interface Analysis **33**: 932-939
- Zorn, N., M. R. Hernandez, et al. (1992). "Collagen gene expression in the developing tree shrew sclera." Investigative ophthalmology and visual science **33**: S1053.

Appendix 1

I Figures

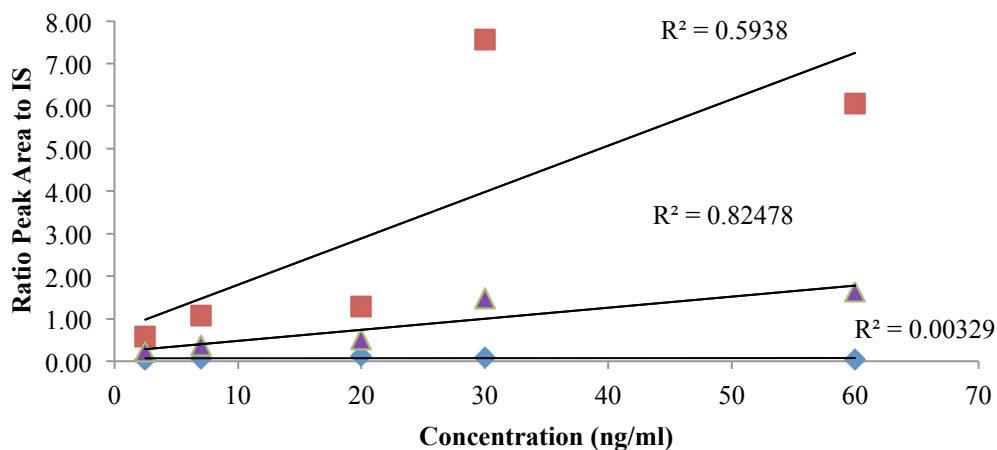


Figure A2.1 Analyte calibration in aqueous tissue using strong cation SPE method. Atenolol is shown in the red square, propranolol is shown in blue diamonds and timolol by green triangles.

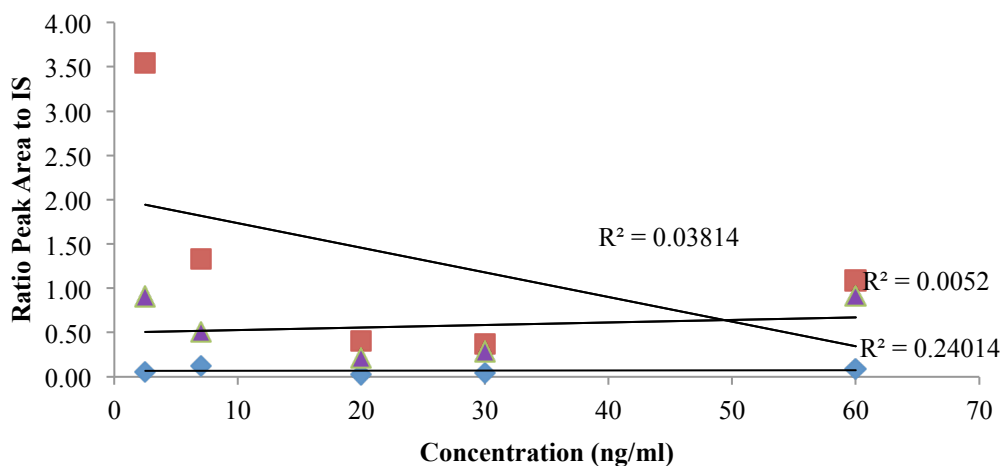


Figure A2.2 Analyte calibration in lens tissue using strong cation SPE method. Atenolol is shown in the red square, propranolol is shown in blue diamonds and timolol by green triangles.

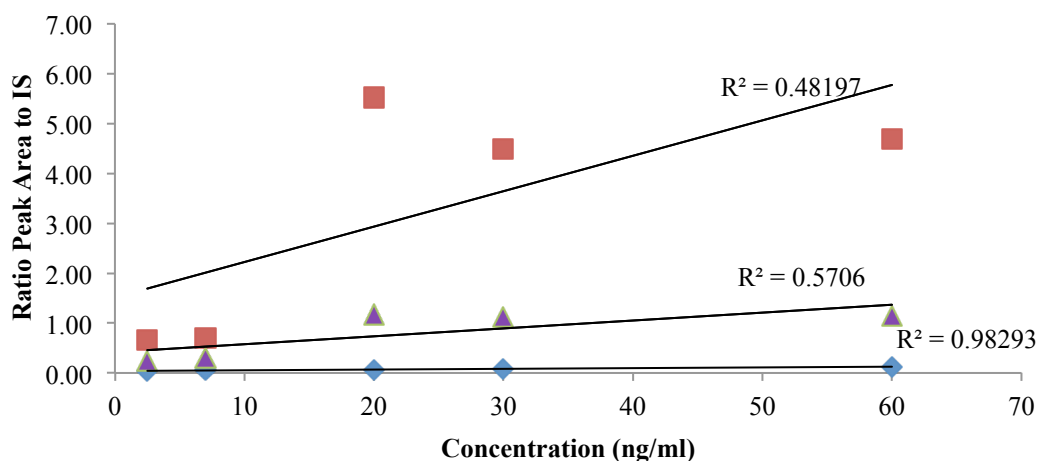


Figure A2.3 Analyte calibration in retinal tissue using strong cation SPE method. Atenolol is shown in the red square, propranolol is shown in blue diamonds and timolol by green triangles.

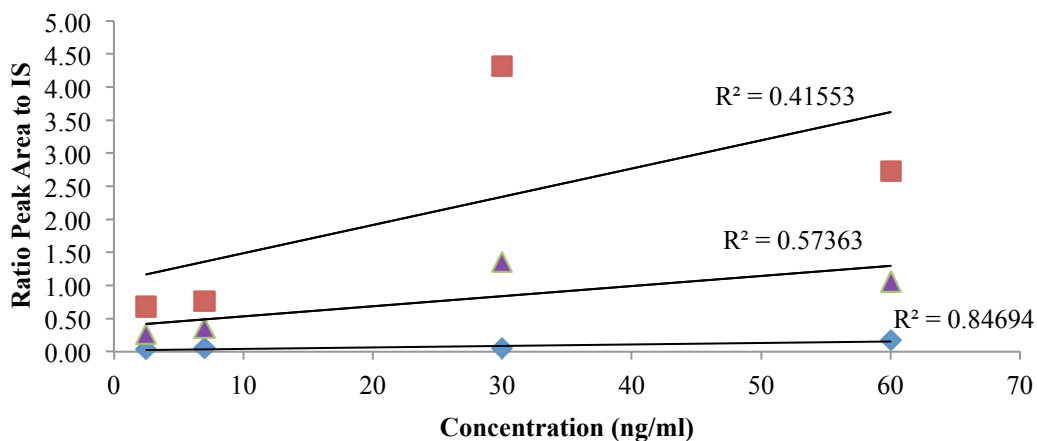


Figure A2.4 Analyte calibration in vitreous tissue using strong cation SPE method. Atenolol is shown in the red square, propranolol is shown in blue diamonds and timolol by green triangles.

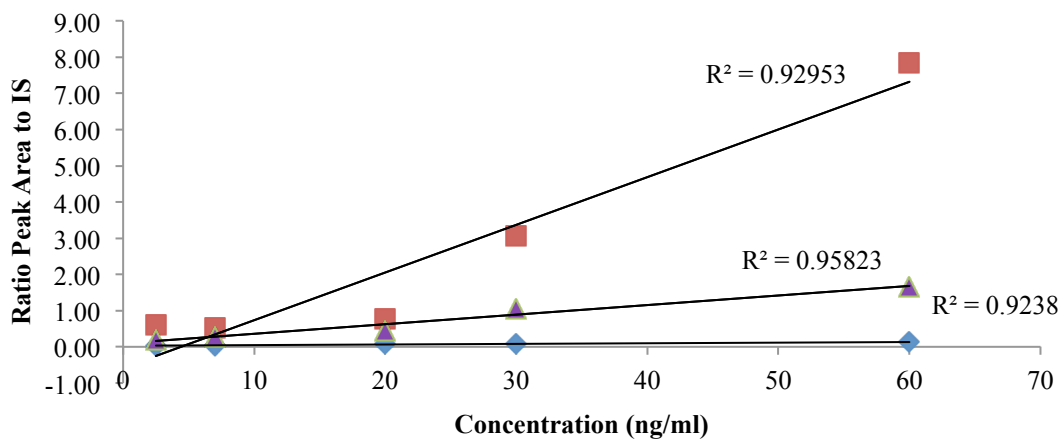


Figure A2.5 Analyte calibration in iris and CB tissue using strong cation SPE method. Atenolol is shown in the red square, propranolol is shown in blue diamonds and timolol by green triangles.

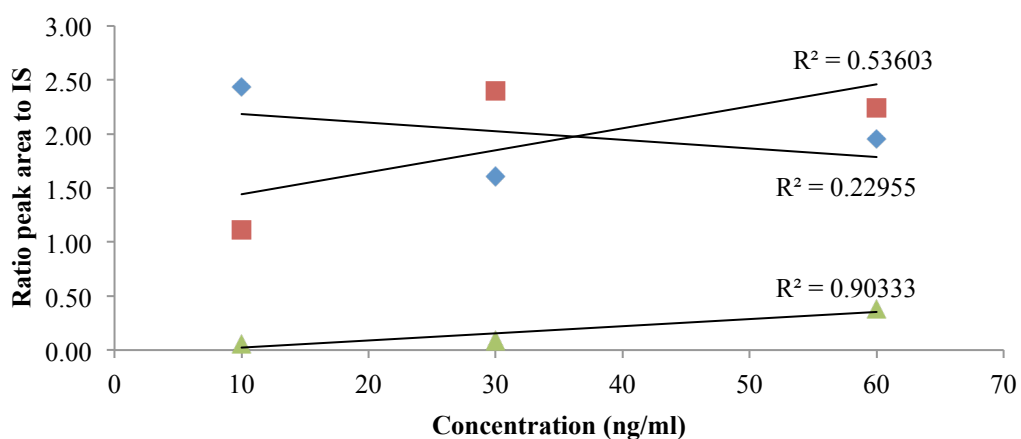


Figure A2.6 Analyte calibration in vitreous tissue using LLE method. Atenolol is shown in the red square, propranolol is shown in blue diamonds and timolol by green triangles.

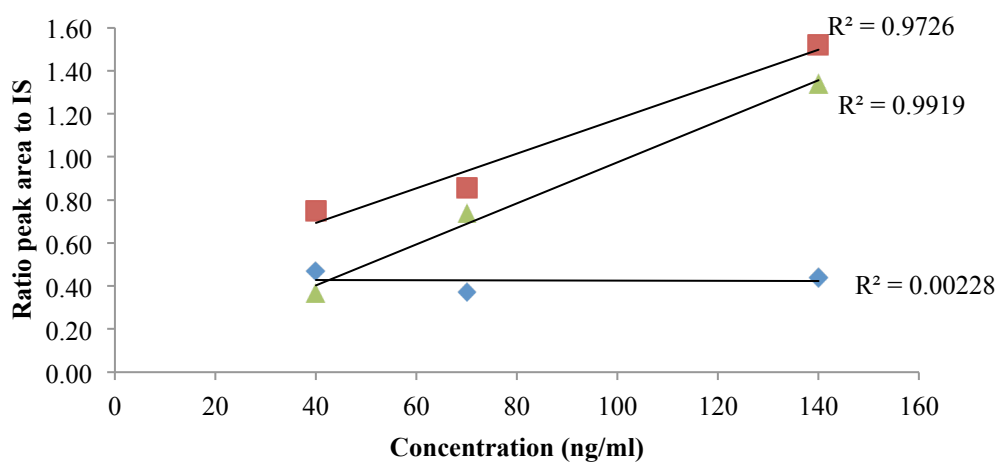


Figure A2.7 Analyte calibration in vitreous tissue using weak cation SPE method. Atenolol is shown in the red square, propranolol is shown in blue diamonds and timolol by green triangles.

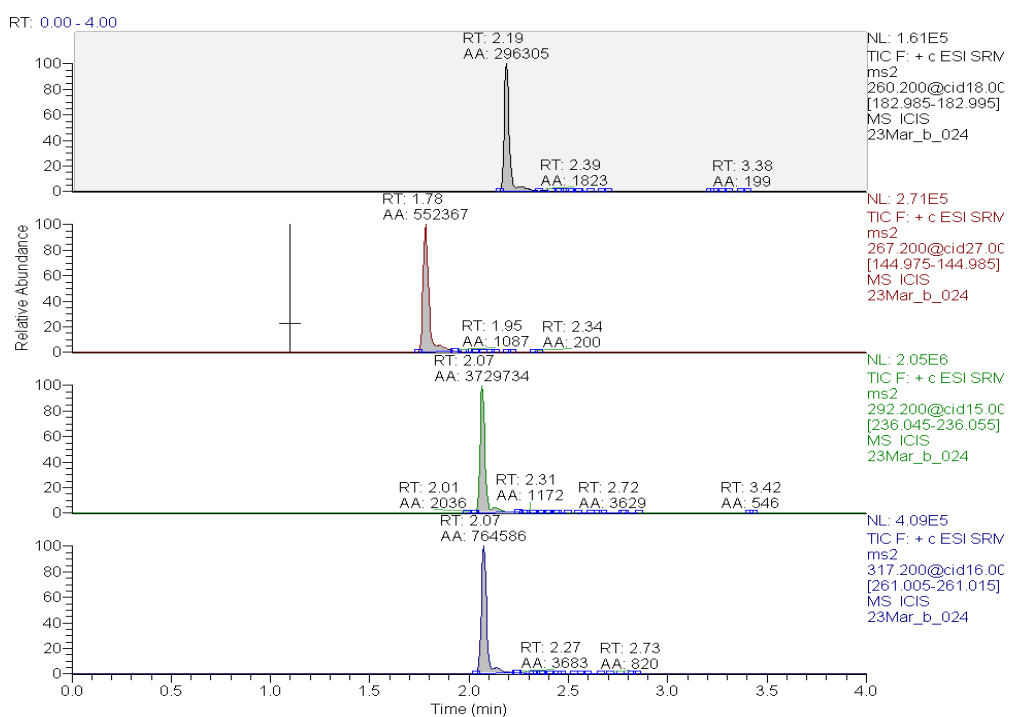


Figure A2.8 Chromatograph showing peaks obtained for propranolol, atenolol, levobunolol and timolol in descending order, prepared in vitreous tissue at 30ng/ml.

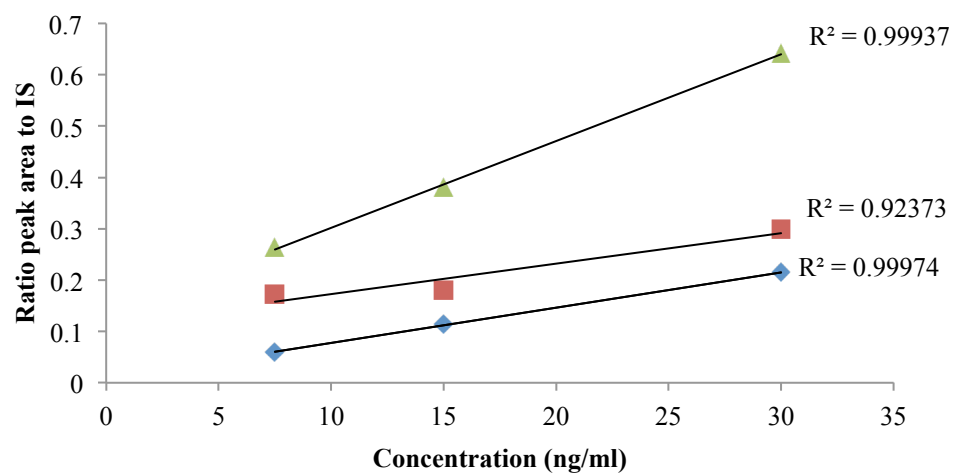


Figure A2.9 Analyte calibration in lens tissue using PP method. Atenolol is shown in the red square, propranolol is shown in blue diamonds and timolol by green triangles.

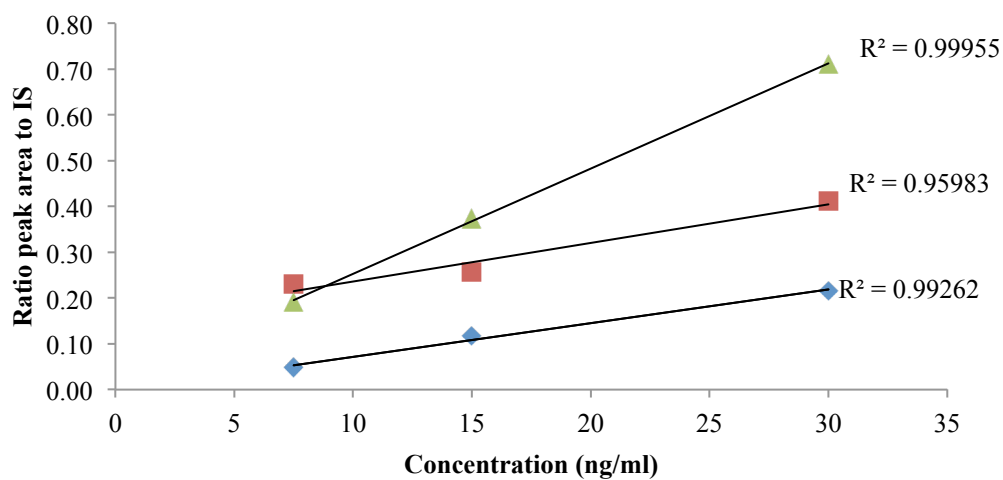


Figure A2.10 Analyte calibration in aqueous tissue using PP method. Atenolol is shown in the red square, propranolol is shown in blue diamonds and timolol by green triangles.

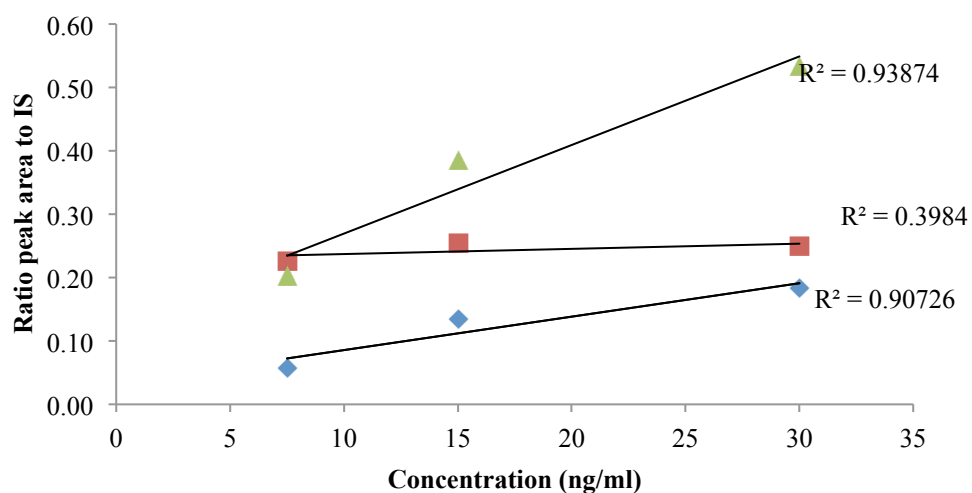


Figure A2.11 Analyte calibration in vitreous tissue using PP method. Atenolol is shown in the red square, propranolol is shown in blue diamonds and timolol by green triangles.

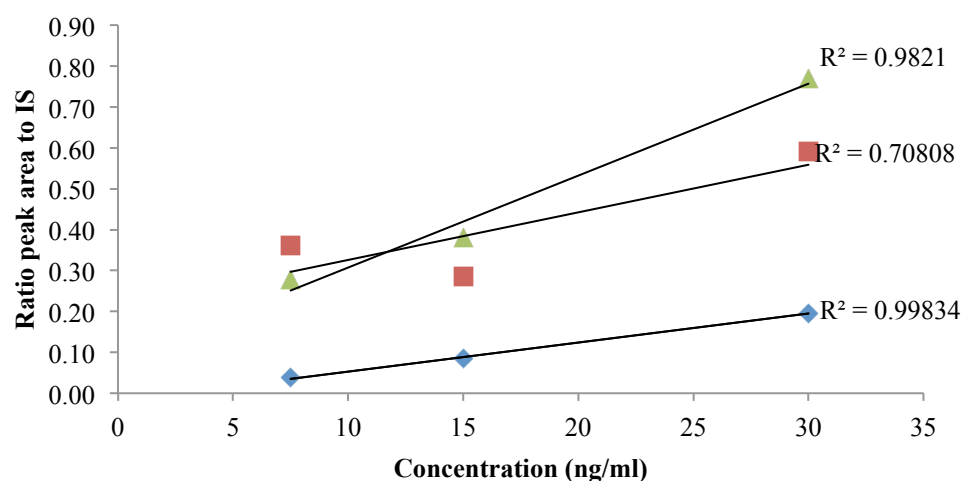


Figure A2.12 Analyte calibration in iris and CB tissue using PP method. Atenolol is shown in the red square, propranolol is shown in blue diamonds and timolol by green triangles.

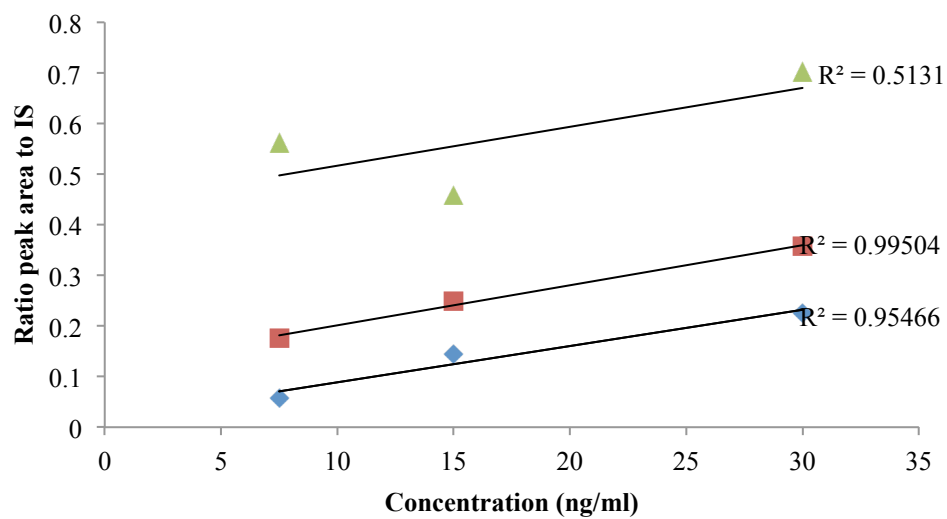


Figure A2.13 Analyte calibration in retinal tissue using PP method. Atenolol is shown in the red square, propranolol is shown in blue diamonds and timolol by green triangles.

II Tables

Concentration (ng/ml)	Analyte			
	Atenolol	Propranolol	Timolol	Levobunolol
60	10307417	167240	2180722	1314818
30	9266780	242555	3197300	3030337
20	16232988	1696681	9118619	20679628
7.5	12103937	986342	6267240	22733818
2.5	9467299	342824	3194829	15419274

Table A2.1 Peak areas obtained for the iris and CB at different analyte concentrations using strong cation SPE method.

Concentration (ng/ml)	Peak Areas				Response		
	Propranolol	Atenolol	Timolol	Levobunolol	Propranolol	Atenolol	Timolol
60	50328	57692	9729	25755	1.95	2.24	0.38
30	35899	53602	2075	22384	1.60	2.39	0.09
10	89446	40894	2220	36720	2.44	1.11	0.06

Table A2.2 Peak areas obtained for vitreous tissue at different analyte concentrations using LLE method.

Tissue	Sample (ng/mL)	Peak Areas					Response		
		Propranolol	Atenolol	Timolol	Levobunolol		Propranolol	Atenolol	Timolol
Aqueous	7.5	4649	22472	18685	97727		0.05	0.23	0.19
	15	11127	24422	35716	95459		0.12	0.26	0.37
	30	18517	35324	60899	85709		0.22	0.41	0.71
Iris and CB	7.5	738	7093	5443	19617		0.04	0.36	0.28
	15	1689	5728	7589	19954		0.08	0.29	0.38
	30	6344	19103	24887	32316		0.20	0.59	0.77
Vitreous	7.5	2869	11233	10101	49630		0.06	0.23	0.20
	15	9465	17975	27264	70701		0.13	0.25	0.39
	30	17073	23141	49553	92897		0.18	0.25	0.53
Lens	7.5	3474	10083	15372	58393		0.06	0.17	0.26
	15	6902	10974	23185	60877		0.11	0.18	0.38
	30	12123	16891	36282	56527		0.21	0.30	0.64
Retina	7.5	3209	9901	31512	56045		0.06	0.18	0.56
	15	7811	13383	24692	53933		0.14	0.25	0.46
	30	12537	19877	39105	55648		0.23	0.36	0.70

Table A2.3 Peak areas obtained for vitreous tissue at different analyte concentrations using the protein precipitation method.

		1 hour			2 hours		
		A	T	P	A	T	P
Aqueous Humor	MEAN (ng/g)	18330.6	8693.9	59476.0	291579.4	103987.3	21050.1
	ST DEV	9672.3	10865.0	110173.1	126373.4	64776.2	19418.7
	% RSD	52.8	125.0	185.2	43.3	62.3	92.2
Lens	MEAN (ng/g)	820175.0	920822.1	1086643.3	636446.8	719344.6	931732.6
	ST DEV	562067.5	580096.0	647980.3	675691.9	827036.8	1157937.2
	% RSD	68.5	63.0	59.6	106.2	115.0	124.3
Iris and CB	MEAN (ng/g)	3918645.5	4000190.0	2900288.0	5648975.3	7086282.4	5477539.7
	ST DEV	1081874.6	1031391.3	1164048.5	3860671.6	5436312.3	4592061.0
	% RSD	27.6	25.8	40.1	68.3	76.7	83.8
Vitreous	MEAN (ng/g)	2488782.2	2664050.7	2341116.7	1322672.0	1534305.3	1161267.6
	ST DEV	1499320.1	1161110.2	1069469.7	503996.3	665680.6	503318.3
	% RSD	60.2	43.6	45.7	38.1	43.4	43.3
Choroid	MEAN (ng/g)	2184422.9	2348847.8	1993284.7	1286745.5	1701992.0	1808303.0
	ST DEV	972723.9	1122876.4	1199006.0	584887.6	866628.6	488160.0
	% RSD	44.5	47.8	60.2	45.5	50.9	27.0
Retina	MEAN (ng/g)	823097.6	500352.0	396704.5	658442.3	1015460.6	941353.9
	ST DEV	447080.0	281156.0	316960.3	300196.9	520824.4	783622.9
	% RSD	54.3	56.2	79.9	45.6	51.3	83.2
		3 hours			5 hours		
		A	T	P	A	T	P
Aqueous Humor	MEAN (ng/g)	278071.2	90348.7	11603.9	426322.7	299861.8	8092.5
	ST DEV	278020.4	82476.5	3508.4	503702.2	403028.5	2367.8
	% RSD	100.0	91.3	30.2	118.2	134.4	29.3
Lens	MEAN (ng/g)	1080261.2	1411827.3	2098176.0	3254825.9	3999928.5	5555175.2
	ST DEV	622471.0	621041.3	1081656.3	5477959.9	6350758.8	7734968.1
	% RSD	57.6	44.0	51.6	168.3	158.8	139.2
Iris and CB	MEAN (ng/g)	3911952.7	4729750.4	3469115.6	1793911.8	2752960.4	2498376.5
	ST DEV	1425624.2	1960541.4	1688556.9	723404.9	1357143.5	1105842.0
	% RSD	36.4	41.5	48.7	40.3	49.3	44.3
Vitreous	MEAN (ng/g)	2237097.6	2672322.2	3964785.8	1353967.3	1455005.6	1921175.6
	ST DEV	823806.1	603849.4	2877186.8	681948.5	721406.6	1577145.1
	% RSD	36.8	22.6	72.6	50.4	49.6	82.1
Choroid	MEAN (ng/g)	2371452.7	3351082.5	2023744.7	1001350.7	1405179.4	926596.9
	ST DEV	503160.9	2200487.7	493233.9	718365.5	793228.6	462650.3
	% RSD	21.2	65.7	24.4	71.7	56.5	49.9
Retina	MEAN (ng/g)	1014077.8	1117875.9	1239795.4	505394.7	565084.0	601352.0
	ST DEV	419949.6	520948.6	741121.4	235911.3	313441.0	285907.1
	% RSD	41.4	46.6	59.8	46.7	55.5	47.5

		7 hours		
		A	T	P
Aqueous Humor	MEAN (ng/g)	183305.9	85827.2	12094.4
	ST DEV	155500.7	72902.1	10657.4
	% RSD	84.8	84.9	88.1
Lens	MEAN (ng/g)	857607.4	1236232.9	2088372.2
	ST DEV	307243.4	579595.2	1161280.7
	% RSD	35.8	46.9	55.6
Iris and CB	MEAN (ng/g)	3113789.4	3851192.0	3920405.3
	ST DEV	1231387.2	1440369.6	1754936.0
	% RSD	39.5	37.4	44.8
Vitreous	MEAN (ng/g)	1365959.3	1449447.1	4975076.2
	ST DEV	393311.4	461992.1	2181792.3
	% RSD	28.8	31.9	43.9
Choroid	MEAN (ng/g)	1525380.7	3391224.1	841740.0
	ST DEV	344322.8	2095166.6	304648.0
	% RSD	22.6	61.8	36.2
Retina	MEAN (ng/g)	836239.8	847515.1	968555.3
	ST DEV	174170.8	221711.3	165669.8
	% RSD	20.8	26.2	17.1

Table A2.4 Mean concentrations in ng/g, standard deviation (STDEV) and % relative standard deviation of atenolol (A), timolol (T) and propranolol (P) in each ocular tissue, at 1, 2, 3, 5 and 7 hours after the perfusion procedure was terminated (n=5).

PUBLICATIONS

Mains, J., Wilson, C and Urquhart A. (2011) "ToF-SIMS analysis of ocular tissues reveals biochemical differentiation and drug distribution." *European Journal of Pharmaceutics and Biopharmaceutics* **79**: 328-333.

Mains, J., Wilson, C and Urquhart A. (2011) "ToF-SIMS analysis of dexamethasone distribution - in the isolated perfused eye. " *Investigative ophthalmology and visual science* **52**: 8413-8419.

Mains, J., Wilson, C and Urquhart A. (2011) "A pharmacokinetic study of a combination of beta adrenoreceptor antagonists – in the isolated perfused ovine eye. " *European Journal of Pharmaceutics and Biopharmaceutics*, In Press.

Mains, J., Wilson, C, Urquhart A, Damien-Iordache, V. A finite element model of Brimonidine distribution in the rabbit eye. [Submitted to IVOS]

Wilson, C, Tan L.E, **Mains J.** Principles of retinal drug delivery from within the vitreous in Drug product development for the back of the eye. Springer link 2011

Mains, J., Wilson, C, Urquhart A, Damien-Iordache, V. Finite element model of topical brimonidine distribution in the rabbit eye [Poster Presentation] In PharmsciFair 2011, Prague, Czech Republic

Mains, J., Wilson, C and Urquhart A, Analysis of drug movement in the ovine eye by ToF-SIMS [Poster Presentation] In AAPS 2010, Los Angeles, USA



Research paper

A pharmacokinetic study of a combination of beta adrenoreceptor antagonists – In the isolated perfused ovine eye

Jenifer Mains, Lay Ean Tan, Clive Wilson, Andrew Urquhart*

Strathclyde Institute of Pharmacy and Biomedical Sciences, University of Strathclyde, Scotland, United Kingdom

ARTICLE INFO

Article history:

Received 10 June 2011

Accepted in revised form 10 November 2011

Available online xxxxx

Keywords:

Ocular

Pharmacokinetics

Mass spectrometry

Isolated perfused

Beta adrenoreceptor antagonist

ABSTRACT

The treatment of posterior eye diseases, such as diabetic retinopathy and age-related macular degeneration, is of growing interest as the number of people affected by these conditions continues to rise. This study utilises the methods of cassette dosing and the perfused ovine eye model – to reduce animal usage and therefore animal time – to show that for a series of beta adrenoreceptor antagonists, lipophilicity is a key physicochemical property that governs drug distribution within the eye. Following intravitreal injection, lipophilic beta adrenoreceptor antagonists penetrate to the posterior eye, where they bind to the choroid and reside in the retina at greater concentrations than more hydrophilic beta adrenoreceptor antagonists, which preferentially penetrate to the anterior eye.

© 2011 Published by Elsevier B.V.

1. Introduction

Interest in drug disposition in posterior eye disease has increased in recent years especially when treating certain disease states – such as diabetic retinopathy and age-related macular degeneration – where effective treatment is currently limited. Understanding the factors that influence drug disposition can potentially improve treatment options in these conditions by enabling improved drug targeting to the desired site of action and prediction of toxicity problems. The difficulty with describing ocular drug disposition mainly arises from the fact that it is not just a matter of taking a simple blood sample from the specimen at various time points and creating a concentration versus time profile although, in the fluid based ocular structures, namely the aqueous and vitreous humour, it is possible to sample a very small volume of fluid without the need for total eye enucleation. However, this technique cannot be applied to the remaining tissues present in the eye. For this reason, an animal is required for each time point, and repeat experiments are necessary. Therefore, in order to obtain information regarding the movement of substances within the eye, many animals are required to cover a significant time range, and each tissue has to be subjected to analysis individually. This leads to large animal requirements, prolonged analytical time and also the problem of inter-animal variability. In an attempt to overcome these problems, cassette dosing can be used. Cassette dosing

involves administering a series of drug compounds to the animal simultaneously in one dose, the 'cassette'. Commonly, a small cassette is used of approximately 2–10 compounds, at a low dose of up to about 1 mg/kg/compound for systemic studies [1,2]. The benefits of cassette dosing include reduced animal usage and reduced animal variability along with reduced analytical time, especially during the method development process. One major issue regarding cassette dosing is the potential for drug interactions between the drugs contained in the cassette. Possible sources of interaction are competition for clearance pathways, competition for protein binding, activation of certain clearance pathways, effects on blood flow and enzyme induction, solubility problems and difficulty in developing an analytical technique when using a set of diverse compounds [3,4]. In order to reduce these issues, it is desirable to keep the number of compounds relatively small and the dose of each to a minimum. The idea of using cassette dosing in ocular pharmacokinetic (PK) studies is a relatively new concept with only a few studies published. One *ex vivo* study of drug partitioning in bovine tissue and a pharmacokinetic study of drug distribution in the rat model using cassette dosing have been successfully completed [5], and another study successfully administered a cassette of five compounds via intravitreal injection to rabbit eyes [6]. Although solid PK data were generated, some variability between the pharmacokinetics of cassette dosing and the pharmacokinetics of individual dosing was noted. However, the results were still regarded as an adequate representation of PK data, and cassette dosing deemed useful for compound screening [6].

Another method of effectively generating ocular PK data without the need for large animal requirements is through the use of an isolated perfused eye system. The isolated perfused eye has

* Corresponding author. Strathclyde Institute of Pharmacy and Biomedical Sciences, University of Strathclyde, 161 Cathedral Street, Glasgow, Scotland G4 0RE, United Kingdom. Tel.: +44 141 548 5947.

E-mail address: andrew.urquhart@strath.ac.uk (A. Urquhart).

been used extensively in a variety of animal models including cat, rat, bull, horse, dog and frog [7–11], and in addition, it has also been used on human eyes [12,13]. More recently, the isolated perfused eye has been utilised in PK studies as an alternative to performing ocular drug distribution studies in live animals. The isolated perfused eye offers several advantages when compared to using an animal during a PK study, including no anaesthetic requirements or concern over animal comfort, control over the physiological environment, reduced animal usage as waste eyes from the food industry can be utilised, controlled drug administration and control of exposure to substances from systemic circulation into the ocular system [14]. Limitations include a lack of neural control of the eye as well as differences between perfusion parameters selected and conditions typically experienced in vivo [15]. In this work, the isolated perfused ovine eye model was used. Ovine eyes have been used previously in isolated perfused eye experiments to investigate the effect of pH on the corneal stroma [16] and carrier mediated uptake of neutral amino acids into the choroid [17]. The relative similarity of the ovine eye size and shape to human eyes and ease of handling make it a useful model in drug distribution studies. Our group has previously demonstrated the use of the isolated perfused ovine eye model through the investigation of fluorescent microparticle distribution in the vitreous and drug distribution using time-of-flight secondary ion mass spectrometry [18,19]. In this study, we present for the first time how the isolated perfused ovine eye can be combined with the method of cassette dosing as a suitable means of generating ocular PK data, reducing both the number of animals required to be utilised during the experimental work and analytical time. We also show that drug lipophilicity plays an important role in the extent of ocular drug distribution following drug administration via an intravitreal injection.

2. Materials and methods

2.1. Isolated ovine eye procedure

Perfusion of the isolated ovine eyes was based on a method detailed previously by Koerberle [20]. Briefly, ovine eyes were collected on ice from a local abattoir, within 1–2 h of slaughter, and warmed to room temperature. One of the long ciliary arteries that typically wrap around the optic nerve was then identified and cannulated in order to supply the perfusion fluid to the eye. Details of the composition of the perfusion fluid administered into the eyes via the ciliary artery are presented in Table 1; all components were purchased from Sigma–Aldrich (Dorset, UK). The eye was placed on the stage of the perfusion system on its side, with the cornea facing outwards, to mimic typical in vivo eye positioning and covered with polyethylene film to prevent dehydration. The cannula was then attached to the filter of the perfusion fluid port, and the perfusion process was initiated at an initial rate of approximately 0.2 ml/minute increased to 1 ml/minute over the course of

Table 1
Composition of perfusion fluid administered to isolated perfused eye.

Chemical	Concentration
Tissue culture medium	1000 ml
Sodium bicarbonate	2.2 g/l
Atropine sulphate	0.005 g/l
EDTA	0.2922 g/l
Penicillin G	100 kU/l
Streptomycin	75.6 kU/l
Gentamycin	0.08 g/l
Insulin bovine	50 U/l
Bovine holo-transferrin	0.0025 g/l
Sodium selenite	2.4 µg/l

Please cite this article in press as: J. Mains et al., A pharmacokinetic study of a combination of beta adrenoreceptor antagonists – In the isolated perfused ovine eye, Eur. J. Pharm. Biopharm. (2011), doi:10.1016/j.ejpb.2011.11.006

30 min. During the perfusion procedure, viability of the isolated perfused ovine eye was determined by monitoring the arterial perfusion pressure, the intraocular pressure (IOP), glucose consumption and lactate dehydrogenase (LDH) activity detailed by Koerberle [20].

2.2. Administration of a beta adrenoreceptor cassette

To investigate the impact of physicochemical properties on drug disposition following intravitreal administration, three different beta adrenoreceptor antagonists were used, atenolol (purity ≥98%), timolol (purity ≥98%) and propranolol (purity ≥99%) – all purchased from Sigma–Aldrich). All three beta adrenoreceptor antagonists were administered to the eye in a cassette. A solution containing atenolol, timolol and propranolol each at a concentration of 5 mg/ml was prepared in deionised water. The solution was then passed through a 0.22 µm syringe filter to remove any particulates. Once the eye had reached maximum perfusion rate and arterial perfusion pressure and intraocular pressure were maintained, the drug cassette was administered into the vitreous. The dose delivered to the eye was 500 µg of each of the three drugs in a total injection volume of 100 µl. The injection was performed using a 1 ml syringe and 23G needle, inserted 5 mm into the vitreous approximately 3–4 mm from the limbus in the posterior direction. Following injection, the needle was drawn very slowly from the eye in order to minimise leakage from the injection site. The perfusion procedure was terminated at five set time points 1, 2, 3, 5 and 7 h post-dosing with the beta adrenoreceptor cassette. For each time point used in the study, five eyes were perfused, dosed and analysed.

2.3. Dissection and ovine ocular tissue preparation

On completion of the perfusion procedure, a 30G needle was inserted into the anterior chamber of the eye, and the aqueous humour was removed. To reduce the risk of cross-tissue contamination, eyes were then frozen in liquid nitrogen before further dissection. The anterior section was removed by creating a small incision into the sclera approximately 3 mm from the edge of the cornea and was then cut away in a circular manner. From this, the lens was lifted away from the iris and ciliary body, and the iris and ciliary body were removed by tweezing the tissue off the sclera. In the posterior section, the eye was placed on its side, and the frozen vitreous was carefully removed using tweezers, ensuring that the retinal tissue did not contaminate the vitreous sample. The retina was then gently lifted away from the head of the optic nerve, and the choroid was also gently lifted away from the sclera. All tissues were then homogenised individually. To the retina, choroid, iris and ciliary body and lens, 1 ml of deionised water was added before homogenisation. Following this, 6 ml of methanol was added to each tissue sample, and samples were ultrasonicated for 2 min. Immediately, the samples were centrifuged for 20 min at a speed of 3000 rpm, and 100 µl was added to 900 µl of deionised water before injection into the UPLC-MS/MS.

2.4. Analysis and quantification of tissue samples

UPLC-MS/MS was performed on a Thermo TSQ Quantum Ultra with HFSI-II heated electrospray ionisation probe (Thermo Scientific). The XCalibur data system was used for system control and also data processing. Analyte separations were performed on an Acquity, BEH UPLC C₁₈ column (100 mm length, 2.1 mm internal diameter) with a 1.7 µm particle size. The mobile phase was composed of 0.1% formic acid in HPLC grade water (A) and 0.1% formic acid in methanol (B) at an initial ratio of 95:05 (A:B). A gradient method was selected for compound elution at 500 µl/min, using

the following ratios of mobile phase: 95% A for 0.5 min decreased to 0% using a linear gradient over 0.5 min and held for 1 min, then restored to starting 95% A before the next injection. Samples were analysed in positive mode with selective ion monitoring mode selected to detect the daughter ion of the compounds.

2.5. Analytical method validation

Analytical method validation was performed on all ocular tissues investigated: the aqueous humour, the lens, the iris and ciliary body, the vitreous humour, the retina and the choroid, for all three beta adrenoreceptor antagonists. In order to prepare the samples for the method validation, all tissues were homogenised and spiked with 1 ml of drug compound series and 1 ml of internal standard. The samples were then processed for analysis using the method detailed previously before injection into the UPLC-MS/MS. The method was calibrated and assessed for linearity over the concentration range of 5–100 ng/ml for each individual ocular tissue, using eye tissue from a different animal for each concentration. Weighted linear regression of $1/x^2$ was selected as a suitable method, and acceptable correlation coefficients were obtained for all three drugs in the vitreous, retina, aqueous and lens tissues (>0.97). Weighted linear regression was selected as this method applies focus to data points with lower variance and as a result has less dependence on data associated with high variance, unlike ordinary linear regression, where deviations at higher concentrations tend to have a greater impact on the shape of the calibration curve than deviations at lower concentrations [21,22]. In the choroid, sensitivity was lost at the lowest concentration in the calibration range, and as a result, the calibration curve in this tissue was prepared in the range of 7.5–100 ng/ml. Acceptable accuracy of between 75% and 120% of the ideal value was achieved for all three drugs in the vitreous, retina, aqueous, lens and iris and ciliary body tissues [23]. For the choroid, a slight deviation in accuracy was noted for propranolol (130%). The choroid is a thick melanin rich tissue, and as a result, sample preparation was more challenging and not as clean as the other samples, explaining this deviation. Intraday precision of drug peak area to internal standard peak area was less than 15% and for the interday precision less than 20%.

3. Results and discussion

Three beta adrenoreceptor antagonists (atenolol, timolol and propranolol) were selected for investigation in this study due to their individual physicochemical properties (see Table 2 for values). All three drugs had similar molecular weights (267 a.m.u., 316 a.m.u. and 260 a.m.u., respectively) removing molecular weight influences on drug distribution within the eye [24,25]. All three drugs were basic compounds and had very similar pKa values; since all three drugs were positively charged at physiological pH, pKa would have had little influence on the distribution of each drug. Where a distinct difference did occur in the physicochemical properties of each of the drug compounds was in their partition coefficients. Partition coefficient has been shown to have a large influence on the distribution of drugs within ocular tissues, with hydrophilic molecules thought to distribute and be cleared from the anterior section of the eye and lipophilic molecules thought to distribute and be cleared from the posterior section of the eye [26]. An intravitreal cassette dosing study performed previously in rabbits failed to show clear differences in the impact of partition coefficient on drug distribution within ocular tissues [6]. However, within the drug series selected, all of the drugs were very lipophilic molecules, and this would have accounted for the lack of correlation in drug distribution and partition coefficient. Previous work investigating the impact of beta adrenoreceptor antagonist

lipophilicity on drug distribution following systemic administration in the rat demonstrated that increased tissue accumulation occurred with increasing drug lipophilicity [27]. In this study, atenolol was selected due to its low logP and is the most hydrophilic of the three compounds with a logP of 0.16. Propranolol was selected to be the most lipophilic molecule, with a logP much greater than atenolol at 2.4. Finally, timolol was selected as an intermediate compound with a logP equal to 1.8 sitting between the logP of other two compounds, but leaning more towards the more lipophilic region of the scale.

Following intravitreal drug administration, the corresponding concentration maxima of drug within tissue (C_{Max}) and the time required to reach C_{Max} (T_{Max}) of all three drug molecules in each individual tissue were obtained (see Table 3 for details). The highest concentration of atenolol measured in the vitreous was 2489 $\mu\text{g/g}$ and was recorded in the first hour. Atenolol then appears to move quickly into the iris and ciliary body with C_{Max} recorded to be 5649 $\mu\text{g/g}$ at 2 h post-dosing. Maximal concentrations in the choroid and in the retina were noted simultaneously at 3 h post-dosing and were 2237 and 1014 $\mu\text{g/g}$, respectively, whereas the C_{Max} of the aqueous humour and the lens was seen at 5 h post-dosing and measured to be 426 and 3255 $\mu\text{g/g}$, respectively. In contrast to the data for atenolol, the C_{Max} of timolol was measured in the vitreous humour occurred at the 3 h time point, post-drug administration, however, only at a concentration of 2672 $\mu\text{g/g}$ which is only slightly higher than the concentration of 2664 $\mu\text{g/g}$ seen at 1 h post-dosing. In a similar manner to atenolol, timolol moved quickly into the iris and ciliary body with T_{Max} occurring at 2 h after drug administration, with a corresponding C_{Max} of 7086 $\mu\text{g/g}$. Peak concentrations in the aqueous humour and the lens again occur at 5 h post-dosing, with C_{Max} recorded to be 300 and 4000 $\mu\text{g/g}$, respectively. In this instance, the retina mirrors vitreous humour and not the choroid, with a maximum concentration of 1118 $\mu\text{g/g}$ recorded in the retina at the 3 h time point. The choroid, in contrast to atenolol, reaches a concentration of 3391 $\mu\text{g/g}$ towards the end of the experiment at a T_{Max} of 7 h. With propranolol, again high concentrations were detected in the vitreous in the initial phase of the experiment, with a C_{Max} of 2341 $\mu\text{g/g}$ occurring at 1 h post-administration. In the anterior segment of the eye, the peak aqueous humour concentration occurred at 5 h post-dosing, although concentrations of propranolol in the aqueous humour were generally low throughout the experiment and C_{Max} was determined to be only 108 $\mu\text{g/g}$. As with the other drugs, peak levels of propranolol in the iris and ciliary body occurred at the 2 h time point, and peak levels of propranolol in the lens occurred at 5 h. C_{Max} for both tissues was very similar and was determined to be 5478 $\mu\text{g/g}$ and 5555 $\mu\text{g/g}$, respectively. In similarity to timolol, a peak level in the retina of 1240 $\mu\text{g/g}$ occurred 3 h post-dosing, and in the choroid, a peak level of 4975 $\mu\text{g/g}$ was seen at 7 h after drug administration.

Focusing on the concentration versus time profile for each tissue obtained for each individual drug. For atenolol, there is an initial dip in the vitreous concentration at 2 h, where the drug appears to move quite quickly into the iris and ciliary body (Fig. 1). At this point, it was noted that the drug began to move into the aqueous humour. At 3 h post-dosing, a slight increase in the concentration measured in the vitreous was noted before the concentration again reduced and began to level off at 5 h post-dosing. Corresponding to the vitreous concentration increase, noted at 3 h, there was a dip in the concentration measured in the iris and ciliary body. The iris and ciliary body appeared to act as a reservoir, taking up a high concentration of drug initially before releasing drug back into vitreous when the concentration in the vitreous fell. At the three hour time point, the vitreous supplies the posterior tissues and increases in choroid and retina concentrations also occurred. The concentration time profiles of the choroid and the

Please cite this article in press as: J. Mains et al., A pharmacokinetic study of a combination of beta adrenoreceptor antagonists – In the isolated perfused ovine eye, Eur. J. Pharm. Biopharm. (2011), doi:10.1016/j.ejpb.2011.11.006

Table 2
Physicochemical properties of the drugs within the drug cassette.

Beta adrenoceptor antagonist	pKa	logP	Structure
Atenolol	9.5	0.16	
Timolol	9.2	1.8	
Propranolol	9.3	2.4	

Table 3
 C_{Max} and T_{Max} obtained for atenolol, timolol and propranolol in each individual ocular tissue.

Tissue	C_{Max} (ng/g)	T_{Max} (h)
<i>Atenolol</i>		
Aqueous	426.32	5
Iris and ciliary body	5648.98	2
Lens	3254.83	5
Vitreous	2488.78	1
Retina	1014.08	3
Choroid	2237.10	3
<i>Timolol</i>		
Aqueous	299.86	5
Iris and ciliary body	7086.28	2
Lens	3999.93	5
Vitreous	2672.32	3
Retina	1117.88	3
Choroid	3391.22	7
<i>Propranolol</i>		
Aqueous	59.48	1
Iris and ciliary body	5477.54	2
Lens	5555.18	5
Vitreous	2341.12	1
Retina	1239.80	3
Choroid	4975.08	7

retina appear to mirror each other, suggesting steady state exchange of drug between the two tissues. Another larger dip in the iris and ciliary body concentration occurred after 5 h, where atenolol moved out of the iris and ciliary body and into the other anterior tissues, the aqueous humour and the lens.

Focusing on the concentration versus time profiles generated for timolol (Fig. 2), a similar pattern of drug distribution to atenolol was seen, with differences in concentration profile occurring in the retina and in the choroid. Initially, timolol moved quickly out from the vitreous humour and into the iris and ciliary body within the first 2 h of the experiment. Differing from atenolol, at the 2 h time point, we had also seen rapid movement of timolol from the vitreous humour and into the retina, with concentrations in the retina rising steadily over the first 3 h as drug began to move in the posterior direction. At 3 h post-administration, timolol appeared to

move back from the iris and ciliary body into the vitreous which, at the point, feeds the posterior retina and choroid tissues. Increases in drug movement into the anterior chamber occurred again at 5 h post-dosing, with increases in aqueous and lens concentrations in response to a corresponding dip in the concentration achieved in the iris and ciliary body. Finally, towards the end of the experiment, drug began to accumulate in the choroid, which facilitated rising concentrations in the retina.

Propranolol moved in the anterior direction from the vitreous to the iris and ciliary body in the first 2 h, but again the drug also moved in the posterior direction, and the levels in the retina began to rise too (see Fig. 3). Propranolol was then dislodged from the iris and ciliary body at 3 h post-administration and moved back into the vitreous tissue, with simultaneous increases in concentrations detected in the retina and in the choroid. This effect was seen across all three drugs, and it is also possible that the increased vitreous concentrations were not only due to drug dislodgement from the iris and ciliary body but from drug movement through the lens into the vitreous humour. Tan et al. have noted from the ocular fluorophotometry in live rabbit eyes that intravitreally injected sodium fluorescein penetrated the lens at 2 h after dosing, but the substance did not continue a forward diffusion into the anterior chamber but unloaded the absorbed fluorescein back into the vitreous humour 3 h later [28]. This coincides with the study by Stepanova and colleagues, who showed that when fluorescein was initially placed in the central section of the lens, it rapidly moved towards the posterior pole of the lens and out into the vitreous humour, with no fluorescein shown to move in the anterior direction [29]. In this case, it was postulated that fluorescein movement was caused by a vectorial fluid flow in the lens that opposes diffusion, most likely mediated by the transport system present in the lens epithelium. After 5 h, another fall in the iris and ciliary body concentration occurred, corresponding to an increase in the concentration of propranolol in the lens. At the end of the experiment, as with timolol, a spike in the concentration of propranolol detected in the choroid occurred and fed the retina with a rich supply of drug. However, the concentration of propranolol bound to the choroid was much greater than the concentration of timolol measured.

Please cite this article in press as: J. Mains et al., A pharmacokinetic study of a combination of beta adrenoceptor antagonists - In the isolated perfused ovine eye, Eur. J. Pharm. Biopharm. (2011), doi:10.1016/j.ejpb.2011.11.006

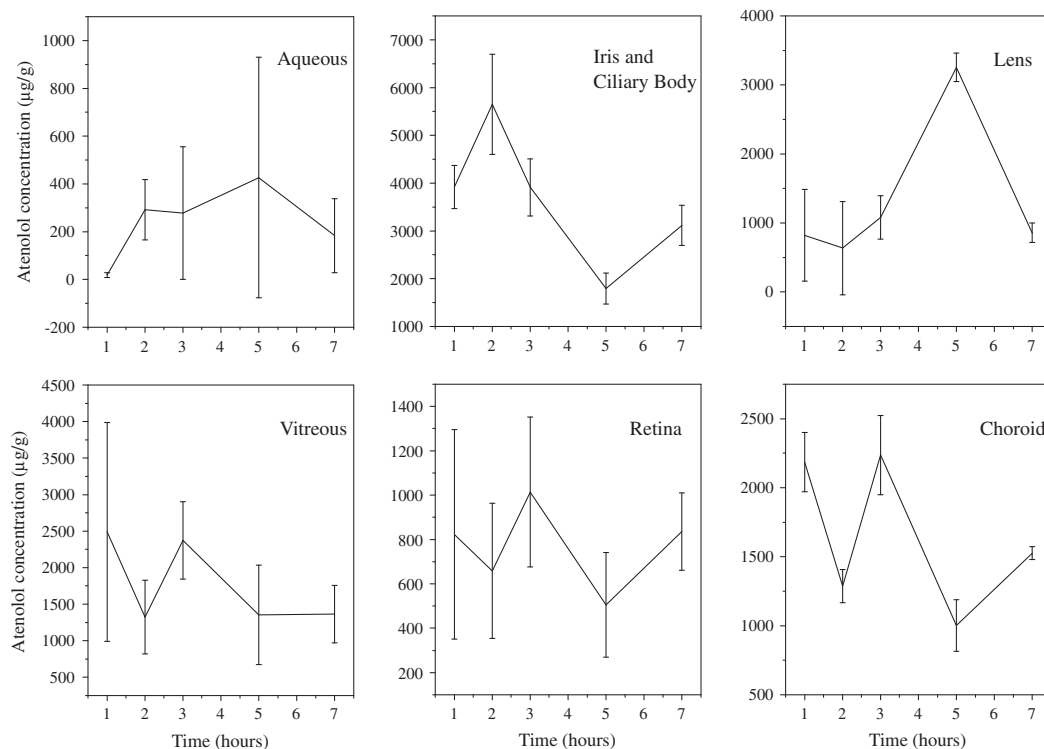


Fig. 1. Mean concentration ($n = 5$) versus time profile obtained for atenolol in each individual ocular tissue. Error bars show standard deviation from the mean.

Directly comparing the C_{Max} achieved for each of the three beta adrenoreceptor antagonists used shows key differences in drug distribution patterns (see Fig. 4). In the anterior segment of the eye, differences in C_{Max} occurred in all three tissues investigated, the aqueous humour, the lens and the iris and ciliary body. In the aqueous humour, the highest C_{Max} was achieved by the most hydrophilic molecule, atenolol, followed by a reduction in C_{Max} according to decreasing hydrophilicity, with timolol higher than propranolol. More hydrophilic compounds have been shown to penetrate and have greater diffusivity within the water based aqueous humour than more lipophilic drug compounds [26]. Therefore, an increase in the aqueous humour C_{Max} of the three beta blocking compounds with decreasing logP was due to an increase in the ease of drug diffusion into the aqueous humour because of drug hydrophilicity. More hydrophilic compounds are also subject to removal through the aqueous clearance system and will migrate from the vitreous into the anterior section of the eye before removal [30,31]. Therefore, a higher concentration of the more hydrophilic drug, atenolol, moved in the anterior direction than the other two more lipophilic drugs. In contrast to a previous study, where T_{Max} in the aqueous humour was shown to increase with increasing logP, no significant difference between the compounds was recorded for T_{Max} , with T_{Max} determined to be 5 h post-dosing for atenolol and timolol, and 1 h for propranolol [26]. The difference in trends in T_{Max} could be related to the molecular size of the compounds used in the previously study, as the logP of the compounds corresponded to a progressive increase in molecular size [23], whereas in this study, no such relationship be-

tween size and partition coefficient existed. Significant differences in C_{Max} were noted in the iris and ciliary body with timolol, showing the greatest binding to this tissue followed by atenolol and then closely followed by propranolol, with a difference between the two of 200 µg/g. For the lens, a progressive increase in penetration into this tissue was seen with increasing drug lipophilicity. Movement of compounds within the lens has previously been investigated using fluorescein as a drug marker [29,32]. In the rabbit eye, it was demonstrated that fluorescein penetrated into the lens at both the anterior side and the posterior side, with little resistance created by the lens capsule. Resistance to fluorescein entry into the lens was, however, caused by the lens epithelium. For this reason, compounds with a higher partition coefficient will more readily penetrate the epithelial barrier than more hydrophilic drugs, explaining the rank order in drug penetration into the lens tissue with increasing lipophilicity [32].

In the posterior segment, and at the site of initial drug administration, little difference in the C_{Max} measured in the vitreous humour across the drug series was noted. The C_{Max} of timolol appeared to be the greatest, but the difference was small with a large variance. A difference in T_{Max} also occurred across the tissues, with the T_{Max} of atenolol and propranolol recorded at 1 h and the T_{Max} of timolol determined to be 3 h. The vitreous has been shown to experience an initial drug diffusion stage over the first hour following administration, followed by a gradual drug elimination phase, explaining the T_{Max} of one hour obtained for atenolol and propranolol [26,33]. As discussed previously, all three drugs also show an increase in measured drug levels at three hours, due to drug dis-

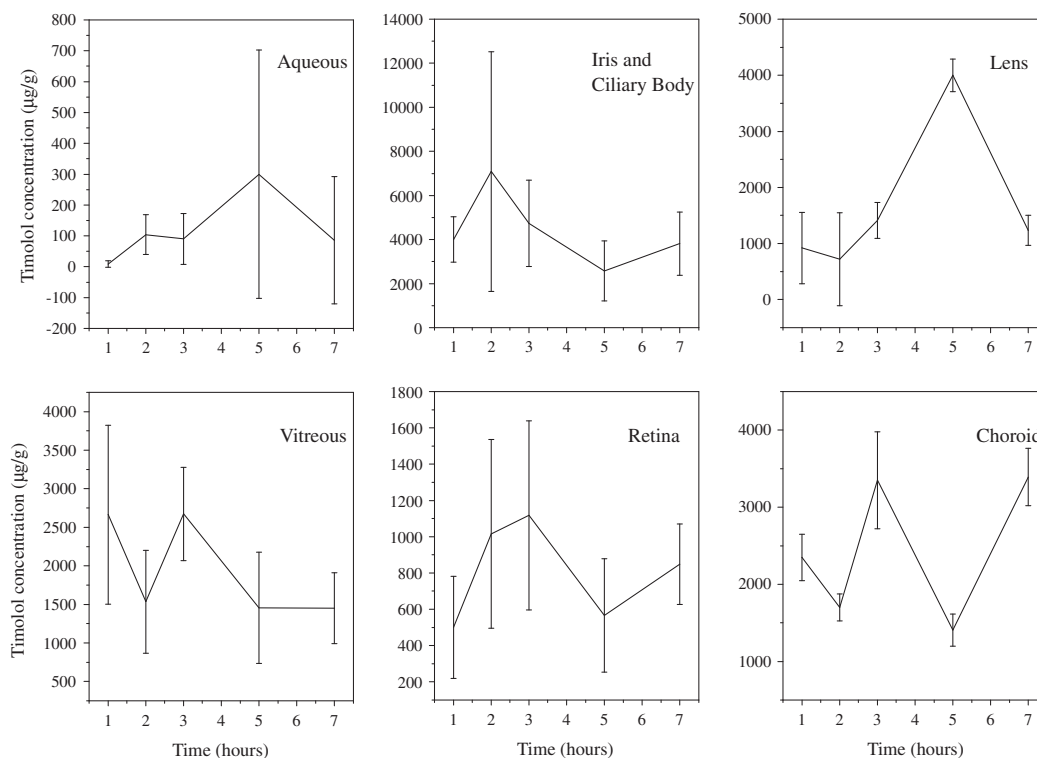


Fig. 2. Mean concentration ($n = 5$) versus time profile obtained for timolol in each individual ocular tissue. Error bars show standard deviation from the mean.

placement from the iris and ciliary body and re-equilibrating through the lens back into the vitreous. As a result, for all three drugs, similar drug levels were obtained at both one hour and three hours post-dosing. For timolol, the level obtained at three hours was just slightly greater than the level obtained at one hour, accounting for the apparent difference in T_{Max} compared to the other drugs in the series. In the remaining posterior tissues, the retina and the choroid, a pattern in the extent of drug movement was seen. In the retina, a stepwise increase was noted with increasing lipophilicity, with atenolol having the lowest C_{Max} , followed by timolol and then by propranolol with the greatest C_{Max} . The retina mirrored the choroid with a progressive increase in C_{Max} with increasing lipophilicity. The increase in choroid levels with increasing lipophilicity is in keeping with previous observations from the rat eye following a trans-scleral injection of a beta blocker drug series [5]. However, in this case, the choroid did not mirror the retina as retinal levels decreased with increasing lipophilicity. The lack of correlation could be explained by the difference in route of administration, as following trans-scleral injection, the beta blocker drug mix would reach the choroid before penetrating into the vitreous. The more lipophilic drugs would have bound to the choroidal melanin, and as a result, less drug would be free to move into the vitreous. Lipophilic drugs are subject to retinal clearance and will migrate towards the posterior pole before subsequent elimination [20,26]. As a result, a progressive increase in drug levels in the posterior eye with increasing lipophilicity is seen, as more hydrophilic drugs tend to move towards the anterior section

of the eye. T_{Max} differed also in the choroid, with C_{Max} occurring much earlier for atenolol at 3 h post-dosing, whereas drug accumulation on the choroid with time occurred for timolol and propranolol, with C_{Max} determined at 7 h post-dosing. The delay in reaching C_{Max} was probably caused by progressive drug accumulation on the melanin contained in the choroid over the course of the perfusion. Beta adrenoreceptor antagonists have previously been shown to bind to melanin of the choroid/RPE (retinal pigmented epithelium) with a high percentage of the available drug accumulating on the melanin [34]. It has been reported that all drugs known to bind to melanin are basic or have some element of basicity in their structure, and in addition to this, all drugs were known to have a positive logP and therefore a degree of lipophilicity [35]. All three drugs used in this study were basic compounds, with varying levels of lipophilicity. It is interesting that the extent of binding to the choroid tissue increased with increasing drug lipophilicity. This differs from the results obtained in the iris and ciliary body, where a stepwise increase in drug tissue binding with increasing lipophilicity was not demonstrated and timolol had the highest C_{Max} out of the three drugs investigated. This difference may be influenced by the clearance mechanisms operating within the eye, as propranolol is very lipophilic and subject to retinal clearance, less propranolol would be available in the anterior section of the eye than the less lipophilic timolol, accounting for the reduced levels experienced on the iris and ciliary body. In addition, although a higher concentration of atenolol would have migrated towards the anterior eye, the more hydrophilic nature of atenolol

Please cite this article in press as: J. Mains et al., A pharmacokinetic study of a combination of beta adrenoreceptor antagonists – In the isolated perfused ovine eye, Eur. J. Pharm. Biopharm. (2011), doi:10.1016/j.ejpb.2011.11.006

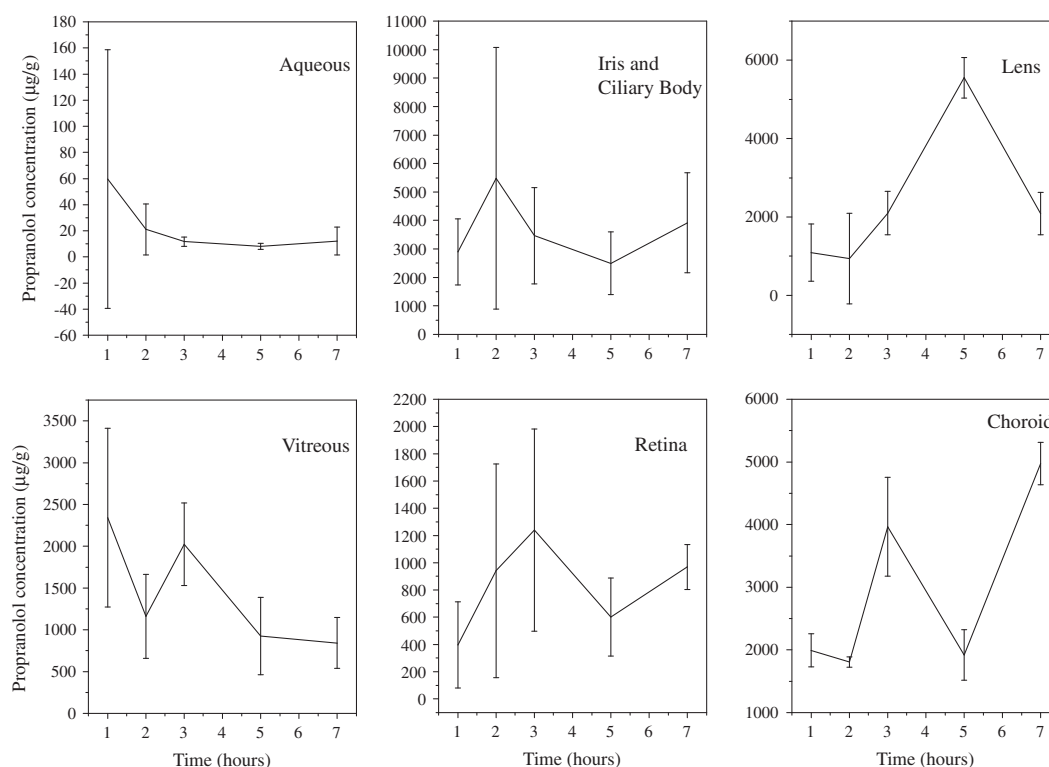


Fig. 3. Mean concentration ($n = 5$) versus time profile obtained for propranolol in each individual ocular tissue. Error bars show standard deviation from the mean.

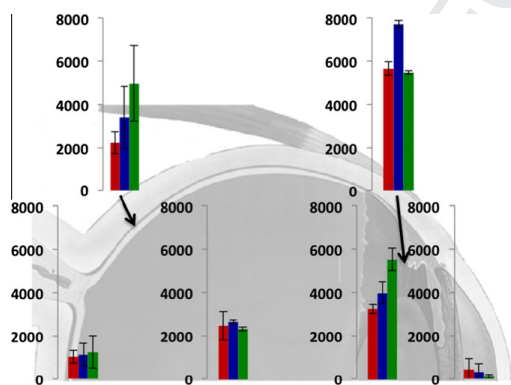


Fig. 4. C_{Max} (y axis in $\mu\text{g/g}$) obtained for atenolol (red column), timolol (blue column) and propranolol (green column) in each ocular tissue ($n = 5$) shown at the position of the tissue within the eye. Error bars show standard deviation from the mean. Moving from left to right, retina, choroid, vitreous, lens, iris and ciliary body and finally aqueous humour. (For interpretation of the references to colour in this figure legend, the reader is referred to the web version of this article.)

within these tissues is slightly different. The uveal tract is known to contain two types of melanin, pheomelanin and eumelanin, whereas the choroid is thought to contain mainly eumelanin. Pheomelanin is a lighter coloured pigment, and the content of pheomelanin varies between eyes with a higher ratio of pheomelanin/eumelanin existing in lighter coloured eyes [36]. The pheomelanin content of the iris, choroid and RPE has been previously shown to be low for all three tissues; however, distinct differences in content existed across the tissue range with 1% pheomelanin content in the iris, 0.1–0.5% in the RPE and a negligible amount in the choroid [37]. The basic melanin composition between the tissues also differs, with differences in the elemental composition of melanin contained in the iris, the choroid and the RPE previously demonstrated [38]. In the human eye, differences in eumelanin content of the melanocytes of the iris and the melanocytes of the choroid were apparent. Although not statistically significant, eumelanin content in the choroidal melanocytes was shown to be greater in the melanocytes of the choroid compared to the melanocytes of the iris [39]. In the bovine eye, differences in the amino acid content of melanin containing tissues were apparent, with amino acid content higher in the choroid than in the iris and the RPE [37]. It is likely that the structural differences in the varying types of melanin played a role in the differences in the extent drug accumulation in the choroid; however, investigations directly comparing drug binding to the different melanin binding tissues of the eye are limited. Further work is still required on drug accumulation on melanin isolated from the choroid and the iris of the ovine eye in

would have reduced the extent of atenolol binding to the melanin of the iris and ciliary body. Although the iris and ciliary body and the retina are both melanin rich tissues, the melanin structure

Please cite this article in press as: J. Mains et al., A pharmacokinetic study of a combination of beta adrenoreceptor antagonists – In the isolated perfused ovine eye, Eur. J. Pharm. Biopharm. (2011), doi:10.1016/j.ejpb.2011.11.006

order to determine the importance of both melanin biochemistry and melanin composition within ocular tissues.

In addition to melanin binding phenomena, drug transporter systems are thought to have a key role in the transfer of materials at the RPE and therefore drug movement from the vitreous to the retina and the choroid [40,41]. Various drug transporter systems have previously been shown to play a role in drug distribution in the posterior eye, including P-glycoprotein, organic cation transporters and organic anion transporters [42–44]. Although the involvement of drug transport systems in the extent of drug penetration of the drug series into the retina and the choroid was out with the scope of this study and remains unclear, the impact of drug lipophilicity on drug levels with the retina and choroid has been demonstrated. The potential involvement of drug transport systems cannot be disregarded and therefore should be taken into consideration when interpreting the results.

This work has demonstrated that cassette dosing using the isolated perfused ovine eye is a suitable means of carrying out drug distribution studies, significantly reducing both the number of animals utilised during the experimental work and analytical time. The results reported here have clearly shown that drug lipophilicity plays an important role in the extent of ocular drug distribution following drug administration via an intravitreal injection. Drugs with greater lipophilicity will penetrate to the posterior eye, residing in the retina and the choroid at greater levels than those seen for more hydrophilic drugs. This will impact on the drug candidate selection process for the treatment of posterior eye diseases such as age-related macular degeneration and diabetic retinopathy, where the desire is to penetrate to the back of the eye at desirable drug concentrations. Further work is still required in order to understand the impact both drug transport mechanisms and melanin biochemistry/tissue composition have on drug distribution within the choroid and the iris and ciliary body.

Acknowledgement

JM acknowledges AstraZeneca and University of Strathclyde for the studentship. We thank Anthony Atkinson from AstraZeneca R&D, Charnwood for assistance with UPLC-MS/MS measurements.

References

- [1] B.L. Ackermann, Ackermann, Results from a bench marking survey on cassette dosing practices in the pharmaceutical industry, *Journal of the American Society for Mass Spectrometry* 15 (2004) 1374–1377.
- [2] P. Manitspikul, R.E. White, Whatever happened to cassette-dosing pharmacokinetics?, *Drug Discovery Today* 9 (2004) 652–658.
- [3] R.E. White, P. Manitspikul, Pharmacokinetic theory of cassette dosing in drug discovery screening, *Drug Metabolism and Disposition* 29 (2001) 957–966.
- [4] L.W. Frick, K.K. Adkison, K.J. Wells-Knecht, P. Woollard, D.M. Higton, Cassette dosing: rapid in vivo assessment of pharmacokinetics, *Pharmaceutical Science & Technology Today* 1 (1998) 12–18.
- [5] R.S. Kadam, U.B. Kompella, Influence of lipophilicity on drug partitioning into sclera, choroid-retinal pigment epithelium, retina, trabecular meshwork, and optic nerve, *The Journal of Pharmacology and Experimental Therapeutics* 332 (2010) 1107–1120.
- [6] J.W. Proksch, K.W. Ward, Cassette dosing pharmacokinetic studies for evaluation of ophthalmic drugs for posterior ocular diseases, *Journal of Pharmaceutical Sciences* 97 (2007) 3411–3421.
- [7] A.H. Friedman, A.L. Marchese, The isolated perfused frog eye: a useful preparation for the investigation of drug effects on retinal function, *Journal of Pharmacological Methods* 5 (1981) 215–234.
- [8] H. Ripps, L. Mehaffey, I.M. Siegel, G. Niemyer, Vincristine-induced changes in the retina of the isolated arterially-perfused cat eye, *Experimental Eye Research* 48 (1989) 771–790.
- [9] E.-N. Su, D.-Y. Yu, V.A. Alder, P.K. Yu, S.J. Cringle, Altered vasoactivity in the early diabetic eye: measured in the isolated perfused rat eye, *Experimental Eye Research* 61 (1995) 699–711.
- [10] M. Wiederholt, S. Bielka, F. Schweig, E. Lütjen-Drecoll, A. Lepple-Wienhues, Regulation of outflow rate and resistance in the perfused anterior segment of the bovine eye, *Experimental Eye Research* 61 (1995) 223–234.
- [11] I.A. Shiels, S.D. Sanderson, S.M. Taylor, Arterially perfused eye model of uveitis, *Australian Veterinary Journal* 2 (1999) 100–104.
- [12] B.G. Dijkstra, A. Schneemann, P.F. Hoyng, Flow after prostaglandin E1 is mediated by receptor-coupled adenylyl cyclase in human anterior segments, *Investigative Ophthalmology and Visual Science* 40 (1999) 2622–2626.
- [13] J. Gottanka, D. Chan, M. Eichhorn, E. Lütjen-Drecoll, C.R. Ethier, Effects of TGF- β 2 in perfused human eyes, *Investigative Ophthalmology and Visual Science* 45 (2004) 153–158.
- [14] G. Niemyer, Retinal research using the perfused mammalian eye, *Progress in Retinal and Eye Research* 20 (2001) 289–318.
- [15] D.-Y. Yu, E.-N. Su, S.J. Cringle, P.K. Yu, Isolated preparations of ocular vasculature and their applications in ophthalmic research, *Progress in Retinal and Eye Research* 22 (2003) 135–169.
- [16] M.J. Doughty, Use of a corneal stroma perfusion technique and transmission electron microscopy to assess ultrastructural changes associated with exposure to slightly acidic pH 5.75 solutions, *Current Eye Research* 33 (2008) 45–57.
- [17] J.E. Preston, M.B. Segal, G.J. Walley, B.V. Zlokovic, Neutral amino acid uptake by the isolated perfused sheep choroid plexus, *Journal of Physiology* 408 (1989) 31–43.
- [18] L.E. Tan, A model of ageing vitreous: implications for drug delivery, in: SIPBS, University of Strathclyde, Glasgow, 2010, p. 272.
- [19] J. Mains, C. Wilson, A. Urquhart, ToF-SIMS analysis of ocular tissues reveals biochemical differentiation and drug distribution, *European Journal of Pharmaceutics and Biopharmaceutics*, in press.
- [20] M. Koeberle, Investigation of factors involved in the disposition and pharmacokinetics of memantine in the isolated bovine eye, University of Strathclyde, Glasgow, 2002.
- [21] N.V. Nagaraja, J.K. Paliwal, R.C. Gupta, Choosing the calibration model in assay validation, *Journal of Pharmaceutical and Biomedical Analysis* 20 (1999) 433–438.
- [22] T. Singtoroj, J. Tarning, A. Annerberg, M. Ashton, Y. Bergqvist, N.J. White, N. Lindgardh, N.P.J. Day, A new approach to evaluate regression models during validation of bioanalytical assays, *Journal of Pharmaceutical and Biomedical Analysis* 41 (2006) 219–227.
- [23] H. Hendrickson, E. Laurenana, M. Owens, Quantitative determination of total methamphetamine and active metabolites in rat tissue by liquid chromatography with tandem mass spectrometric detection, *AAPS Journal* 8 (2006) 709–717.
- [24] I. Fatt, Flow and diffusion in the vitreous body of the eye, 37 (1975) 85–90.
- [25] J. Kathawate, S. Acharya, Computational modeling of intravitreal drug delivery in the vitreous chamber with different vitreous substitutes, *International Journal of Heat and Mass Transfer* 51 (2008) 5598–5609.
- [26] H. Atluri, A.K. Mitra, Disposition of short-chain aliphatic alcohols in rabbit vitreous by ocular microdialysis, *Experimental Eye Research* 76 (2003) 315–320.
- [27] T. Rodgers, D. Leahy, M. Rowland, Tissue distribution of basic drugs: Accounting for enantiomeric, compound and regional differences amongst blocking drugs in rat, *Journal of Pharmaceutical Sciences* 94 (2005) 1237–1248.
- [28] L.E. Tan, W. Orilla, P. Hughes, S.T. S. J. Burke, C.G. Wilson, Effects of vitreous liquefaction on intravitreal distribution of sodium fluorescein, fluorescein dextran and fluorescent microparticles, *Investigative Ophthalmology and Visual Science* 52 (2011) 1111–1118.
- [29] L.V. Stepanova, I.Y. Marchenko, G.M. Synchev, Direction of fluid transport in the lens, *Bulletin of Experimental Biology and Medicine* 139 (2005) 50–51.
- [30] M. Araie, D.M. Maurice, The loss of fluorescein, fluorescein glucuronide and fluorescein isothiocyanate dextran from the vitreous by the anterior and retinal pathways, *Experimental Eye Research* 52 (1991) 27–39.
- [31] P.M. Beer, S.J. Bakri, R.J. Singh, W. Liu, G.B. Peters, M. Miller, Intraocular concentration and pharmacokinetics of triamcinolone acetonide after a single intravitreal injection, *Ophthalmology* 110 (2003) 681–686.
- [32] R.J. Kaiser, D.M. Maurice, The diffusion of fluorescein in the lens, *Experimental Eye Research* 3 (1964) 156–165.
- [33] T. Hu, Q. Le, Z. Wu, W. Wu, Determination of doxorubicin in rabbit ocular tissues and pharmacokinetics after intravitreal injection of a single dose of doxorubicin-loaded poly-[β]-hydroxybutyrate microspheres, *Journal of Pharmaceutical and Biomedical Analysis* 43 (2007) 263–269.
- [34] L. Pitkanen, V. Ranta, H. Moilanen, A. Urtti, Binding of betaxolol, metoprolol and oligonucleotides to synthetic and bovine ocular melanin, and prediction of drug binding to melanin in human choroid-retinal pigment epithelium, *Pharmaceutical Research* 24 (2007) 2063–2070.
- [35] B. Leblanc, S. Jezequel, T. Davies, G. Hanton, C. Taradach, Binding of drugs to eye melanin is not predictive of ocular toxicity, *Regulatory Toxicology and Pharmacology* 28 (1998) 124–132.
- [36] G. Prota, D.-N. Hu, M.R. Vincenzi, S.A. McCormick, A. Napolitano, Characterization of melanins in human irides and cultured uveal melanocytes from eyes of different colors, *Experimental Eye Research* 67 (1998) 293–299.
- [37] Y. Liu, L. Hong, K. Wakamatsu, S. Ito, B.B. Adhyaru, C. Cheng, C. Bowers, J.D. Simon, Comparisons of the structural and chemical properties of melanosomes isolated from retinal pigment epithelium, iris and choroid of newborn and mature bovine eyes, *Photochemistry and Photobiology* 81 (2005) 510–516.

Please cite this article in press as: J. Mains et al., A pharmacokinetic study of a combination of beta adrenoreceptor antagonists – In the isolated perfused ovine eye, *Eur. J. Pharm. Biopharm.* (2011), doi:10.1016/j.ejpb.2011.11.006

- [38] T.P. Dryja, M. O-Neil-Dryja, D.M. Albert, Elemental analysis of melanins from bovine hair, iris, choroid and retinal pigment epithelium, *Investigative Ophthalmology and Visual Science* 18 (1979) 231–236.
- [39] K. Wakamatsu, D. Hu, S.A. McCormick, S. Ito, Characterisation of melanin in human iridal and choroidal melanocytes from eyes with various colored irides, *Pigment Cell Melanoma Research* 21 (2007) 97–105.
- [40] M.E. Smith, M.C. Kincaid, C.E. West, *Basic Science, Refraction, and Pathology. The Requisites in Ophthalmology*, first ed., Mosby-Year Book Inc., 1999.
- [41] C.G. Wilson, E.M. Semenera, P.M. Hughes, O. Olejnik, Eye structure and physiological function, in: E. Touitou, B.W. Barry (Eds.), *Enhancement in Drug Delivery*, Taylor and Francis Group, LLC, 2007, pp. 473–486.
- [42] Y. Han, D.H. Sweet, D. Hu, J.B. Pritchard, Characterization of a novel cationic drug transporter in human retinal pigment epithelial cells, *Journal of Pharmacology and Experimental Therapeutics* 296 (2001) 450–457.
- [43] K. Hosoya, Y. Ohshima, K. Katayama, M. Tomi, Use of microdialysis to evaluate efflux transport of organic anions across the blood-retinal barrier, *AAPS Journal* (2003) 583.
- [44] H. Steuer, A. Jaworski, B. Elger, M. Kausmann, J. Keldenich, H. Schneider, D. Stoll, B. Schlosshauer, Functional characterization and comparison of the outer blood-retinal barrier, *Investigative Ophthalmology and Visual Science* 46 (2005) 1047–1053.

UNCORRECTED PROOF

Please cite this article in press as: J. Mains et al., A pharmacokinetic study of a combination of beta adrenoreceptor antagonists – In the isolated perfused ovine eye, *Eur. J. Pharm. Biopharm.* (2011), doi:10.1016/j.ejpb.2011.11.006

ToF-SIMS Analysis of Dexamethasone Distribution in the Isolated Perfused Eye

Jenifer Mains, Clive G. Wilson, and Andrew Urquhart

PURPOSE. To illustrate the ability of time-of-flight secondary ion mass spectrometry (ToF-SIMS) to characterize and demonstrate the spatial distribution of dexamethasone within ocular tissues.

METHODS. Dexamethasone sodium phosphate was administered to perfused and nonperfused ovine eyes via intravitreal injections. The vitreous humor, the lens, and the retina of the eyes were then removed and divided into front, middle, and back sections. ToF-SIMS analysis was performed on each cross-section of the vitreous humor using Bi³⁺ cluster source and images of drug distribution within the sections generated.

RESULTS. In the positive ion spectra, four key drug fragment peaks were identified and in the negative ion spectra, one key drug peak was identified. All five important drug peaks were successfully imaged in each tissue section and their distribution within the section illustrated. The drug was shown in the nonliving eye to move by diffusion alone, whereas in the living eye the drug was shown to distribute faster within the vitreous and penetrate through to the back of the retina and also into the lens.

CONCLUSIONS. The results illustrate the ability of ToF-SIMS to characterize and provide spatial information about drug distribution within ocular tissues. Key differences in drug movement through the vitreous humor, toward both the anterior and the posterior tissues, in the living eye and the nonliving ovine eye were demonstrated, showing that dexamethasone sodium phosphate distribution through the vitreous is not determined by diffusion alone. (*Invest Ophthalmol Vis Sci*. 2011;52:8413–8419) DOI:10.1167/iops.11-8199

Dexamethasone (see Fig. 1 for chemical structure) is a glucocorticoid drug currently used in the treatment of various inflammatory disease states, including inflammatory conditions of the eye such as uveitis and conjunctivitis. Dexamethasone has been administered to the eye using various routes of administration, including topical, systemic, and intravitreal injection (IVI). Using the topical route of administration, dexamethasone has been shown to be of benefit as an inhibitor of inflammation after ocular surgical procedures such as vitrectomy or lensectomy. It has also been used topically in combination with antibiotics to reduce anterior eye inflammation.¹ Although dexamethasone has been shown to be useful in the

treatment of anterior eye inflammation, after topical administration dexamethasone experiences poor penetration into vitreous and posterior eye tissues²; as a result of this, topical treatment will have little effect in the treatment of posterior eye inflammatory conditions. The systemic route of dexamethasone administration has also been shown to be no better than the topical route, with only 0.1% of the injected dose penetrating into the eye.² To penetrate to the back of the eye and treat posterior eye inflammation, the intravitreal route of administration is a more feasible option. Using the intravitreal route, dexamethasone has been shown to reduce inflammation and lessen the breakdown of the blood–ocular barrier^{3,4} and, more recently, a dexamethasone implant has been shown to improve vision in patients with macular edema.⁵ Although dexamethasone administration via the intravitreal route has been shown to benefit patients with macular edema, it has been associated with numerous adverse events,^{6–8} with the two principal side effects reported to be cataract formation⁸ and increased intraocular pressure.^{6,7}

Determining the extent of dexamethasone drug distribution within ocular tissues has involved the use of various different analytical techniques. Standard analytical methods often used in determining ocular pharmacokinetics, including high-performance liquid chromatography^{9,10} and liquid chromatography–mass spectrometry,⁴ have been developed and used previously in the rabbit eye. In addition to these methods, tracking the movement of radiolabeled dexamethasone has also been performed.¹¹ To prepare ocular tissues for analysis via these commonly used methods, each ocular tissue is typically extracted and is then homogenized before performing a method of drug extraction from the tissue. The destructive nature of the standard analytical techniques has led to the desire to investigate alternative routes of measuring drug distribution within ocular structures and has included the development of a fluorescence polarization immunoassay method¹² and also a nuclear magnetic resonance (NMR) imaging method.¹³ Using ¹H- and ¹⁹F-NMR, Midelfart and colleagues¹³ were able to demonstrate the presence of dexamethasone and various amino acids in the aqueous humor of the rabbit eye, without the need for lengthy drug extraction techniques required when performing standard analytical techniques on ocular tissue samples. Although this technique was shown to be a useful alternative technique in detecting drug presence within the aqueous humor, drug detection may not be as straightforward in one of the more complicated tissues of the eye such as the lens and the retina. In addition to this, NMR provided no spatial awareness of the drug location within the tissue. Interest in mapping drug distribution within ocular tissues has recently increased, especially when the target site of action is the posterior eye, which is particularly difficult to reach. Posterior eye conditions such as diabetic retinopathy^{14,15} and age-related macular degeneration^{16,17} have limited effective treatment options available and understanding spatial drug distribution patterns in ocular tissues could potentially improve treatment options in these conditions.

From the Strathclyde Institute of Pharmacy and Biomedical Sciences, University of Strathclyde, Glasgow, Scotland.

Supported by a studentship from AstraZeneca and the University of Strathclyde (JM).

Submitted for publication July 11, 2011; revised August 29, 2011; accepted September 14, 2011.

Disclosure: J. Mains, None; C.G. Wilson, None; A. Urquhart, None

Corresponding author: Andrew Urquhart, Strathclyde Institute of Pharmacy and Biomedical Sciences, University of Strathclyde, 161 Cathedral Street, Glasgow, Scotland, G4 0RE; andrew.urquhart@strath.ac.uk.

Investigative Ophthalmology & Visual Science, October 2011, Vol. 52, No. 11
Copyright 2011 The Association for Research in Vision and Ophthalmology, Inc.

8413

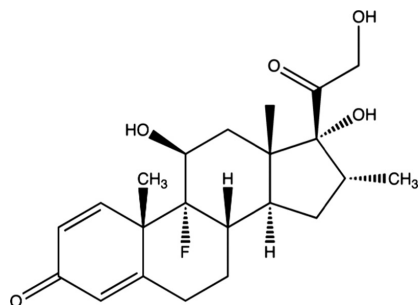


FIGURE 1. The chemical structure of dexamethasone. Note the fluorine atom bonded to the ninth carbon atom in the tetracyclic ring, which provides a unique chemical label for the drug.

Time of flight secondary ion mass spectrometry (ToF-SIMS) is an extremely surface sensitive analytical technique that can characterize the chemical composition of a wide variety of systems, including biological tissue,^{18,19} drug formulations,^{20,21} and polymers.^{22,23} ToF-SIMS of samples requires no sample modification, unlike a similar but well-used technique of matrix-assisted laser desorption/ionization time of flight mass spectrometry (MALDI-ToF/MS),²⁴ which requires the sample to be coated with a matrix. In ToF-SIMS measurements a primary ion beam is fired at the surface of the sample of interest. The primary ions then collide with the sample, causing sample fragmentation and the generation of secondary ions. The secondary ions generated are then accelerated to the detector with a known kinetic energy, enabling an accurate ion mass to be determined from the flight time required by the ion.²⁵ The potential of ToF-SIMS to map drug distribution within ocular tissue, without the need for prior drug extraction, has previously been demonstrated in our group, using amitriptyline as a model basic drug.²⁶ Using ToF-SIMS and the multivariate analytical technique, principal component analysis (PCA), key physiological differences between ocular subtypes were identified and, in addition to this, the presence of the model drug in drug-treated tissue samples was demonstrated. However, this study focused on the use of PCA to data mine mass spectra from specific ocular tissue types to determine drug distribution, rather than use key mass fragments to build ion maps to determine drug distribution. In this study, we present for the first time how the technique of ToF-SIMS can be successfully used to image as well as spatially determine drug distribution in the lens, vitreous, and retinal ocular tissues, after intravitreal drug administration. Moreover, we also demonstrate key differences in the movement and distribution of dexamethasone within the vitreous humor, the lens, and retina of the living eye and the nonliving eye.

MATERIALS AND METHODS

Chemicals

Dexamethasone phosphate disodium salt (purity \geq 98%) was purchased from Sigma-Aldrich (Dorset, UK). Isopropyl alcohol used to clean silicon wafers before sample mounting was obtained from Fischer Scientific (Loughborough, UK).

Ocular Tissue Preparation

Preparation of ocular tissues for intravitreal dexamethasone administration was based on a method detailed previously.²⁶ Briefly, a batch of ovine eyes was collected from a local abattoir within 1 hour of slaughter and then cannulated using one of the long posterior ciliary arteries

that typically wrap around the optic nerve. One long posterior ciliary artery was cannulated because, within the eye, the lateral and medial ciliary arteries merge. It has previously been reported that no difference in ocular blood flow occurred when both arteries were perfused, compared with the perfusion of only one artery.²⁷ In the ovine eye, the long posterior arteries supply the iris, ciliary body, and anterior choroid and also branch out to form the short posterior arteries, which supply the posterior choroid.²⁸ The long posterior ciliary arteries also provide a reinforcing branch to the choroidoretinal artery and this vessel supplies the choroid and the retina via the retinal arterioles, which branch out from the choroidoretinal artery.²⁹ In previous ocular perfusion studies, perfusion of one of the ciliary arteries has been shown to maintain the viability of the eye over a prolonged time period, with slow deterioration of Bruch's membrane^{30,31} and maintenance of oxygen and glucose consumption, indicating retinal tissue perfusion. To establish if flow systems remained operational within the eye, a small volume of perfusion fluid was slowly pumped through the eye and the vortex veins were inspected for fluid exit. On successful initiation of perfusion fluid flow, the eye was introduced into the perfusion system and perfused with physiologic media, based on a method previously used by Koeberle et al.³²

Throughout the experiment, the perfused eye was maintained at 37°C to mimic typical *in vivo* body temperature. Details of the composition of the perfusion fluid administered into the eyes via the ciliary artery are presented in Table 1; all components were purchased from Sigma-Aldrich. A solution containing dexamethasone at a concentration of 100 mg/mL was prepared in deionized water. Once arterial perfusion pressure was maintained, to investigate the distribution of dexamethasone within the ovine eye 100 μ L of the solution was injected into the vitreous of the isolated perfused eye. The injection was administered 5 mm into the vitreous, approximately 3 to 4 mm from the limbus, using a 1-mL syringe and 23-gauge needle. After injection the needle was drawn very slowly from the eye to minimize leakage from the injection site. An IVI was also administered to non-perfused eyes as a control, using the same method used for the perfused eyes. One hour after the IVI, for the isolated perfused ovine eyes, the perfusion procedure was terminated and the perfused eyes were removed from the perfusion kit. Using liquid nitrogen, both the perfused eyes and the nonperfused eyes were then immediately snap frozen before the tissue dissection procedure was performed. In the first instance, the lens was removed by cutting away the anterior eye in a circular manner. From the posterior section, the vitreous was removed by slicing the eye at four positions from the anterior to the posterior section. The sclera was then pressed back to enable cryosectioning of the retina and all tissues were stored at -80°C before sectioning. Using embedding matrix (Shandon M-1; Thermo Fisher Scientific, Cheshire, UK), the lens, vitreous, and retina were mounted onto a cryostat chuck. Each tissue was then cut through the center of the tissue to produce 20- μm -thick sections using a cryostat (Leica CM1850; Leica Microsystems, Milton Keynes, UK). Tissue sections were mounted directly onto 1 \times 1 cm silicon wafers that were previously cleaned with isopropyl alcohol.

TABLE 1. Composition of Perfusion Fluid Administered to Isolated Perfused Eye

Chemical	Concentration
Tissue culture medium	1000 mL
Sodium bicarbonate	2.2 g/L
Atropine sulfate	0.005 g/L
EDTA	0.2922 g/L
Penicillin G	100 kU/L
Streptomycin	75.6 kU/L
Gentamycin	0.08 g/L
Insulin bovine	50 U/L
Bovine holo-transferrin	0.0025 g/L
Sodium selenite	2.4 $\mu\text{g/L}$

ToF-SIMS Analysis

A ToF-SIMS instrument (Ion-TOF IV; ION-TOF GmbH, Münster, Germany) using a Bi³⁺ cluster source and a single-stage reflectron analyzer was used to perform time of flight–secondary ion mass spectrometry. Spectra were acquired in both positive and negative modes by rastering a primary ion energy of 25 kV, along with a pulsed target current of approximately 1 pA and postacceleration energy of 10 kV across the sample surface. Analysis was performed on a sample area of 500 × 500 μm of each tissue. The primary ion dose density was maintained at <10¹² ions/cm² throughout to ensure static conditions. A common insulating effect of biological surfaces is positive primary ion beam induced surface charging. To account for this, low-energy electrons (20 eV) were delivered to the sample surface throughout the analysis. Data processing was performed using imaging software (SurfaceLab 6 Image; ION-TOF GmbH), for spectroscopy and image analysis.

RESULTS

To analyze lens, retina, and vitreous samples by ToF-SIMS, both positive and negative spectra were obtained for all samples. For each of the tissue subtypes and tissue samples, perfused eye samples, and nonperfused eye samples, analysis was performed on three replicates of each sample. ToF-SIMS analysis was also performed on a sample of dexamethasone alone. In ToF-SIMS analysis, the ion beam is rastered across the sample surface and a complete mass spectrum is obtained for each point on the sample hit. From the mass spectra produced, key ions of interest can then be selected and an image of the distribution pattern of the ion in the sample generated. Mass spectra obtained for each sample contained numerous peaks with mass-to-charge ratio (m/z) ranging from 1 to 870. Peaks at the lower end of the mass spectra dominated, with greater peak intensities achieved in the m/z range of 1 to 200, a common occurrence in ToF-SIMS.²² A peak list was generated for both the positive and negative spectra, using a method detailed previously by Urquhart et al.²² Peak lists were initially generated using the pure drug substance sample. Using the positive spectra obtained for the drug and tissue samples, 172 ion peaks were selected and added to form the peak list. In the negative pure drug spectra, 292 ion peaks were selected and added to form the peak list. The positive and negative ion peak lists generated were then applied to each of the tissue samples. Positive spectra obtained from a perfused eye lens sample and a nonperfused lens sample were then directly compared with the positive spectra obtained for the pure drug sample. Using all three spectra, key drug peaks present in the lens samples were identified. This process was repeated for both the retina and the vitreous tissue samples and used to generate a list of

fundamental drug ion fragments to be imaged across the samples. Across the samples in the positive spectra, four significant dexamethasone fragments were identified, attributed to their presence in the spectra obtained for the drug, the lens, the vitreous, and the retina samples (m/z = 63, 109, 187, 289).

Images of the distribution of the significant positive ion drug peaks in the nonperfused eye treated with dexamethasone are shown in Figure 2. A high signal intensity was obtained for drug peak m/z = 63 in the vitreous samples. Similar signal intensities were achieved at the front and the middle of the vitreous, with the greatest signal intensity recorded in the back section of the vitreous toward the retina. A high signal intensity was also seen at the front of the retina, with intensity decreasing in the middle of the retina and becoming extremely low at the back of the retina. In the lens samples, the presence of the molecular ion m/z = 63 was negligible. The remaining three chosen drug peaks (m/z = 109, 187, 289) showed similar intensities in the nonperfused eye. Signals were detectable in the vitreous samples with low intensity at the front and in the middle of the vitreous but increasing in intensity at the back of the vitreous. In the retina, although signal intensity was low, the intensity decreased moving through the retina, with the highest signal intensity detected at the front of the retina, next to the vitreous, and the lowest at the back. Again in the lens samples, the presence of all three drug peaks was insignificant.

Distributions of the significant positive ion drug peaks in the perfused eye samples treated with dexamethasone are shown in Figure 3. For drug peak m/z = 63 in the vitreous samples a high signal intensity, similar to that seen in the back of the vitreous of the nonperfused eye samples, was seen across the front, middle, and back sections of the vitreous. Signal intensities in the retina of the perfused eye samples were higher than those in the nonperfused eye samples. High signal intensities were seen at the front and in the middle sections of the retina, with intensity decreasing at the back of the retina. In the lens samples of the perfused eye, a low intensity of mass peak m/z = 63 was detected at the back of the lens (in contact with the vitreous); however, at the front and in the middle of the lens signal intensities were still insignificant. For drug peak m/z = 109, significant and relatively equal signal intensity was seen in the front vitreous, middle vitreous, front retina, and middle retina, with seemingly even distribution across the samples. At the back of the vitreous and the back of the retina, the signal intensity was slightly reduced. In the lens samples, again a low intensity was detected at the back of the lens, with negligible drug detection at the front and in the middle of the vitreous. A similar pattern of intensity was shown for drug peak m/z = 187 for the retina and vitreous samples, with the

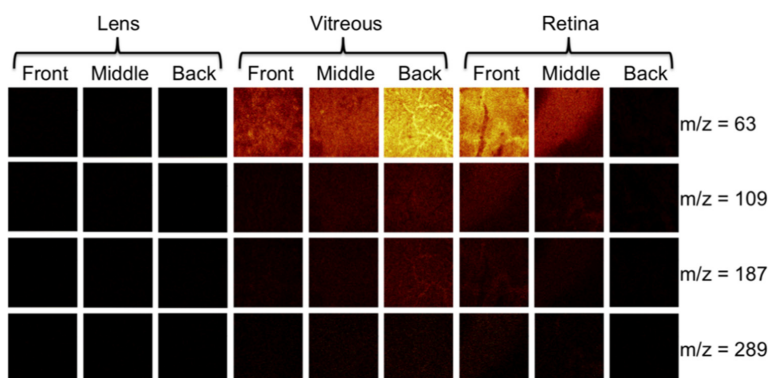


FIGURE 2. ToF-SIMS images showing the spatial distribution of drug-specific dexamethasone sodium phosphate drug fragments detailed by the drug fragments' m/z (mass-to-charge ratio) in the front, middle, and back sections of the lens, the vitreous humor, and the retina. The 500 × 500 μm images were obtained from measurements of positive secondary ions and show images obtained for nonperfused eye tissue sections.

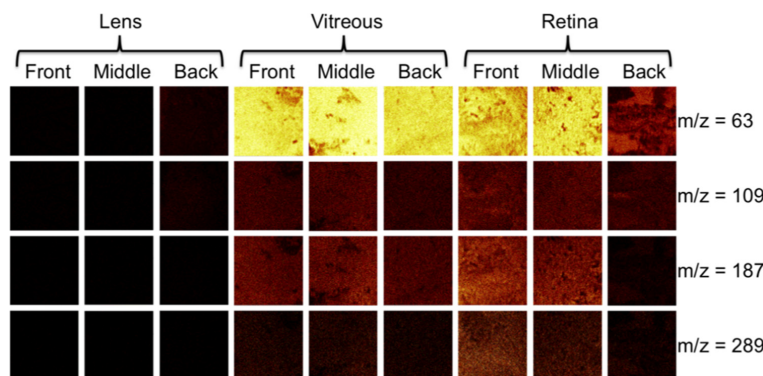


FIGURE 3. ToF-SIMS images showing the spatial distribution of drug-specific dexamethasone sodium phosphate drug fragments detailed by the drug fragments' m/z in the front, middle, and back sections of the lens, the vitreous humor, and the retina. The $500 \times 500 \mu\text{m}$ images were obtained from measurements of positive secondary ions and show images obtained for perfused eye tissue sections.

exception for the lens tissue where for all samples front to back, signal intensities were negligible. For drug mass peak $m/z = 289$, a similar pattern of intensity to drug peak $m/z = 187$ was noted across all samples with reduced signal intensity.

As with the positive spectra, key drug peaks present in the perfused eye and nonperfused eye samples were identified by directly comparing the negative spectra of samples with the negative spectra obtained for the pure drug samples. After this, the process was again repeated for both the retina and the vitreous to generate a complete list of crucial drug ion fragments to be imaged across the sample. Across the samples in the negative spectra, just one critical dexamethasone fragment ($m/z = 19$) was identified due to its presence in the spectra obtained for the drug, the lens, the vitreous, and the retina samples. Distribution of the $m/z = 19$ drug fragment in the nonperfused eye samples treated is shown in Figure 4A. In the nonperfused eye, fluorine signal intensity was low at the front of the vitreous but high in the middle and in the back vitreous samples. Interestingly, a spot of very high signal intensity was seen in the middle vitreous and also in the front of the retina. At the front of the retina, significant peak intensity was recorded and, again, a small area of larger signal intensity was seen. In the remaining retina samples, lower intensities were seen in the middle and at the back of the retina. Peak intensity in the lens samples was marginal. Distribution of the $m/z = 19$ drug fragment in the perfused eye samples treated is shown in Figure 4B. In the perfused eye greater dexamethasone distribution was apparent. Across the vitreous samples, high, evenly distributed signal intensities were seen from front to back, with slightly greater intensity seen at the back of the vitreous. In the retina samples, $m/z = 19$ peak intensity was much greater in

the perfused eye compared with that in the nonperfused eye, with slightly reduced signal intensity at the back of the retina compared with that at the front and the middle retina samples. Again, in the lens samples signal intensities were marginal, with a slightly greater signal intensity noted at the back of the lens (see Fig. 5 for increased clarity).

DISCUSSION

Dexamethasone phosphate was selected for investigation in this work because of its anti-inflammatory effect in both the anterior and the posterior eye and also its structural chemistry. Dexamethasone sodium phosphate is a relatively large, slightly lipophilic drug molecule, with a molecular weight of 516.45 and a log P of 0.56 (Fig. 1). The presence of the fluorine group makes it an ideal candidate for studying distribution using ToF-SIMS, in that fluorine-based anions tend to dominate ToF-SIMS negative ion spectra due to the stability of the fluorine anion.^{33,34}

The four drug peaks identified in the positive ion spectra represent molecular fragments of dexamethasone sodium phosphate. The peak at $m/z = 63$ represents C_5H_3^+ , a commonly encountered hydrocarbon species in positive ToF-SIMS spectra of molecules containing aromatic ring structures.³⁵ It is possible that $m/z = 63$ could be a fragment of an amino acid, such as phenylalanine, tryptophan, or tyrosine; however, due to the uneven distribution within the vitreous of the nonperfused eye, $m/z = 63$ represents a single-ring fragment of the drug. Mass peak $m/z = 109$ represents $\text{C}_7\text{H}_9\text{O}^+$, which represents another single-ring-based structure, arising typically in

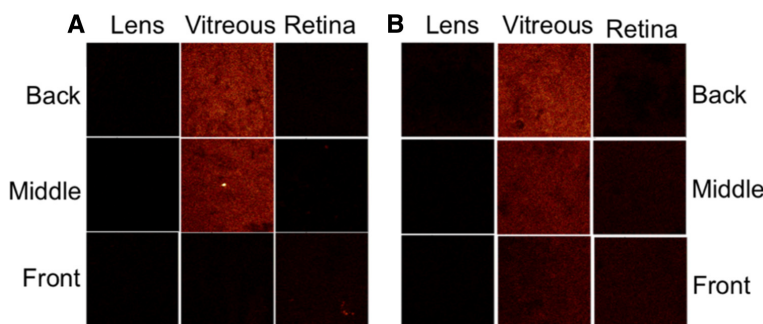


FIGURE 4. (A) F^- ion distribution in the nonperfused eye ($500 \times 500 \mu\text{m}$ images). (B) F^- ion distribution in the perfused eye ($500 \times 500 \mu\text{m}$ images).

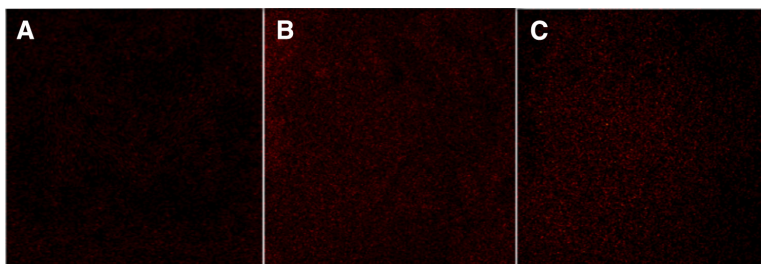


FIGURE 5. Enhanced-contrast ToF-SIMS images, from the perfused eye back of the lens sample, altering saturated pixel percentage from 0.4% to 2.5% as an aid for clarity. (A) $m/z = 19$, (B) $m/z = 63$, and (C) $m/z = 109$. All images are $500 \times 500 \mu\text{m}$.

mass spectrometry of steroid drug structures.³⁶ The peak at $m/z = 187$ remains unassigned, although the similarity in distribution of this ion peak to that of the other drug peaks suggests it is likely to represent a bicyclic ring fragment of the drug. The final drug peak identified in the positive spectra at $m/z = 289$ represents $\text{C}_{18}\text{H}_{25}\text{O}_3^+$, a tricyclic ring fragment generated from dexamethasone.³⁷ In the positive spectra, there is a potential chance that a proportion of the ion intensity measured for each molecular ion fragment could be influenced by the signal generated by molecular ions emitted from biological molecules released from the tissue surface. In the case of negative spectra, the ion intensity signal of the characteristic fluorine ion of the drug was high and is highly unlikely to be influenced by the secondary ions generated from the tissue sample. For this reason, $m/z = 19$ (F^-) was also selected to monitor drug distribution through the eye and to validate the patterns of drug distribution recorded for key drug peaks obtained in the positive spectrum.

All the positive and negative drug fragments selected to monitor drug distribution in ocular tissue cross-sections followed very similar patterns of drug distribution within each of the eye tissue sections; however, it is noted that the signal intensities obtained for each individual ion are not the same. Because the individual ion fragments are generated from the same parent drug compound, in a simplistic view it would be anticipated that each ion fragment would generate the same signal intensity, given that the concentration of the drug contained in the tissue cross-section from which the ion is generated is the same. In ToF-SIMS this is not the case because the yield of secondary ions generated is not a simple process and can depend on several factors. Two important factors, which experience variability and influence secondary ion generation and therefore signal intensity, are the yield of secondary ions generated per impact of the primary ion beam and also the probability that a given particle will be released from the sample surface as a certain ion.³⁸ In addition, there is also the influence of matrix-effect phenomena, where the yield of secondary ions emitted can vary depending on the environment in which they are generated. The sample environment can change during analysis and this again can influence the secondary ion yield, although by using the spectra preprocessing steps discussed previously, the impact of this effect can be limited.³⁹

The nonperfused eye was selected as an initial means of determining the feasibility of imaging drug location within the ocular tissue cross-sections. In the nonperfused eye, flow and circulation within the isolated eye are redundant and, as a result, drug movement will occur by diffusion alone. There are also no clearance systems operating within the nonperfused eye; therefore, no drug would have been removed from the eye during the course of the experiment and drug concentrations would have remained high in the vitreous. In the vitreous of the nonperfused eye, drug fragment distribution was successfully imaged and drug diffu-

sion from the front section of the vitreous to the middle and back sections was evident. In the nonperfused eye a differential concentration gradient is present in the vitreous, providing a motive force, which drives drug movement through the vitreous to the retina, and this is shown by the presence of drug in the positive spectrum in the front section of the retina only (Fig. 2) This is confirmed by the generation of a much greater signal intensity of F^- in the front section of the retina, compared with the middle and back sections, in the negative spectrum (Fig. 4A). Because the drug solution was injected into the front of the vitreous, the lack of uniformity in drug distribution across the vitreous (from front to back) is likely due to the vitreal structure. The vitreous is a fluid-based structure composed of approximately 99% water. However, although composed of predominantly water, the vitreous has a gel-like structure attributed to its viscoelastic properties to collagen, hyaluronic acid, and proteoglycans that are contained within.⁴⁰ It has previously been shown that dexamethasone diffusion through the vitreous is four- to fivefold slower than its diffusion in water.⁴¹ In the nonperfused eye lens images, the drug was not shown to be present due to the lack of flow operating in the dead eye and, thus, the drug did not penetrate into the ocular lens. In addition we also see a potential element of drug clumping in the vitreous and the retina of the nonperfused eye; this could be explained by drug localization on structures contained within these tissues when flow systems are not in operation within the eye.

The perfused eye system has been developed as an effective method of investigating properties of the eye, *ex vivo*, while maintaining arterial flow and nutritional status within the eye.⁴² Advantages of the isolated eye model compared with performing a full animal study include no anesthetic requirements or concern over animal comfort, control over the physiologic environment, reduced animal usage, controlled drug administration, and control of exposure to substances from systemic circulation into the ocular system,⁴³ making it an ideal model in which to study drug distribution. In the vitreous samples of the perfused eye, a more even distribution of the drug across the front, the middle, and the back of the vitreous was evident, when compared with that of the nonperfused eye. Because flow systems remain operational within the perfused eye, drug movement in the vitreous occurs by both diffusion and convection.^{44,45} There has been some debate over the role of convection in drug distribution in the vitreous, with some suggestion that convection plays a role, although the impact is less than that of diffusion,^{44,46} whereas other work has suggested that convection will become important only for larger sized molecules.^{47,48} Although dexamethasone sodium phosphate is regarded as a small drug molecule, it is clear from the images that drug movement within the nonperfused and perfused eye differ, with drug movement in the perfused eye occurring not only in the posterior direction but also in the anterior direction, where it was also detected

in the back section of the lens. Therefore, in this case drug movement is not caused solely by diffusion but also by circulation systems operating within the eye. In the perfused eye, the signal intensity in the retina images was much larger than the signal obtained in the nonperfused eye retina images for both the positive drug fragments and the negative drug fragment F^- . The drug was evident in all retinal cross-sections, demonstrating that dexamethasone sodium phosphate can penetrate from the vitreous completely through the retina to the posterior retina, which is extremely desirable in the treatment of posterior eye disease. The transfer of materials at the retinal pigment epithelium and therefore drug movement from the vitreous to the retina and the choroid is not only controlled by flow systems operating within the eye but is also thought to involve drug transporter systems.^{40,41} Previously, the involvement of transporter systems in ocular drug delivery, such as p -glycoprotein, organic cation transporters, and organic anion transporters, has been demonstrated.⁴²⁻⁴⁴ The involvement of drug transporter systems in dexamethasone movement into the retina was outside the scope of this study; however, the potential impact of drug transporter systems on dexamethasone distribution in ocular tissues should be considered when interpreting the results. Although the signal intensity of drug fragments in the lens is extremely low, the presence of drug within the back section of the lens is apparent, suggesting that dexamethasone will also move toward the anterior eye after intravitreal administration. However, the lack of drug presence in the middle and the front lens sections could suggest that the drug will not move any further forward through the lens and will potentially move back into the vitreous. A similar effect on movement was noted by Tan et al.⁴⁹ with intravitreally injected sodium fluorescein in the rabbit eye. Using ocular fluorophotometry, it was shown that sodium fluorescein will penetrate into the ocular lens 2 hours after dosing; however, the substance did not continue a forward diffusion into the anterior chamber but unloaded the absorbed fluorescein back into the vitreous humor 3 hours later. However, due to the short time course of the experiment it is difficult to determine whether the drug would penetrate further into the lens and through to the anterior chamber. It would be interesting in the future to extend the perfusion time and image the drug moving through and out of the lens tissue.

The results presented in this work illustrate the ability of ToF-SIMS to characterize and provide spatial information about drug distribution within ocular tissues. The capability to characterize drug positioning within an ocular tissue is extremely desirable, such as when determining ocular drug distribution, ocular tissues are homogenized and the drug is then extracted from the tissue. Therefore, no specific information with regard to the spatial positioning of the drug within the tissue can be determined. The ability to map and image drug positioning within individual ocular tissues holds significant value in adding to the understanding of how we can improve drug treatment options in posterior eye disease. Understanding spatial drug distribution within the target site of action, the retina, is especially useful because drug penetration through the retina is key in treating disease states such as diabetic retinopathy and age-related macular degeneration. In addition, here we have also demonstrated key differences in drug movement through the vitreous humor, toward both the anterior and the posterior tissues, in the living eye and the nonliving ovine eye, demonstrating that dexamethasone sodium phosphate distribution through the vitreous is not determined by diffusion alone and will involve the circulatory flow systems operating within the eye and drug transporter systems.

Acknowledgments

The authors thank David Scurr from Laboratory of Biophysics and Surface Analysis, School of Pharmacy, University of Nottingham for assistance with ToF-SIMS measurements.

References

- Notivol R, Bertin D, Amin D, et al. Comparison of topical tobramycin-dexamethasone with dexamethasone-neomycin-polymyxin and neomycin-polymyxin-gramicidin for the control of inflammation after cataract surgery: results of a multicenter, prospective, three-arm, randomized, double-masked, controlled, parallel-group study. *Clin Ther*. 2004;26:1274-1285.
- Weijtens O, Schoemaker RC, Cohen AF, et al. Dexamethasone concentration in vitreous and serum after oral administration. *Am J Ophthalmol*. 1998;125:673-679.
- Barcia E, Herrero-Vanrell R, Díez A, et al. Downregulation of endotoxin-induced uveitis by intravitreal injection of polylactide-glycolic acid (PLGA) microspheres loaded with dexamethasone. *Exp Eye Res*. 2009;89:238-245.
- Earla R, Boddu SHS, Cholkar K, et al. Development and validation of a fast and sensitive bioanalytical method for the quantitative determination of glucocorticoids: quantitative measurement of dexamethasone in rabbit ocular matrices by liquid chromatography tandem mass spectrometry. *J Pharm Biomed Anal*. 2010;52:525-533.
- Haller JA, Bandello F, Belfort R, et al. Randomized, sham-controlled trial of dexamethasone intravitreal implant in patients with macular edema due to retinal vein occlusion. *Ophthalmology*. 2010;117:1134-1146.
- Armaly MF. Statistical attributes of the steroid hypertensive response in the clinically normal eye. *Invest Ophthalmol Vis Sci*. 1965;4:187-197.
- Haller JA, Kuppermann BU, Blumenkranz MS, et al. Randomized controlled trial of an intravitreal dexamethasone drug delivery system in patients with diabetic macular edema. *Arch Ophthalmol*. 2010;128:289-296.
- Williams GA, Haller JA, Kuppermann BD, et al. Dexamethasone posterior-segment drug delivery system in the treatment of macular edema resulting from uveitis or Irvine-Gass syndrome. *Am J Ophthalmol*. 2009;147:1048-1054.
- Eljarrat-Binstock E, Raiskup F, Frucht-Pery J, et al. Transcorneal and transscleral iontophoresis of dexamethasone phosphate using drug loaded hydrogel. *J Control Release*. 2005;106:386-390.
- Kwak HW, D'Amico DJ. Determination of dexamethasone sodium phosphate in the vitreous by high performance liquid chromatography. *Korean J Ophthalmol*. 1995;9:79-83.
- Attia MA, Kassem MA, Safwat SM. In vivo performance of [³H]dexamethasone ophthalmic film delivery systems in the rabbit eye. *Int J Pharm*. 1988;47:21-30.
- Baeyens V, Kaltsatos V, Boisramé B, et al. Optimized release of dexamethasone and gentamicin from a soluble ocular insert for the treatment of external ophthalmic infections. *J Control Release*. 1998;52:215-220.
- Midelfart A, Dybdahl A, Muller N, et al. Dexamethasone and dexamethasone phosphate detected by H and F NMR spectroscopy in the aqueous humour. *Exp Eye Res*. 1998;66:327-337.
- Mason JO 3rd, Nixon PA, White MF. Intravitreal injection of bevacizumab (Avastin) as adjunctive treatment of proliferative diabetic retinopathy. *Am J Ophthalmol*. 2006;142:685-688.
- Porta M, Allione A. Current approaches and perspectives in the medical treatment of diabetic retinopathy. *Pharmacol Ther*. 2004;103:167-177.
- Ding X, Patel M, Chan C-C. Molecular pathology of age-related macular degeneration. *Prog Retin Eye Res*. 2008;28:1-18.
- Wong TY, Liew G, Mitchell P. Clinical update: new treatments for age related macular degeneration. *Lancet*. 2007;370:204-206.
- Börner K, Nygren H, Malmberg P, et al. Localization of Na⁺ and K⁺ in rat cerebellum with imaging TOF-SIMS. *Appl Surf Sci*. 2006;252:6777-6781.

19. Wu L, Lu X, Kulp KS, et al. Imaging and differentiation of mouse embryo tissues by ToF-SIMS. *Int J Mass Spectrom.* 2007;260:137-145.
20. Davies OR, Head L, Armitage D, et al. Surface modification of microspheres with steric stabilizing and cationic polymers for gene delivery. *Langmuir.* 2008;24:7138-7146.
21. Belu AM, Davies MC, Newton JM, et al. TOF-SIMS characterization and imaging of controlled-release drug delivery systems. *Anal Chem.* 2000;72:5625-5638.
22. Urquhart AJ, Taylor M, Anderson DG, et al. TOF-SIMS analysis of a 576 micropatterned copolymer array to reveal surface moieties that control wettability. *Anal Chem.* 2007;80:135-142.
23. Shard AG, Davies MC, Tendler SJB, et al. X-ray photoelectron spectroscopy and time-of-flight SIMS investigations of hyaluronic acid derivatives. *Langmuir.* 1997;13:2808-2814.
24. Marko-Varga G, Fehninger TE, Rezeli M, et al. Drug localization in different lung cancer phenotypes by MALDI mass spectrometry imaging. *J Proteomics.* 2011;74:982-992.
25. Benninghoven A, Hagenhoff B, Niehuis E. Surface MS: probing real-world samples. *Anal Chem.* 1993;65:630-640.
26. Mains J, Wilson C, Urquhart A. ToF-SIMS analysis of ocular tissues reveals biochemical differentiation and drug distribution. *Eur J Pharm Biopharm.* 2011;79:328-333.
27. Shiels IA, Sanderson SD, Taylor SM. Arterially perfused eye model of uveitis. *Aust Vet J.* 1999;77:100-104.
28. Cioffi GA, Granstam E, Alm A. Ocular circulation. In: Kaufman PL, Alm A, eds. *Adler's Physiology of the Eye.* 10th ed. St. Louis: Mosby, 2003;747-784.
29. Simoens P, Ghoshal NG. Arterial supply to the optic nerve and the retina of the sheep. *J Anat.* 1981;135:481-497.
30. Coo FAM, Zonnenberg BA, Trap NH. Prolonged normothermic perfusion of the isolated bovine eye: initial results. *Curr Eye Res.* 1993;12:293-301.
31. Wilson WS, Shahidullah M, Millar C. The bovine arterially-perfused eye: an in vitro method for the study of drug mechanisms on IOP, aqueous humour formation and uveal vasculature. *Curr Eye Res.* 1993;12:609-620.
32. Koeberle MJ, Hughes PM, Skellern GG, et al. Pharmacokinetics and disposition of memantine in the arterially perfused bovine eye. *Pharm Res.* 2006;23:2781-2798.
33. Feng J, Chan C-M, Weng L-T. Influence of chain sequence structure of polymers on ToF-SIMS spectra. *Polymer.* 2000;41:2695-2699.
34. Huang HL, Goh SH, Lai DMY, et al. ToF-SIMS studies of poly(methyl methacrylate-co-methacrylic acid), poly(2,2,3,3,3-pentafluoropropyl methacrylate-co-4-vinylpyridine) and their blends. *Appl Surf Sci.* 2004;227:373-382.
35. Gazi E, Dwyer J, Lockyer N, et al. The combined application of FTIR microspectroscopy and ToF-SIMS imaging in the study of prostate cancer. *Faraday Discuss.* 2003;126:41-59.
36. Williams TM, Kind AJ, Houghton E, et al. Electrospray collision-induced dissociation of testosterone and testosterone hydroxy analogs. *J Mass Spectrom.* 1999;34:206-216.
37. Calza P, Pelizzetti E, Brussino M, et al. Ion trap tandem mass spectrometry study of dexamethasone transformation products on light activated TiO₂ surface. *J Am Soc Mass Spectrom.* 2001;12:1286-1295.
38. Belu A, Graham DJ, Castner DG. Time-of-flight secondary ion mass spectrometry: techniques and applications for the characterization of biomaterial surfaces. *Biomaterials.* 2003;24:3635-3653.
39. Tyler BJ, Royal G, Castner DG. Multivariate analysis strategies for processing ToF-SIMS images of biomaterials. *Biomaterials.* 2007;28:2412-2423.
40. Balazs EA, Denlinger JL. The vitreous. In: Davson H, ed. *The Eye.* New York: Academic Press; 1984:533-589.
41. Gisladdottir S, Loftsson T, Stefansson E. Diffusion characteristics of the vitreous humour and saline solution follow the Stokes Einstein equation. *Graefes Arch Clin Exp Ophtalmol.* 2009;247:1677-1684.
42. Gouras P, Hoff M. Retinal function in an isolated perfused mammalian eye. *Invest Ophtalmol Vis Sci.* 1970;9:388-399.
43. Niemeyer G. Retinal research using the perfused mammalian eye. *Prog Retina Eye Res.* 2001;20:289-318.
44. Fatt I. Flow and diffusion in the vitreous body of the eye. *Bull Math Biol.* 1975;37:85-90.
45. Xu J, Heys JJ, Barocas VH, et al. Permeability and diffusion in the vitreous humor: implications for drug delivery. *Pharm Res.* 2000;17:664-669.
46. Park J, Bungay PM, Lutz RJ, et al. Evaluation of coupled convective-diffusive transport of drugs administered by intravitreal injection and controlled release implant. *J Control Release.* 2005;105:279-295.
47. Missel P. Hydraulic flow and vascular clearance influences on intravitreal drug delivery. *Pharm Res.* 2002;19:1636-1647.
48. Stay MS, Xu J, Randolph TW, et al. Computer simulation of convective and diffusive transport of controlled release drugs in the vitreous humor. *Pharm Res.* 2002;20:96-102.
49. Tan LE, Orilla W, Hughes P, et al. Effects of vitreous liquefaction on intravitreal distribution of sodium fluorescein, fluorescence dextran, and fluorescent microparticles. *Invest Ophtalmol Vis Sci.* 2011;52:1111-1118.



Research paper

ToF-SIMS analysis of ocular tissues reveals biochemical differentiation and drug distribution

Jenifer Mains, Clive Wilson, Andrew Urquhart*

Strathclyde Institute of Pharmacy and Biomedical Sciences, University of Strathclyde, Glasgow, Scotland, United Kingdom

ARTICLE INFO

Article history:

Received 17 January 2011
 Accepted in revised form 12 April 2011
 Available online 21 April 2011

Keywords:

Ocular
 Drug
 Time-of-flight secondary ion mass spectrometry
 Principle component analysis
 Multivariate statistics

ABSTRACT

Time-of-flight secondary ion mass spectrometry (ToF-SIMS) was used to obtain mass spectra from three ocular tissues, the lens, the vitreous and the retina. All three tissues were extracted from control ovine eyes and ovine eyes treated with model drug. To identify variations in surface biochemistry of each ocular tissue, principal component analysis (PCA) was applied to ToF-SIMS data. Interesting physiological differences in Na⁺ and K⁺ distribution were shown across the three tissue types, with other elements including Ca²⁺ and Fe²⁺ distribution also detected. In addition to the identification of small molecules and smaller molecular fragments, larger molecules such as phosphocholine were also detected. The ToF-SIMS data were also used to identify the presence of a model drug compound (amitriptyline – chosen as a generic drug structure) within all three ocular tissues, with model drug detected predominantly across the vitreous tissue samples. This study demonstrates that PCA can be successfully applied to ToF-SIMS data from different ocular tissues and highlights the potential of coupling multivariate statistics with surface analytical techniques to gain a greater understanding of the biochemical composition of tissues and the distribution of pharmaceutically active small molecules within these tissues.

© 2011 Elsevier B.V. All rights reserved.

1. Introduction

Time-of-flight secondary ion mass spectrometry (ToF-SIMS) is an extremely surface sensitive spectrometric technique that can provide detailed chemical information of a wide variety of systems, including biological tissue [1,2], drug formulations [3] and polymers [4]. ToF-SIMS has previously been successfully applied to ocular tissues; however, studies have been limited and mainly focused on physiological composition of retina tissue from a specific animal model [5–10]. Work by Amemiya et al. demonstrated the presence of vitamin A and E in cross sections of rat retina as well as differences in counts obtained in response to light stimulus [5]. Using the same model, the group also showed differences in retina expression of fatty acids (maleic, palmitic, oleic, stearic, arachidonic and docosahexaenoic acid) with the highest counts obtained for maleic acid [6]. The ability of ToF-SIMS to spatially map sample cross sections was not exploited in this retinal work as in each case work focussed on total ion counts measured for the whole-tissue cross section. Total ion count is often not an ideal method of direct comparison between samples due to matrix effects where the ion count achieved can vary depending on the

chemical environment of the sample [11]. Following on from this work, a study by Kim et al. moved onto demonstrate spatial distribution in ocular tissue by mapping the distribution of Na⁺, K⁺, Mg²⁺ and Ca²⁺ in the mouse retina [8]. Very limited work has been carried out on lens tissue using the technique of ToF-SIMS with only one study reporting use of this technique. Kinoshita et al. used the rat model to demonstrate that concentration differences of Ca²⁺, Fe²⁺, Mg²⁺ and Na⁺ existed in 4-month-old rats when compared with 15-month-old rats [12].

Similarly to the lens, limited studies have been performed on the vitreous tissue of the eye. The structure of the vitreous, mainly water, makes it a difficult tissue to prepare and analyse, perhaps explaining the previous lack of use of the ToF-SIMS technique in this tissue. Only one previous study, by Kishikawa et al., has been performed on vitreous tissue, looking at the distribution of various elements, fatty acids and vitamins A and E in patients with diabetic retinopathy and vitreoretinopathy [9]. The vitreous in this case was subjected to a washing stage to facilitate salt removal and was treated as a mass of tissue, analysing the outer layer of the tissue mass rather than a cross section through the tissue. Although ToF-SIMS has been used to consider organic substance distribution within some ocular tissues, ocular tissues have not previously been investigated as a collective to reveal any important physiological differences between tissues. In addition to this, the potential of ToF-SIMS to map drug distribution within ocular tissues has not previously been explored. Interest in mapping drug distribution

* Corresponding author. Strathclyde Institute of Pharmacy and Biomedical Sciences, University of Strathclyde, 161 Cathedral Street, Glasgow, Scotland G4 0RE, United Kingdom. Tel.: +44 0141 548 5947.

E-mail address: andrew.urquhart@strath.ac.uk (A. Urquhart).

within ocular tissues has increased recently, especially when treating certain posterior eye disease states, such as diabetic retinopathy [13] and age-related macular degeneration [14], where effective treatment is currently limited. The process of generating ocular drug distribution data can be time-consuming and requires the eye to be separated into its various ocular tissues. Typically, following separation, ocular tissues are homogenised before the drug is extracted from the tissue, providing no spatial awareness of the drug location within the tissue. The ability to detect drug concentrations directly from a cross section of ocular tissue using ToF-SIMS without the need for extraction method could provide useful distribution information.

Analysis of ToF-SIMS mass spectrum data can be seriously challenging with a simple sample, such as a homopolymer, producing thousands of secondary ion mass peaks [15]. This challenge is increased in magnitude for biological tissue due to the biochemical complexity and composition (from small molecules to kiloDalton weight proteins and polysaccharides) of tissue. It is now commonplace with analytical chemistry to utilise data mining techniques to fully explore large data sets. In the field of ToF-SIMS, both principle component analysis (PCA) [4,16] and partial least squares regression (PLS) [17] are extensively used and have established rules for data pre-processing and processing [16]. PCA is used to establish variance with a data set and determine where the direction of this variance originates. Through the use of PCA, chemically distinct regions in ToF-SIMS data can be identified and key peaks associated with image features selected, in both biological and non-biological samples [18,19]. Prior to carrying out MVA, it is important to select an appropriate means of scaling, as the method selected is widely known to have a major influence on extracting the most useful information from the data set. The use of various data scaling methods has been shown to aid the ability to identify chemical information governing differences within data sets; however, there appears to be no clear guidance on which method is most effective [20]. As a pre-processing step, normalisation is often carried out first before the selected scaling method is applied and PCA carried out. Various types of pre-processing include mean centring, root mean scaling, autoscaling, filter scaling and shift variance scaling. In this study, we show for the first time how PCA can be successfully applied to both positive ToF-SIMS data in order to highlight similarities and differences within the physiological chemistries of the lens, vitreous and retinal ocular tissues. We also present the first use of the ToF-SIMS technique to identify the presence of a model drug compound within these ocular tissues.

2. Materials and methods

2.1. Ocular tissue preparation

A batch of ovine eyes was obtained from a local abattoir within one hour of slaughter. On arrival, the eyes were warmed to body temperature at 37 °C and excess extraorbital tissue and eyelids were removed. Eyes were then cannulated using one of the long ciliary arteries which typically wrap around the optic nerve. A small volume of perfusion fluid was slowly pumped through the eye, whilst the vortex veins were inspected for exit of the perfusion fluid out of eye. Once flow had been established, the eye was introduced into the perfusion system and perfused with physiological media (pH 7.4) based on a method previously used by Koeberle et al. [21]. Eyes were maintained at 37 °C throughout the experiment with a perfusion flow rate of 1 ml/min. Details of the composition of the perfusion fluid administered into the eyes via the ciliary artery are presented in Table 1, all components were purchased from Sigma–Aldrich (Dorset, UK). Once arterial perfusion pressure was maintained, an intravitreal injection of model drug

Table 1
Perfusion media composition.

Chemical	Concentration
Tissue culture medium	1000 ml
Sodium bicarbonate	2.2 g/l
Atropine sulphate	0.005 g/l
EDTA	0.2922 g/l
Penicillin G	100k U/l
Streptomycin	75.6kU/l
Gentamycin	0.08 g/l
Insulin bovine	50 U/l
Bovine holo-transferrin	0.0025 g/l
Sodium selenite	2.4 µg/l

amitriptyline (Fig. 1A) was administered to both eyes. Amitriptyline was identified as a suitable representation of a routinely administered small, generic, biologically active drug molecule. Amitriptyline was selected due to similarities in its basicity, molecular weight and partition coefficient to small drug molecules typically used in the treatment of ocular disease. Intravitreal injections of model drug amitriptyline hydrochloride (Sigma–Aldrich Dorset, UK) were prepared at two concentrations in 100 µl of deionised water. A low dose and a high dose injection were prepared, containing 250 µg and 2000 µg of drug, respectively. The injection was performed using a 1 ml syringe and 23G needle, inserted 1 mm into the vitreous approximately 3–4 mm from the limbus in the posterior direction. Non-perfused eyes, with and without drug administration, were used as controls. To non-perfused eyes with drug administration, intravitreal injection was performed using the same method as perfused eyes. Following exposure for 2 h, the perfusion procedure was ended and perfused eyes were removed from the perfusion kit. All eyes were immediately frozen in liquid nitrogen, and the lens, retina and vitreous were removed. The anterior eye was then cut away in a circular manner and the lens removed. In order to achieve cross sections of the vitreous and the retina, the eye was sliced at four positions from the anterior to the posterior section. The vitreous was removed and the sclera was pressed back for cryosectioning. All tissues were stored at –80 °C prior to sectioning. The lens, vitreous and retina from each eye were mounted onto a cryostat chuck using Shandon M-1 embedding matrix (Thermo-Scientific, Chesire); 20-µm-thick sections were cut through the centre of the tissue on a Leica CM1850 Cryostat (Leica Microsystems, Milton Keynes, UK). Tissue sections were mounted directly onto 1 × 1 cm silicon wafers which were previously cleaned with isopropyl alcohol.

2.2. ToF-SIMS analysis

Time-of-flight secondary ion mass spectrometry was performed on an Ion-TOF ToF-SIMS IV instrument (IONTOF, GmbH, Munster, Germany) using a Bi³⁺ cluster source and a single-stage reflectron analyzer. Samples were mounted on a standard sample stage rather than a cold/cryostage as samples were taken directly from frozen conditions and then exposed to ultra high vacuum removing thawing issues. The standard sample stage also allowed greater sample dimension flexibility. A primary ion energy of 25 keV along with a pulsed target current of approximately 1 pA and post-acceleration energy of 10 keV were employed throughout the analysis. The primary ion dose density was maintained at less than 10¹² ions per cm² throughout to ensure static conditions. Spectra were acquired in both positive and negative mode by rastering the stage under the primary ion beam over a sample area of 500 × 500 µm. Low energy electrons (20 eV) were delivered to the sample surface to compensate for positive primary ion beam induced surface charging, a common insulating effect of biological surfaces. Data

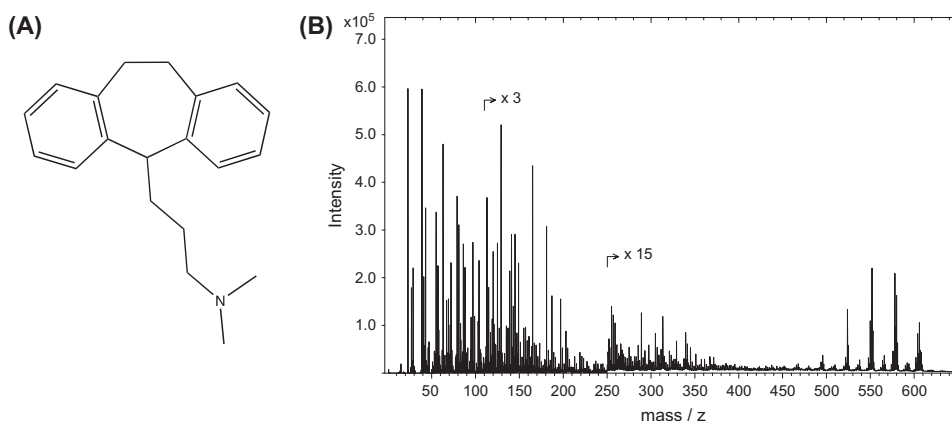


Fig. 1. (A) A schematic showing the structure of amitriptyline. (B) An example of a positive ion spectrum obtained from a vitreous tissue sample.

processing was performed using IonSpec and IonImages software (version 4.0), for spectroscopy and image analysis.

2.3. Multivariate statistics

Statistical analysis was performed using SIMCA-P version 11 (Umetrics, Sweden). Data were exported from IonSpec into Microsoft Excel and divided into three groups: complete sample data, low drug dose data and high drug dose data. The low- and high-dose data sets each contained data for all three tissues from a dosed perfused eye section, a dosed non-perfused eye section and a non-dosed control. Normalisation was carried out as a pre-processing step by dividing total ion count of individual mass peaks obtained for each sample by the total ion count of all peaks calculated for the sample. Following this, mean centring was utilised as an appropriate data scaling method and principle component analysis was performed [29].

3. Results and discussion

In order to analyse lens, retina and vitreous samples by ToF-SIMS, both positive and negative spectra were obtained for all samples. For each of the tissue subtypes and tissue samples, dosed and controls, analysis was performed on three replicates of each sample. Mass spectra obtained for each sample contained numerous peaks with m/z ranging from 1 to 800. Peaks at the lower end of the mass spectra dominated, with greater peak intensities achieved in the m/z range of 1–200 (Fig. 1B). A peak list was generated using a method detailed previously by Urquhart et al. [4]. From the spectra obtained, poor sample separation was observed with the negative ion spectra whereas strong sample separation was shown using the positive ion spectra. It is often the case that with negative spectra, poor sample separation is observed and information obtained using the negative spectrum can often be less specific [4]. The positive ion spectra were used in this study, as they enabled a more interesting and in-depth peak list to be generated and applied to the data. In the positive spectra, 774 ion peaks were selected and added to produce a peak list. After applying the generated peak list to every sample spectrum, the spectra were normalised, before carrying out data processing. To investigate model drug location on the sample surface and identify key model

drug peaks, PCA was performed on the positive ion data sets obtained after scaling each of the data sets. It appears that the selection of a suitable pre-processing method can often depend on the individual data set, with only small differences noted when comparing scaling methods, however, it is noted that PCA of scaled data is a vast improvement on PCA of unscaled data [22]. During the data processing step of this work, we explored the use of mean centring, root mean scaling and autoscaling. Mean centring revealed the greatest information from the data and as a result became the focus of this work. Principle components (PC) 1 and 2 demonstrated the best discrimination between tissue subtypes, separating out clearly the lens, retina and vitreous samples, whilst covering 83% of the cumulative variance.

Fig. 2A shows the scores plot obtained for the first two PC's for the positive ion spectra of all tissue samples, and Fig. 2B shows the scores plot obtained for the control samples of each tissue only. From both plots, it is clear that the three ocular tissue subtypes, the lens, retina and vitreous, group together as three distinct groups, reflecting the physiological differences between the tissues. Often in the analysis of biological samples in the first instance, a salt washing step is employed during sample preparation to reduce the salt concentration, as often salts present within the sample surface are associated with the induction of peak suppression [23]. Salt washing has been shown previously to counteract some effects associated with salt suppression; however, the removal effect of the washing phase reduces the secondary ion yield generated which can result in the loss of important biological information [23]. In this work, no salt washing step was utilised as in this case salts were not viewed as contaminations but as biologically important tissue determinants. Good sample clustering was obtained for all three tissue types without the need for a salt washing step (Fig. 2A). The loadings plot of PC 1 and 2 (Fig. 3A) contains the mass peak data used to create the score plot. Suggested structural ion assignments detailing relevant peaks to PC 1 and 2 are detailed in Table 1 and show that salt peaks were important in determining biological differences between tissue types.

Interesting biochemical information and chemical physiological determinants of ocular subtypes were identified. Positive PC 1 values were strongly associated with physiological salts, with $m/z = 23$ and 39 corresponding to Na^+ and K^+ , respectively (Fig. 2A and Table 1). On PC 2 from Fig. 2A, positive PC 2 values were associated with Na^+ ($m/z = 23$) and negative PC 2 values are associated

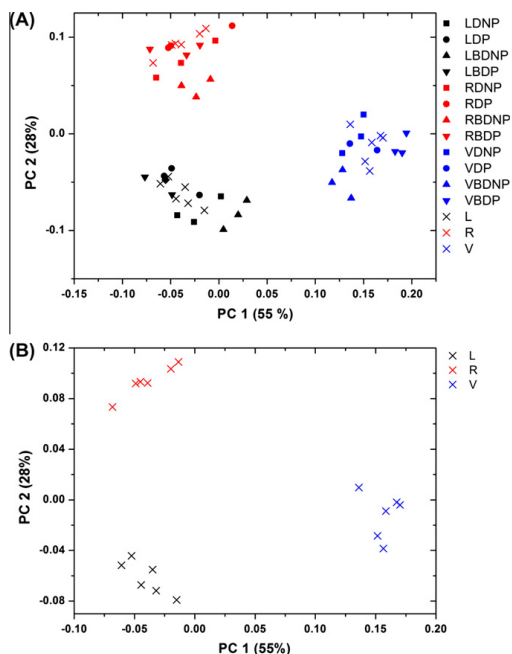


Fig. 2. (A) The scores plot for PC 1 versus PC 2 using positive ion spectra obtained for all ocular tissues samples. L corresponds to lens, V to vitreous and R to retina. DNP corresponds to low dosed non-perfused controls and BDP to high dosed non-perfused. DP corresponds to low dosed perfused samples and BDP to high dosed perfused samples. (B) The scores plot for PC 1 versus PC 2 using positive ion spectra obtained control tissue samples. L corresponds to lens, V to vitreous and R to retina.

with K^+ ($m/z = 39$). The vitreous tissue lies on the positive region of PC 1 demonstrating that this structure is almost completely dominated by Na^+ and K^+ ions. This is in keeping with the known alkali metal composition of the vitreous [24,25]. Other physiological components of the vitreous are likely not to be seen, due to the sheer magnitude of the salt peaks obtained overshadowing any other biochemical peaks obtained. The vitreous tissue has much higher concentrations of Na^+ and K^+ when compared with the lens and the retina, as both of these tissues sit on the negative region of PC 1. The lens and the retina tissues are predominantly separated on PC 2 by differences in Na^+ and K^+ ion concentration. The lens tissue, sits within the negative region of PC 2, demonstrates a high K^+ concentration ($m/z = 39$) rather than a high Na^+ concentration ($m/z = 23$). The lens is known to contain Na^+ , K^+ and Ca^{2+} with these ions thought to control fluid circulation and nutrient movement [26]. It is extremely interesting that the ovine lens appears to be a richer source of K^+ than Na^+ , as previously the human lens has been reported to contain Na^+ concentrations twice that of K^+ [27]. The difference in K^+ prevalence between the human lens and ovine lens represents an interesting species variation in lens tissue electrolyte composition. The retinal tissue sits within the positive region of PC 2, demonstrating that the retina is very different to the lens in the sense that it is dominated by the Na^+ ions rather than the K^+ ions. Differences in Na^+ and K^+ concentrations between the lens and retina have not been previously reported and this shows an interesting difference in ion importance within these tissues.

In addition to Na^+ and K^+ , Ca^{2+} ions ($m/z = 41$) were also detected in the tissue samples; however, two ion peaks of $m/z = 41$

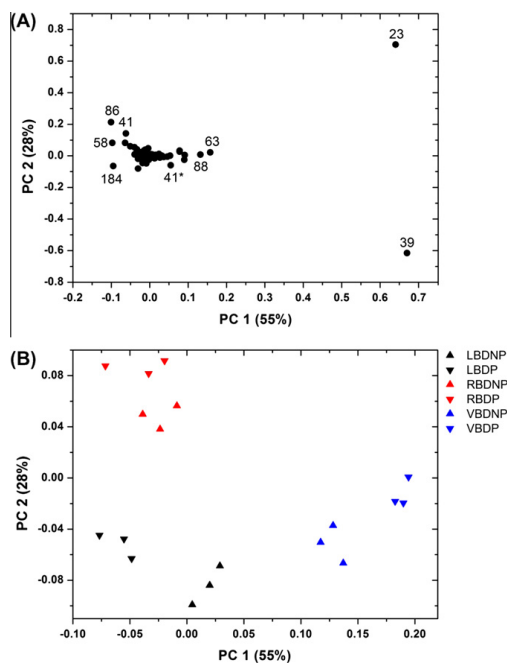


Fig. 3. (A) The loadings plot for PC 1 versus PC 2 demonstrating ion fragments controlling sample discrimination for positive ion spectra. (B) The scores plot for PC 1 versus PC 2 using positive ion spectra obtained high dosed tissue samples. B represents the scores plot for PC 2 versus PC 3 using positive ion spectra obtained for all ocular tissues samples. L corresponds to lens, V to vitreous and R to retina. DNP corresponds to low dosed non-perfused controls and BDP to high dosed non-perfused. DP corresponds to low dosed perfused samples and BDP to high dosed perfused samples.

were obtained, one of which represented Ca^{2+} and the other representing an organic hydrocarbon peak [2]. The first peak at 41 was associated with a positive value on PC 1, whereas the second peak at 41 sat on the negative region of PC 1. On PC 2, positive directionality was associated with the first peak at 41 and negative values associated the second m/z of 41. The retina sat within the negative region of PC 1 and the position region on PC 2, with positioning influenced by the second m/z of 41. The presence of Ca^{2+} in the retina is already well established with the presence of Ca^{2+} in the retina of mice demonstrated previously using ToF-SIMS [8]. Although Ca^{2+} is also present in the lens and vitreous, the Ca^{2+} content in the retina is high [28] due to the essential role of Ca^{2+} in the visual process [29]; therefore, the second peak with $m/z = 41$ in Fig. 2B represented Ca^{2+} . A peak of $m/z = 63$ was also detected and associated with positive directionality on PC 1 and also positive directionality on PC 2. A positive value on both PC 1 and PC 2 was associated with the vitreous tissue. Copper ($m/z = 63$, Cu^{2+}) is known to reside in the human vitreous, and the levels are often found to be increased during vitreoretinal diseases such as diabetic retinopathy [30]. The ocular tissues used in this work come from healthy ovine eyes sacrificed at a young age; therefore, it is unlikely the ocular tissues investigated would have increased Cu^{2+} levels. In addition, the positioning of ion $m/z = 63$ on Fig. 3A shows only a weak pull in the positive direction; therefore, it is likely this peak is commonly found in all three ocular tissues investigated and relates to a typical hydrocarbon species $C_5H_3^+$, commonly seen in positive ion spectra

and likely deriving from phenylalanine, tryptophan and tyrosine, which contain aromatic ring structures [31].

Using ToF-SIMS, we were not only able to detect small molecules, but interestingly we were able to detect smaller fragments of larger molecules found in ocular tissues. Phosphocholine fragments, including the phosphocholine head group $C_5H_{15}NPO_4^+$ with m/z 184, were shown to be present in the ocular tissue samples (Fig. 3A and Table 2). Negative PC 1 values were strongly associated with $C_5H_{15}NPO_4^+$, however, another ocular constituent, vitamin A is also known to fragment and produce ions with a corresponding m/z of 184 [5,32]. The lens tissue sits within the negative regions of PC 1 and 2 and is dominated by the peak at a m/z of 184. The lens is well known to contain vitamin C [33]; however, vitamin A content is of the lens is unclear. On the other hand, the retinal content of vitamin A [5] is well established due to the essential role of vitamin A in the visual process [34]. If the peak at $m/z = 184$ was induced by a fragment of vitamin A, it would feature on the positive side of PC 2, where the retina samples lie and not where the lens samples sit. The lens is composed of fibre cells, which are surrounded by a phospholipid bilayer and as a result phosphocholine concentrations are likely to be high. Due to the position and importance of mass peak of $m/z = 184$ in the distribution of the lens samples, m/z of 184 represents $C_5H_{15}NPO_4^+$. In addition to the phospholipid fragment identified, other potential fragments of larger molecules were also detected. A negative pull on PC 1, where the retina samples are positioned, was associated with a mass peak of $m/z = 86$ and represents either another phosphocholine fragment or the amino acid leucine [35].

In addition to the identification of physiological ocular constituents on PC 1 and PC 2, information about the location of amitriptyline is also evident on these components. Within each of the tissue subtypes, sample grouping of model drug-treated samples and untreated samples is evident. In the vitreous tissue samples, both the high dosed perfused samples and the high dosed non-perfused samples group together. Within the lens and the retina samples, grouping is present within samples treated with a high dose of drug, but only within samples that were dosed and non-perfused (Fig. 3B). The model drug was administered directly into the vitreous of treated eyes that were either perfused or non-perfused. In the non-perfused eye, drug movement through the eye occurred by diffusion alone resulting in drug not being cleared out of the eye due to the lack of blood flow. Therefore, the highest drug concentrations would likely be seen in non-perfused, treated eyes where the total dose remained in the eye and was not cleared. This explains the grouping together of the non-perfused-treated eye samples within the tissue groups for all three ocular tissues.

Table 2
Ion fragments (m/z) and structural assignment for positive ion spectra.

m/z	Positive ion structure
22.9930	Na^+
29.0409	$C_2H_5^+$
30.0378	CH_4N^+
38.9687	K^+
40.9660	Ca^+
43.0565	CH_3CO^+
44.0529	$C_2H_6N^+$
55.0568	Fe^+
63.0214	$C_5H_3^+$
70.0728	$C_4H_8N^+$
71.9842	FeO^+
72.0860	$C_5H_{12}N^+$
86.1090	$C_4H_8NO^+$ or $C_3H_{12}N^+$
94.9363	$C_7H_{10}^+$
104.1218	$C_5H_{14}NO^+$
147.0273	$C_2H_5O_4PNa^+$
184.1090	$C_5H_{15}NPO_4^+$

In perfused eye samples, ocular flow systems were enabled, resulting in drug movement through the eye by both diffusion and convection processes, in addition to this, drug clearance from the vortex veins was also in operation [36]. This clearance accounts for the lack of grouping between perfused-treated eye samples of the lens and retina. For the vitreous, the grouping together of perfused-treated samples suggests that a significant drug concentration still remained present within the vitreous. As the vitreous is an avascular structure, movement within the vitreous will often remain slow, even whilst flow systems are in operation within the eye. For this reason, a significant drug concentration remained within the vitreous, explaining the grouping in this tissue. Although the presence of the drug molecule is evident in PC 1 versus PC 2 (Fig. 2A), the biochemical composition of the individual ocular tissue dominates the multivariate analysis and has overshadowed peaks related to the model drug. Two peaks remain undetermined on PC 1 and PC 2, m/z of 58 and m/z of 88, and are possible fragments of the model drug (Fig. 3A). The difficulty in identifying drug peaks could be related to the dose of drug administered to the eye and/or the similarity of the drug structure to organic tissue constituents. However, even with these difficulties, the presence of the drug is evident on PC 1 and PC 2 and is a highly promising result.

This work has demonstrated that PCA can be applied to ToF-SIMS data in order to gain key physiological chemical information of ocular tissues and identify important physiological differences between ocular subtypes. The ability to detect and identify physiological constituents holds significant value in adding to the understanding of the structural components of the lens, vitreous and retinal tissues. PCA has also successfully detected model drug presence within ocular tissues, showing differences between ocular tissues treated with model drug and control ocular tissues. Although challenges arose in identifying specific drug fragments, this preliminary piece of work shows good promise in the use of the ToF-SIMS technique to identify drug location within ocular tissues. However, further work is still required in order to progress the use of ToF-SIMS in identifying drug distribution in ocular tissues. Studies focusing on a drug containing distinct chemical groups not typically seen in the ocular tissues analysed, such as a fluorinated compound, is of interest and would aid the identification of specific drug fragments.

Acknowledgements

JM acknowledges AstraZeneca and University of Strathclyde for the studentship. We thank Dr David Scurr from Laboratory of Biophysics and Surface Analysis (LBSA), School of Pharmacy, University of Nottingham for assistance with ToF-SIMS measurements.

References

- [1] K. Börner, H. Nygren, P. Malmberg, E. Tallarek, B. Hagenhoff, Localization of Na^+ and K^+ in rat cerebellum with imaging TOF-SIMS, *Applied Surface Science* 252 (2006) 6777–6781.
- [2] L. Wu, X. Lu, K.S. Kulp, M.G. Knize, E.S.F. Berman, E.J. Nelson, J.S. Felton, K.J.J. Wu, Imaging and differentiation of mouse embryo tissues by ToF-SIMS, *International Journal of Mass Spectrometry* 260 (2007) 137–145.
- [3] A.M. Belu, M.C. Davies, J.M. Newton, N. Patel, TOF-SIMS characterization and imaging of controlled-release drug delivery systems, *Analytical Chemistry* 72 (2000) 5625–5638.
- [4] A.J. Urquhart, M. Taylor, D.G. Anderson, R. Langer, M.C. Davies, M.R. Alexander, TOF-SIMS analysis of a 576 micr patterned copolymer array to reveal surface moieties that control wettability, *Analytical Chemistry* 80 (2007) 135–142.
- [5] T. Amemiya, H. Gong, K. Takaya, M. Tozu, Y. Ohashi, Changes of vitamins A and E in the rat retina under light and dark conditions detected with TOF-SIMS, *Applied Surface Science* 203–204 (2003) 738–741.
- [6] T. Amemiya, M. Tozu, Y. Ohashi, Time-of-flight secondary ion mass spectrometry can replace histochemistry demonstration of fatty acids in the retina, *Japanese Journal of Ophthalmology* 48 (2004) 287–293.

- [7] H. Gong, T. Amemiya, K. Takaya, M. Tozu, Y. Ohashi, Time-of-flight secondary ion mass spectrometry of fatty acids in rat retina, *Applied Surface Science* 203–204 (2003) 734–737.
- [8] J.H. Kim, J.H. Kim, B.J. Ahn, J.H. Park, H.K. Shon, Y.S. Yu, D.W. Moon, T.G. Lee, K.W. Kim, Label-free calcium imaging in ischemic retinal tissue by TOF-SIMS, *Biophysical Journal* 94 (2008) 4095–4102.
- [9] Y. Kishikawa, H. Gong, T. Kitaoka, T. Amemiya, K. Takaya, M. Tozu, T. Hoshi, Y. Ohashi, Elements and organic substances in epiretinal proliferative tissue excised during vitreous surgery: analysis by time-of-flight secondary-ion mass spectrometry, *Japanese Society of Microscopy* 52 (2003) 349–354.
- [10] Y. Kishikawa, T. Suematsu, T. Kitaoka, M. Tozu, T. Hoshi, Y. Ohashi, Analysis of internal limiting membranes of secondary macular hole and idiopathic macular hole by time-of-flight secondary ion mass spectrometer, *Investigative Ophthalmology and Visual Science* 46 (2005) 5422.
- [11] S. Jung, M. Foston, M.C. Sullards, A.J. Ragauskas, Surface characterization of dilute acid pretreated populus deltoides by ToF-SIMS, *Energy & Fuels* 24 (2010) 1347–1357.
- [12] A. Kinoshita, H. Gong, T. Amemiya, K. Takaya, M. Tozu, Y. Ohashi, Trace elements in lenses of normal Wistar Kyoto rats, *Applied Surface Science* 203–204 (2003) 742–744.
- [13] M. Porta, A. Allione, Current approaches and perspectives in the medical treatment of diabetic retinopathy, *Pharmacology & Therapeutics* 103 (2004) 167–177.
- [14] T.Y. Wong, G. Liew, P. Mitchell, Clinical Update: new treatments for age related macular degeneration, *The Lancet* 370 (2007) 204–206.
- [15] M.C. Davies, R.A.P. Lynn, J. Hearn, A.J. Paul, J.C. Vickerman, J.F. Watts, Surface chemical characterization using XPS and TOF-SIMS of latex particles prepared by the emulsion copolymerization of functional monomers with methyl methacrylate and 4-vinyl pyridine, *Langmuir* 11 (1995) 4313–4322.
- [16] J.L.S. Lee, I.S. Gilmore, M.P. Seah, Quantification and methodology issues in multivariate analysis of ToF-SIMS data for mixed organic systems, *Surface and Interface Analysis* 40 (2008) 1–14.
- [17] M. Taylor, A.J. Urquhart, D.G. Anderson, R. Langer, M.C. Davies, M.R. Alexander, Partial least squares regression as a powerful tool for investigating larger combinatorial polymer libraries, *Surface and Interface Analysis* 41 (2009) 127–135.
- [18] B. Tyler, Interpretation of TOF-SIMS images: multivariate and univariate approaches to image de-noising, image segmentation and compound identification, *Applied Surface Science* 203–204 (2003) 825–831.
- [19] M.S. Wagner, D.J. Graham, B.D. Ratner, D.G. Castner, Maximizing information obtained from secondary ion mass spectra of organic thin films using multivariate analysis, *Surface Science* 570 (2004) 78–97.
- [20] M.R. Keenan, P.G. Kotula, Optimal scaling of TOF-SIMS spectrum-images prior to multivariate statistical analysis, *Applied Surface Science* 231–232 (2004) 240–244.
- [21] M.J. Koerberle, P.M. Hughes, G.G. Skellern, C.G. Wilson, Pharmacokinetics and disposition of memantine in the arterially perfused bovine eye, *Pharmaceutical Research* 23 (2006) 2781–2798.
- [22] B.J. Tyler, G. Rayal, D.G. Castner, Multivariate analysis strategies for processing ToF-SIMS images of biomaterials, *Biomaterials* 28 (2007) 2412–2423.
- [23] A.M. Piwowar, N.P. Lockyer, J.C. Vickerman, Salt effects on ion formation in desorption mass spectrometry: an investigation into the role of alkali chlorides on peak suppression in time-of-flight-secondary ion mass spectrometry, *Analytical Chemistry* 81 (2009) 1040–1048.
- [24] E.A. Balazs, J.L. Denlinger, The Vitreous, in: H. Daveson (Ed.), *The Eye*, Academic Press, 1984, pp. 533–589.
- [25] C.S. Nickerson, J. Park, J.A. Kornfield, H. Karageozian, Rheological properties of the vitreous and the role of hyaluronic acid, *Journal of Biomechanics* 41 (2008) 1840–1846.
- [26] D.C. Beebe, Lens, in: P.L. Kaufman, A. Alm (Eds.), *Adler's Physiology of the Eye*, Mosby Inc., St Louis, Missouri, 2003, pp. 117–158.
- [27] N. Dilsiz, A. Olcucu, M. Atas, Determination of calcium, sodium, potassium and magnesium concentrations in human senile cataractous lenses, *Cell Biochemistry and Function* 18 (2000) 259–262.
- [28] H.H. Hess, The high calcium content of retinal pigmented epithelium, *Experimental Eye Research* 21 (1975) 471–479.
- [29] A. Akopian, P. Witkovsky, Calcium and retinal function, *Molecular Neurobiology* 25 (2002) 113–132.
- [30] N.S. Konerirajapuram, K. Coral, R. Punitham, T. Sharma, N. Kasinathan, R. Sivaramakrishnan, Trace elements iron, copper and zinc in the vitreous of patients with various vitreoretinal diseases, *Indian Journal of Ophthalmology* 52 (2004) 145–148.
- [31] H. Zhou, C.M. Chan, L.T. Weng, K.M. Ng, L. Li, Relationship between the structure of polymers with well-defined fluorocarbon segmental lengths and the formation of secondary ions in SIMS, *Surface and Interface Analysis* 33 (2002) 932–939.
- [32] E. Gazi, J. Dwyer, N. Lockyer, P. Gardner, J.C. Vickerman, J. Miyan, C.A. Hart, M. Brown, J.H. Shanks, N. Clarke, The combined application of FTIR microspectroscopy and ToF-SIMS imaging in the study of prostate cancer, *Faraday Discussions* 126 (2003) 41–59.
- [33] E.R. Berman, *Biochemistry of the Eye*, Plenum Press, New York, 1991.
- [34] L. Quadro, W.S. Blamer, D.J. Salchow, S. Vogel, R. Piantadosi, P. Gouras, S. Freeman, M.P. Cosma, V. Colantuoni, M.E. Gottesman, Impaired retinal function and vitamin A availability in mice lacking retinol-binding protein, *EMBO Journal* 18 (1999) 4633–4644.
- [35] M. Aranyosiova, M. Michalka, M. Kopani, B. Rychly, J. Jakubovsky, D. Velic, Microscopy and chemical imaging of Behcet brain tissue, *Applied Surface Science* 255 (2008) 1584–1587.
- [36] S. Tsuboi, J.E. Pederson, Volume flow across the isolated retinal pigmented epithelium of cynomolgus monkey eyes, *Investigative Ophthalmology and Visual Science* 29 (1988) 1652–1656.

